Electronic transfer within a microbial fuel cell. Better understanding of Experimental and Structural Parameters at the Interface between Electro-active Bacteria and Carbon-based Electrodes

David Pinto

Université Pierre et Marie Curie

Ecole doctorale 397 – Physique et Chimie des Matériaux

Laboratoire Chimie de la Matière Condensée de Paris

Matériaux Hybride et Nanomatériaux

TRANSFERT ELECTRONIQUE AU SEIN D'UNE PILE A COMBUSTIBLE MICROBIENNE

Compréhension des Paramètres Expérimentaux et Structuraux à l'Interface entre une Bactérie électro-active et une Electrode carbonée

---

Présentée par : **David PINTO**

Thèse de doctorat de Chimie des Matériaux

Dirigée par : **Pr. Christel Laberty-Robert et Dr. Thibaud Coradin**

Présentée et soutenue publiquement le **14 Novembre 2016**

Devant le jury composé de :

Dr. Sara Cavaliere	Maitre de Conférence HDR à l'Université de Montpellier, France – ICGM	Rapporteur
Dr. Elisabeth Lojou	Directrice de Recherche CNRS à l'Unité de Bioénergétique et Ingénierie des Protéines	Rapporteur
Pr. Abraham Esteve Núñez	Professeur à l'Université of Alcalá, Madrid, Spain – Bioelectrogenesis	Examinateur
Pr. Claude Jolivalt	Professeur à l'Université Pierre et Marie Curie, Paris 6, France – LRS	Examinatrice
Dr. Eric Lafontaine	Docteur HDR, Responsable de domaine scientifique à la DGA	Examinateur
Dr. Thibaud Coradin	Directeur de Recherche CNRS à l'Université Pierre et Marie Curie, Paris, France – LCMCP	Co-directeur de Thèse
Pr. Christel Laberty-Robert	Professeur à l'Université Pierre et Marie Curie, Paris, France – LCMCP	Directrice de Thèse

ELECTRONIC TRANSFER WITHIN A MICROBIAL FUEL CELL

Better understanding of Experimental and Structural Parameters at the Interface between Electro-active Bacteria and Carbon-based Electrodes

Presented by: **David PINTO**

Doctoral thesis of Material Chemistry

Supervised by: **Pr. Christel Laberty-Robert et Dr. Thibaud Coradin**

Thesis presented and defended on **14th November 2016**

« La vie, c'est comme une bicyclette,
il faut avancer pour garder l'équilibre. »
– *Albert Einstein*

TABLE OF CONTENTS

Chapter 2 – External Parameters Affecting Bacterium Adhesion and Microbial Fuel Cell Performanced 59

GENERAL INTRODUCTION

Over the last decades, the energetic question takes up a large part of the world research effort to both discover and develop an energetic mix to limit our dependency on non-renewable energy including petroleum, coal nuclear plants. Fossil fuels are non-renewable, that is, they draw on finite resources that will eventually dwindle, becoming too expensive or too environmentally damaging to retrieve. In contrast, renewable energy resources-such as wind and solar energy-are constantly replenished and will never run out. They are already developed and, for some of them, commercialized.

Fuel cells are another example of technology based on a sustainable process [1,2]. Basically, the most common hydrogen/oxygen fuel cell is based on the hydrogen oxidation and the oxygen reduction to form water and generates two electrons per electrochemical reaction. However, even if oxygen is already available in air, hydrogen has to be produced. Currently, hydrogen is obtained from catalytic reforming of petroleum but renewable processes are already under development for example the electrolysis of water [3]. To develop low temperature fuel cell technologies, two main questions need to be solved (i) the installation of a clean and efficient H_2 network and the education of population about hydrogen use [4]. (ii) Other limitations need to be solved such as the use of Pt as catalyst for both hydrogen oxidation and oxygen reduction [5]. Sustainable and inexpensive alternatives need to be found to make this technology competitive.

In fuel cell, biofuel cells using a concept close to conventional hydrogen/oxygen fuel cell are very interesting technology [6,7]. The main difference is in the substitution of platinum by a biological component carrying out the oxidation and/or the reduction reactions. In microbial fuel cell, a bacterium acts as a catalyst and oxidizes molecules based on its metabolism. Interestingly, this system can use short and cheap molecules as fuel. These short organic molecules can be sugars or organic contaminants in water which are generally unusable in conventional energy producing technology due to their low energy content. Even if electrical performances of these systems are not comparable to H_2/O_2 fuel cell, they can be made economically-viable by combining energy production with other valuable functions such as depollution, carbon dioxide valorization, hydrogen production and water desalinization [8]. Finally, MFC are theoretically easy to produce, cheap and necessitate a source of bacteria and fuels depending on bacterium strains. Bacterial communities can also be adapted to fuels available in their working environment [9].

Therefore, MFCs must be studied via a multidisciplinary approach involving microbiological understanding of electroactive bacterium [10] or micro-organism and understanding the electronic transfer at the complex bacterium/electrode interface [11]. Moreover, material sciences and engineering are also needed to develop adapted electrode materials to be colonized by bacteria. Altogether electroactive bacterium sourcing and characterization, electronic transfer understanding, electrode material and cell designing are key parameters that need to be intensively studied in order to elaborate efficient MFCs with a long-term stability.

In this general context, **the present thesis focusses on the interactions existing between the bacterium and the electrode in the anodic compartment of a MFC**. The main objective is to determine the best conditions for a bacterium to adhere to the anode and to form a conductive biofilm in order to perform external electron transfer. For this project, the electroactive wild strain *Shevanella oneidensis* is chosen as a model bacterium. Commercial and home-made fibrous electrodes are used as anodic material.

To achieve this objective, **experimental and structural parameters are varied to evaluate their influence on the bacteria/electrode interfaces** with the help of microbiological, electrochemical and chemical engineering methodologies.

A first chapter will briefly present how biofuel cell and more particularly microbial fuel cell are studied as a promising way to produce energy by combining it with other functions. The way a biofuel cell works and how the micro-organisms interact with the anode will be described together with an overview of the recent advances in term of global comprehension and material sciences.

In a first part of the second chapter, various experimental parameters are evaluated stimuli to optimize the colonization of carbon felt electrode by *S. oneidensis* strain to form an electrically conductive biofilm. It will be demonstrated that the particular aero-anaerobic optional *S. oneidensis* strain is able to grow and perform external electron transfer to a solid electrode even in presence of oxygen. Moreover, the state of growth of the bacteria as well as the nature of the electrolyte will be examined as parameters to obtain various electrochemical behaviors. Polarization in unusual aerated medium will be evaluated and defined as one of the most influencing parameters to colonize the electrode. Dual- and single-compartment (half-cell) MFC reactors are employed to electrochemically characterize the effect of these parameters on fuel cell performances. Electrochemistry, characterization of complete MFC (polarization and power curve), scanning electron chemistry, and biological test of viability are used to characterize the MFC.

In a second part of the second chapter, *S. oneidensis* is embedded in a hybrid SiO_2-carbon felt electrode, composed of a silica gel synthetized by the aqueous sol-gel route and then, included in a carbon felt. By this way, bacteria are encapsulated in a 3D matrix without requiring a colonization step. The electrochemical response of the bacterium is then correlated to the inorganic gel (composition and structure).

Finally, **in a third chapter**, based on an experimental observation that such commercial carbon felts are underused due to the carbon nature and their architecture, a new electrode is designed and synthetized to respond basic requirements such as the average fibers diameter, porosity and thickness. The electrode is produced by electrospinning combined with a heat-treatment at high temperature under various conditions to provide an electrical conductivity network. Finally, electrospun carbon papers are characterized by classical techniques including electrochemistry, impedance spectroscopy, fourier transform infrared spectroscopy, Raman spectroscopy, scaning electron microscopy and viability test such as epifluorescence optical microscopy and couting on plate. The carbon paper was then colonized by *S. oneidensis* and evaluated as new and promising category of home-made electrodes.

CHAPTER I

LITERATURE REVIEW

Table of Contents – Chapter 1

1.1. GENERAL ENERGETIC CONTEXT

In 2015, the world energy consumption was considerably high, around 13 371 Mtoe (million tonnes of oil equivalent; 1 toe = 11 630 kWh) with 80% coming from fossil fuels. Among the 13 371 Mtoe, 1 800 Mtoe is for Europe and 246 Mtoe for France. World energy demand increases by 0.7% in 2015. According to IEA, global energy demand will increase by ca. 1.2% per year between 2008 and 2035. In parallel, if there is controversy on the amount of fossil fuel remaining on Earth, it is certain that reserves are finite and their accessibility is becoming more complex. Rapid decline of limited fossil fuel resources will increase the market price and lead to the development of new energy sources, independent on finite resources. Moreover, COP21 conference indicates the importance of a global carbon-emission reduction to regulate climate degradation and made life sustainable everywhere on Earth.

To tackle climate change and energy transition, new technologies were developed to eventually replace fossil fuel by sustainable energy. Renewable energy such as wind power, solar energy, hydropower represents great insight for energy transition but they are intermittent and highly dependent on power plant localization. To compensate variability and intermittence in renewable energy availability, research has been initiated and intensified to develop energy storage and punctual supply. Batteries are efficient for energy storage and redistribution but they need a primary energy production. Meanwhile, fuel cells [1] allow continuous energy production as long as they are supplied by fuel (such as hydrogen) and represent a complementary alternative to non-renewable energy for our future energy mix.

1.2. GENERAL ASSESSMENTS ABOUT BIOFUEL CELLS

1.2.1. From fuel cell to biofuel cell

A fuel cell is an electrochemical device that allows continuous generation of energy by converting chemical energy into electrical energy while anodic and cathodic tanks are supplied in fuel and combustible [2,12]. In this way, fuel cell differs from batteries which need to be recharged thanks to an external source [13,14]. Fuel cells are based on the inverse electrolysis process, named “Fuel Cell Effect” observed by Christian Friedrich Schönbein in 1838 and applied in 1839 by William Grove who constructed the first Fuel Cell, using platinum electrodes. Grove results were intensively studied and improved by Francis Bacon (5 kW alkaline fuel cell) in the 1960s due to the emulation around the “space race” [15]. Fuel cells were firstly commercialized in 2007 for stationary backup power units and then continuously developed until now [16,17].

Indeed, fuel cell works as an autonomous and versatile sustainable device. Hydrogen is commonly used as fuel and oxygen as combustible **(Figure 1.1)**. For the most part, pure hydrogen is nowadays fabricated by hydrocarbons reforming which is based on petroleum resources and emits carbon dioxide. Nevertheless, water splitting process opens a green issue to produce highly pure hydrogen and oxygen, particularly if using renewable energy. In this case, a fuel cell can be compared to a battery: during high energy productivity of intermittent sources,

hydrogen is produced by water splitting and stored. Then during low productivity (ex. night for solar energy), energy stored in hydrogen form may be released using fuel cell effect.

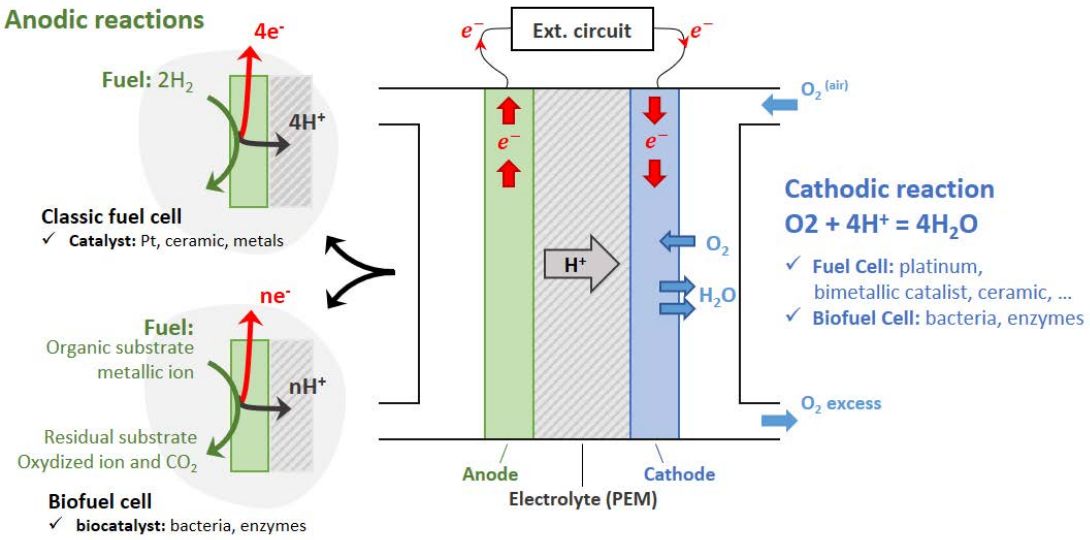

Figure 1.1 - Comparison between Hydrogen Fuel Cell and Biofuel Cell

In a hydrogen fuel cell, hydrogen oxidation produces protons and electrons that diffuse respectively through an electrolyte and the external circuit to participate in the reduction of oxygen at the cathodic side of the cell. In fuel cells, the low reaction rate of both oxidation and reduction, mainly due to the oxygen which implies four exchanged electrons, require catalysts and/or specific conditions to be efficient:

(i) For SOFC (Solid Oxide Fuel Cell) working at high temperature, technical ceramic catalyst is used if a temperature of at least 500°C [18] is maintained, consuming one part of the energy produced.

(ii) For PEMFC (Proton Exchange Membrane Fuel Cell), low temperatures are acceptable but a highly pure gas is mandatory as a complement to expensive and rare catalysts based on platinum or bimetallic compound such as PtCr or PtTi [5,19].

(iii) In both case, hydrogen storage [4] represents an important challenge in term of security and users' education.

Combustive are already available in sufficient amount. The oxygen must be extracted from the air and the hydrogen is currently produced from catalytic reforming of petroleum. However, renewable hydrogen production must be available in the next decade (water splitting). Meanwhile, others renewable technologies such as photovoltaic or wind energy are developed. Even if biofuel cell only starts to be potentially competitive in term of performance, they represent a promising alternative. Cheap electrode materials (carbon or stainless steel) are easy to find as well as biocatalysts for microbial fuel cell. Moreover, the micro-organisms can be selected as function of the combustive available in the MFC working conditions.

1.2.2. Microbial Fuel Cells and Enzymatic Fuel Cells

In biofuel cell, oxidation and reduction are performed by biological catalysts such as purified enzymes for enzymatic fuel cell (EFC), bacteria or other type of micro-organisms (yeast, algea, …) for microbial fuel cell (MCF) [7,20,21]. Fuels converted by these devices are usually sourced from biomass owing to the natural sourcing of the catalysts. Various sugars (glucose, …) or carboxylates (lactate, pyruvate, acetate, …), metallic ions, carbon dioxide or hydrogen are involved in the process as converted fuel. Microbial and enzymatic fuel cells differ in their adaptability for a specific environment. EFC consists in the immobilization of an enzyme on a conductive material. Consequently to the substrate-specificity of enzymes, EFC only converts one type of substrate for a specific enzyme. At the opposite, bacteria-based MFC assimilates a large diversity of substrates.

1.2.2.1. Enzymatic Fuel Cell.

Biochemical transformations are commonly catalyzed by specific biological catalysts, such as enzymes. In 1833, Payen A. and Persoz J.F. firstly extracted an enzyme from malt, the diatase responsible for amidon hydrolysis. Then, Schwann T. isolated Pepsine before the emergence of the Enzyme-Substrate model by Henri and Brown in 1902. Thirty years later, a large panel of enzymes were crystallized (urease, pepsine, trypsine, …) and Warburg O. explained basics of enzymes purification, a critical advance for enzymatic biochemistry. Gradually, enzymes scope became more diverse and proved its relevance in medical field, analytical chemistry and agro-food industry.

EFC is based on the use of immobilized enzymes (oxidoreductases, EC1) on an electrode to ensure electrocatalytic degradation of fuel-substrate [7]. Electrons flow from active sites of enzymes to the electrode occur thanks to the tunnel effect. Three major ways of immobilization are reported: surface adsorption (Van der Waals interaction) [22], covalent grafting via specific amino-acids [23] and encapsulation into conductive matrix [24,25]. Immobilized enzyme on an electrode may serve as a sensor to dose specific molecules, usually a molecule of biological interest or a pollutant, with an impressive sensitivity. Indeed, in potentiostatic monitoring configuration enzymatic bio-sensors are only limited by the current sensitivity of the potentiostat which is already high (picoamps) [26,27]. Also, enzymes are able to efficiently convert a large concentration of substrate for power generation (EFC-mode). As a result of immobilized enzyme selectivity and thus of electrode selectivity for a specific substrate, compartment separator (semi-permeable membrane) is optional [28–31]. Conventionally, the membrane prevents fuel crossover, causing side reaction, catalysts poisoning and finally loss of performance. For example, in a hydrogen fuel cell, platinum catalyzes both anodic and cathodic redox reactions. Therefore, without membrane, oxidation and reduction potentially happen on both electrodes. In hydrogen/oxygen fuel cell, the separator has to be impermeable to gas (fuel and combustible) in order to prevent combustion and needs to be a good ionic conductor for proton crossover.

Enzyme-substrate dependence, immobilization, enzymes less sensitive to poisoning and deactivation, membrane-less architecture, miniaturization, both direct and mediated electron transfer strategies are the main advantages counterbalancing enzymes cost, dependence on co-factor (co-enzymes, organic molecules or metallic ions) [32] and relative instability in soft conditions [33]. A few systems are currently under development for portable devices powering (fructose/dioxygen EFC: 850 $\mu W.cm^{-2}$ [34] ; ethanol/air EFC: ca. 12 $mW.cm^{-2}$ [35]) and implantable EFC (Glucose/O_2 EFC already implanted in rats: 24.4 $\mu W.mL^{-1}$ [36] ; [37,38]).

Recently, hybrid systems combining MFC (bioanode) and EFC (biocathode) were proposed as alternatives of full-enzyme fuel cell. For example, Cooney *et al.* reach an OCV of 1V and 26 W/m^3 for several days with lactate/O_2 hybrid MFC/EFC using *Shewanella oneidensis* at the anode and the laccase at the cathode [39].

1.2.2.2. Microbial Fuel Cell.

In 1911, Potter M.C. observed an electrical current generation from micro-organisms for the first time by measuring electrode potential of various materials immerged in yeast and bacteria solution [6] . Even though Potter observations were fundamental, they generated few interest to micro-organisms generating bioelectricity. Biofuel cell studies were really reinitiated in 1966 during a symposium of Lewis K. proposing basic and advanced principles of microbial and enzymatic fuel cells including critical points remaining unsolved (oxygen sensitivity of enzymes, …) [40]. Interest in MFC increases during 1990s with the idea of adding shuttles in solution to promote bacteria-electron transfers. Moreover, a crucial stage has been reached in 1999 when Kim *et al.* [41–43] and then Rabaey *et al.* [44,45] refuted the systematic need of an external mediator which were toxic for bacteria viability and expensive.

With pure, mixed or enriched inoculum it is possible to extract from 10 $mW.m^{-2}$ to more than 10 $W.m^{-2}$ [10]. MFC starts to be competitive with an increase of performance by 6 from 1999 to 2009. But, in comparison with solar cells (1 $kW.m^{-2}$), it appears that MFC needs to be improved in term of power and current production. This could be achieved with the aid of synthetic biology, material science and engineering to optimize architectures. Nevertheless, future MFC consists in mixing power production with another highly valuable application. For example, based on the work of Shizas *et al.* [46], Logan and Rabaey developed the concept of powering wastewater treatment plant by the valorization of loss wastewater energy. They calculated that wastewater contains 9.3 times as much energy as that currently used to treat it [10,47–49]. Conceptually, this theoretical result indicates the potential valorization of the power contained in domestic wastewater. Based on these conclusions, Liu *et al.* empirically demonstrated the possibility to extract a significant quantity of power by wastewater circulation in a laboratory scaled MFC (ca. 20 $mW.m^{-2}$, in 2004) [50]. Since nowadays, the concept is intensively studied. In a report published in 2013, Zhen *et al.* demonstrated higher performance (6 $W.m^{-3}$) and conclude by confirming the promising application of MFC to treat low-strength domestic wastewater [51].

MFC are suitable for both stationary and portable applications. MFC can be easily transported for energy production in isolated environment to power electronic devices (cellphone, …) [52], small robots (Eco-bot II and III) [53,54], etc. Moreover, MFC can be designed to answer specific requirements to serve as an operational source of energy in non-electrified place. This technology does not need fuel (fuel generator, hydrogen, …) thanks to the possibility to select the micro-organisms in order to use fuel available where MFC are used (wastewaters, effluents).

Even if MFC power efficiency is lower than other renewable energy, the valorization of end-life substrates justifies the exponential increase in research publications about MFC and more generally Microbial Electrochemical Technologies (METs) [8].

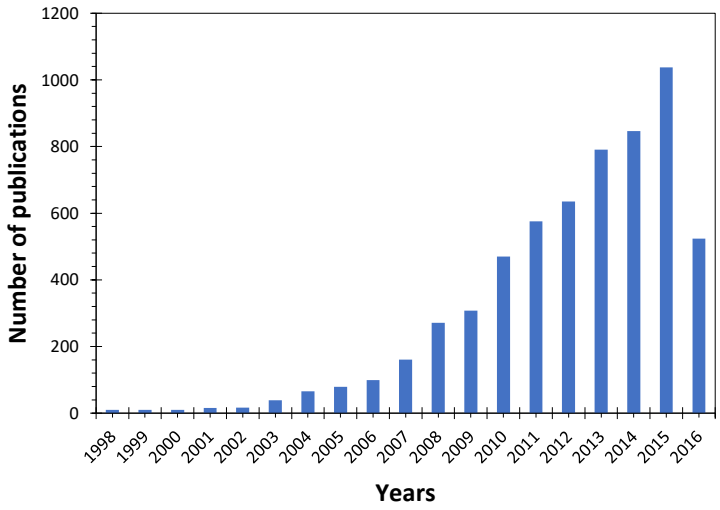

Figure 1.2 - Number of published journal articles on MFCs containing the phrases "microbial fuel cell". Source: Web of Sciences on 07/08/2016

1.2.3. Microbial Electrochemical Systems

Microbial Electrochemical System (MES) is a general class of electrochemical systems adapted from the very original class of MFC but with different bacteria localization, separator configuration and applications (biosensing or electrical/chemical production). The application of MES determines if the system consumes or produces electricity **(Figure 1.3)**. They are also named Microbial Electrochemical Technologies (METs).

Energy productive MES:

(i) *Microbial Fuel Cell* **(Figure 1.3.A)** As described in part 1.2.2. and 1.3.1., MFC allows electrical power harvesting based on carbon source oxidation (electron donor) via bacteria metabolism. Electrons are produced by the respiration and transferred to the anode (final electron acceptor). By this way, a MFC supplies an external device or resistor. [50]

(ii) *Biosensor.* If a MFC is monitored in a potentiostatic three electrodes configuration (reference electrode, working and counter electrodes), a substrate oxidized by

bacteria can be dosed electrochemically. Current produced by electrons flow must be precisely measured by a potentiostat (I > 100 pA). [55,56]

(iii) *Microbial Remediation Cell.* Exoelectrogenous bacteria accept various fuels as carbon source or co-substrate. Similarly to MFC, specific strains named Dissimilatory Metal-Reducing Bacteria (DMRB) are able to couple the oxidation of organic electron donors and reduction of metal pollutants from industry (electron acceptors). DMRB are useful for reduction of heavy metal-ions pollutants. [57–59]

(iv) *Microbial Desalination Cell* **(Figure 1.3.D)**. Schematically, a MDC is an MFC associated with a third chamber between anodic and cathodic sides. This chamber is separated into anodic and cathodic chambers with two membranes: an anion-exchange membrane and a cation-exchange membrane. While MDC works, bioelectricity is harvested. Additionally, anions and cations from sea water migrate to the anodic and cathodic side, respectively. [60–62]

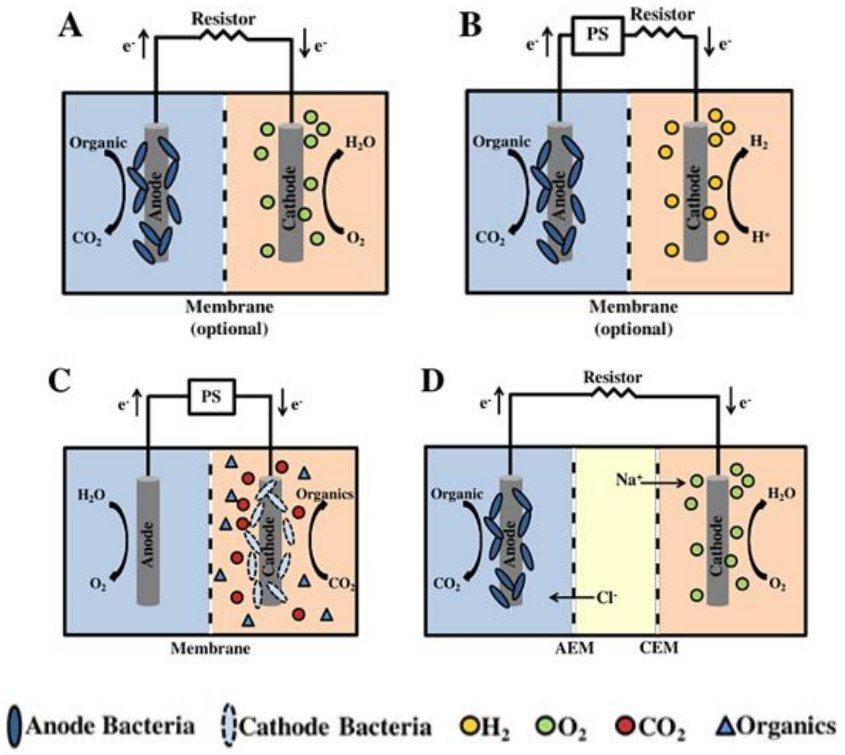

Figure 1.3 – Four typical MXC, where X corresponds to application:
(A) Microbial Fuel Cell, adaptable for biosensing; **(B)** Microbial Electrolysis Cell for hydrogen production; **(C)** Microbial Electrosynthesis for CO_2 valorization; **(D)** Microbial Desalination Cell, including ionic gradient middle chamber. *Wang H. and Ren Z.J., 2013* [8]

Energy consumers MES:

(v) *Microbial Electrolysis Cell* **(Figure 1.3.B)**. By applying a bias to the MFC, cell voltage must be enough to work in water splitting mode inducing dihydrogen production (protons reduction). [61]

(vi) *Microbial Electrosynthesis, CO_2 valorization* **(Figure 1.3.C)**. In contrast with other microbial electrochemical systems, MES anodic side is free of bacteria and the cathode is colonized by bacteria able to recover carbon dioxide and convert it into small organic

molecules with electrons provided by the cathode. MES discovery is based on the verified hypothesis of electron flow from an electrode to a bacterium (reverse classical electron transfer). [63–65]

1.3. MICROBIAL FUEL CELLS

1.3.1. Principle of MFC electricity generation

Microbial Fuel Cell converts chemical energy into electrical energy through metabolic activity of micro-organisms and more particularly bacteria respiration in the case of this thesis work. These bacteria are defined as *exoelectrogenic*, "*exo*" for exocellular and "*electrogen*" to define their ability to produce electricity by transferring electrons to chemical or solid substrate [66]. To compare MFC with a conventional fuel cell, the bacterium acts as a biocatalyst.

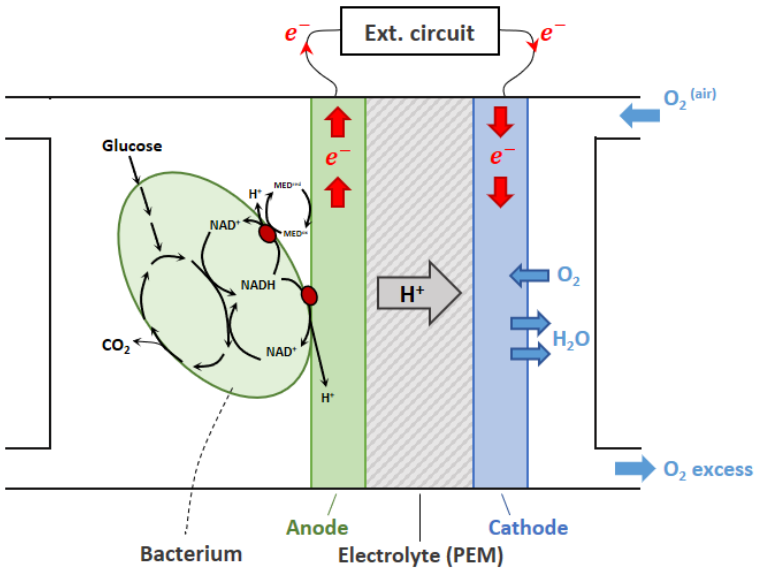

Figure 1.4 – Developed scheme of a Microbial Fuel Cell.
Micro-organism (in green) converts glucose into carbon dioxide, protons (diffusing through the membrane to the cathode) and electrons transferred to anode and cathode via external circuit.
Adapted from: Rabaey K., Verstraete W. [67]

Basically, a MFC is composed of an anode in a first compartment, a cathode in another compartment. Both compartments are separated by an ion-permeable membrane. The anode is colonized by bacteria which oxidize fuel (organic matter) in a final product (ex. pyruvate for lactate), electrons, protons and CO_2. Such a CO_2 production is less damageable than CO_2 produced from fossil fuel as it results from biomass conversion. Electrons flow from the anode to the cathode via an external circuit (device or resistor) and protons diffuse through the membrane from the anodic compartment to the cathodic compartment. Most of the time, at the cathode protons and electrons react with oxygen from air leading to it reduction into water **(Figure 1.4)** [10,66,67,9,68].

In comparison with enzymatic fuel cell, microbial fuel cell catalysts are easily regenerated by bacteria growth in specific conditions without requiring expensive step of isolation or purification. Moreover, in 2002 Kim *et al.* studied the lifetime of a MFC under cycling

condition beyond 3 or 5 years. The diversity of bacteria able to exoelectrogenic activity in MFC-mode is robust and versatile. Consequently, they present numerous metabolic profitable pathways to generate electricity from a large diversity of electron donors **(Figure 1.5)**. MFC are less specific than EFC resulting in a higher conversion yield for a complex chemical environment (wastewater, industry effluents, …) [9].

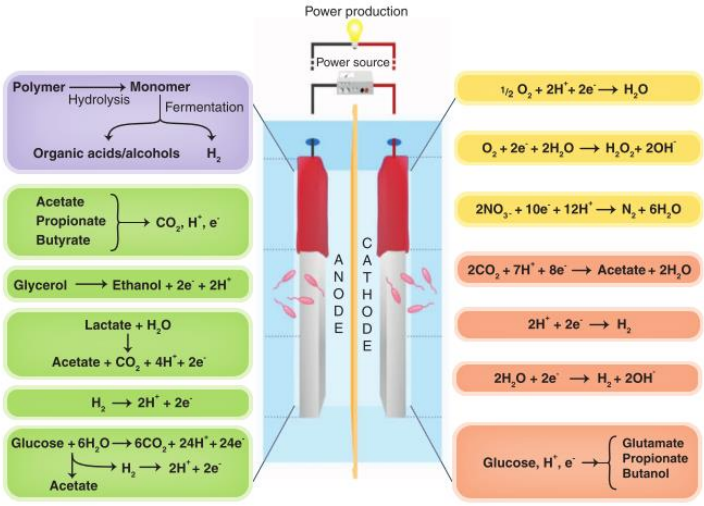

Figure 1.5 – General overview of anodic and cathodic BES/MET (non-exhaustive).
At the anode, simple molecule or gas are oxidized while CO_2, H_2O, glucose and protons are reduced at the cathode. *Reaction in: Purple*, do not directly result in current generation. *Green*, produce energy. *Yellow*, occur spontaneously (without bias). *Red*, require power addition to occur. *Bruce and Rabaey* [9]

1.3.2. Microbial Electron Transfer

Bacteria are now well-known to transfer electrons obtained by respiration mechanism. This ability to donate electrons to a surface is a critical point in the elaboration of microbial fuel cells and more generally, microbial electrochemical systems. Electron production happens by the oxidation of electron donors (lactate, acetate, glucose, …) inside the cell using bacterial respiration. Resultant electrons flow to electron acceptors (conductive surface, fumarate, …). For the electron transfer to occur, electrons have to cross the cell wall before reducing electron acceptors.

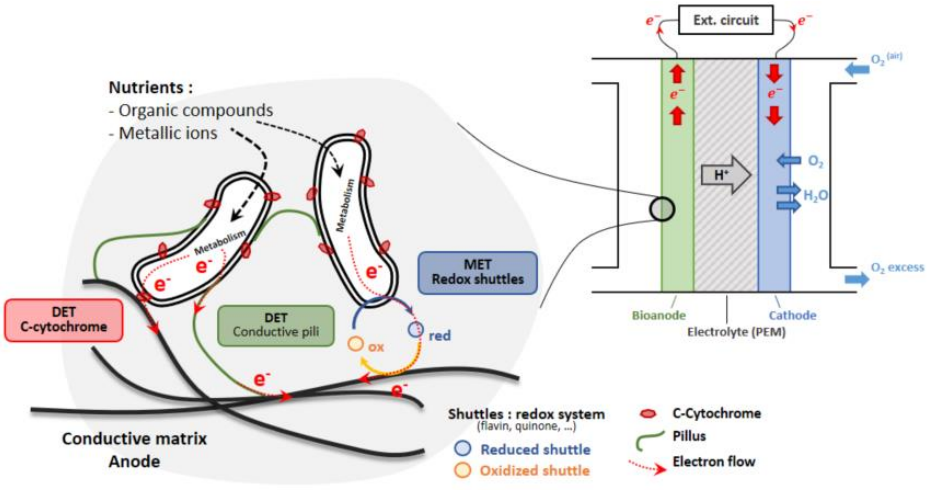

Figure 1.6 – Extracellular electron transfer representation:
Direct electron transfers (DET), mediated electron transfers (MET); indirect electron transfers (IET) are similar to MET using electron donor synthetized by fermentative micro-organisms

Intensive studies about extracellular electron transfer (EET) were carried out in order to better understand transfer pathways. Currently, three types of electron transfer are defined and presented on **Figure 1.6**: indirect electron transfer (IET), mediated electron transfer (MET) and direct electron transfer (DET). These transfers are not exclusive and may occur simultaneously depending on bacteria nature. For example, *Shewanella oneidensis (S. oneidensis)* carries out MET and DET while *Geobacter sulfurreducens (G. sulfurreducens)* only performs DET.

1.3.2.1. Indirect Electron Transfer.

Most cells and bacteria strains transfer electrons by indirect electron transfer. For IET, fermentative bacteria consume carbon sources and convert it into metabolite products such as hydrogen or alcohol. These fermentative products are redox species in reduced state and contain electrons that can be donated to an electron acceptor. As a matter of fact, they are secreted by bacteria and diffuse to react at the electrode surface.

1.3.2.2. Mediated Electron Transfer.

Mediated transfer is based on the use of soluble intermediate molecules to facilitate electron shuttling from the inside of the bacteria to the outside at the electrode surface. The mediators also named shuttles are redox molecules that approach the cell and diffuse inside to be reduced by electrons from their initial oxidized state to a more reduced one and consequently oxidized again at the electrode. Misunderstanding usually remains on the difference between MET and IET. They are based on the same principle, but in MET, shuttles are reusable intermediates while in IET fermentative metabolites are not **(Figure 1.7)**.

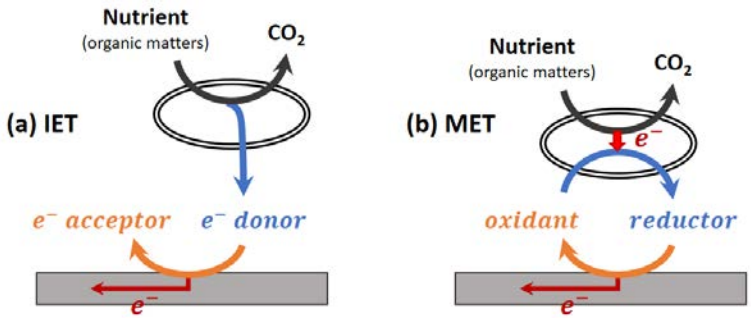

Figure 1.7 – Difference in electron transfer mechanism between IET **(a)** and MET **(b)**

Since Potter ambiguous discovery of bioelectricity generation (cf. part 1.2.2) [6], shuttles have been extensively used as electron transfer promotors in MFC due to their high reversibility. Originally, synthetic mediators were added to culture to palliate incapacity of bacteria such as *Escherichia coli* to directly transfer electrons [69]. Many artificial redox molecules were demonstrated to allow MET: neutral red, methyl viologen, methylene blue, AQDS, thionin [67,70–72] or immobilized mediators at electrode surface [73]. Due to their toxicity and cost, mediators are restricted to isolated experiments and are inefficient if scaling-up is proposed [74]. Moreover, in the early 2000s, Rabaey *et al.* demonstrated *Pseudomonas aeruginosa* ability to self-produced pyocyanin as mediators to operate MET without external addition of synthetic molecules [44,45,72,75]. Accumulation of mediators in batch condition was demonstrated to involve electron

transfer and bioelectricity generation [76]. On the contrary, changing medium to regenerate carbon source concentration dramatically decreases the monitored current. This observation allows to conclude on the mediator-driven characteristic of *Pseudomonas aeruginosa* or *Escherichia coli* while other bacteria such as *G. sulfurreducens* presents a membrane-driven characteristic [67]. For *S. oneidensis*, both membrane-driven (DET) and mediator-driven (MET, flavin [77–79]) behaviors have been demonstrated.

1.3.2.3. Direct Electron Transfer.

Initially, cells were considered as structure incapable to transfer electrons directly, without the assistance of redox mediators owing to their inherent non-conductive nature. Cell membranes are made off isolative materials such as polysaccharides. But the growth of certain bacteria at the surface of iron or manganese oxides suggested direct interaction between them. Multi-heme c-type cytochrome proteins were suggested as responsible for electron diffusion from the inside to the outside of bacteria through the cell wall [72]. By mutagenesis experiments on genes specific to c-type cytochromes, it was demonstrated that c-cytochromes (localized in the outer membrane, inner membrane and periplasm space) facilitate the interaction between bacteria and metal oxide during dissimilatory metal reduction forming an electron chain transfer (ETC) [80–82]

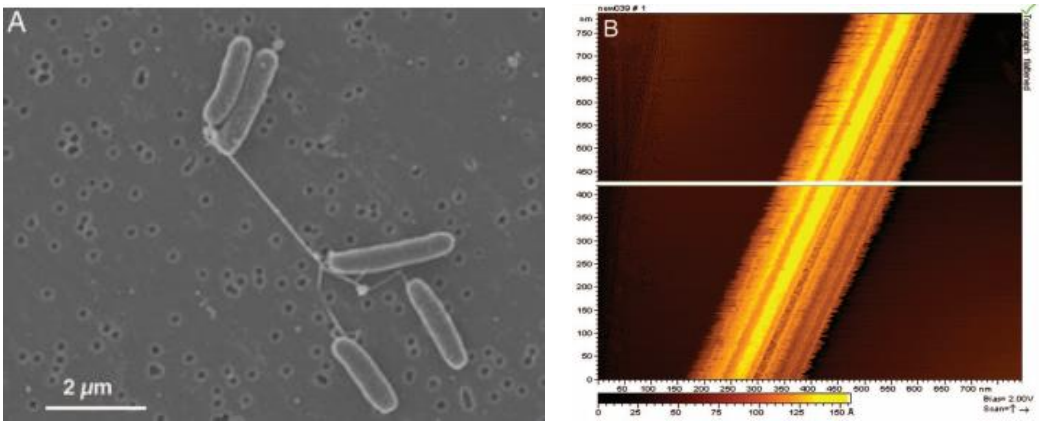

Figure 1.8 – Evidence of nanowires production by *S. oneidensis*: **(A)** Scaning electron microscopy of *S. oneidensis* showing pilus connection between two *S. oneidensis* bacteria. **(B)** STM analysis of a single nanowire demonstrating conductivity in white. *Gorby et al.* [83]

Considering that membrane-bounded c-cytochromes as open doors for electron transfer, only the first layer of bacteria at the electrode surface must be electroactive. In 2005, Gorby *et al.* observed connecting pili between *S. oneidensis* or *S. oneidensis* and a solid conductive surface. By scanning tunneling microscopy, they demonstrated the conductivity of these thick nanowires **(Figure 1.8)** [83]. Complementary to these results, in 2010 El-Naggar *et al.* confirmed previous results by growing *S. oneidensis* on SiO_2 wafer between gold deposited nano-electrodes. It appears that nanowires are conductive and electron transfer is observed at long range scale at a speed of 10^9 electrons.s^{-1} (AFM at 100 mV applied) **(Figure 1.9)** [84]. In 2006, Reguera et *al.* observed conductive pili production by *G. sulfurreducens* by atomic force microscopy.

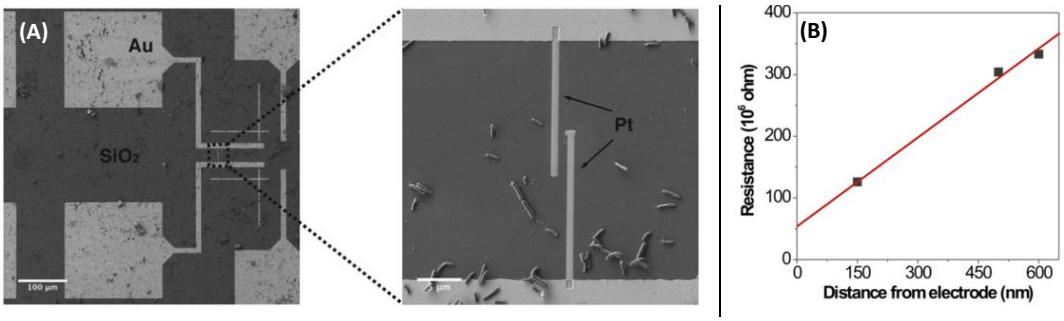

Figure 1.9 – (A) *S. oneidensis* on nano-fabricated Au/Pt contact. **(B)** Resistance along conductance appendant. El-Naggar *et al.* [84]

Two mechanisms are proposed for pili conductivity: (i) metal-like conductivity based on delocalization of electron through π-orbital amino acids conjugation. (ii) electron-hopping conductivity based on the hopping of electrons through c-cytochromes along the pilus. A mutation on the gene which encoded for mtrC and omcA c-Cyts (see section 1.3.3.1) of *S. oneidensis* leads to the formation of non-conductive appendage. This suggests that c-Cyt along pili are responsible for electrical conductivity (electron-hopping conductivity – **Figure 1.10.A**)[83]. For *G. sulfurreducens* controversy remains between electron-hopping hypothesis [85] and metal-like conductivity [86,87]. Other authors suggest a mix of both conductivity [88] **(Figure 1.10)**.

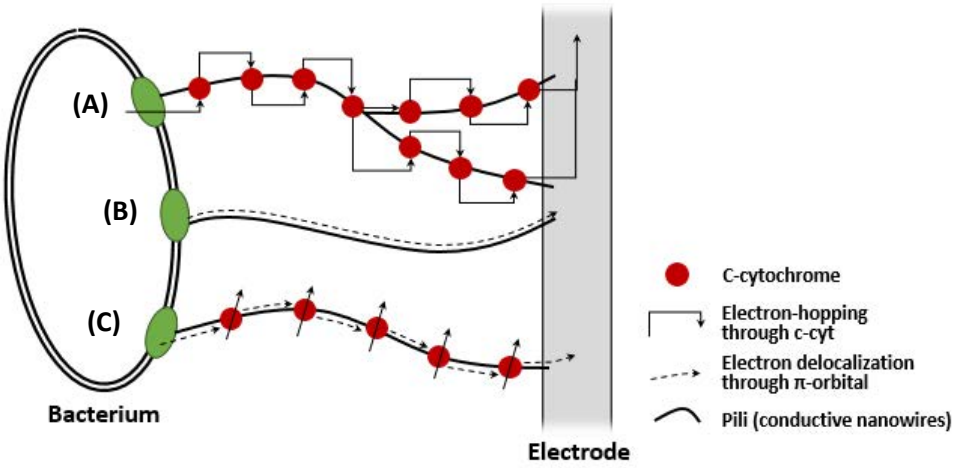

Figure 1.10 – Representation of proposed mechanisms for electron transfer between the membrane cell and the electrode through conductive nanowires/pili: **(A)** Electron-hopping through c-Cyt [83,85], **(B)** metal-like conductivity by electron delocalization along π-orbital of amino acid conjugation [86,87], **(C)** Bonanni hypothesis of mixed comportments [88]. Adapted from: Bonanni *et al.* [88] and Malvankar *et al.* [89]

1.3.3. Exoelectrogenic bacterium

A large diversity of electroactive bacteria exists and has been referenced for their ability to electron transfer and participates to bioelectricity generation in a MFC system. From the first bacteria that demonstrate self-mediated characteristic (*Shewanella putrefaciens IR-1*) to the recent extremophiles, *G. sulfurreducens*, *Pseudomonas aerudinosa*, *Geothrix propionicus*, … a large variety of bacteria was highlighted for their performances as biocatalysts [10,9,90]. Microbial fuel cells are based on promoted extracellular electron transfer by bacteria. Three reasons explain why bacteria transfer electrons [10]: (i) Bacterial respiration on metal oxides (*Geobacter*

and *Shewanella*). (ii) Electrons sharing between bacteria, Gorby *et al.* observed the formation of thick conductive appendages connecting *Pelotomaculum thermopropionicum* (fermentative bacteria) and *Methanothermobacter thermautotrophicus* (methanogen bacteria). Gorby hypothesized that bacteria form these conductive structures to support interspecies electron transfer [83]. (iii) Quorum sensing (i.e. inter-bacteria communication) was suggested to enhance electron transfer [91].

1.3.3.1. *Shewanella oneidensis*.

In 1988, Nealson *et al.* firstly isolated a gram-negative γ-proteobacteria from sediments of Lake Oneida in New York responsible of the high level of reduced manganese (Mn^{2+}) in water. This bacterium was geographically named *S. oneidensis MR-1* for Manganese-Reducing 1. *S. oneidensis* is a bacillus bacterium and an optional anaerobic bacterium which grows and survives in oxygenated medium **(Figure 1.11)**. This strain is classified in the class of Dissimilatory Metal Reducing Bacteria (DMRB) due to its ability to reduce manganese and few other heavy metals such as iron, uranium or lead [92]. This metal-reducing aptitude comes with its EET conductive network formed by c-cytochromes which present multiple heme in the inner membrane (CymA), the periplasm (MtrA) and outermembrane (MtrC, OmcA). By applying mutation on gene responsible of these c-Cyts, Myers proved their implication in MnO_2 reduction (mutants present a reduction-rate 45 to 75% slower than wild type) [82]. Riboflavin was suggested as soluble shuttles by Marsili *et al.* after experiencing high current drop when biofilm supernatant was removed [77].

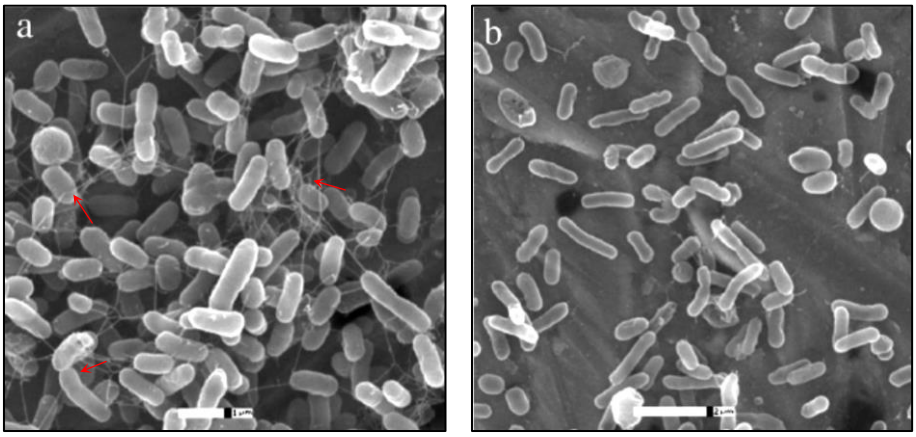

Figure 1.11 – Morphology of electroactive *S. oneidensis* strain on a palladium **(a)** and gold **(b)** substrates: with (a) or without (b) formation of conductive pili (red arrow)

1.3.3.2. Pure culture versus mixed culture.

System comparison is challenging due to the advantages and limitations of a large diversity of strategies employed to develop MFC: single or dual chamber, electrode material employed, separator nature. As an example, in 2008, Ishii *et al.* demonstrated +22% in power density for a mixed culture comparing to a pure culture *of G. sulfurreducen* (single chamber MFC, air cathode) [93]. In the same time, Nevin *et al.* emphasized comparable or higher power production for *G. sulfurreducens* rather than an enriched consortium of bacteria (dual chamber

MFC, ferrycianide cathode) [94]. In addition, Kim and Paraneswaran show that in enriched culture, some bacteria cannot grow by their own without co-cultured strains and support for fuel degradation [42,95].

Moreover, for power harvesting applications, pure cultures appear less efficient than mixed cultures extracted from real media (wastewater, sludge, sewage, …) or artificially composed of bacteria consortia. Single cultured *G. sulfurreducens* only degrades short organic molecules such as acetate [69]. A large diversity of substrates may be degraded by a consortium and this synergetic behavior allows extracting a higher quantity of energy from a complex medium. On the contrary, pure cultures are efficient to observe specific bacteria-electrode interactions or bio-energy production mechanisms and to understand how to optimize the overall MFC.

1.3.4. Biofilm

A biofilm consists in surface-associated pure or mixed bacteria embedded in a self-produced extracellular polymeric substance (EPS) [96] composed of DNA, proteins, polysaccharides and electron transfer facilitators (redox shuttles, …) [97–99]. Microbial species close to the electrode surface are engaged in an adhesive structure. Unlike isolated planktonic cells also named “floating cells” which mainly transfer electron by MET, bacteria forming biofilm may transfer electrons by MET and DET pathways [45,100]. They form community where micro-organisms communicate in a balance of cooperation and competition [101]. It is important to notice that all bacteria are not electroactive in both pure or mixed biofilms **(Figure 1.12)**. Certain bacteria are inactive (represented in brown) but secrete molecules which facilitate EET or break massive organic matters into more adapted fuels for exoelectrogenic bacteria **(Figure 1.12)** [10].

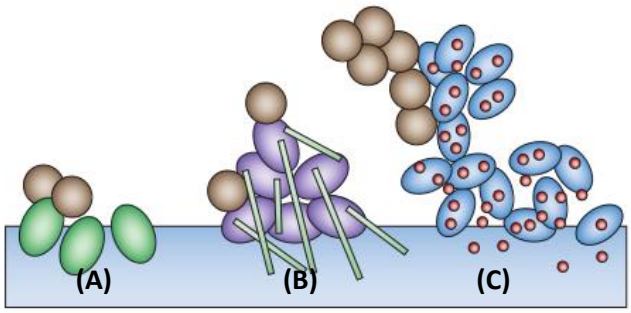

Figure 1.12 – Bacteria forming communities at the electrode surface engaged in: **(A)** membrane-bounded C-Cyt DET, **(B)** pili DET, **(C)** MET. Inactive bacteria are represented in brown, DET-engaged bacteria in green and purple, MET-engaged bacteria in blue (shuttles diffusing in red). Logan *et al.* [10]

A biofilm forms a complex architecture changing as a function of metabolic, physiological and ecological states. While biofilms enhanced electron transfer [102,103] due to potential conductive facilitators (c-Cyt, nanowires, shuttles), diffusion can be slowed down by the biofilm tortuosity and compactness. The loss of fuel diffusion deeply into the biofilm as well as acidification due to entrapped protons may cause the decline of biofilm activity and current generation [104,105]. Biofilm can exceed 50 to 80 µm thick, this structure presents cells engaged in electron transfer, cooperative cells forming a compatibilizing environment for exoelectrogenic

bacteria and competitive cells [106]. Moreover, dynamic nature of biofilm causes its formation, degradation and regeneration engaging MFC performances.

1.4. MICROBIAL FUEL CELLS EFFICIENCY: KEY FACTORS

Efficiency of microbial fuel cells depends on many parameters to optimize cell voltage, current and power density. In comparison with standard fuel cells or enzymatic fuel cells, microbial fuel cells performance depends on the metabolic activity of a micro-organism which adds more complexity to perform MFC optimization. Relevant factors that affect MFC efficiency are related to the global cell conception and architecture, the electronic transfer at bacteria-electrode interface and the inherent metabolic activity of the bacterium **(Figure 1.13)** [107].

The performance of a microbial fuel cell is described by polarization and power curves (potential and power in function of current) commonly used for classic fuel cells [108]. A polarization curve can be divided in three main domains of low (zone A), intermediate (zone B) and high (zone C) relative density of current **(Figure 1.14)**. As an initial approach, each domain is specifically affected by the factors stated above.

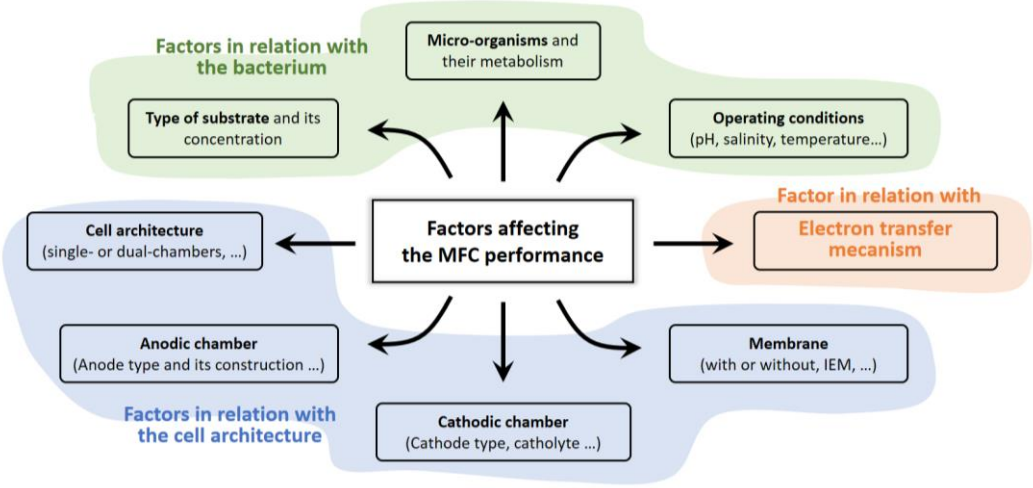

Figure 1.13 – Factors affecting the performance of the MFC. *Adapted from: Aghababaie et al.* [109]

(A) At low current, the system is theoretically governed by Nernst and Buttler-Volmer equations. At the open circuit current (i=0), the OCP is defined by the redox potential of the species responsible for the electronic transfer. Therefore, the bacterium nature, its metabolic activity and pathways efficiency to transfer electrons are determinant. Activation losses are predominant and occur during the electron transfer from the bacterium to the electrode by the intermediate of a mediator (if needed). These losses may be minimized by improving the electrode surface (high surface area, roughness, catalyst) and by the formation of an adapted, conductive biofilm. For low current, an over-potential results from activation losses which affects the anode potential: $E_a = E_{eq} - \eta_a$.

(B) At intermediate current, the internal resistance becomes damageable resulting in predominant ohmic losses. Therefore, the cell voltage linearly decreases following the ohmic low: $E = E^{i=0} - R_{int} i$. The internal resistance (R_{int}) includes ohmic losses due

to (i) electron flow through the electrode, interconnection and external circuit; (ii) ions flow through both anodic and cathodic electrolyte (ionic strength) and the ion exchange membrane (if present). An effective mean to decrease ohmic losses is to control the MFC architecture by using highly conductive electrodes materials, low resistive membranes or a membrane-less reactor, by increasing ionic strength of the electrolytes (in function of the bacterium tolerance) and by ensuring that all contacts are not limiting electron flow.

(C) At higher current concentration losses are mainly due to a low rate of mass transport. The fuel is limited by diffusion gradients which lead to a lack of nutrients and mediators through the as-formed biofilm and an accumulation of protons in the biofilm and the anolyte. The lack of diffusion of proton and species to reduce (O_2) leads to a decrease of the number of exchanged electrons in the system and high degradation at the limiting current of the cell.

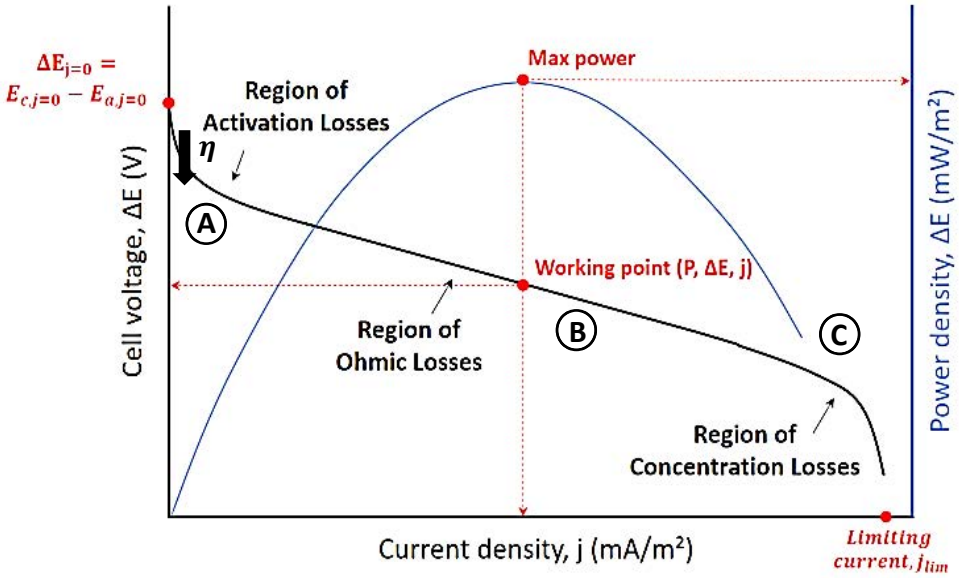

Figure 1.14 – Polarization and power curves: the working point is defined as the cell voltage and the current density for the maximum power density provided by a fuel cell.

1.4.1. Factors related to the bacterium

To elaborate a microbial fuel cell, the choice of the bacterium is important. Two main factors have to be considered: its ability to generate bioelectricity and its electron transfer pathways. Numerous strains are reported and classified including consideration of electron transfer pathways. As examples, *Saccharomyces cerevisae*, *Escherichia coli*, *Actinobacillus succinogenes*, *Proteus mirabilis* and *Vulgaris* or *Pseudomonas fluorescence* are not able to transfer electrons by DET (cytochrome, pili) and require a mediator. On the contrary, *Rhodoferax Ferrireducens*, the families of *Shewanella*, *Geobacteraceae* and *Geobacter* work without addition of mediator and transfer electron by DET and/or MET (self-production of shuttles). As previously described, it appears that real or mounted consortia of bacteria produce more energy rather pure culture. This observation is explained by a complex synergetic effect: in a consortium, a chain reaction of degradation (a bacterium degrades a nutrient and produces a

suitable product for the metabolism of another bacterium, etc.) is established [110]. This process maximizes the energy recovered for a quantity of fuel [10,109].

The choice of the fuel is determinant. A large diversity of pure nutrients (glucose, lactate, acetate, butyrate, …) as well as real or formulate fuels (organic, chemical, industrial wastewaters, …) were tested in MFC based on specific strains or consortia [109]. The fuel choice is complex and has to be done in relation with the selected bacterium or consortium of bacteria. For example, the energy recovered by dissimilatory iron-reducing bacteria from acetate (non-fermentable electron donor) is 66% higher than butyrate [111]. Also, Lee *et al.* indicates a low conversion of glucose by *G. sulfurreducens* (3%) in comparison with the higher conversion rate of acetate by the same strain (42%) [112]. More recently, Speers and Reguera confirmed that lactate-fed *G. sulfurreducens* produce less power than acetate-fed bacteria. Speers and Lee demonstrated that a bacterium metabolism accepts various nutrients, but as function of the encoded enzymes, an electron donor is more suitable than another one. For example, *G. sulfurreducens* encodes for glycolate oxidase which poorly degrades lactate while *S. oneidensis* encodes for lactate dehydrogenase which efficiently converts lactate [113]. For consortia, real fuels are preferable due to their complex composition presenting a large diversity of nutrients as well as bacteria strains. Moreover, nutrient concentration affects power production. Jiang showed that increasing nutrient concentration from 100 to 850 $mg.L^{-1}$ rises power output from 0.2 to 1.2 $W.m^{-3}$ (single-chamber MFC, air-cathode, inoculum: wastewater) [114].

1.4.2. Factors related to the cell architecture

Most of the ohmic losses are related to the cell architecture. As described in part 1.4, electrodes materials have to be highly conductive, porous, to present a large surface area and to facilitate both bio-reaction at the anode (adhesion of bacteria, no toxicity, …) and the reduction at the cathode (combustive choice, catholyte, catalysts, …). Space between the electrodes must be optimized as well as their dimension, to limit internal resistance due to diffusion rate and reaction rate. Wang and Zuo demonstrated an increasing of cathode performance as well as specific surface area or geometric surface area, respectively [115,116]. The separator intensively participates to the cell internal resistance. Several tests were done to determine its effect; they showed higher power and current density in absence of membrane. However, the membrane acts as a separator and prevents both chambers to be poisoned. Global cell architecture and the mode of cycling (batch or continuous-fed modes) may influence ohmic losses, mass transport rate and therefore the fuel cell performance.

1.4.3. Factors related to the electronic transfer

The electrons produce by a bacterium are transferred by two mains pathways: DET or MET (cf. 1.3.3). For DET transfer, the bacterium must be in contact with the electrode or close to the electrode to produce a conductive appendage from its membrane to a conductive surface. High surface area is necessary to promote bacteria adhesion in direct contact. For MET, a mediator is mandatory. This mediator is synthetized by the cell or added to the medium. In both cases, shuttles have to meet few requirements: (i) oxidized and reduced forms should easily diffuse through the bacterial membrane, (ii) the redox potential of the mediator should match

the electron transfer potential (electron transfer chain). Both redox states of the shuttle (iii) must not interfere with metabolic activity of the bacterium, (iv) must be chemically stable and soluble (no precipitation inside or outside of the cell). (v) Electrochemical kinetics of oxidation and reduction for the mediator should be fast [21].

1.5. MICROBIAL FUEL CELLS MATERIALS & ARCHITECTURE

In term of materials and cell designing, three major points must be taken in account to elaborate a MFC: (i) the anode and cathode materials, (ii) the separator between each compartment and (iii) the global architecture of the MFC. Intensive survey concerning materials and cell engineering leads to a great diversity of systems.

1.5.1. Anode materials

To be selected as an effective electrode (anode and cathode), materials must be chosen considering a balance of required properties. High (i) conductivity, (ii) specific surface area, (iii) porosity, (iv) low sensibility to corrosion and bio-corrosion, (v) non-clogging or fouling by bacteria, EPS (exopolysaccharides) and resultant reduced metals are mandatory as inherent properties for MFC stability and efficiency. To ensure bacteria viability and colonization, electrode must be (vi) cytocompatible and non-toxic (for colonized electrodes). To be easily scalable at larger sized, electrodes have to be (vii) inexpensive, widely available and easy to made.

1.5.1.1. Carbon-based materials.

Carbon rods and carbon sheets (flat graphite) are widely used as *anodic electrodes* in MFC due to their high conductivity, biocompatibility, non-toxicity, chemical stability and low sensibility to corrosion. There are accessible, easy to use and cheap [50,117–119]. To enhance bacterial adhesion, rods are gently abraded to improve their roughness. Main drawbacks of carbon rods and sheets are due to their low specific surface area and low porosity. However, if compactness is not mandatory, inexpensive and mechanically resilient carbon rods and sheets remain materials of choice. Also, carbon rods are commonly considered as model materials [120].

To palliate these issues, more technical 2D and 3D commercial carbon architectures **(Figure 1.15)** were used leading to a large diversity of systems [121,122]:

- **(i) Carbon papers** (Torray™ paper) [122–124] are made by precipitating thin layers of carbon powder (or wide fibers) supplemented or not with a binder on PTFE substrate. They are porous, rigid, easy to connect but brittle and highly expensive (around 1000 dollars/m²).
- **(ii) Carbon cloth, tissue, mesh** [125] consist in wide woven carbon fibers (micrometric, ca. 10 µm). They are flexible, robust and present a higher specific surface area and porosity than carbon papers but are as expensive.
- **(iii) Carbon fiber veils** [126] are thick and continuous randomly looped carbon fibers.

(iv) Graphite granules [127–130] consist in micrometric pieces of conductive carbon (activated or not). In a MFC, graphite granules are compacted to ensure electrical contact between individual granules.

(v) Graphite fibers brush [131]. This electrode is made of wide carbon fibers radially assemble around a titanium stem (collector). This brush presents a high specific surface area but they are easy to clog and quite uneasy to entirely colonize.

(vi) Carbon and graphite felt [118,127,132,133] consists in a 3D organization of randomly align fibers (ca. 12 µm in diameter). This smooth structure is largely open resulting in a high porosity and specific surface area (ca. 0.2 $m^2.g^{-1}$).

Chaudhuri *et al.* compare carbon rods and felts in a two-chambers MFC using *Rhodoferax Ferrireducen* as anodic micro-organism revealing current three time higher for felts compared with rods. This current increase appears related to the higher specific surface area (x3) and bacteria quantity at the surface (x2.7) [118].

(vii) Carbon foams (Reticulated Vitreous Carbon, RVC) [121] present similar porosity to carbon felts. However, its structure made of rigid interconnected carbon walls (sponge structure) is less resistant than carbon felts and more expensive.

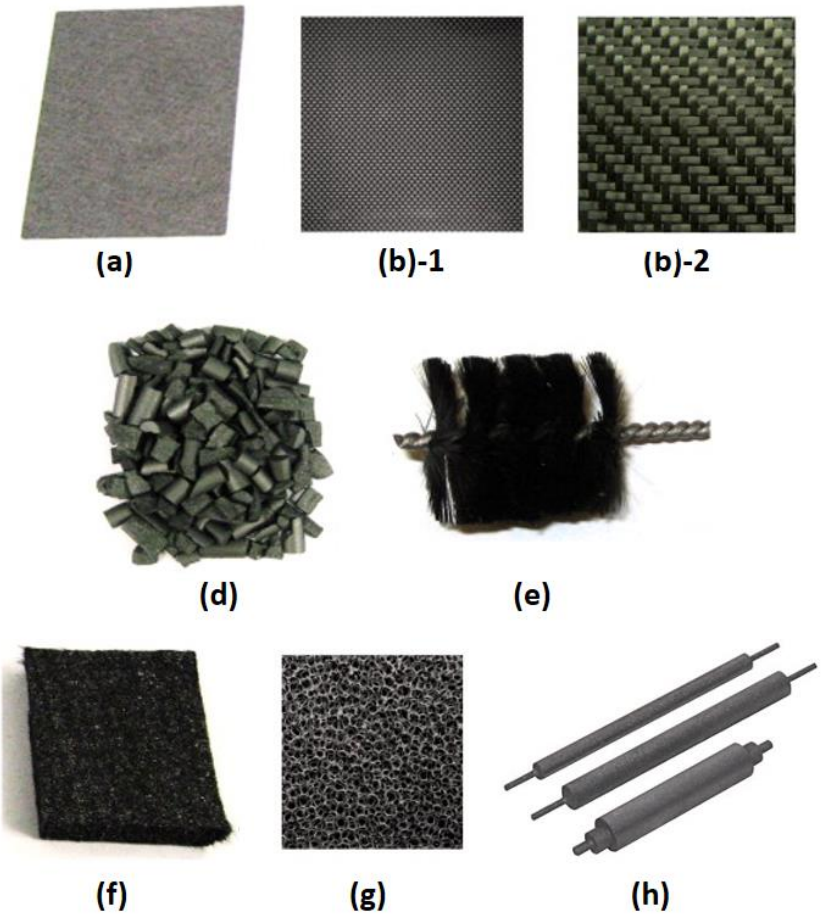

Figure 1.15 – Photograph of various carbon-based electrode materials for MFC: **(a)** carbon paper (type Torray™), **(b)-1** carbon cloth, **(b)-2** carbon mesh, **(d)** carbon granules, **(e)** carbon fibers brush, **(f)** carbon felt, **(g)** carbon foam RVC, **(h)** carbon rods

The comparison between the MFC performances as function of the anodic material is complex due to three parameters: (i) A large diversity of carbon-based materials are available. (ii) Generally, the use of a carbon-based material implies specific surface treatment; in consequence, performances are not solely related to materials. (iii) Anodic and cathodic materials are not only mounted in MFC, the performances are also related to the process, the MFC assembly and the cell architecture. These parameters vary from one experiment to another. Moreover, the normalization of the results differs in the various publications (normalization by the mass, the volume, the specific or the geometric surface area of the anode or the cathode).

However, carbon-based materials described above can be divided in five categories: (i) Carbon plates and carbon rods are generally dedicated to theoretical investigation due to their high simplicity. They deliver the lowest density of power as a consequence of their inherent simplicity, low roughness and active surface. Recently, ITO and FTO (Indium or Fluorine doped Tin Oxide) were used as conductive glass for application implying photo-sensitive micro-organisms or to combine optical and confocal microscopy with electrochemistry [134]. (ii) 2D carbon papers have been widely used since nowadays even if highly expensive. Without surface treatments, power density in a range of 20 to 250 $mW.m^{-2}$ are reported. (iii) 2D fibers materials (carbon cloth, tissue, mesh, fiber veils) offer high specific surface and are integrated in reactors which present impressive performances (> 250 $mW.m^{-2}$). Due to their availability, less expensive price and facility to use, they were continuously used. (iv) Based on the advantages of the previous 2D materials, technical 3D carbon-based materials, such as carbon felts or carbon fibers brush, are currently intensively used as anode materials. Most of the actual advances in MFC and more generally MES involve these materials. As function of the surface treatments and the conditions of use, power densities from 50 up to 1000 $mW.m^{-2}$ are reported. Both carbon felts and fiber brushes are widely available, easy to use and can be supply for a reasonable cost. (v) Finally, graphite granules are another type of anodic material. Carbon granules present the advantage to fill a large anodic volume with an impressive compactness without impeding anolyte circulation.

To summarize, the anodic material must be chosen as function of the experimental aim (theoretical, empirical studies or power delivery), cost/availability balance and the considered surface treatment. Currently, technical materials such as carbon felt or carbon fiber brush demonstrated promising performances. Home-made materials such as polymer matrix covered with carbon suspension or bucky papers are another promising option.

1.5.1.2. Surface Treatment on Carbon based materials.

To enhance anode electrode efficiency in term of bacteria adhesion, biofilm formation, electron transfer and collection, carbon-based surface may be treated. Based on the work of Wang *et al.* [135], Feng *et al.* shown that a carbon fiber brush heated and acid treated generates higher power rather than raw fiber brush (+34%) **(Figure 1.16.b)** [136]. In 2006, Cheng and Logan proposed an ammonia treatment of carbon cloth to enhance MFC performance consisting in a heat treatment of 1h at 700°C under gas feeding (5% NH_3 in a helium gas vector). They

demonstrated that the acclimation time (before current production begin) decreases by 60%, the maximum power increases by 48% and coulombic efficiency rises 60% from the initial 30% without ammonia treatment **(Figure 1.16.a)** [131,137,138]. Considering this results, Cheng and Wang have demonstrated that chemical surface modifications by charged groups ($-COO^-$) favor bacteria adhesion and enhance MFC performance.

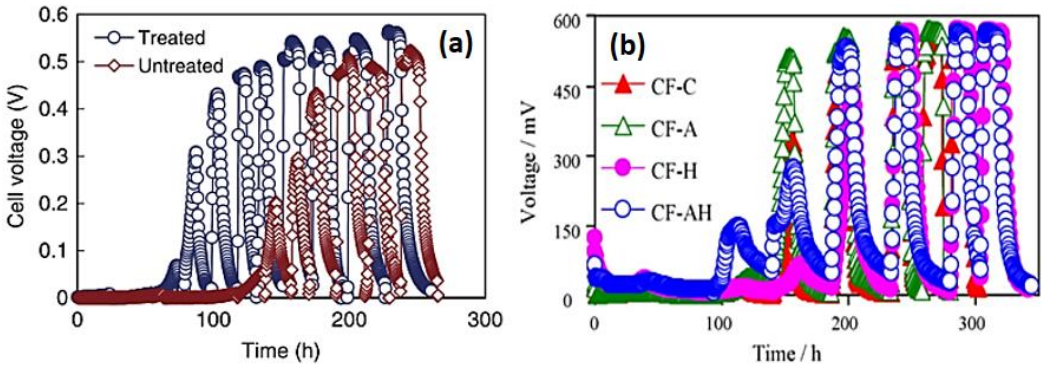

Figure 1.16 – Acclimation time (lag time) amelioration and cell voltage for a waste water MFC demonstrated by **(a)** Cheng and Logan [red: untreated, blue: ammonia treated fiber brush] [137] and **(b)** Feng *et al.* [acid- (CF-A), heat- (CF-H), and acid- and heat-treated (CF-AH) anodes] [136]

Also, surface modification can be achieved by the immobilization of conductive carbon nanotubes, graphene suspensions, manganese/iron oxide, neutral red [71] or AQDS (anthraquinone-1,6-disulfonic acid, a quinone generally used as a pigment for metabolic assay, electrochemical mediator) [139] at the surface. It increases both specific surface area and roughness; moreover, it may charge the surface. In 2010, Peng *et al.* demonstrated the effect of adsorbed carbon nanotubes on glassy carbon on current production by *S. oneidensis* suspension in turn-over condition [140]. Also, an increase of 20% in power production was demonstrated when carbon nanotubes are embedded in polymer (Layer-By-Layer method) on Torray™ carbon paper **(Figure 1.17)** [141].

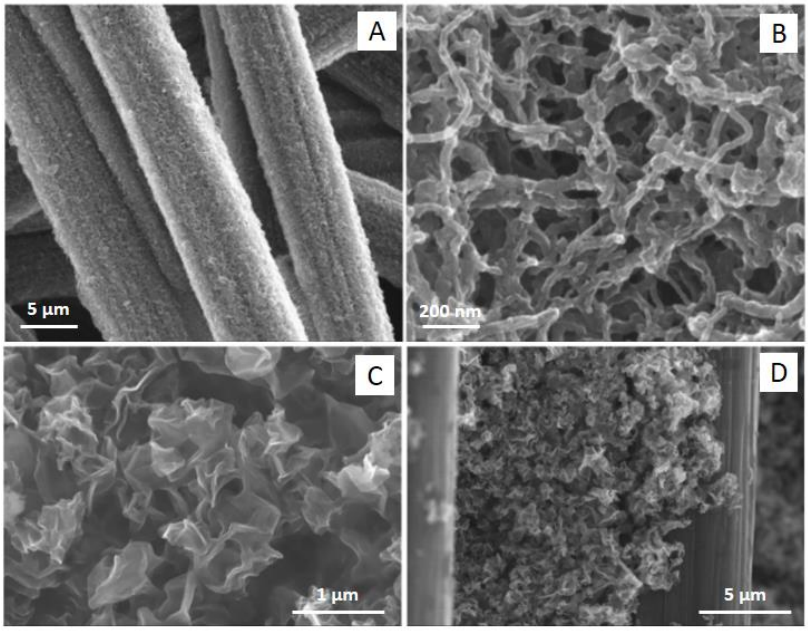

Figure 1.17 – SEM observation of carbon paper covered by **(A-B)** carbon nanotubes [141] or **(C-D)** reduce graphene oxide [142]

It appears that reduced graphene oxide (r-GO) sheets and particles induce significant increase of power production in MFC [142]. In 2003, Schröder *et al.* proposed a protocol to deposit a layer of polyaniline (PANI) by electrodeposition on platinized based carbon electrodes. This treatment increased their current densities from 0.29 mA.cm^{-2} for a deposition of polyaniline to 1.45 mA.cm^{-2} for the final electrode. It is worth noting that these currents were obtained with fermentative *Escherichia coli* bacteria [143]. In 2007, Qiao *et al.* prepared PANI/CNT nanocomposites paste on nickel foams. Evaluation of performance for *Escherichia coli* culture with glucose as carbon source indicated again a current rise from 20 to 100 µA.cm^{-2} for 20 wt.% CNT addition to PANI **(Figure 1.18)**. Performance obtained by Qiao was 18 times higher than the ones referenced in the literature for similar systems since 2007. Similar studies were performed since nowadays using various conductive polymers with or without carbon inclusions such as CNT [121,144–146] or graphene. This strategy needs further efforts to be considered as a viable surface treatment for system scaled up with large volume of electrode. Performances remain quite stable but paste formulation includes highly expensive components. Conductive polymers are unfriendly, complex to synthetize with sufficiently large molecular weight (polymeric length) in adequate quantity. Moreover, the carbon suspensions used (CNT and graphene) are expensive and difficult to implement without damageable perturbation (homogeneous dispersion, stability).

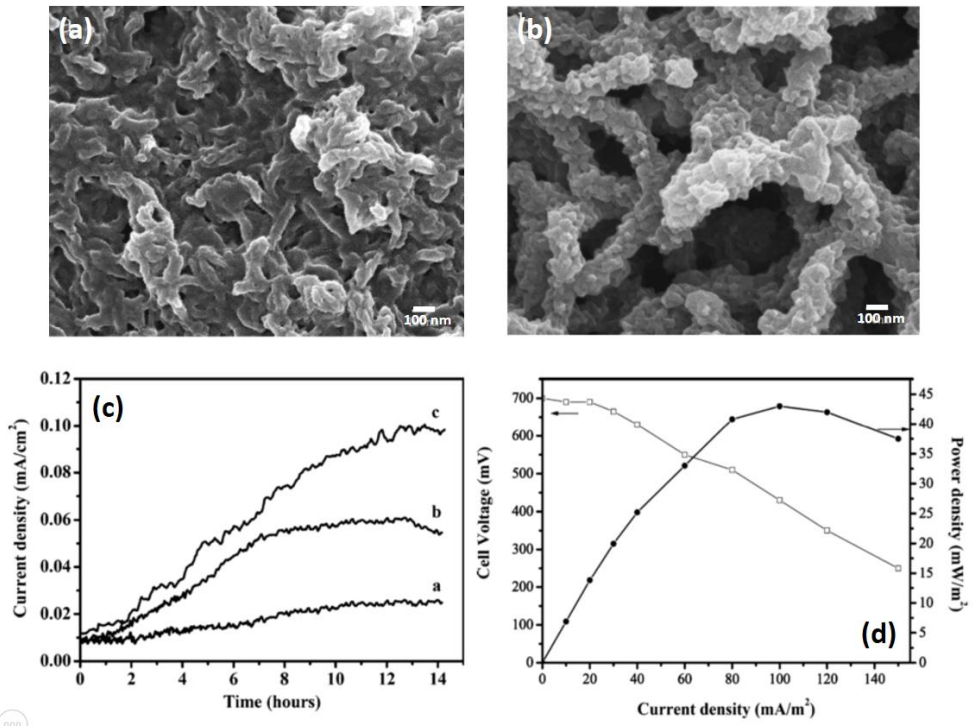

Figure 1.18 – Nickel foams covered by PANI or PANI/CNT nanocomposite layer. SEM images of **(a)** PANI and **(b)** PANI/CNT composite, **(c)** current monitoring in presence of glucose at 0.1V, **(d)** polarization curve. *Qiao et al* [147].

In 2011, Xie *et al.* developed another approach in which non-conductive and well-controlled geometries were covered with CNT by immerging the supports in a concentrated CNT dispersion. As a first step, Xie used a polyester foam coated with a 200 nm thin layer of CNT. The smooth, highly porous and conductive structure might be compared with carbon felts and

presented a performance 2.5 times higher than carbon tissues [148]. In 2012, Xie improved its concept and performance by using a polyurethane sponge structure and graphene [149].

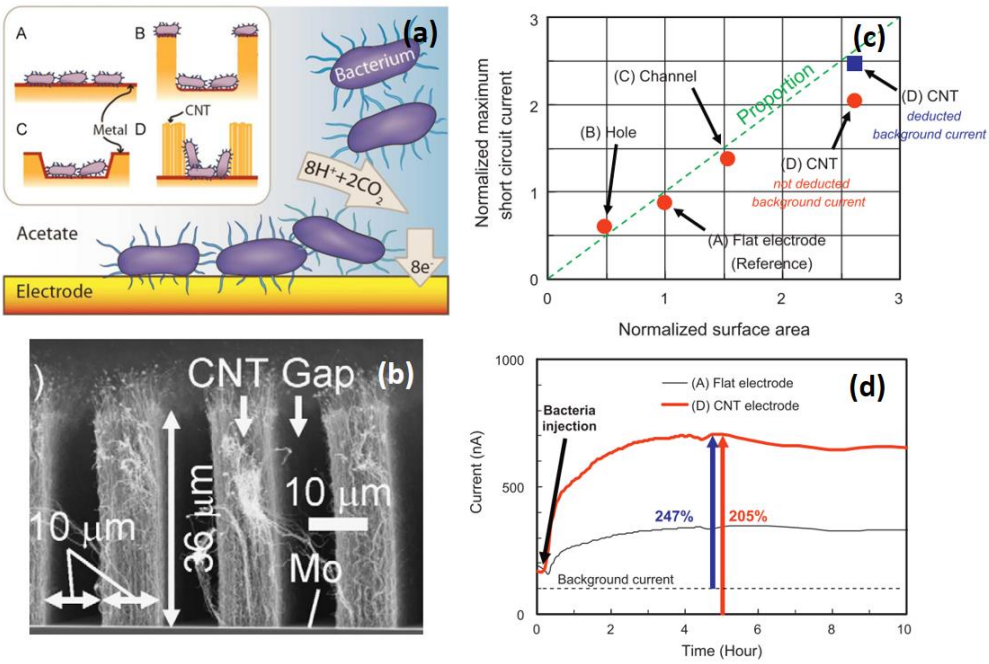

Figure 1.19. Relation between Surface area (roughness) and current production (bacterial activity). **(a)** Schematic representation of bacteria on a (A) flat electrode or on an electrode presenting (B) hole, (C) channel, (D) vertically aligned CNT. **(b)** SEM of vertically aligned CNT. **(c)** Linear relation between current and surface area. **(d)** Current increase between flat and vertically aligned CNT. *Shogo et al.* [150].

Advances in surface modification, increasing roughness and surface architecture at cells scale, lead to a general increase of MFC performance. Shogo *et al.* evaluated surface geometry effect on current production suggesting a higher bacteria adhesion and bacteria quantity in direct contact, close to the surface. Shogo found a linear relationship between surface area and current production **(Figure 1.19)** [150].

1.5.1.3. Metallic and metal coated materials.

Metals are compatible with MFC if they meet basic requirements such as a low sensibility to corrosion and cyto-compatibility. Therefore, iron or copper are not suitable for aqueous MFC applications. On the contrary, precious metals (platinum, gold [151,152]) or chemically stable metals in MFC cycling condition (titanium [119], stainless steel [153]) may be adapted as anode electrode. In 2008, Dumas *et al.* indicated lower efficiency of stainless steel plate electrodes compared to graphite electrodes in MFC (*G. sulfurreducens*) due to lower average surface roughness and non-optimized biofilm/electrode interface [154]. By replacing stainless steel plate by a stainless steel micro-structured grid, Pocaznoi dramatically increase MFC performance reaching equivalent or higher performance rather than carbon cloth, demonstrating the interest of using stainless steel-based electrodes [153]. Combination of stainless steel and reduced graphene oxide seems to demonstrate long time stability (min. 40 days) of biofilm/electrode interface with higher current density [155]. Park and Zeikus explored metal and molecular coating on carbon-based materials. Mediators such as neutral red

(electron mediator, generally use as indicator of cell viability) and Mn^{4+} were linked on carbon electrode and characterized as MFC anode using *S. putrefaciens* (model bacterium). In both case electricity productions indicated a significant increase of fuel conversion in comparison with non-treated electrodes [156,157]. In this case, reduced MnO_2 acts as a solid intermediate (mediators) in the electron transfer chain.

1.5.2. Cathode materials.

To perform efficient microbial fuel cells, relevant cathodes are mandatory. Cathode reduction was described as a limiting factor for MFC productivity [158]. Several reactions may be selected as cathodic reduction. For laboratory experiments, ferricyanide [45,102,157], iron, permanganate [159,160], copper, … cathodic solutions are relevant due to their well-known behaviors, high redox potential and simplicity. Cost, toxicity and low viability of these redox couples are disadvantages for scale-up MFC and working in real environment.

Most of the time, oxygen reduction is selected for microbial fuel cell applications. Even if the reaction rate is lower than potassium ferricyanide or permanganate reduction and the oxygen solubility in water is low, oxygen reduction presents the advantage of a high redox potential (> +0.8 mV vs. SHE). In 2006, Cheng *et al.* applied a paste made of a commercial 10 wt.% Pt/C powder and a binder (5% Nafion or 2% PTFE) on a commercial carbon cloth [161]. Chronoamperommetric measurements indicate no significant effect in decreasing platinum loading from 2 to 0.1 $mg.cm^{-2}$. If PTFE-binder was replaced by Nafion, for a known Pt-loading (0.5 $mg.cm^{-2}$) the cathode potential became more positive (+12%) and the power in MFC-mode increases by 34%. Besides, MFC power decreases with Pt-loading. In previous research, various air-cathodes were proposed and tested: platinum coating (0.25 to 0.5 $mg.cm^{-2}$) on graphite electrode [162,163], with or without proton exchange membrane [164]. More recently, fuel cell electrospun air-cathodes were developed and showed significant performances at low Pt-loading (0.05 to 0.1 $mg.cm^{-2}$) in comparison with commercial electrodes developed by Nissan [165,166].

Regarding platinum cost and availability, decreasing noble-metal loading is crucial for MFC sustainability. Non-precious metals catalysts were proposed by Zhao *et al.* in 2005: an iron phtalocyanine (iron-based catalyst, FePc) and a cobalt tetramethoxyphenylporphyrin (cobalt-based catalyst, CoTMPP). Both catalysts were pasted on graphite foils and evaluated as cathode in MFC-mode (Pt-carbon as anode). CoTMPP performance was slightly better than FePc, but they presented performance similar to commercial platinum-coated cathode, demonstrated the possibility to substitute platinum for cheaper (yet more complex) materials [167].

Another way to replace platinum by cheapest materials is to apply the MFC strategy to the cathode using micro-organisms as catalysts for the cathodic-reduction [168]. In 2005, Bergel *et al.* build a model MFC composed of two compartments separated by a proton exchange membrane (Nafion), an abiotic platinum anode and a stainless steel cathode covered by a seawater biofilm. Platinum is chosen as model anodic material to ensure no limitation due to a deficiency in electron transfer. MFC works under continuous circulation of modified seawater

media in both anodic and cathodic compartments. MFC performances were firstly measured with the stainless steel cathode covered with a seawater biofilm in presence of an electrolyte composed of seawater supplemented in air. Maximum power of 0.3 $W.m^{-2}$ was observed. Then the biofilm was removed from the stainless steel, and the MFC was characterized in the same condition. By removing the seawater biofilm, Bergel *et al.* observed a loss in power density of 95% (0.015 $W.m^{-2}$). To resume, Bergel *et al.* observed a higher power production in presence of a seawater biofilm compared to a cathode without biofilm attached at the surface. They explained this difference by the catalytic effect of the biofilm for oxygen reduction reaction and demonstrated promising application of bacterial cathode to replace expensive platinum catalyst [169]. Aldrovandi *et al.* confirmed this result with a membrane-less MFC for wastewater. They demonstrated that power production limitation was due to the lack in diffusion and not in the catalytic activity [170].

In parallel, to perform valuable free platinum MFC, Clauwaert *et al.* proposed to couple MFC power generation and denitrification at the cathode. The denitrification is a biochemical process which takes place in environment presenting low concentration of oxygen. Denitrifying bacteria participate in the nitrogen cycle by the deoxygenation (bio-reduction) of nitrate ions (NO_3^-) in nitrite ions ($NO_3^- + 2H^+ + 2e^- = NO_2^- + H_2O$), then in NO, N_2O and at the end in N_2. Carbon granules were chosen as electrodes. Effluent from a previous MFC and a mix of aerobic and anaerobic sludges were respectively used as anolyte and catholyte, in which potassium nitrate was added to the catholyte at various concentrations. Clauwaert demonstrated efficient denitrification and performance (density of power and current) proportional to the quantity of nitrate available [171]. Moreover, this experience proved that coupling bioelectricity production with another valuable application such as denitrification is viable.

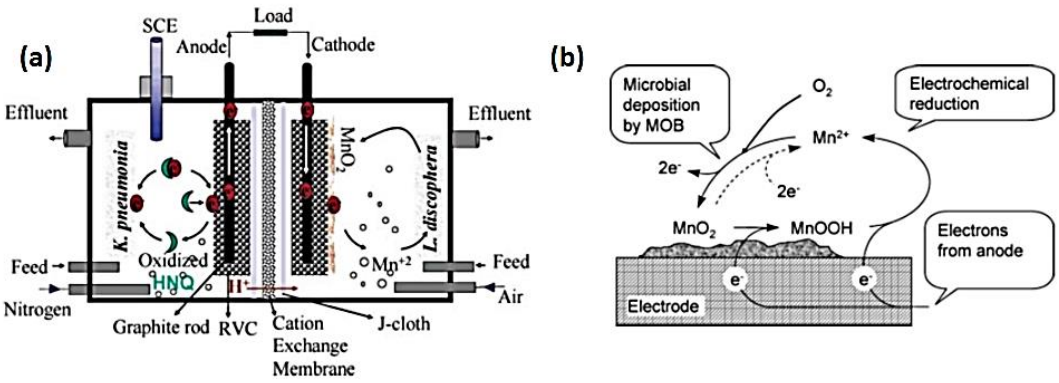

Figure 1.20 – Glucose/MnO2 full-MFC [172]. **(a)** Scheme of the MFC, glucose is microbially oxidized at the anode (mediator: 2-hydroxy-1,4- naphthoquinone) and **(b)** manganese oxide microbially mineralized is reduced at the cathode without mediator.

Emergence of adapted micro-organisms to cathodic reactions led to the development of mediator-assisted biocathodes. In 2005, based on previous works of Lewandowski group, Rhoads *et al.* used the ability of *Leptothrix discophora* to biomineralize manganese ions as manganese oxide [172]. They worked with a PEM-MFC and reticulated vitreous carbon foams electrodes. *K. pneumonia* ensure glucose oxidation and deliver electrons to the systems. At the cathodic side, *L. discophora* biomineralized manganese oxide (MnO_2) from Mn(II) dissolved in

the cathodic medium at the electrode surface. Resulting MnO_2 is consecutively reduced in manganese oxide hydroxide (manganite, MnOOH) and Mn(II) by the electron from the bioanodic oxidation of glucose **(Figure 1.20)**. Equivalent studies has been performed with a ferric/ferrous iron couple [173]. A mix of iron- and manganese-oxide [174] defined as mediators was deposited on cathode surface. This mediator ensures the electron transfer to bacteria responsible of oxygen reduction (final electron acceptors).

Another recently explored option is to replace cathodic bacteria by specific algae (photosynthetic cathode, CO_2 valorization [158]), yeasts or enzymes [39] (enzyme-substrate specificity, membrane-less MFC/MEC).

1.5.3. Separator: proton exchange membrane

In hydrogen fuel cell, the membrane is necessary to avoid hydrogen and oxygen (gas) to merge and promote channel for protons diffusion from the anode to the cathode (H^+-pump). In microbial fuel cells, these problematics are less damageable: (i) no incompatible gas are used in MFC, (ii) protons are available in the entire fuel cell and electrodes ensure their directional flow. MFC may function without membrane, but for dual chambers MFC, the membrane allows separating each electrolyte and avoiding undesirable substrates to diffuse and poisoned the opposite electrode. Moreover, the membrane serves as barrier to keep the bacteria in the appropriate compartment and limits oxygen diffusion in the anodic compartment. The main disadvantage of the membrane is the increasing of the MFC internal resistance due to (i) solution conductance and (ii) protons diffusion loss.

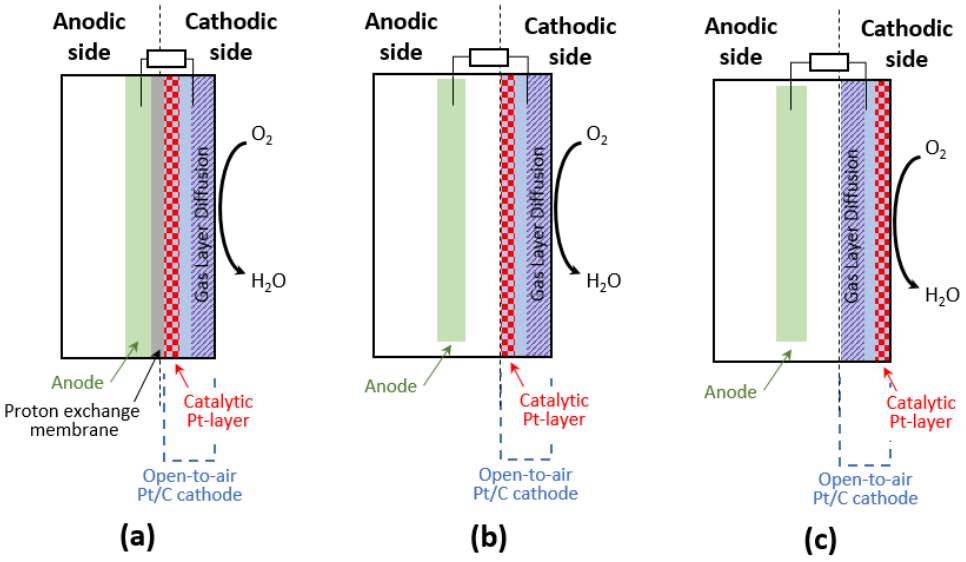

Figure 1.21 – Schematic representation of the catalytic Pt-layer positioning (vs. anodic side) in **(a)** a conventional fuel cell or a dual-compartments MFC with a separator or **(b, c)** in a membrane-less MFC (without separator). **(b)** Pt-loading facing the anolyte, **(c)** Pt-loading facing the air.

Gil *et al.* described ideal working conditions for MFC and concluded that compartmentless MFC complemented with a *highly efficient* air cathode (oxygen scavenger) is preferable to maximize MFC performance [175]. Moreover, Rozendal *et al.* indicate that catholyte

pH increases with time due to competitive cations diffusion (Na^+, K^+, … vs. H^+) and the formation of basic species. Even if anolyte pH remains stable (buffered medium), pH modification in the cathodic side leads to power degradation [176]. Moreover, other studies indicate possible decrease of the anolyte pH causing biological activity degradation or biocatalyst deactivation. Finally, decreasing the internal resistance by hot-pressing Nafion® directly onto carbon cloth cathode was proposed and demonstrated as beneficial for MFC performances by Liu's group and others [121,177]. Yan *et al.* proposed a membrane-less architecture with impressive performance if the Pt-loading of the cathode faces the anolyte [164,176]. In presence of a separator, facing the Pt-loading in the direction of the anolyte directly on the membrane seems logical (refer to **Figure 1.21** for a schematic representation). In absence of the membrane, the question of bio-poisoning of the platinum is important due to the possible deactivation of the platinum catalyst if polluted by bacteria or biofilm. Based on these considerations, Yan *et al.* demonstrated that facing the anolyte with the Pt-loading is preferable (than facing with the GDL) even if bacteria can colonize the surface of the loading. Also, it was suggested that long term biofilm formation on the cathode prevents oxygen to diffuse in the anodic compartment [176]. Recent results published by Kim *et al.* demonstrated that the way the membrane is integrated in the MFC has more impact than the nature of the membrane [178].

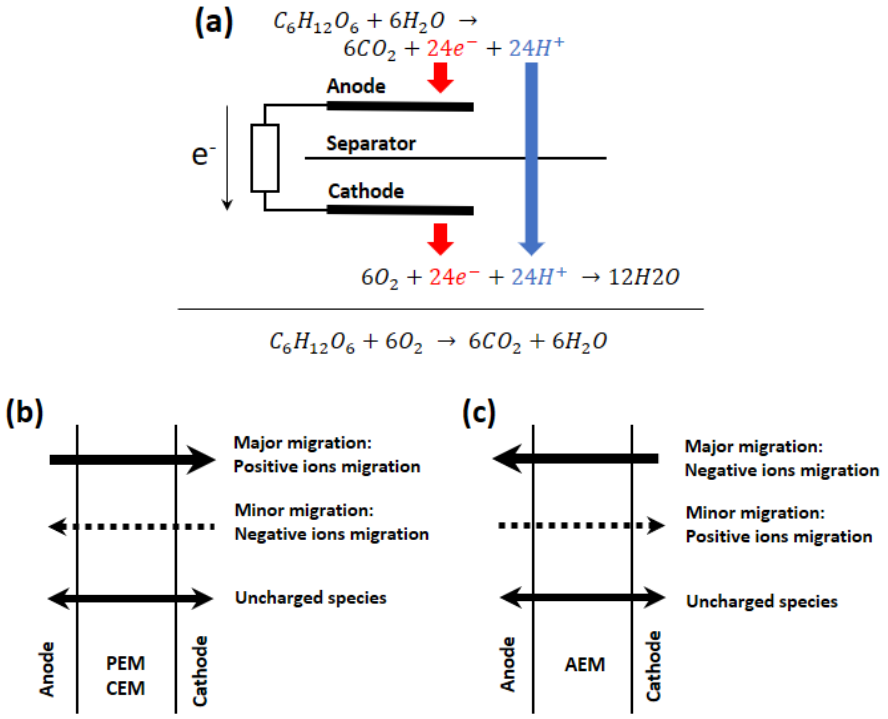

Figure 1.22 – (a) Simplified MFC representation of electrons, protons and ions flux with **(b)** a PEM or a CEM, **(c)** a AEM membrane. *Adapted from: Harnish et al.* [179]

A large diversity of available membranes.

In an MFC or more generally in an electrochemical system composed of two electrodes oppositely polarized, an electrical field is created and induces spontaneous migration of ions in solution. Positive and negative ions migrate to the oppositely-charged electrodes while neutral

species are not affected by the field. As a result, ion flux is controlled by ion exchange membrane depending on its composition. Ion exchange membranes are commonly composed of hydrophobic polymers grafted with charged groups. They are divided in two categories as function of the grafted groups **(Figure 1.22)**: (i) Cation exchange membranes (CEM) grafted with negative groups ($-SO_3^-$) only allow positive ions (protons, Nafion® PEM) to diffuse. (ii) On the contrary, anion exchange membranes (AEM) exhibit positive grafted groups ($-NR^{4+}$) promoting the diffusion of negatively charged ions. For both CEM and AEM, minor parasite migrations are observed (respectively, anion and cation) [179].

Most of the time, dual-chambers MFC applications used proton exchange membranes (PEM) to separate both compartment and avoid substrates and micro-organisms to poison and deactivate the cathode catalysts (and conversely). AEM and CEM comparison indicated great properties of AEM for single-chamber MFC with air cathode due to the low diffusion of interfering cations such as Na^+, K^+, Ca^{2+} or Mg^{2+} (buffer). Biofouling of the membrane affects both CEM and AEM. Moreover, non-ionic exchange membranes alternatives were investigated to replace CEM, PEM or AEM: Ultrafiltration membrane [180], cellulose nitrate, polycarbonate, regenerated cellulose, nylon membranes [132], wool, glass fiber[181], salt bridge [177]. Internal resistance, pH gradient effect, compartments isolation and oxygen diffusion were intensively studied and reported [132,177,182,183].

1.5.4. Global cell architectures

The power produced by an MFC is dependent on the global architecture and dimensioning of the cell. The H-type geometry probably is the oldest proposed architecture. However, it suffers from a high internal resistance and mass-transfer losses due to the large space between electrodes and the bulky reactor volume. However, this geometry is suitable for gas recovery and gas analysis in MES-mode for example. An evident strategy to improve the internal resistance is to decrease the distance between the anode and the cathode for a specific membrane. The dual-chamber cube reactor allows the variation of this distance. It was used since 1980 and clearly described by Bennetto *et al.* in 1990 [184]. Based on the cube geometry, the single-chamber cube reactor was firstly reported by Sell in 1989 and intensively described by Logan and co-workers since 2004 (with and without membrane to separate the compartments) **(Figure 1.23)** [164,185]. In a single-chamber cube reactor, the catholyte is no more require, an open-air cathode replaces the aqueous aerated air-cathode **(Figure 1.25.a, Figure 1.25.b, Figure 1.25.e to Figure 1.25.g)**. By varying the anode position, Liu *et al.* have demonstrated an increase in power density from 720 $mW.cm^{-2}$ to 1210 $mW.cm^{-2}$ for 4 cm and 3 cm inter-electrode distance. But, decreasing this distance to 1 cm leads to a decrease in power density by 50%, even though internal resistance is lower. This is probably due to oxygen diffusion through the PEM and may be solved by a continuous circulation of the bacterial anolyte [186]. Moreover, it was demonstrated that adding four PTFE/Carbon diffusion layers to the air cathode increases power density [187]. Recently, air-cathodes were tested in single-chamber open-air cathode using various carbon-catalysts mix [188–190].

Zuo *et al.* improved air-cathode dual-compartments reactor by replacing flat air-cathode by two tubular air-cathodes in a cathodic compartment filled with water **(Figure 1.24)**. Tubular cathode consisted in an ultrafiltration membrane coated with graphite paint and a mix of CoTMPP (20%) and carbon catalyst mixture [115]. Power density was not improved in comparison with classic air-cathode/CEM systems, but may be attributed to high resistivity of ultrafiltration membrane [178].

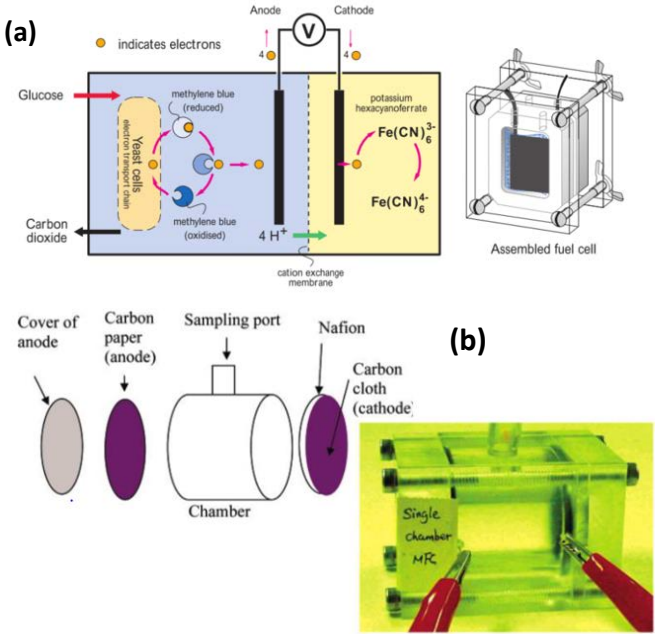

Figure 1.23 – Cubic reactor architectures: **(a)** dual-chamber cube reactor [184] and **(b)** single-chamber cube reactor [164] with an open-air cathode.

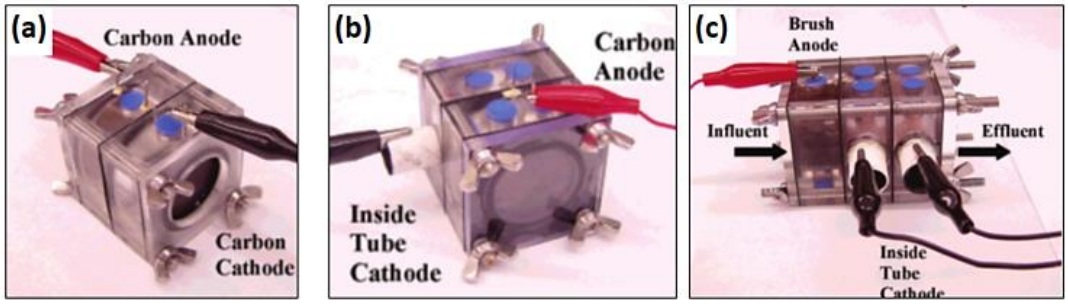

Figure 1.24 – Comparison between **(a)** flat air-cathode and **(b-c)** tubular air-cathode for cubic MFC architecture [115].

Other architectures were developed as function of the applications. Some of them are reported below:

(i) *Single-chamber air-cathode bottle* was developed for pure culture studies. They need a simple reactor easy to use, that could be autoclavable and adapted easily in a dual-chamber reactor **(Figure 1.25.a)** [131].

(ii) *A horizontal tubular single-chamber air-cathode* was used with eight carbon rods and a Nafion membrane for wastewater treatment. This system permitted a continuous

circulation of wastewater. It removed 80% of the chemical oxygen demand (COD, indirect test of the organic compounds amount in water) and generate 28 $mW.cm^{-2}$ **(Figure 1.25.b)** [50].

(iii) *Various H-type architectures* were developed for aqueous air-cathode to satisfy specific problematics: gas sparging **(Figure 1.25.c)** [191], anaerobic condition **(Figure 1.25.d)** [192] in both compartments, etc.

(iv) *Planar architecture* was designed to reduce internal resistance based on hydrogen fuel cell feedback, but it appears that oxygen diffusion may be damageable for bacteria activity in the anodic side **(Figure 1.25.f)** [193].

(v) Two types of cylindrical/tubular fuel cell based on continuous-flow of fuel in the anodic compartments exist: the vertically organized tubular reactor with anode and cathode organized in stack [194] and the horizontally organized tubular reactor where the cathode is wrapped around the anodic compartment (and conversely) [195]. These reactors may produce high power density due to their high surface area available and continuous flow **(Figure 1.25.e)**.

(vi) In 2006, Ringeisen *et al.* build a micro fuel cell composed by two chamber each 1.2 cm^3 in continuous-fed mode with carbon felt electrodes and *S. oneidensis DSP10* as active micro-organism **(Figure 1.25.g)** [196].

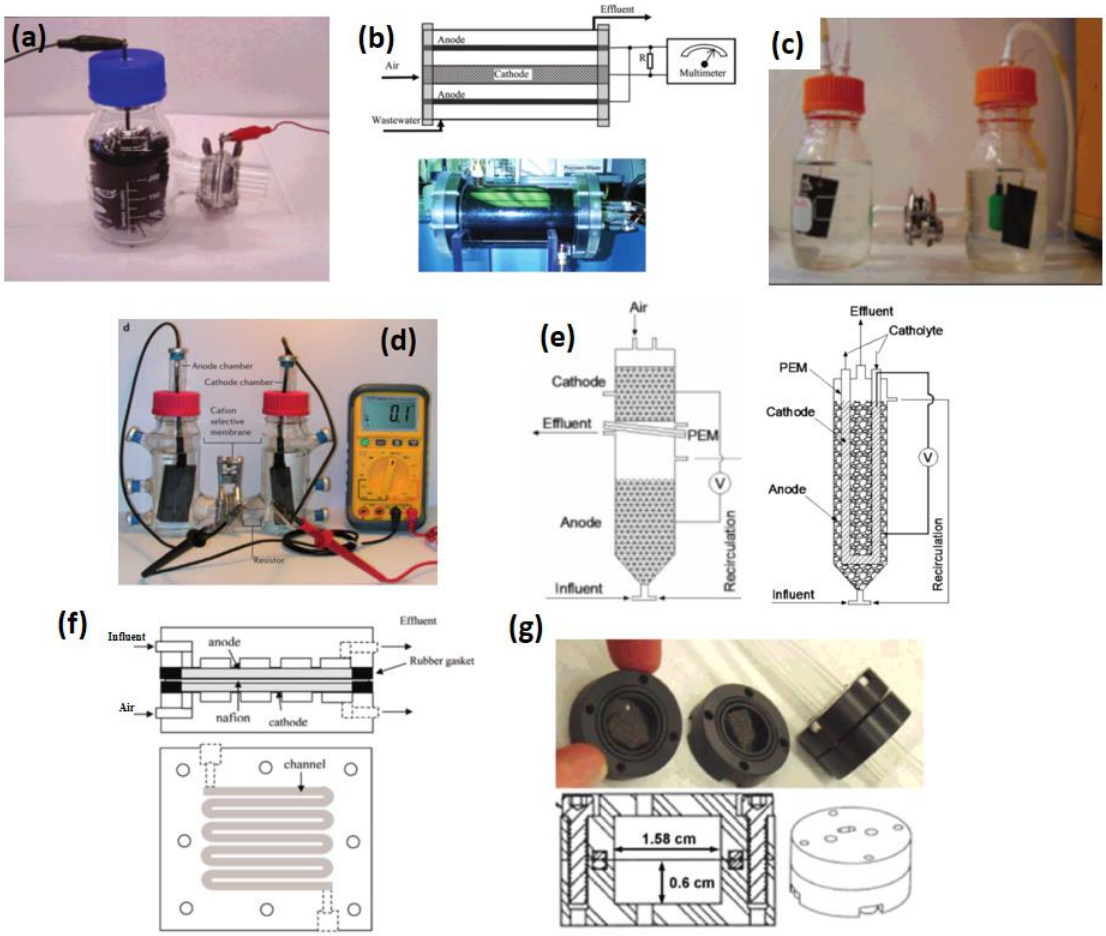

Figure 1.25 – MFC architectures: **(a)** *Single-chamber air-cathode bottle* [131], **(b)** *horizontal tubular single-chamber air-cathode* [50], *H-type architectures* ***(c)*** gas sparging **(Figure 1.22.c)** [191], **(d)** anaerobic condition [192], **(e)** Cylindrical/tubular [194,195], **(f)** *Planar architecture* [193], **(g)** Micro fuel cell [196]

1.6. CONCLUSION & THESIS OBJECTIVES

A large diversity of research in the field of microbial fuel cell and more generally in the field of microbial electrochemical systems has led to numerous reactor architectures, electrode materials and treatments and colonization strategies. To elaborate a microbial fuel cell, five major focus of research must be explored. (i) The micro-organisms involved in the MFC must be chosen carefully as function of the experimental aim and constraints. (ii) The nature and the modification of anodic material must be evaluated. Anodic electrochemical behavior must be understood as well as the interactions between the micro-organism and the chosen material. (iii) The cathode appears as a crucial part of the reactor. The strategy selected has to be chosen carefully not to be limiting for MFC performance. In other words, to ensure the reduction at the cathode of all the electrons provided by the cathode, both mass and charge transfers must be considered and optimized. (iv) The necessity of a separator or not must be evaluated and the separator must be chosen as function of the cell architecture, the nature of the micro-organisms, the cathodic reaction and experimental objectives. (v) Global cell architecture regulates most of the ohmic losses and depends on chosen anodic, cathodic and separator materials.

(i) How to select the micro-organisms?

An electroactive micro-organism is a specific cell able to convert a chemical energy into an electrical energy and to transfer electrons by the intermediate of direct, indirect or mediated electron transfer pathways. Two strategies are currently reported in the literature. Pure culture implies the choice of one micro-organism and the application of growth and colonization conditions specific to this micro-organism. For a MFC, the micro-organism is a bacterial strain. Another strategy consists in the use of a community of bacteria either artificially composed or sampled from a real environment. Both strategies present advantages and disadvantages. A pure culture is a simple system easier to control and characterize, but due to the absence of synergetic effect, electron donors are limited for a specific strain. Bacterial communities exhibit a global synergetic behavior which allows the use of complex or real fuel. But, the characterization of the colonies is more complex due to the variability from a strain to another one. Moreover, a strain can take the lead in the biofilm formation and form a biofilm mostly composed of a specific strain from the community.

In this work: *Shewanella oneidensis* is selected as the bacterium strain and is provided by the *Centre de Ressources Biologique de l'Institut Pasteur*. This strain is selected for its aero-anaerobic optional behavior and the possibility to grow in aerobic medium. Moreover, the aim of this work is to evaluate the interaction between an electroactive bacterium and the anodic material. *S. oneidensis* is also selected for its ability to inherently transfer electrons by both direct and mediated pathways.

(ii) How to select the anodic material?

Carbon-based materials are widely used as anodic materials for MFC, but stainless steel based materials represent a qualitative alternative. Surface treatments are employed to

enhance the properties of the material and the performance of the global MFC. The anodic material must be chosen as function of the objectives. Most of the theoretical or empirical approaches to understand the bacterium bio- and bioelectro-chemistry are carried out with the simplest materials (carbon or stainless steel plates and rods, platinum electrode). To enhance the performances of the MFC, technic and treated 3D materials are promoted (carbon felt or fibers brush, carbon or stainless steel foam, grid or cloth).

In this work: Carbon felt is used as a reference material for the evaluation and the comprehension of the bacteria adhesion, the biofilm formation and the electron transfer. A home-made carbon paper made by electrospinning methodology will be also evaluated as an innovative carbon-based electrode for MFC.

(iii) How to select the cathodic material and strategy?

Oxygen reduction is mainly promoted as cathodic reaction of reduction at the cathode ($E^0(O_2/H_2O) = 1.23\,V\ vs.\ NHE$). Numerous strategies have been tried and evaluated to perform oxygen reduction at the cathode, but platinum electrode or carbon electrode covered with a layer or nanoparticles of platinum remains the most efficient catalytic electrode. Iron and cobalt based catalysts were recently studied and remain promising but necessitate further efforts. Another option is to apply the MFC by using a micro-organism at the cathode strategy to the cathode: oxygen reduction can be performed by enzymes or specific bacterium strains. But it is also possible to add a second aim to a MFC by performing hydrogen production (algae, bacteria) or water denitrification (bacteria) at the cathode instead of oxygen reduction. These last strategies are recent and under study.

In this work: At the lab-scale, this work focalizes on the anodic part of the MFC. As a consequence, ferricyanide electrolyte ($K_3Fe(CN)_6$ and NaCl) is generally used with a carbon felt cathode. Air cathodes are also used.

(iv) How to select the separator? Is it necessary?

In a dual-compartments reactor or open-to-air cathode single-compartment, the separator has several utilities: (i) while using an air cathode, the membrane avoids the diffusion of oxygen in the anodic compartment. For anaerobic strict bacteria, the absence of oxygen in the anolyte is determining for MFC performance. (ii) Several membranes limit the increasing of salinity by avoiding osmotic effect and acidification by promoting protons diffusion. (iii) The separation between the anodic and the cathodic compartments limits bacteria and electrolytes components to crossover and contaminate opposite compartment. Membrane-less MFC was determined as promising for specific MFC architecture, generally with bacterial communities which are composed of anodic and cathodic micro-organisms.

In this work: Both membranes-less reactor (single-compartment reactor) and dual-compartments reactor with a membrane to separate the anodic and the cathodic compartment are used to evaluate MFC performances. Ultrafiltration membrane (0.2 µm in porosity) is firstly

used, then reactors are optimized by using Nafion® membranes. Nafion® is cationic-exchange membrane mainly dedicated to proton diffusion.

(v) Consideration on the global cell architecture.

The reactor architecture regulates most of the ohmic losses. Various architectures have already been studied, and the choice is dependent on the MFC working conditions. Continuous fed-batch reactor needs a continuous circulation of the catholyte and/or the anolyte while batch reactors are performed in stationary configuration. Recently single-compartments reactor equipped of an open-to-air cathode are promoted due to their versatility and simplicity to use for long or short time experiments.

In this work, both single- and dual-compartment reactors are used with control of the distance between the anode and the cathode and of the volume of anolyte and catholyte. Batch reactor and semi-continuous fed-batch (possible renewal of the electrolyte and addition of nutrient) are employed.

To summarize, the design of an MFC firstly depends on the chosen micro-organism, its pathways available for electron transfer to the electrode (DET and/or MET) and the physiological constraints inherent to the micro-organism. The electrode material depends on the strategy employed to perform electron transfer to the electrode and on the bacterium behavior. The cell architecture is chosen as function of the previous bacterium and material selected. Moreover, the cell architecture has to be compatible with the type of reactor (batch or continuous fed-batch).

In this work, reactors architectures, electrodes materials and global MFC strategy will be employed to study the interaction existing between *Shewanella oneidensis* strain and carbon-based anodes by electrochemical methodologies.

In a first step, the behavior of the bacterium in a single-compartment MFC reactors, without separator to isolate the electrodes, will be evaluated in various conditions. For this work, carbon felt electrodes are used as anode and cathode. Following external parameters will be evaluated as promotor of the electrode colonization and electron transfer: (i) oxygen availability, (ii) electrolyte nature (growth medium or PBS medium), and (iii) the state of growth of the *S. oneidensis*.

In a second part, the effect of the anode (working electrode) polarization at potential from -0.3 to +0.5 V vs. Ag/AgCl/KCl will be demonstrated in both single- and dual-compartment to determine the beneficial effect of a polarization step for *S. oneidensis* to colonize the electrode and to perform EET. These polarizations are carried with strictest and symmetrical electrode potential (anode and cathode are polarized at opposite potential). Electrodes are polarized under unusual aerobic condition, in order to demonstrate the ability of *S. oneidensis* to transfer electrons to the anode even in presence of a competitive electron acceptor.

In a third step, *S. oneidensis* will be encapsulated in an artificial biofilm to limit growth of bacteria that can block the electrode porosity This artificial biofilm is an inorganic matrix of silica gel produced by the aqueous route (alkoxysilane replaced by sodium silicate). The electrochemical behavior of *S. oneidensis* will be monitored as a function of the matrix composition (inorganic network tightness) in polarized or non-polarized condition. This study will allow us to study how stress modify electron transfer from bacteria to the electrodes.

Finally, an innovative electrode made by carbonization of electrospun fibers (80 to 150 µm in diameter) will be synthetized, characterized and evaluated as a bio-anode for MFC in comparison with a commercial carbon felt wide fibers (12 µm in diameter).

CHAPTER 2

EXPERIMENTAL PARAMETERS AFFECTING BACTERIUM ADHESION AND MICROBIAL FUEL CELL PERFORMANCES

FROM THE BIOFILM FORMATION TO THE CONCEPTION OF AN ARTIFICIAL BIOFILM

Table of Contents – Chapter 2

2.1. INTRODUCTION AND OBJECTIVES

A microbial fuel cell is a device which performs the conversion of chemical energy into electrical energy [197,198], similarly to a conventional fuel cell [199]. In this technology, the model platinum catalyst is replaced by a micro-organism acting as a unit of conversion. Based on its metabolism, the micro-organism is able to oxidize small organic molecules and to transfer electron to other bacteria, to an external electron acceptor such as the oxygen or to reduce a metallic oxidant in order to externalize its electrons. In microbial fuel cell configuration, the electrons are externally transferred by the bacteria to the electrode [152]. The main objective of the microbial fuel cell is to produce energy by the valorization of combustive unusable with conventional technologies (i.e. valorization of domestic and industrial wastewaters or effluents, or polluted soils). But, the scope of application of this technology can also be extended to produce hydrogen, to passively desalinate water or to the valorization of the carbon dioxide [8].

To construct a bio-anode for a microbial fuel cell (or more generally for microbial electrochemical systems), the electrode material is exposed to bacterium, a community of bacterium or a real inoculum sampled from a specific environment [10]. During the exposition, the bio-anode is colonized by the micro-organisms and a biofilm is formed at the surface. The external electron transfer occurs by direct, indirect and mediated pathways from the bacteria to the conductive electrode surface. This transfer highly depends on the interaction between the bacterium and the electrode surface. Moreover, the formation of a local environment promoting electron transfer to the anode depends on the bacterium nature and several external parameters, especially the bacterium response to external stimuli.

In this chapter, a microbial fuel cell based on the colonization of technical tri-dimensional electrodes (carbon felts) by the electroactive *Shewanella oneidensis* wild strain will be explored [77,200,201]. The objective is to characterize the ability of *S. oneidensis* to transfer electrons by both direct and mediated pathways in specific experimental condition in order to better understand the external electron transfer (EET) and the close interaction existing between the electron collector (final electron acceptor) and the micro-organism acting as a catalyst.

To reach this objective, (i) in a first step, the ability of a carbon-based electrode to act as a preferential surface for EET will be explored by an evaluation of its conductivity and of its electrochemical behavior in presence of conventional electrochemical probes. (ii) In a second stage, the growth of *S. oneidensis* will be studied so as to determine the optimal conditions for carbon felt colonization. The colonization process will be studied in various conditions that are supposed to act as external stimuli to enhance the colonization and the formation of a conductive and active biofilm. The effect of chemical and biological parameters (oxygen presence, bacterial state of growth, complexity of the seeded electrolyte) will be assessed as relevant external parameters. Turning to physical parameters, the electrode will be poised symmetrically at negative and positive specific potentials and the effect of the polarization evaluated under unusual aerobic conditions for microbial fuel cell. The aim is to characterize the ability of *S. oneidensis* to acclimate the presence of oxygen due to its optional aero-anaerobic

specificity and to perform EET to the electrode even if the oxygen acts as a competitive electron acceptor. To conclude, (iii) in a third part, *a S. oneidensis* SiO_2-carbon felt bio-anode will be designed by the encapsulation of the bacterium in an inorganic matrix of silica gel made by the aqueous sol-gel route, incorporated into a conductive carbon felt. The electrochemical behavior of the encapsulated bacterium and its ability to form a biofilm and to perform EET will be evaluated as a function of the silica gel formulation.

Both of the studies of *S. oneidensis* ability to perform an electron transfer without structural restriction by the colonization of a 3D-electron or trapped in an artificial biofilm by encapsulation into a silica gel will conduct to a better understanding of the surface/bacteria interaction. This information will lead to experimental condition to form efficient bio-anode and to increase the performance of the microbial fuel cell.

2.2. CARBON FELT AS AN ANODIC CARBON-BASED ELECTRODE

2.2.1. How an electrochemical reaction occurs?

For an electrochemical reaction to occur, two conditions are required: the charge transfer and the mass transfer. The charge transfer principle implies that reactants are in contact with the electrode and able to exchange electrons with it. For this electron transfer to occur, the species must diffuse through the bulk solution to the electrode surface as described by the mass transfer principle [8].

To be thermodynamically favorable, the Gibbs energy of a reaction must be negative or equal to zero ($\Delta_r G = \Delta_r H - T\Delta_r S \leq 0$). The Gibbs energy is composed by (i) an enthalpic term of reaction $\Delta_r H$ characteristic of both reactants and reaction stability and, (ii) an entropic term $-T\Delta_r S$ characteristic of associated change in the system disorder. Generally, $\Delta_r H$ is fixed by the nature of the reactants and Gibbs energy varies as function of $-T\Delta_r S$. Chemical reaction generally necessitates an increase of temperature to occur.

An electrochemical system is composed of a redox reactant and a solid « pseudo-reactant » able to exchange electrons with the oxydo-reductant system, the working electrode. This electrode is set-up at a specific potential of reaction E_r with a potentiostat in a three-electrodes configuration. By varying the potential, the reaction is facilitated ($E_r \sim E_{Nernst}$) or blocked ($E_r \neq E_{Nernst}$).

$$E_{Nerst} = E^0 + \frac{RT}{nF}\ln\frac{[Ox]}{[Red]}$$

E^0, standard potential of the redox couple. R, ideal gases constant (8.314 J.K^{-1}.mol^{-1}). T, temperature in Kelvin. n, number of electron exchanged during the reaction. F, Faraday constant (96500 C.mol^{-1}). $[Ox]$ and $[Red]$, concentration of oxidant and reducer.

By varying the potential around the Nernst potential of the redox couple, the reduction or the oxidation is promoted. For an applied electrode potential lower than the Nernst potential, the electrode presents an excess of electrons, the reaction current is negative and the reduction

occurs to consume the excess of electrons. On the contrary, for a higher potential, the electrode presents a lack in electrons, the oxidation occurs and electrons are transferred to the electrode **(Figure 2.1)**. The reaction current is positive. Most of the common redox couples have a reaction potential between -3 and 3 V vs. NHE (Normal Hydrogen Electrode) that are accessible in a 3-electrodes potentiodynamic experiments monitored by a potentiostat [202].

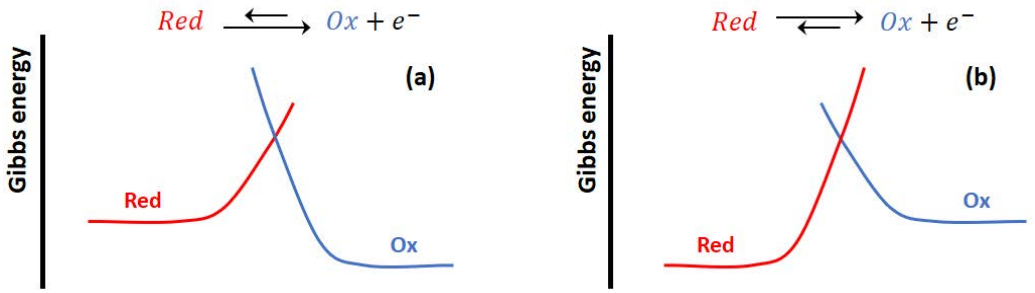

Figure 2.1 – Effect of the applied electrode potential on the reduction or the oxidation sense of reaction. **(a)** Oxidation for $E_{apply} < E_{eq}$ and **(b)** Reduction for $E_{apply} > E_{eq}$ (adapted from Bard and Faulkner, 2001 [202])

2.2.1.1. Charge transfer.

The reaction is thermodynamically favorable if the energy states of the reactants is higher or equivalent to the energy states of the products ($\Delta_r G \leq 0$). However, for the reaction to occur in a reasonable time scale, the kinetic reaction rate also has to be favorable. The reaction pathway which leads to a more favorable final energy state (lower than the reactants energy state) involves an activation energy barrier with an instable intermediate at a higher energy state. By modifying the temperature and/or the entropic contribution, the energy barrier can be passed away and the reaction accelerated **(Figure 2.2)**.

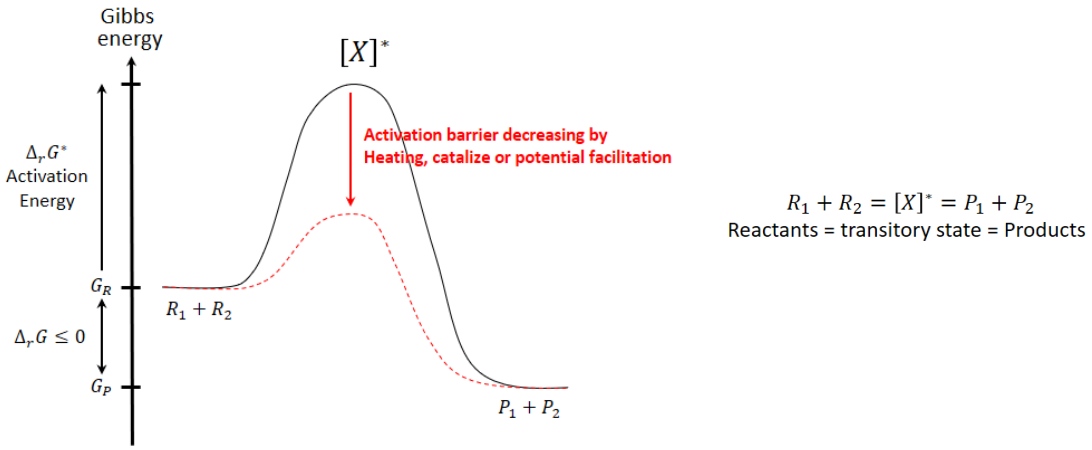

Figure 2.2 – Reactional pathway from the reactants R_1 and R_2 to the products P_1 and P_2 by the instable component [X]* at the activation energy barrier.

During an electrochemical reaction at a solid surface, electrons are exchanged at the surface of a conductive material in a way that depends on the potential applied to the electrode. For a wisely chosen potential, the activation energy barrier intensity may decrease to facilitate the reaction. This phenomenon is described in the Butler-Volmer equation which introduces two

kinetics parameters: (i) the exchange current i_0, that indicates the fast or slow nature of the equilibrium. This current is measured at the equilibrium potential ($\log(i_o) = f(E = E_{eq}) = f(\eta = 0)$): i_0 is low for slow reaction rates and high for fast reactions **(Figure 2.3)**. (ii) The cathodic coefficient of transfer α (defined between 0 and 1) and the anodic transfer coefficient $1 - \alpha$. They indicate the direction of the reaction (oxidation or reduction). The exchange current and the coefficients of transfer are determined using the Tafel plot **(Figure 2.4)**.

$$\text{Butler-Volmer equation: } i = i_0 \left(e^{-\frac{\alpha n F}{RT}(E - E_{eq})} - e^{\frac{(1-\alpha) n F}{RT}(E - E_{eq})} \right)$$

i_0, the exchange current. α, the generic coefficient of transfer. R, ideal gases constant (8.314 J.K^{-1}.mol^{-1}). T, temperature in Kelvin. n, number of electron exchanged during the reaction. F, Faraday constant (96500 C.mol^{-1}). E, the applied potential and E_{eq}, the equilibrium potential for $i = 0 = f(E = E_{eq})$.

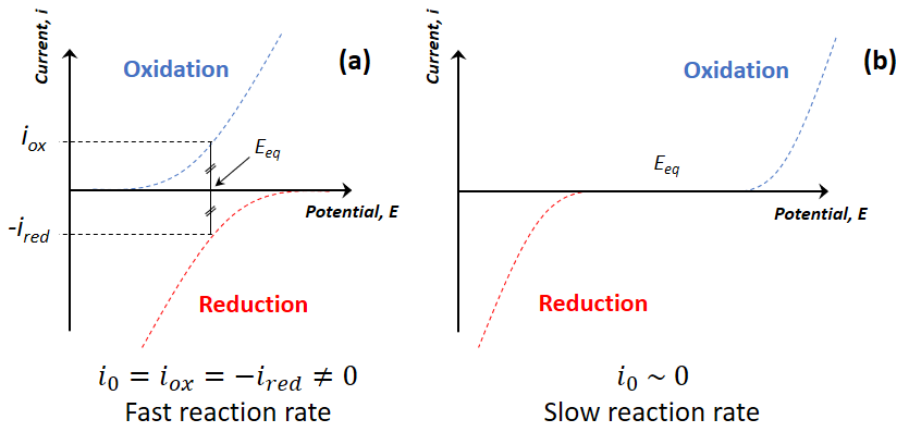

Figure 2.3 – Schematic evaluation of the exchange current i_0 for a fast **(a)** or a slow **(b)** reaction rate.

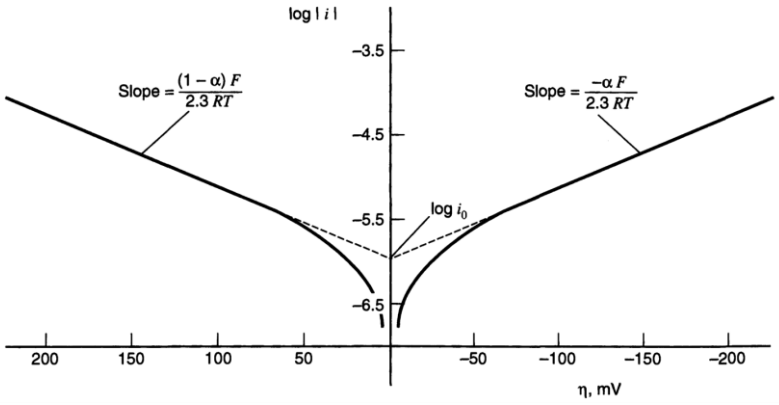

Figure 2.4 – Tafel plots for anodic and cathodic branches in function of the current-overpotential curve $Ox + e^- = Red$ with $\alpha = 0.5$, $T = 298K$, and $i_0 = 10^{-6}\ A.cm^{-2}$. [202]

In an electrochemical reaction the role of the electrode is two-fold. The electronic exchange happens at the electrode surface and electrons are received or delivered through the electrode. Moreover, to catalyze a reaction, the electrode can be made of a specific catalytic material (Pt, Pt/C, Iridium oxide, …). For example, to accelerate the reduction of the oxygen in water (a multi-electronic redox reaction), platinum may be used as a catalyst to improve the

dissociation of the H-H and O=O covalent bonds to form water molecules. This catalytic property is ensured by the adhesion and the positioning of the reactants on the catalytic surface. Thus, the chemical nature and the surface condition of the electrode is critical for specific reactions such as the reduction of oxygen in PEMFC (cf. 1.2.1) [203].

2.2.1.2. Mass transfer.

For an oxido-reduction reaction to occur, the reactants have to reach the electrode surface if they are not initially adsorbed on it. This progressive migration is described by the mass transfer phenomena and occurs via three different mechanisms **(Figure 2.5)**.

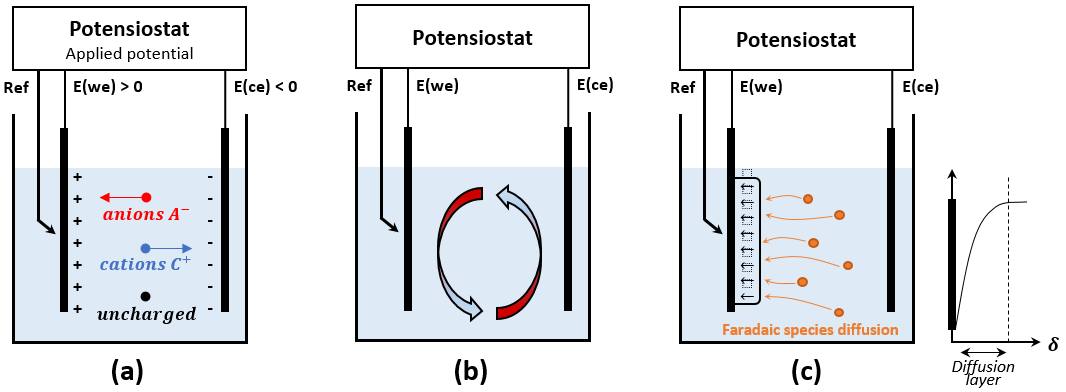

Figure 2.5 – Mechanisms of species migration in a three electrodes configuration:
(a) migration in an electrical field, **(b)** migration by convection, **(c)** diffusive mechanism

(i) During an electrochemical reaction, the working electrode is polarized and an electrical field is established between the working and the counter electrodes. Ionic species migrate towards the electrode charged at the respective opposite sign due to the applied electrical field, while uncharged species are not influenced.
The influence of this migration has to be limited in presence of faradaic species. To minimize this, a supporting electrolyte (also named background salt) is employed to shield the electrical field and to limit unintended migration of faradaic redox species. Small unreactive (non-faradaic) ions such as sodium, potassium and chloride are traditionally used.

(ii) Natural or forced convection in a gradient of pressure or temperature leads to the mobility of the species in solution. This convection ensures the mixing of the reactants and is employed in specific electrochemical experiments such as rotating disk electrode experiments to minimize the diffusion layer due to the consumption of reactants at the electrode surface.

(iii) The main mechanism of migration is the diffusion. The driving force is the concentration gradient established between the surface and the bulk solution. Indeed, the local environment is depleted in reactants when they react at the surface of the electrode. The diffusion phenomenon is described by the Fick law:

$$\overrightarrow{J_d} = -D * \overrightarrow{grad}\, c$$

In this equation, D is the diffusion coefficient, usually expressed in cm².s^{-1}, which describes the mobility of a species in a particular environment. Indeed, this coefficient depends on the chemical nature of the species (hydrodynamic radius) and the medium viscosity. Generally, the coefficient of diffusion is between 10^{-4} à 10^{-6} cm².s^{-1}.

The diffusion layer thickness is related to the dimension of the gradient of concentration which corresponds to the variation of concentration from the electrode to the bulk solution (where the concentration is maximal and constant). The thickness of the layer is described by the δ parameter related to the diffusion, the chemical nature of the mobile species and the electrode geometry (1D dimension, radius).

For an electrode of large dimension, the Cottrell infinite planar electrode model, also applied to « locally plate » electrode is verified and implies the assimilation of δ to $\delta' = \sqrt{D\tau}$. Indeed, the high dimension of the electrode suggests the invariance of the surface at the molecular scale. As a consequence, δ' is solely related to the diffusion (via the coefficient of diffusion, D) and the characteristic duration of the experiment, τ. Moreover, τ is inversely proportional to the scan rate. In other words, the diffusion layer is thinner when scan rate is high. The expression of the faradaic current intensity is related to the Randles-Sevcik law:

$$i_{pic} = 0.4463 * (nF)^{3/2} * \left(\frac{\upsilon D}{RT}\right)^{1/2} * A * c \xrightarrow{T=25°C} 269\,000 n^{3/2} * \upsilon^{1/2} * D^{1/2} * A * c$$

n, the number of exchanged electrons. F, the Faraday constant (96500 C.mol^{-1}). R, the ideal gas constant (8.314 J.K^{-1}.mol^{-1}). T, the temperature in K. υ, the scan-rate in V.s-1. D, the coefficient of diffusion in cm².s^{-1}. A, the surface area in cm² and c, the concentration in mol.cm^{-3} [204].

Therefore, the current at the oxidation/redox potential E_{pic} is proportional to the square root of the scan rate and to the concentration. At potentials higher than E_{pic}^{ox} or lower than E_{pic}^{red}, redox species are not consumed, the thickness of the diffusion layer increases. As a result, the current of oxidation i_{ox} and reduction i_{red} decrease and converge to 0.

For electrodes with low dimension, such as microelectrodes, the characteristic dimension of the diffusion layer is larger than the dimension of the electrode ($a < 50\ \mu m \ll \delta \Leftrightarrow a/\delta \ll 1$). The diffusion layer of diffusion takes the form of a half-sphere with an invariable dimension. At this scale the fast diffusion leads to a homogeneous concentration of reactant and the establishment of a stationary state characteristic of the microelectrodes. This layer is independent to the characteristic duration of the experiment τ but highly dependent on the 1D dimension of the electrode (the radius). In this condition, the maximum faradaic current is expressed by the equation:

$$i_{\max} = 4nFD * c * r$$

with n the number of exchanged electrons, F the Faraday constant (96500 C.mol^{-1}), D the coefficient of diffusion, c the concentration of the redox species and r the radius of the cylindrical electrode [204].

To summarize, a chemical reaction can occur at the surface of an electrode if it is thermodynamically favorable ($\Delta_r G \leq 0$). Moreover, the reaction only occurs in reasonable duration if the kinetic parameters are in accordance. These parameters are determined by the reactional pathway, that is affected by the temperature of the reaction and the presence of catalysts. In the case of an electrochemical reaction, the applied electrode potential influences the intensity of the activation energy barrier **(Figure 2.2)**. The mass transfer and the charge transfer are two critical steps to be optimized to ensure the feasibility of an electrochemical reaction.

2.2.2. Carbon felt as carbon-based electrode for electrochemistry

To evaluate the influence of the external parameters on the colonization and on the current production by *Shewanella oneidensis*, a carbon felt is used as a working electrode. Carbon-based electrodes present a high chemical and electrochemical stability. They are usually cytocompatible, non-toxic and barely sensitive to corrosion unlike common metals such as copper or nickel. Moreover, carbon-based materials are resilient, easy to use and available in various morphologies.

The carbon felt used as electrode for this study is supplied from Morgan Carbon company as a roll of 1 cm thick, black and smooth mat easy to shape due to its impressive mechanical strength and resilience. This mat is composed of loosely intertwined conductive carbon fibers. The fibers are composed of carbon at 99.9% and slightly oxidized or substituted at the surface (WDF grade) [205]. They form a network of fibers spaced by 50 to 100 µm. Each fiber is a stack of 8 to 10 fibrils and measures a few millimeters in length for 10 to 12 µm in diameter **(Figure 2.6)**. Due to this aggregation of fibrils, the fibers present small channels which increase the global roughness. Also, undefined nanoparticles are aggregated at the surface. It results from this architecture, a large porosity (more than 95% of air) and a large specific surface area which is evaluated to 0.15-0.2 m².g^{-1} with a cylindrical fiber model ($A_{spe} = 2/\rho r$ [1], where ρ is the density and r the radius).

To act as an electrode for microbial fuel cell, the electronic conductivity of a given material must be clearly known and understood. Due to its smooth structure, the carbon felt is

[1] **Demonstration: Specific surface area of n fibers**

$V_{cylinder} = \pi r^2 l$ and $A_{cylinder} = 2\pi rl$
Weight of a single cylinder $m = \rho V_{cylinder} = \pi r^2 l\rho$
Weight of n cylinders: $M_{n\ cylinders} = mn = \pi r^2 l\rho n$
And Surface Area of n cylinder: $A_{n\ cyclinders} = V_{cylinder} n = 2\pi rln$
Thus, $A_{spe}^{n\ cylinders} = A_{n\ cylinders}/M_{n\ cylinders} = 2\pi rln/(\pi r^2 l\rho n) = 2/r\rho$
By considering a cylinder as a fiber, $A_{spe}^{n\ cylinders} = A_{spe}^{fibers} = 2/r\rho$

flexible and compressible. When the mat is compressed the fibers get closer and additional electronic pathways are created by new junction between fibers. The electronic conductivity therefore varies as function of the compression and may increase from 20 $mS.cm^{-2}$ to 40 $mS.cm^{-2}$. Moreover, as a bio-electrode, the carbon felt must be able to function in aqueous condition. However, as such, they exhibit a hydrophobic surface. To improve their hydrophilicity, two treatments are possible: (i) an oxidation in acidic condition of the carbon felt to form hydrophilic groups at the surface and (ii) the deposition of a hydrophilic layer of polymer at the surface of the fibers. An electrochemical characterization of the raw and treated carbon felt is required to evaluate the electrochemical responses of the felt as an electrode and the beneficial effect of the hydrophilic treatment (cf. part 2.2.3).

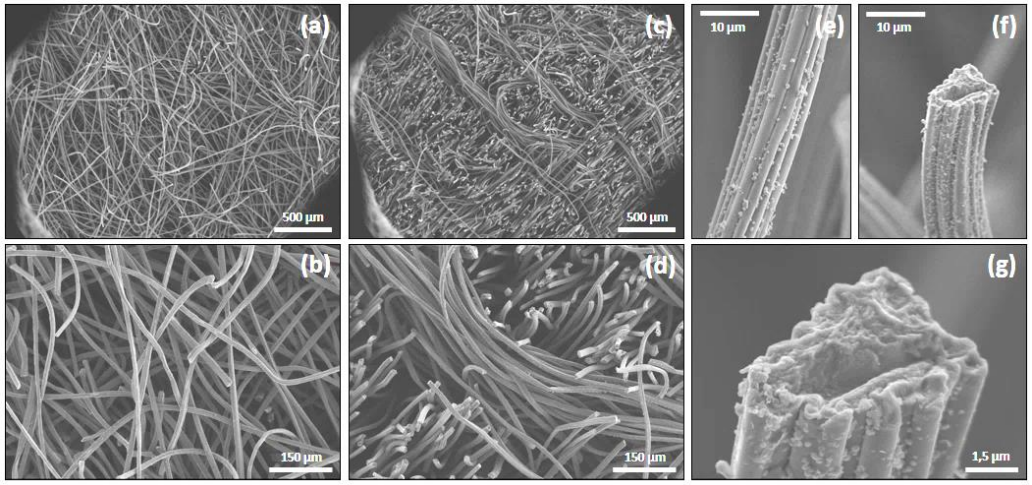

Figure 2.6 – Scanning electron microscopy of the microscopic structure of a carbon felt supplied by Morgan Carbon. **(a-b)** Randomly organized fibers in the plan. **(c-d)** Woven structure perpendicularly to the plan. **(e-g)** Aggregate of fibrils which form fiber.

2.2.3. Electrochemical characterization of a carbon felt

A carbon felt is a complex hydrophobic organization of rough carbon fibers. The properties of this conductive architecture as an electrode for electrochemical system or as bio-anode/cathode must be evaluated. In this part, the capacitive behavior of a carbon felt is compared to a platinum nanowire electrode and the surface of both electrodes are studied and compared in term of capacitive current. To characterize the faradaic behavior of the felt and the accessibility of the fibers, a positively-charged probe (Hexaammineruthenium(III) chloride, $Ru(NH_3)_6Cl_3$, Sigma-Aldrich) and a negatively-charged probe (Potassium ferrocyanide, $K_4Fe(CN)_6$, Sigma-Aldrich) are used. Two treatments (acid and polymer) are described to enhance the hydrophilicity of a raw carbon felt and their electrochemical efficiency is assessed in comparison with a raw carbon felt. For all measurements, 1 cm^3 cubic carbon felts (1 cm square in shape) are used and three electrolytes are employed: (i) 130 mM NaCl to evaluate the capacitive behavior, both (ii) 130 mM NaCl + 0.3 mM $K_4Fe(CN)_6$ and (iii) 130 mM NaCl + 0.3 mM $Ru(NH_3)_6Cl_3$ to evaluate the faradaic behavior. A 30 mL single-compartment reactor is filled with 20 mL of the chosen electrolyte. The measurements are performed in a three-electrodes configuration: the working electrode corresponds to the carbon felt (or a platinum wire for comparison), a

twisted platinum wire is used as counter electrode and an Ag/AgCl/KCl electrode as reference (V vs. Normal Hydrogen Electrode = -0.2 V vs. Ag/AgCl/KCl).

2.2.3.1. Capacitive behavior of a raw carbon felt.

The capacitive current is related to the capacitor effect. The polarized electrodes may be considered as the positive and the negative plate of a condenser. Under an electrical field induced by the external polarization, positive and negative ions migrate to the negatively and positively charged plate electrodes, respectively. The accumulation of charges Q at an applied potential E leads to the formation of a double layer or capacitance C, mathematically expressed as $Q = CE$. During a voltammetric experiment, the capacitive current resulting in the accumulation of ions from the support electrolyte to the electrode surfaces corresponds to a square pattern ($i = f(E_{apply})$). At the vertex potential, the scan direction change and a condenser discharge effect happens resulting in a rounded configuration at the capacitive square angles. The charge linearly varies with the monitored current i and the time t: $Q = it$, and the capacitance C can be expressed as the product of the specific capacitance κ and the capacitive surface area A_c. As a result, the capacitive current may be expressed as:

$$i_c = \frac{CE}{t} = Cv = \kappa A_c v = \frac{F * V}{cm^2 * s}$$

i_c, the capacitive current (A). A_{spe}, the specific surface area (cm²). v, the scan rate (V.s^{-1}) and κ, the specific capacitance equivalent to 20 µF.cm^{-2} for the carbon and 87 µF.cm^{-2} for the platinum [206].

Platinum wire (0.5 cm in diameter) and carbon felt (1 cm^3, 1 cm square in shape) immersed in a 130 mM NaCl electrolyte present a square cyclic voltammogram characteristic to a capacitive response of the support electrolyte. The water reduction phenomenon ($2H^+ = H_2 + 2e^-$) is observed around -0.2 V vs. Ag/AgCl/KCl. The measured surface area is the projected capacitive surface area corresponding to the accessible surface to small non-faradaic ions (Na^+ and Cl^-). The capacitive surface is calculated *via* the capacitive current i_c measured at $i_{ox} = -i_{red} = i_c$ and is equal to ca. 243 cm² for 1 cm^3 carbon felt (0.12 g). This value corresponds to ca. 0.2 m².g^{-1} and is in accordance with the specific surface calculated geometrically based on both the carbon density and the radius of carbon fibers **(Figure 2.7)**.

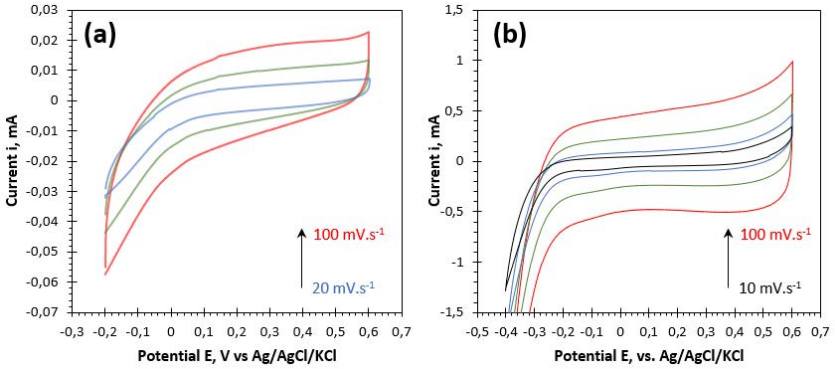

Figure 2.7 – Cyclic voltammogram for a platinum wire **(a)** and a 1 cm^3 carbon felt **(b)** working electrode immersed in a solution of 130 mM NaCl. Platinum wire and Ag/AgCl/sat. KCl are respectively used as counter electrode and reference electrode.
Caption: **— 10 mV.s^{-1}** in black, **— 20 mV.s^{-1}** in blue, **— 50 mV.s^{-1}** in green and **— 100 mV.s^{-1}** in red.

The maximum surface area for carbon felt or a similar architecture is the specific surface area. The capacitive surface is equivalent or slightly lower. For an aqueous electrolyte, the equivalence between these two types of surface area depends on the accessibility of the conductive surface to ions, the hydrophilic/hydrophobic balance, the pores dimension and the surface chemistry. The faradaic surface corresponds to the reactive surface. For conventional electrodes, the faradaic surface is generally smaller than the capacitive surface. The advantage of a 3D architecture such as the carbon felt is to develop a high surface for a low volume and weight.

2.2.3.2. Faradaic behavior of a raw carbon felt.

The faradaic current corresponds to the flow of electrons produced by an oxido-reduction reaction and then transferred at the surface of a conductive electrode. In cyclic voltammetry experiment, the faradaic current is expressed as a sigmoidal wave of oxidation or reduction which depends on the chemical nature and the scan rate of the redox reaction. Moreover, the nature of the electrode and the surface reactivity affect the cyclic voltammetric pattern (surface accessibility, conductivity, …). The Nernst equation describes most of the electrochemical phenomena related to the faradaic reaction in cyclic voltammetry methodology. Kinetics of reaction at the electrode surface are defined by the Buttler-Volmer equation (cf. 2.2.1). The peak potential and its current intensity is mathematically determined by the Randles-Sevcik in the case of a fast and reversible redox system.

The electrochemical behavior of a redox system can be identified based on the cyclic voltammogram shape. Three type of redox systems are identified (i) fast and reversible, (ii) slow and quasi-irreversible or (iii) quasi-reversible redox systems **(Figure 2.8)** [207].

(i) If the charge transfer at the electrode is faster than the diffusion of the active species from the bulk solution to the electrode surface (mass transfer), the system is considered as **reversible and fast**. In this case, narrow and symmetrical faradaic peaks are observable in cyclic voltammetry. The potential of the oxidation peak E_p^{ox}, of the reduction peak E_p^{red} and the difference of peak potential (DPP) $\Delta E_p = E_p^{ox} - E_p^{red}$ are independent of the scan rate v. The DPP is invariable and equal to $59/n\ mV$ (at 25°C, n is the number of electrons involved in the redox reaction). The peak intensity is described by the Randles-Sevcik equation and linearly proportional to the square root of the scan rate, $v^{1/2}$.

(ii) In the opposite case (charge transfer slower than mass transfer), the system is **quasi-irreversible and slow**. The exchange coefficient α, which defined the affinity for the oxidation or the reduction direction of reaction, is introduced by the Buttler-Volmer equation. The peak intensity remains proportional to the square root of the scan rate $\sqrt{v}$ and is mathematically calculated at 25°C as:

$$i_p = 299\,000 * \alpha^{1/2} n^{3/2} A D^{1/2} v^{1/2} c$$

i_p, the current intensity of the faradaic peak at E_p. α, the exchange coefficient. n, the number of electrons implied in the reaction. A, the surface area. D, the coefficient of diffusion. v, the scan rate of reaction and c, the redox species concentration

The peak potential varies with the scan rate and is proportional to the logarithm of the scan rate,$E_p = f(\log v)$. Consequently, E_p^{red} decreases and E_p^{ox} increases leading to ΔE_p increasing.

(iii) If the charge transfer is slow but the reaction is reversible, the opposite reaction must be taken into account. This system is defined as **quasi-reversible**. The peak intensity, i_p, increases with the scan rate, but not linearly as it is observed for a reversible redox system. Moreover, the current intensity of the peak is inferior to the intensity obtained for a reversible system. ΔE_p increases with the scan rate, v, and is superior to $59/n\ mV$ (25°C).

To summarize,

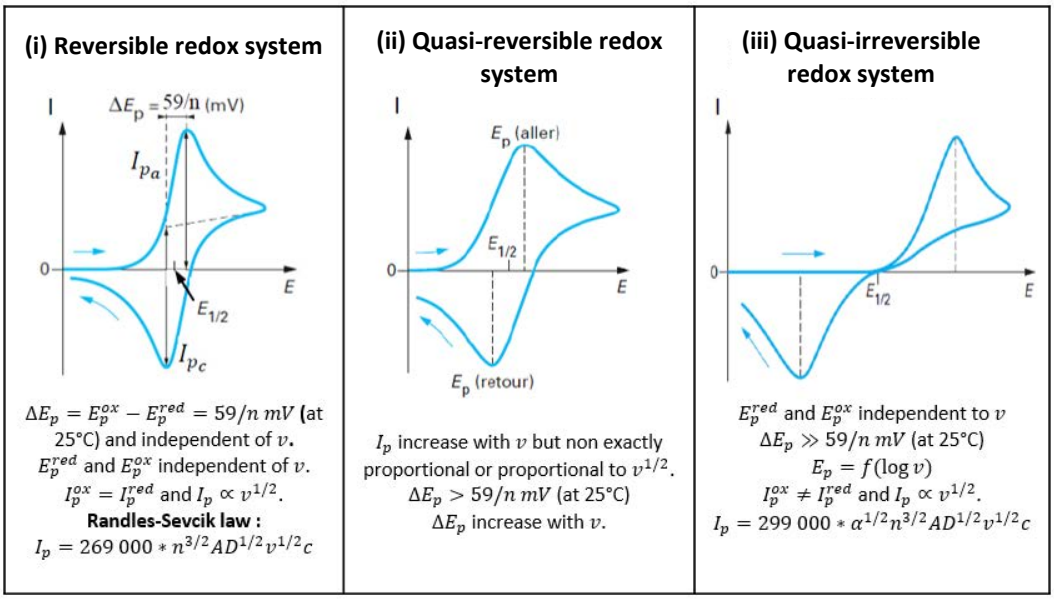

Figure 2.8 – Electrochemical patterns in cyclo voltammetric mode and main criteria to define the **(a)** reversible, **(b)** quasi-reversible or **(c)** quasi-irreversible behavior of the redox system. (adapted to *Trémillon 1993* [207])

Electrochemical characterization of a raw carbon felt

The cyclovoltammetric behavior of both negative ($Fe(CN)_6^{4-}$) and positive ($Ru(NH_3)_6^{3+}$) probes are first evaluated on an ideal platinum wire ($r = 0.25\ mm, L = 20\ cm$, geometric surface area $A_g = 3.14\ cm^2$) and compared to the cyclic voltammogram behavior obtained for a 1 cm^3 cubic carbon felt. As expected, $Fe(CN)_6^{3-}/Fe(CN)_6^{4-}$ and $Ru(NH_3)_6^{3+}/Ru(NH_3)_6^{2+}$ redox couples are reversible on **platinum wire** and the respective faradaic peaks are narrow and well-defined. For potentials lower than -0.2 V vs. Ag/AgCl/KCl, a sigmoidal wave is observable and attributed to the H^+/H_2 redox couple **(Figure 2.9)**. The peak potentials of oxidation and reduction

are independent of the scan rate of the experiment. Therefore, the ΔE_p is stable, at around 50 mV which is close to the limit ΔE_p for a reversible system (59 mV for a mono-electronic reaction at 25°C). The potential of oxidation and reduction peaks remains stable for $0 < v < 0.1\ V.s^{-1}$ **(Figure 2.10)**. The current intensity of the faradaic peaks evolves proportionally to the scan rate square root, $\sqrt{v}$ **(Figure 2.11)** following the Randles-Sevcik model.

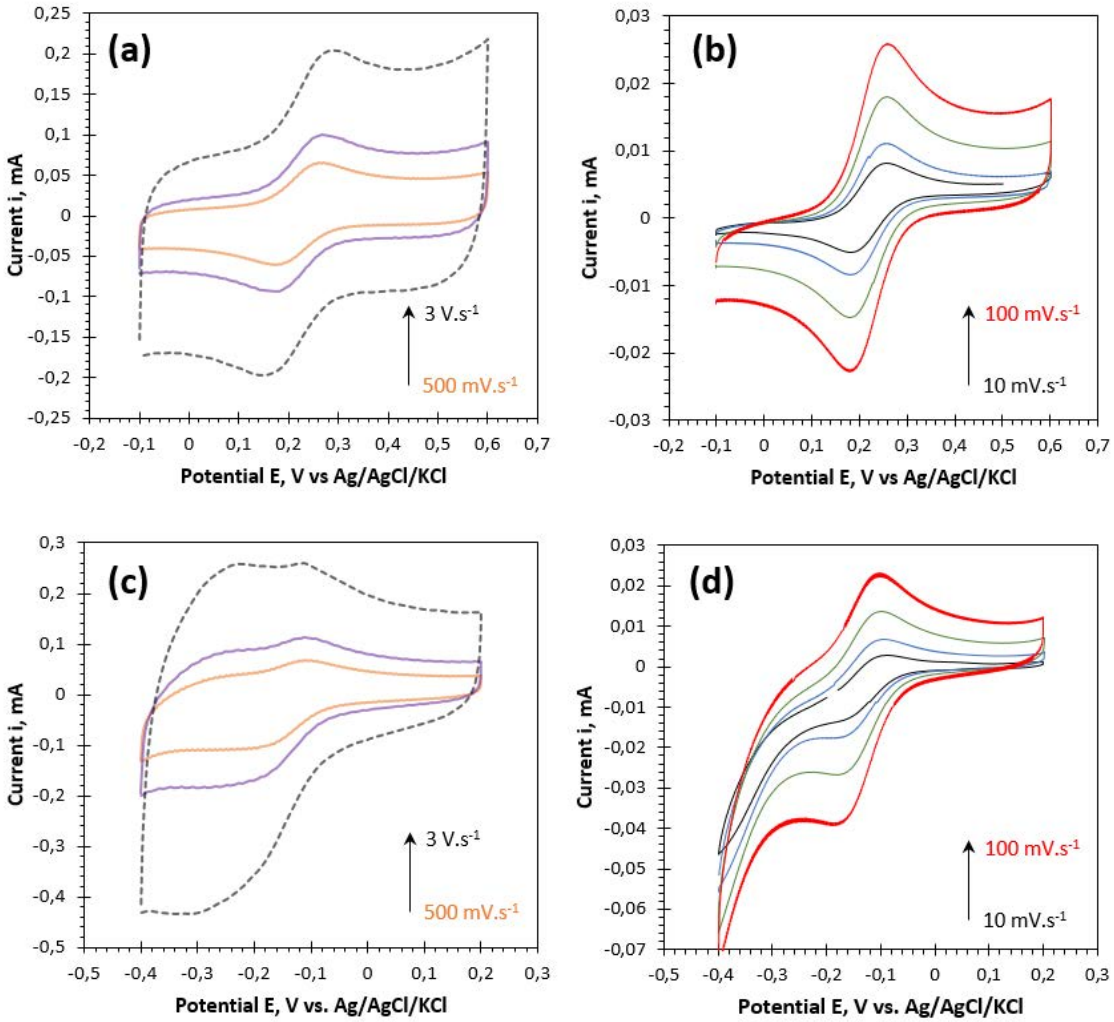

Figure 2.9 – Electrochemical characterization of a platinum wire as working electrode (WE). Platinum wire and Ag/AgCl/sat. KCl are respectively used as counter and reference electrodes: Cyclic voltammogram characterization against 0.3 mM $K_4Fe(CN)_6$ **(a-b)** and against 0.3 mM $Ru(NH_3)_6Cl3$ **(c-d)**.
Caption: **— 10 mV.s^{-1}** in black, **— 20 mV.s^{-1}** in blue, **— 50 mV.s^{-1}** in green, **— 100 mV.s^{-1}** in red, **— 500 mV.s^{-1}** in orange, **— 1 V.s^{-1}** in purple and **- - - 3 V.s^{-1}** in black (dotted line).

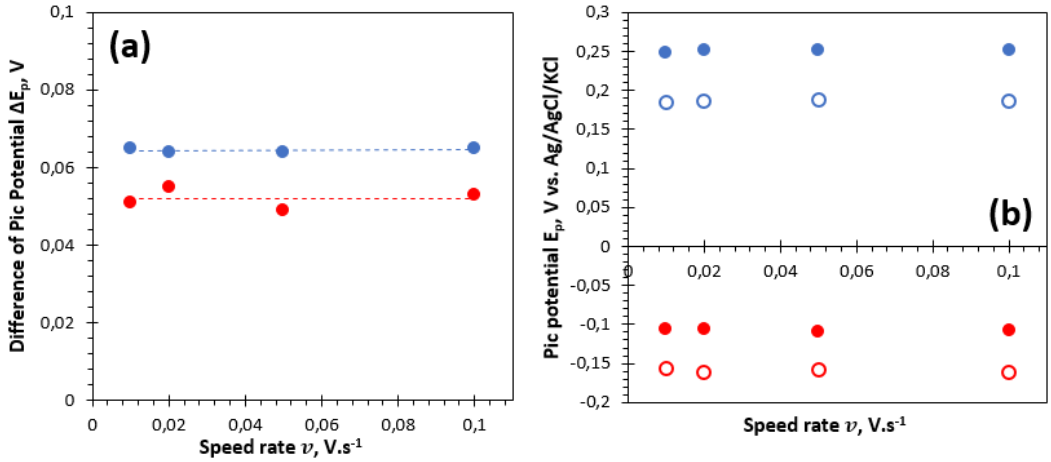

Figure 2.10 – Evolution of the difference of peak potential ΔE_p **(a)** and evolution of the pics potential **(b)** in function of the scan rate for a **platinum wire working electrode**. Based on the results of the **Figure 2.9.**
Caption: **(a)** • **$Fe(CN)_6^{4-}/Fe(CN)_6^{3-}$** redox couple, • **$Ru(NH_3)_6^{2+}/Ru(NH_3)_6^{3+}$** redox couple.
(b) • $Fe(CN)_6^{4-}$ oxidation, ○ $Fe(CN)_6^{3-}$ reduction, • $Ru(NH_3)_6^{2+}$ oxidation and ○ $Ru(NH_3)_6^{3+}$ reduction.

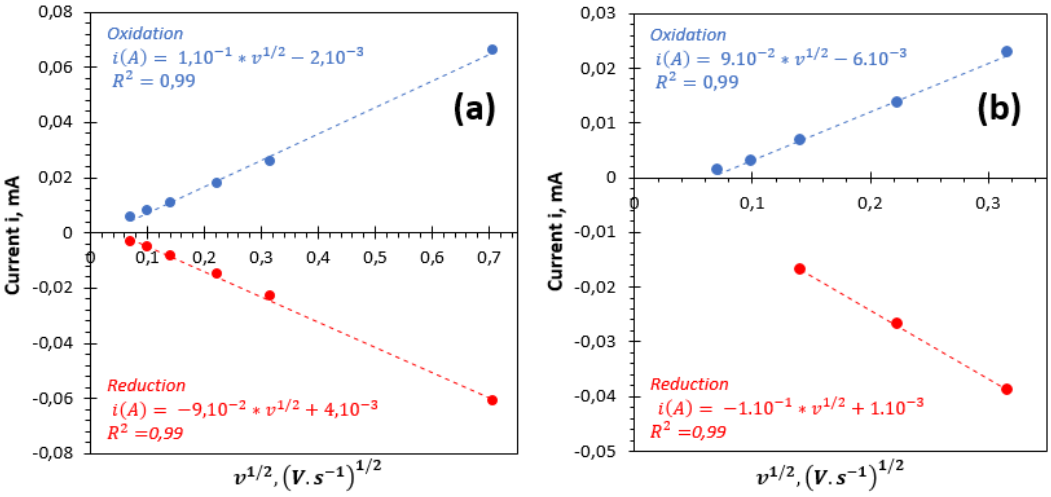

Figure 2.11 – Randles-Sevcik model applied to the maximum i_{pic} at the oxidation and reduction peak potentials based on the results of the **Figure 2.9 for a platinum wire** working electrode. Faradaic current for the redox couples: **(a)** $Fe(CN)_6^{3-}/Fe(CN)_6^{4-}$ ($K_3Fe(CN)_6$ probe) and **(b)** $Ru(NH_3)_6^{4+}/Ru(NH_3)_6^{3+}$ ($Ru(NH_3)_6Cl_3$ probe).

The pattern changes when using a **carbon felt** as working electrode. The couple of redox pics are wider than for a platinum wire electrode, but they remain characteristic of a reversible reaction **(Figure 2.12.e, Figure 2.12.f)**. The potential of reduction (E_{pic}^{red}) and oxidation (E_{pic}^{ox}) decreases and increases, respectively, with the scan rate square root **(Figure 2.14.b)**. As a consequence, the DPP increases with $\sqrt{v}$. The Ru-based probe appears less sensitive to the ΔE_p increases than Fe-based probes **(Figure 2.14.a)**. Moreover, at high scan rate (> 100 $mV.s^{-1}$), in presence of faradaic probes, an elliptic pattern with a slope of ca. 45° is observable **(Figure 2.12.c, Figure 2.12.d)**. In the absence of probes, the monitored capacitive current at high scan rate is squared and characteristic, which means that the elliptic current measured in presence of probes is faradaic and results from a charge transfer. Thus, this elliptic signal is not representative of a resistive behavior. However, for $v \leq 100\ mV.s^{-1}$ the current intensity of the faradaic peaks linearly increases with $\sqrt{v}$ **(Figure 2.13)**. Considering a mono-electronic

reaction $n = 1$ $(Fe(CN)_6^{4-} = Fe(CN)_6^{3-} + e^-$ and $Ru(NH_3)_6^{2+} = Ru(NH_3)_6^{3+} + e^-)$, a concentration of probes of 0.33 10^{-6} mol.cm^{-3} and the diffusion coefficient of iron (D_{Fe} = 0.77 10^{-5} cm².s^{-1}) and ruthenium (D_{Ru} = 0.55 10^{-5} cm².s^{-1}) from the literature, the faradaic surface area is determined from the Randles-Sevcik model [204,208]. The calculated faradaic surface area is equal to ca. 138 cm² for the $K_4Fe(CN)_6$ probe and ca. 111 cm² for the $Ru(NH_3)_6Cl_3$ which correspond to 56% (A_c = 240 cm², **Figure 2.13.a**) and 40% (A_c = 280 cm², **Figure 2.13.b**) of the capacitive surface area, respectively.

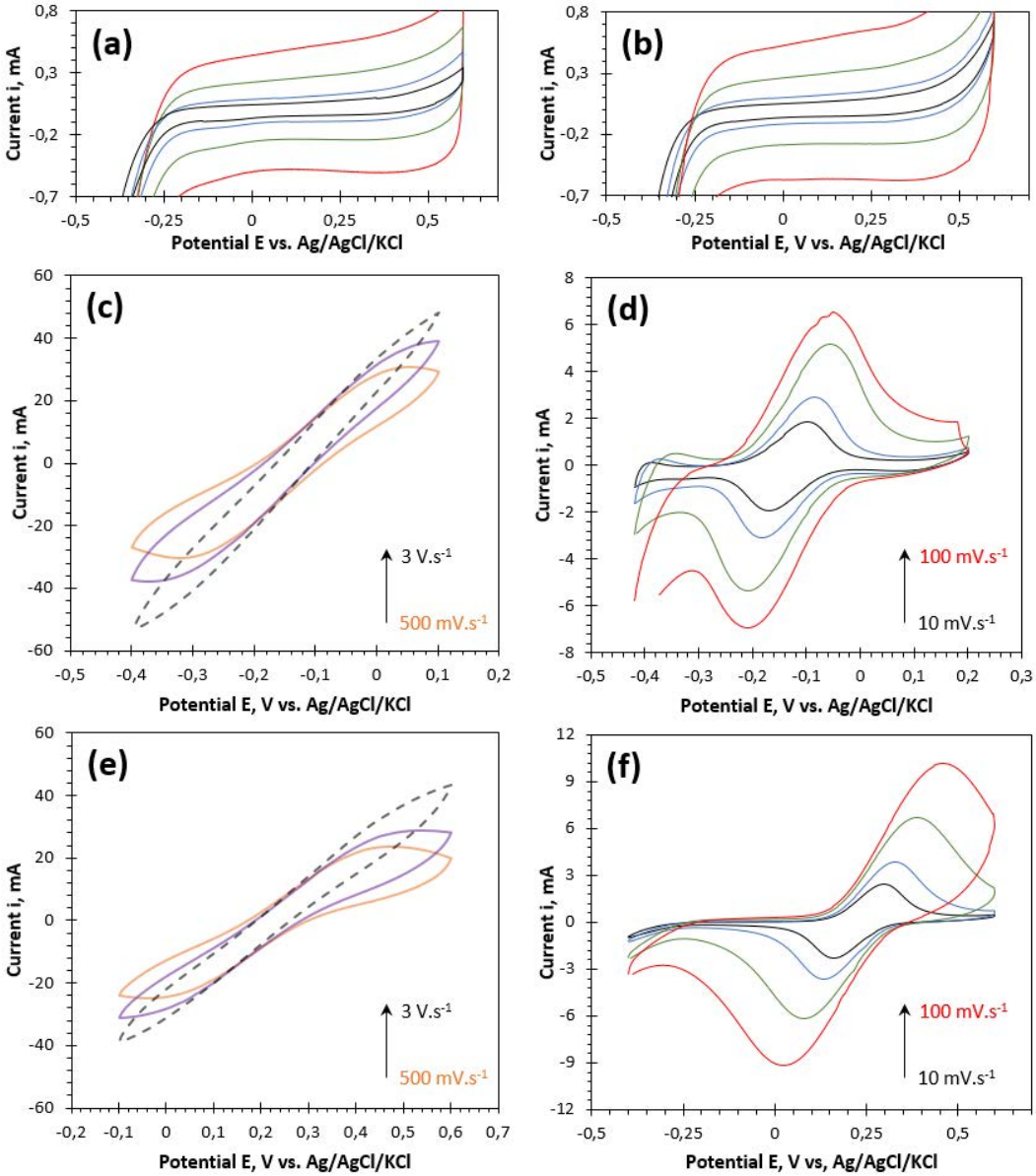

Figure 2.12 – Electrochemical characterization of a 1 cm³ raw carbon felt as working electrode (WE). Platinum wire and Ag/AgCl/sat. KCl are respectively used as counter and reference electrodes:
(i) Cyclic voltammogram of the capacitive current of the WE_1 used for characterization against $K_4Fe(CN)_6$ **(a)** and of the WE2 used for characterization against $Ru(NH_3)_6Cl3$ **(b)**. Both electrodes are immersed in a solution of 130 mM NaCl. (ii) Cyclic voltammogram of the faradaic response against electrochemical probes: **(c, e)** WE1 immersed in a solution of 130 mM NaCl and *0.3 mM of $K_4Fe(CN)_6$*. **(d, f)** WE_2 immersed in a solution of 130 mM NaCl and *0.3 mM of $Ru(NH_3)_6Cl_3$*.
Caption: **— 10 mV.s^{-1}** in black, **— 20 mV.s^{-1}** in blue, **— 50 mV.s^{-1}** in green and **— 100 mV.s^{-1}** in red, **— 500 mV.s^{-1}** in orange, **— 1 V.s^{-1}** in purple and **- - - 3 V.s^{-1}** in black (dotted line).

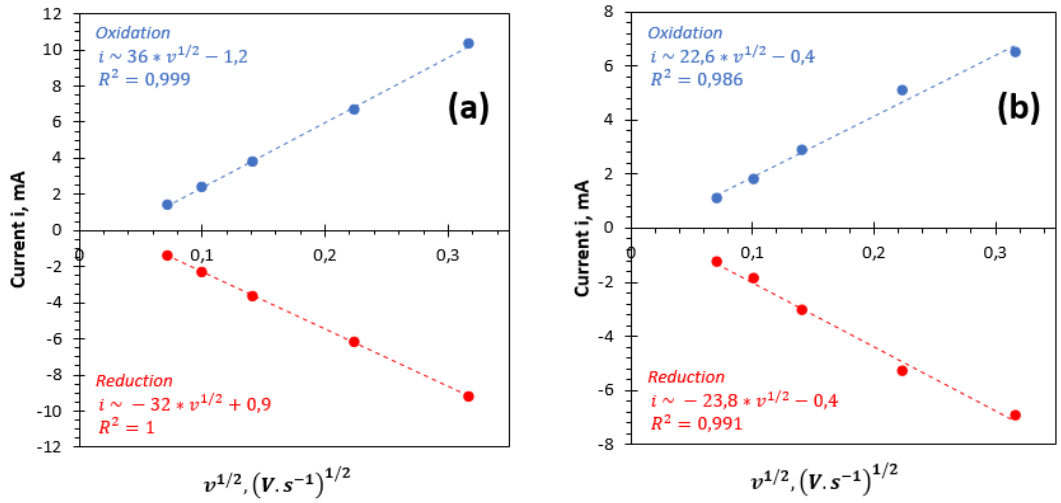

Figure 2.13 – Randles-Sevcik model applied to the maximum i_{pic} at the oxidation and reduction peak potentials based on the results of the *figure 2.8* **for a carbon felt** working electrode. Faradaic current for the redox couples: **(a)** $Fe(CN)_6^{3-}/Fe(CN)_6^{4-}$ ($K_3Fe(CN)_6$ probe) and **(b)** $Ru(NH_3)_6^{4+}/Ru(NH_3)_6^{3+}$ ($Ru(NH_3)_6Cl_3$ probe).

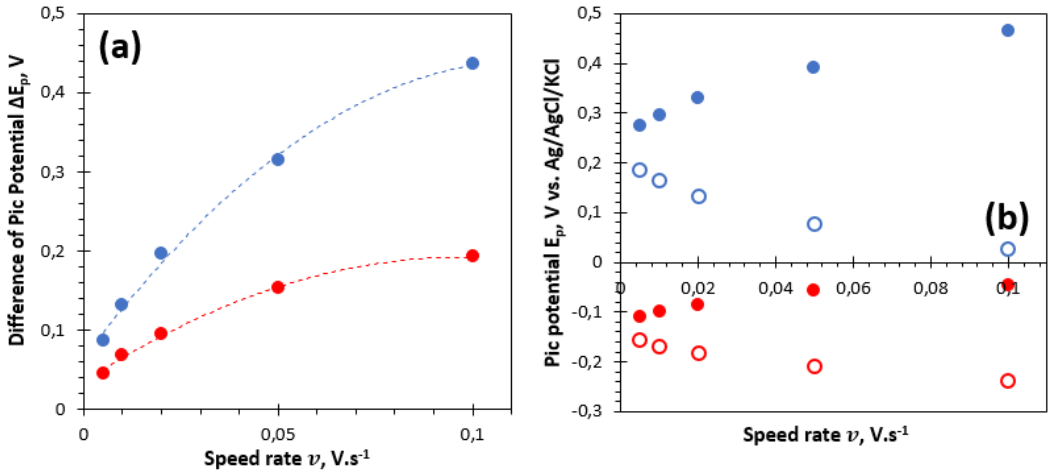

Figure 2.14 – Evolution of the difference of peak potential ΔE_p (a) and evolution of the pics potential (b) in function of the scan rate for a **carbon felt working electron**.
Caption: (a) • **$Fe(CN)_6^{4-}/Fe(CN)_6^{3-}$** redox couple in blue, • **$Ru(NH_3)_6^{2+}/Ru(NH_3)_6^{3+}$** redox couple in red.
(b) • **$Fe(CN)_6^{4-}$ oxidation**, ○ **$Fe(CN)_6^{3-}$ reduction** in blue, • **$Ru(NH_3)_6^{2+}$ oxidation** and ○ **$Ru(NH_3)_6^{3+}$ reduction** in red.

The peak potential deviation, the lowest proportionality of the current intensity of the faradaic peaks with scan rate (cycling duration) and the elliptic pattern at high scan rate all indicate a non-ideal redox reactivity at the surface of the carbon felt. $Fe(CN)_6^{3-}/Fe(CN)_6^{4-}$ and $Ru(NH_3)_6^{3+}/Ru(NH_3)_6^{2+}$ are two highly-reversible redox couples and, cyclic voltammetry as confirmed on the platinum electrode. As a consequence, these observations on carbon felt working electrode are not due to the redox system but can be attributed to the interactions between the surface and the probes. The carbon felt presents the advantage of a high specific surface area and porosity, but the hydrophobicity of the carbon leads to its low wettability by an aqueous electrolyte. A likely explanation of the Ep deviation is a slower circulation and renewal of the faradaic species into the felt, notably due to the hydrophobicity of the carbon and the tortuosity the fibers architecture. As a consequence of a slower mass transfer, the

products of reaction may accumulate for a longer duration near the surface, inducing an increasing of the over potential and a lack in reversibility.

2.2.3.3. Hydrophilic treatment effect on the faradaic current.

Despite the use of carbon felt as an electrode for electrochemistry, the carbon hydrophobicity makes the diffusion of the electrolyte toward the felt more difficult than in a hydrophilic architecture. The objective of this part is to evaluate the interest of a hydrophilic treatment of a carbon felt foreseeing its use in aqueous media. Treated carbon felt and raw carbon felts will be compared in term of structure and electrochemistry. Two surface treatments were undertaken: (i) an acid attack to form hydrophilic groups (−OH, −COOH) at the surface of the carbon to increase the wettability of the carbon surface. However, the formation of hydrophilic groups creates defaults in the highly conjugated carbon atomic architecture. A degradation of electronic conductivity can be observed at the carbon fiber surfaces. (ii) The deposition of a hydrophilic polymer at the surface of the fibers to create hydrophilic anchor in the fibers architecture. However, such a coating may decrease the accessibility of the faradaic species to the conductive network.

(i) **Acid treatment.** Cubic carbon felt electrodes are immersed in concentrated nitric acid (70%) for 24h. The treated cubic carbon felts are washed with water until neutralization. Then, the felts are dried to remove the residual traces of acid, sterilized in an autoclave, immersed in a sterile PBS buffer and stored at 4°C.

(ii) **Polymer treatment.** The objective is to entirely or partially cover the carbon fibers with a hydrophilic polymer to facilitate the diffusion of an aqueous electrolyte through the felt [133]. A protocol was previously developed to cover the fibers with sodium alginate, a natural and biocompatible polymer. First, the carbon felt is immersed in ethanol (95%) to remove air from the felt porosity (95 v.% of felt volume). Then the ethanol-loaded carbon felt is immersed in a solution of water and glycerol (75:25 ratio) for 1h30 under stirring. This intermediary mobile phase is necessary since sodium alginate is not soluble in ethanol. Then, the water/glycerol-containing felt is immersed into a 1 wt.% sodium alginate aqueous solution for 1h30 under stirring. During this three steps, the felt is manually compressed to facilitate the impregnation by the mobile phase. Finally, the treated carbon felt is rinsed and dried at 90°C for 24h.

Both the treated carbon felts instantaneously sink in water, PBS or MR1 (growth culture medium, see 2.3.1) medium revealing an enhanced diffusion of the electrolyte into the felt **(Figure 2.15)**. The carbon felt treated with sodium alginate remains hydrophilic after a long period in humid or dried atmosphere. SEM imaging revealed that the carbon fibers are not entirely covered with sodium alginate **(Figure 2.16)**. They present a patchy covering with sodium alginate pieces **(Figure 2.16.a)** or ribbons **(Figure 2.16.b)** between or around them. The alginate acts as a glue and agglomerates the fibers **(Figure 2.16.c, Figure 2.16.d)**. This configuration may imply a loss in active surface area. In parallel, it was checked by SEM that the micro-architecture of the carbon felt treated by acid attack was similar to the raw carbon felt micro-structure (data not shown).

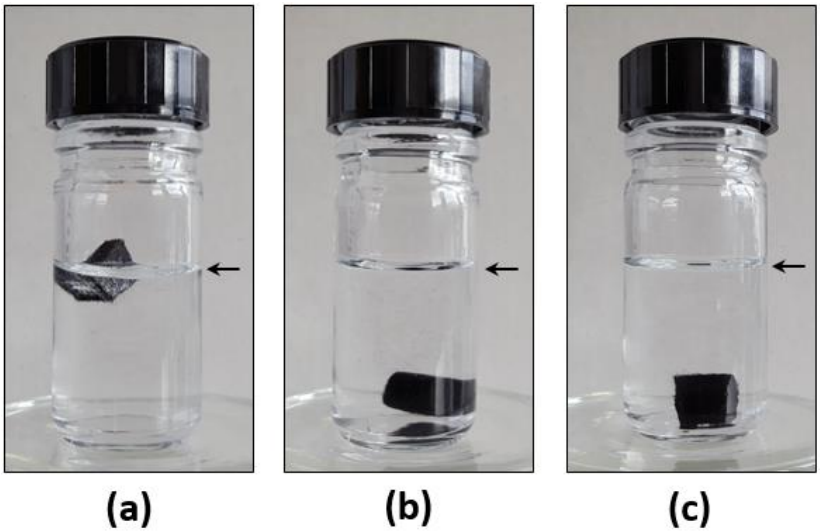

Figure 2.15 – Immersion of the raw and treated carbon felts in Milli-Q water: **(a)** raw hydrophobic carbon felt and hydrophilic carbon felt treated by **(b)** sodium alginate deposition on the carbon fibers, or by **(c)** acid attack the carbon fibers surface.

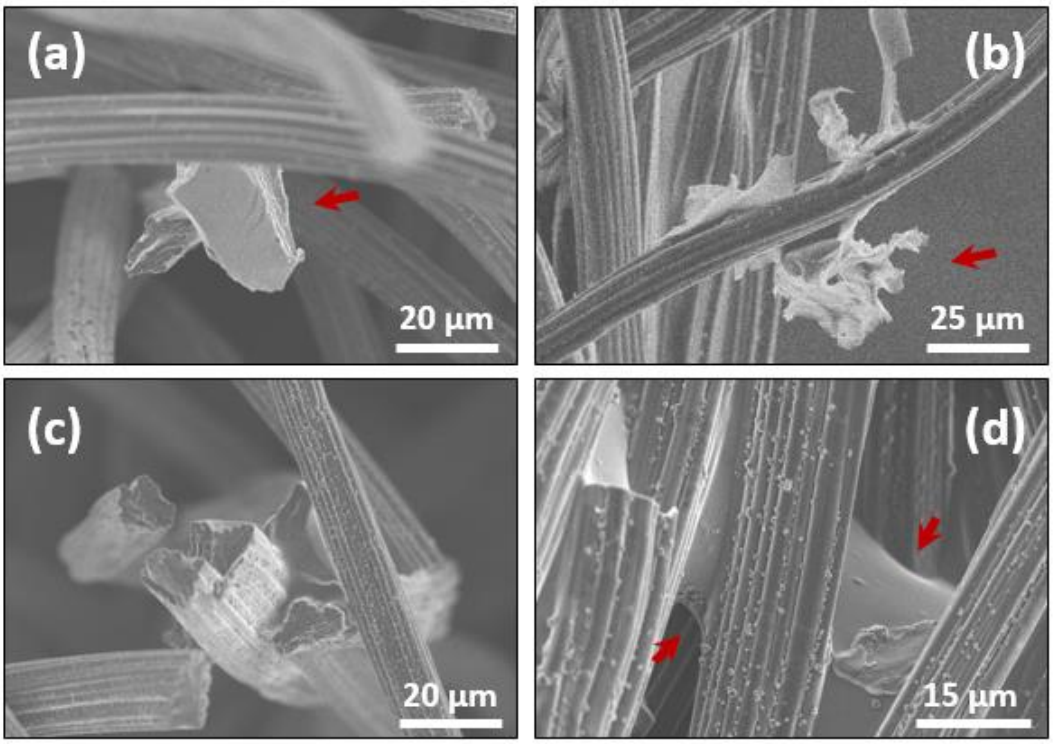

Figure 2.16 – SEM observation of a **dry** carbon felt after a polymer hydrophilic treatment. **(a, b)** Sodium alginate agglomerate on a fiber. **(c, d)** effect of the sodium alginate on fibers agglomeration, the polymer act as a glue between the fibers **(d)**. Red arrows indicate visible sodium alginate.

To characterize the treatment effect on the electrochemical behavior, the electro-reactivity is evaluated by cyclic voltammetry on a control raw felt, and on both treated carbon felts with a positive and a negative probe. The raw and modified carbon felt are mounted as a working electrode in a three-electrodes reactor with a platinum wire as a counter electrode and an Ag/AgCl/KCl reference. Capacitive surface areas are calculated individually based on the cyclic voltammogram obtained for a 130 mM NaCl electrolyte for the control raw electrode (A_c = 120 cm²), the electrode treated with sodium alginate (A_c = 250 cm²) and nitric acid-treated one

(A_c = 90 cm²). The monitored current is normalized by the capacitive surface area corresponding to the electrode tested. The concentration of probes is fixed at 0.33 mM.

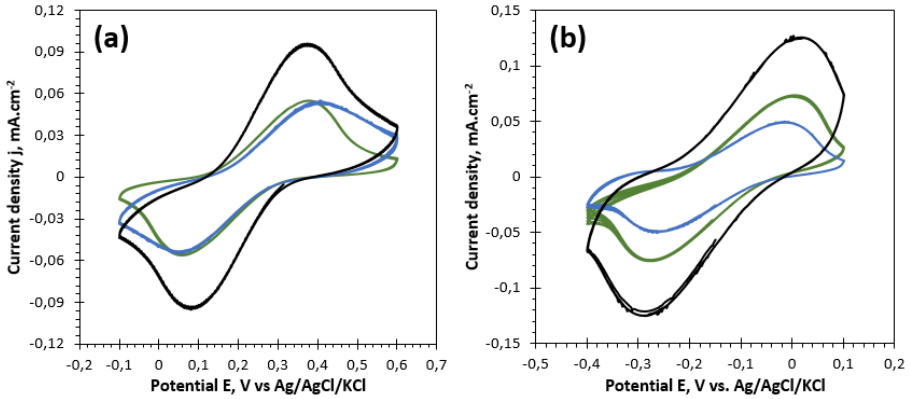

Figure 2.17 – Effect of a hydrophilic treatment of a 1 cm3 carbon felt on the surface reactivity. Cyclic voltammogram at *100 mV.s^{-1}* against **(a)** a negative redox probe ($Fe(CN)_6^{3-}/Fe(CN)_6^{4-}$) and **(b)** a positive redox probe ($Ru(NH_3)_6^{4+}/Ru(NH_3)_6^{3+}$). Currents normalized by specific surface areas ($j = i_{measured}\kappa v/i_{capacitif}$, with $\kappa = 0.2\ F.m^{-2}$ and $v = 100\ mV.s^{-1}$). Currents are normalized by the capacitive surface area (A_c) based on an initial cyclo voltammetry in a 130 mM NaCl electrolyte.
Two hydrophilic treatments are compare to a raw carbon felt: — hydrophobic **raw carbon felt** in black (A_c = 120 cm²). — carbon felt treated with **sodium alginate** in blue (A_c = 250 cm²). — carbon felt treated with **HNO_3** in green (A_c = 90 cm²).

The redox reversibility (DPP, ΔE_p), the peak potential deviation and the current intensity of redox peaks vary as a function of the treatment applied to the felt and of the probe charge **(Figure 2.17)**. **For a negative probe ($K_4Fe(CN)_6$)**, the normalized faradaic current densities of oxidation decrease by 48% for the carbon felt treated with nitric acid (HNO_3_CF) and by 51% for carbon fibers coated with sodium alginate (Alginate_CF) in comparison with the raw carbon felt **(Figure 2.17.a)**. Both hydrophilic treatments lead to the accumulation of negative charges (negatively charged polymer or functional groups, −COOH or −OH) which make the surface more repulsive for negatively-charged faradaic species. Moreover, the DPP increases from 260 mV for the raw carbon felt to 309 mV for the Alginate_CF and to 316 mV for the HNO_3_CF which means a loss of reversibility. This is most likely due to the creation of hydrophilic defaults (−OH, −COOH) or the partial isolation of the fibers by a non-conductive polymer. On the contrary, for **a positive probe ($Ru(NH_3)_6Cl_3$)**, there is no equivalence in term of faradaic current intensity between the treatments **(Figure 2.17.b)**. The loss in current density $\%j_{loss}$ ($mA.cm^{-2}$) in comparison with the current measured for a raw carbon felt is about 44% for the HNO_3_CF and 75% for the Alginate_CF **(Figure 2.18.b)**. Adhesion phenomena may explain the loss of current density for the HNO_3_CF. The positively charge oxidant or reducer can be adsorbed electrostatically on the negatively-charged surface and obstructs the access of the faradaic surface to fresh redox species. As a consequence, the mass transfer may be limited. In term of redox reversibility, the DPP slightly decreases from 311 mV (raw carbon felt) to 297 mV (HNO_3_CF) and 227 mV (Alginate_CF). The enhancement of the reversibility can be explained by the trapping of the faradaic species in the hydrophilic carbon felt structure. In this case, mass transport is less damageable due to the direct availability of the redox species closed to the fibers **(Figure 2.18.a)**.

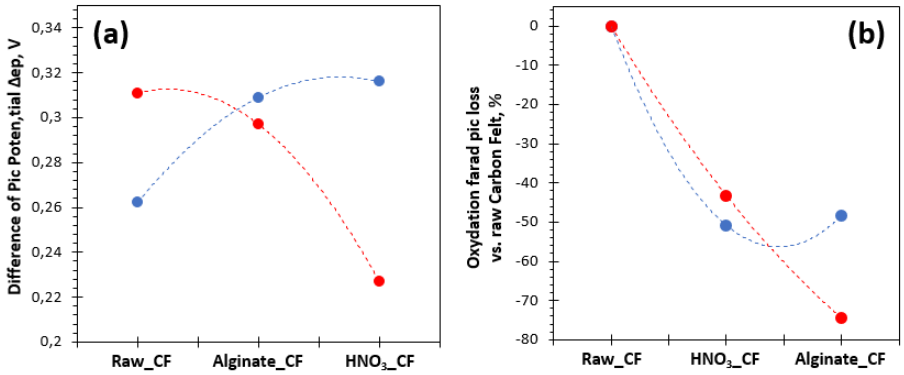

Figure 2.18 – Evaluation of the redox reversibility in function of the hydrophilic treatment **(a)** and evaluation of the loss in the oxidation peak intensity ($j_p\ A.cm^{-2} = j_p^{ox,\ treated\ CF} - j_p^{ox,\ raw\ CF}$ *and* $\%j_{loss} = (j_p - j_p^{raw\ CF})/j_p^{raw\ CF}, noralized\ by\ A\_c$) vs. raw carbon felt **(b)**. Results based on the data of the **figure 2.17**. Caption: • $K_4Fe(CN)_6$ in blue, • $Ru(NH_3)_6Cl_3$ in red. *Alginate_CF means carbon felt treated with Na-alginate.*

In conclusion, both hydrophilic treatments have already proved their ability to overcome the carbon felt hydrophobicity. The HNO_3_CF and the Alginate_CF sink in aqueous medium without forced impregnation, while raw carbon felt floats over or just under the surface of the aqueous solution. In this case, it is necessary to compress the felt a few times to overcome the hydrophobicity of the carbon and to allow the diffusion of the aqueous electrolyte inside the felt. After a few hours (> 10h) the raw carbon felt sinks in the aqueous solution. However, the positive effect of the hydrophilic treatment on the electrochemical properties of the carbon felt is not confirmed. The current density at E_p dramatically decreases for treated carbon felts (from 44% to 75% of the $j_p^{raw\ CF}$). This decrease is dependent of the nature of the redox couple and involves several complex, probably competitive, phenomena. In particular, hydrophilization appears to favor electrolyte diffusion in the bulk (i.e. within the pores) of the felts but are detrimental to their interaction with their surface (i.e. with the fibers). From now on, the carbon felts used in all the experiments are untreated and immersed in the electrolyte for 10 to 20 hours before use to improve the diffusion of the aqueous media and therefore of the bacteria or cathodic redox species.

2.2.3.4. Dimensional effect and probes concentration effect.

The dimension of the carbon felt electrode influences the electrode capacitive surface area and the electrode weight. To evaluate the dimensional effect of the felt on redox reaction yield, five volumes of carbon felt are evaluated in a three-electrodes configuration (against a platinum wire). For all the volumes tested, the thickness is kept at 1 cm, the length and the width are varied as indicated in **Table 2.1**.

Electrode no	Volume, cm^3	Thickness, cm	Length, cm	Width, cm
1	0.25	1	0.5	0.5
2	0.5	1	0.5	1
3	1	1	1	1
4	1.5	1	1.5	1
5	2	1	2	1

Table 2.1 – Selected carbon felt geometry.

Both capacitive surface area and weight of the felt samples increase linearly with the geometric volume of electrode. On the contrary, the non-normalized faradiac current i_p increases until an electrode volume of 1.5 cm^3, from ca. 2 mA to ca. 17 mA for a probe concentration of 0.75 mM. For higher volumes the current goes down **(Figure 2.19.a)**. The mass current density and the surface current density are respectively determined by the ratios $j_p^{mass}(mA.mg^{-1}) = i_p/m_{CF}$ and $j_p^{surface}(mA.cm^{-2}) = i_p/A_c$, with m_{CF} the weight of the carbon felt in mg and A_c the capacitive surface area in cm². These ratios reveal an optimum of current density at 0.15 mA.mg^{-1} and 0.18 mA.cm^{-2} for an electrode volume of 1 cm^3. Thus, even if the currents are normalized, a variation is clearly observed and confirms a dimensional effect on the diffusion of the electrolyte through the felt. The electrodes are immersed but the impregnation happens naturally. If the felts are not compressed to observed the real effect of both carbon hydrophobicity and fibers architectures. In the felt is compressed, the phenomena observed are forced. Moreover, in natural diffusion condition, the observed diffusion corresponds to the diffusion of electrolyte into compressed carbon felt after several hours of immersion. The same observations were made with a positive probe ($Ru(NH_3)_6Cl_3$) (data not shown). Furthermore, the effect of the probes concentration has been investigated in order to determine if in the conditions of experiment, the quantity of probes is correctly set. By decreasing the concentration from 0.75 mM to 0.33 mM (2.3 times less concentrated electrolyte), the measured current density linearly decreases by a factor between 2 and 3 in accordance with the concentration variation **(Figure 2.19.b)**.

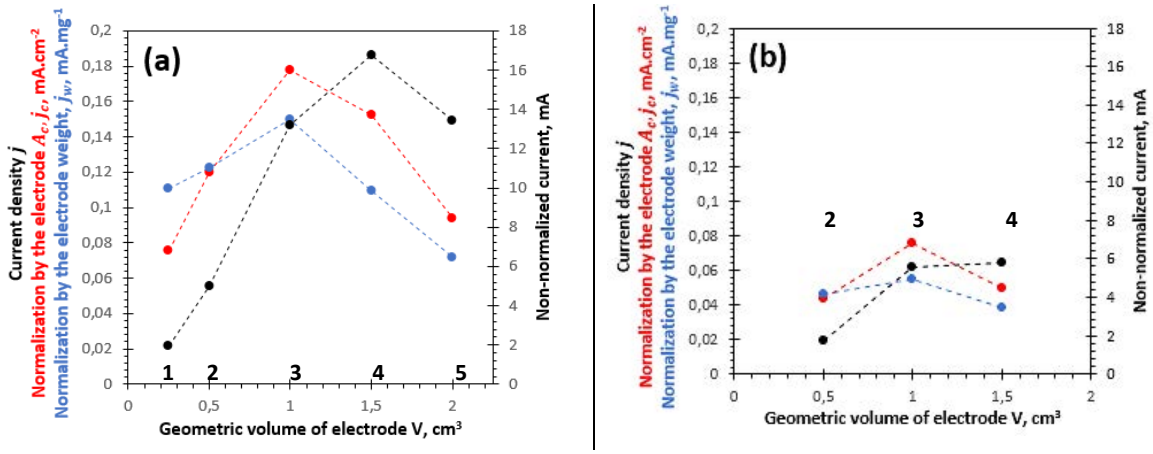

Figure 2.19 – Effect of the carbon felt electrode dimension and of the probe ($K_4Fe(CN)_6$) concentration: **(a)** 0.75 mM and **(b)** 0.33 mM. **The carbon felts are not treated**. The measured current density is the addition of the faradaic and the capacitive currents $(j_p = j_p^{capa} + j_p^{fara})$ and the capacitive current is negligible in comparison with the faradaic current: $j_p^{capa} \cong 2\% \ll j_p^{fara} \Rightarrow j_p \cong j_p^{fara}$. By multiplying the concentration by 2.3, the current is increased by a factor comprised between 2 and 3. Caption: faradaic current of oxidation at $j_p^{ox}(E_{pic}^{ox})$:
• **non-normalized** in black. • **normalized by capacitive surface area** in red. • **normalized by the electrode weight** in blue.

As previously mentioned, the fiber organization differs over the felt volume. The fibers are randomly organized on the top and the bottom of the felt. Perpendicularly to the horizontal plan, the fibers are « woven » and organized in a preferential direction **(Figure 2.6)**.

Taking as hypothesis that the woven organization is equivalent to a network of linear channel (between the woven fibers), it will promote electrolyte diffusion from the peripheral surface to the carbon felt core.

Increasing the planar dimension of carbon felt, the peripheral surface (woven structure) progressively became less predominant in comparison with the horizontal surface. In this condition, the beneficial effect of the diffusive channel corresponding to the woven fibers organization perpendicularly to the horizontal plan is counterbalancing by increasing the channels length. The core of the felt, where most of the fibers density is, remains inaccessible to the electrolyte.

Additionally, the same measurements have been carried out with a hydrophilic treated carbon felt by sodium alginate deposition (in liquid phase) and an electrolyte concentrated in $K_4Fe(CN)_6$ at 0.33 mM **(Figure 2.20)**. Considering the non-normalized current, the mass density of current decreases from ca. 50 µA.mg^{-1} (equivalent to the raw carbon felt) at 0.5 cm^3 to ca. 30 µA.mg^{-1} at 1.5 cm^3. This loss in current density is related to the alginate deposited on the fibers which increase the weight of the electrode. The surface current density slightly decreases from 24 µA.cm^{-2} to 18 µA.cm^{-2}. This quite stable density of current without high dependence on the geometrical features of the felt may be related to the hydrophilic treatment which promotes the electrolyte diffusion in the entire carbon felt. In comparison to the raw carbon felt, here the current densities are lower because of the resistivity added by the patchy repartition of alginate and the previously described adhesion and trapping phenomena.

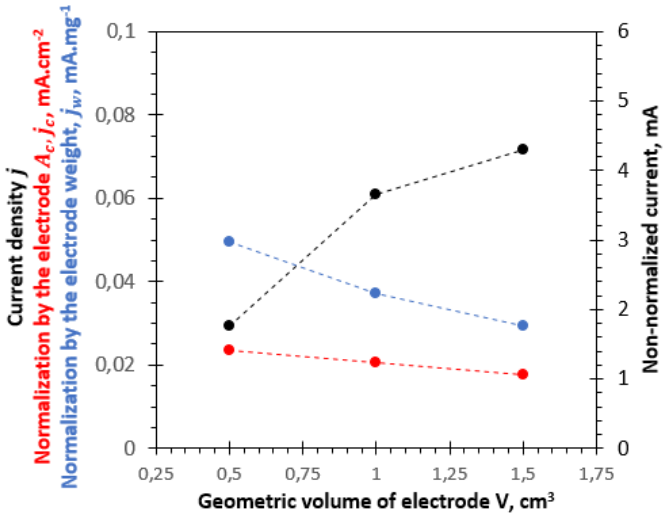

Figure 2.20 – Effect of the carbon felt electrode dimension for a probes ($K_4Fe(CN)_6$) concentrated at 0.33 mM. **With a hydrophilic treatment based on sodium alginate** deposition on the fibers, there is no optimal geometry at Length = 1 cm, Width = 1 cm and Thickness = 1 cm. $j_p^{capa} \cong 2\% \ll j_p^{fara} \Rightarrow j_p \cong j_p^{fara}$ (cf. figure 2.19).
Caption: faradaic current of oxidation at $j_p^{ox}(E_{pic}^{ox})$: • **non-normalized** in black. • **normalized by capacitive surface area** in red. • **normalized by the electrode weight** in blue.

2.3. BACTERIA GROWTH CONDITIONS AND ACCLIMATION

The electroactive bacterium strain *Shewanella oneidensis* (CRBIP 17.141) is provided by the Biological resource center of the Pasteur Institute and selected due to its well-known ability

to produce and transfer electrons based on the degradation of short organic molecules such as lactate or glucose. Moreover, in the scope of the electroactive (or exoelectrogenic) bacterium, *Shewanella oneidensis* is an aero-anaerobic optional strain able to grow in presence or absence of oxygen which is supposed to change its electrochemical behavior. This ability suggests different possible pathways to culture *Shewanella oneidensis* strain depending on the presence of pure or multiple carbon sources, electron donors (lactate, glucose, …) and electron acceptors (oxygen, fumarate, …). To evaluate the biological growth of *Shewanella oneidensis* strain under aerobic and anaerobic conditions and to implement an efficient and reproducible growth, a protocol was set up based on the previous work of Bretscheger [92] and Baron [77,209]. The growth protocol was divided in two parts: the microbial pre-culture phase and the microbial culture phase.

2.3.1. Media and solutions for growth.

Luria-bertani broth medium: Tryptone (10 $g.L^{-1}$), Yeast Extract (5 $g.L^{-1}$), NaCl (5 $g.L^{-1}$) in milli-Q water, pH 7 (LB Broth Lennox from sigma-aldrich). Sterilization by autoclaving at 120°C for 20 min and then by ultrafiltration on a 0.2 µm sterile membrane.

Medium for strain conservation at -80°C: 20% of Luria-bertani (LB) broth and 30% of glycerol in milli-Q water, pH 7. Sterilization by autoclaving at 120°C for 20 min and then by ultrafiltration on a 0.2 µm sterile membrane.

Basal MR1 medium:

(i) NH_4Cl (8.5 mM, 0.46 $g.L^{-1}$), K_2HPO_4 (1.3 mM, 0.225 $g.L^{-1}$) , $MgSO_4.7H_2O$ (0.23 mM, 0.057 $g.L^{-1}$), KH_2PO_4 (1.6 mM, 0.225 $g.L^{-1}$) and $(NH_4)_2SO_4$ (1.7 mM, 0.225 $g.L^{-1}$) are dissolved in milli-Q water. The raw medium is supplemented with 0.1 vol.% of a solution of trace elements and a solution of selenite. Sterilization is performed by autoclaving at 120°C for 20 min.

(ii) At room temperature, 0.1 vol.% of a solution of vitamins and a solution of amino acids mare added to the medium.

(iii) MR1-L medium: MR1 medium supplemented with 30 mM of sodium lactate as sole arbon source and electron donor.

(iv) MR1-L/F: MR1 medium supplemented with 30 mM of sodium lactate (carbon source and electron donor) and 30 mM of sodium fumarate as sole (anaerobic condition) or co-electron donor (aerobic condition).

(v) The pH is adjusted at 7 and a final sterilization is performed by ultrafiltration on a 0.2 µm sterile membrane.

Solution of trace elements (in milli-Q water): Na_2-$EDTA.2H_2O$ (8.1 µM, 3 $g.L^{-1}$), $FeSO_4.7H_2O$ (4 µM, 1.1 $g.L^{-1}$), $CoCl_2.6H_2O$ (0.8 µM, 190 $mg.L^{-1}$), $ZnCl_2$ (0.31 µM, 42 $mg.L^{-1}$), $NiCl_2.6H_2O$ (0.1 µM, 24 $mg.L^{-1}$), $Na_2MoO_4.2H_2O$ (0.087 µM, 18 $mg.L^{-1}$), H_3BO_4 (4.8 µM, 300 $mg.L^{-1}$), $CuCl_2.2H_2O$ (0.01 µM, 2 $mg.L^{-1}$), $MnCl_2.4H2O$ (0.25 µM, 50 $mg.L^{-1}$). Adjust pH to 6.5 before sterilization by autoclaving at 120°C for 20 min.

Solution of selenite (in milli-Q water): NaOH (12.5 µM, 500 $mg.L^{-1}$), $Na_2SeO_3.5H_2O$ (11.4 µM, 3 $mg.L^{-1}$), $Na_2WO_4.2H_2O$ (12.1 µM, 4 $mg.L^{-1}$) . Sterilization by autoclaving at 120°C for 20 min.

Solution of vitamins (in milli-Q water): 4-aminobenzoic acid (0.29 µM, 4 mg.L^{-1}), D-(+) biotin (0.041 µM, 1 mg.L^{-1}), nicotinic acid (0.81 µM, 10 mg.L^{-1}), Ca-(+) pantothenate (0.21 µM, 5 mg.L^{-1}), Pyridoxamine dihydrochloride (0.41 µM, 10 mg.L^{-1}), Thiaminium dichloride (0.29 µM, 10 mg.L^{-1}), Riboflavin (1.32 µM, 50 mg.L^{-1}). Sterilization by ultrafiltration on 0.2 µm sterile membrane.

Solution of amino acids (in milli-Q water): L-glutamic acid (13.6 mM, 2 g.L^{-1}), L-arginine (11.5 mM, 2 g.L^{-1}), DL-serine (19.6 mM, 2 g.L^{-1}). Sterilization by ultrafiltration on 0.2 µm sterile membrane.

2.3.2. Growth protocol

2.3.2.1. Preparation of the pre-cultures.

Shewanella oneidensis bacteria from the strain CRBIP 17.141 are stored at -80°C in 1.5 mL of a conservative medium made of Luria-Bertani (20%) broth and glycerol (30%). A fraction of *S. oneidensis* strain is inoculated in 10 mL of oxic and sterile Luria-Bertani (LB) broth medium for 24h at 30°C and 150 rpm. 100 µL of this first pre-culture is then sub-cultured in 10 mL of fresh oxic LB broth medium for 24h in the same conditions. This step serves to replace the dead or non-cultivable bacteria by an intense multiplication of cultivable bacteria. Moreover, it increases the bacteria density to fix the density of bacteria inoculated and to limit the lag-phase during the growth.

2.3.2.2. Preparation of the culture and growth curve determination.

50 mL of growth medium (MR1, MR1-L or MR1-L/F) is inoculated at 2% (or 1%) with 1 mL (or 2 mL) of pre-cultivated cells suspended in the same medium. Bacteria are cultured in sterile flasks (75 cm^2, max. 200 mL) for at least 30h at 30°C and 150 rpm. The density of cells is determined by measuring the optical density of the culture at 600 nm (OD_{600}) with a spectrophotometer and the growth curve is obtained by measuring and plotting the OD_{600} as function of the culturing time.

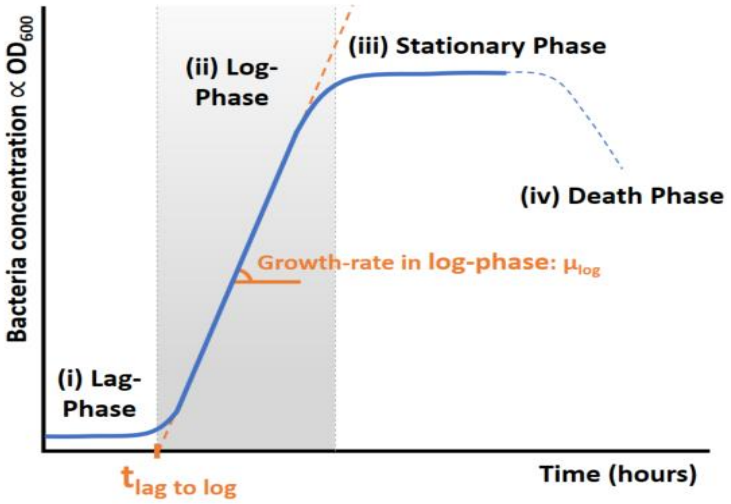

Figure 2.21 – Growth curve model for micro-organisms.
(i) Lag-phase, µ = 0. (ii) Log-phase, µ max. (iii) Stationary phase, µ = 0. (iv) Death phase, µ < 0

In batch cultivation (limited amount of nutrient initially added without medium renewal), the growth curve is composed by four phases **(Figure 2.21)**: (i) the lag-phase characterized by a zero-growth rate (μ = 0) in which inoculated bacteria are maturing for future division. They adapt themselves to new growth medium and conditions. The age of the used pre-cultured influences the lag-phase duration since older bacteria have to restore their physiology before multiplication. (ii) The log-phase in which the growth rate is maximized and constant. During this period, bacteria multiplication is exponential and most of the bacteria are viable. Thereafter, the constant growth-rate in log-phase μ_{log} will define the multiplication speed as the slope during the linear growth (OD_{600} linear increasing). The interception of the slope with the abscissa axis indicates the $t_{lag-log}$ time which characterizes an approximate lag-phase duration. (iii) The stationary phase resulting in a constant bacteria density over time (μ = 0) where growth rate and death rate are equivalent. This bacterial growth limitation is usually related to the predominance of a growth-limitation factor such as the synthesis of growth inhibitor by the bacteria community or the depletion in a critical component in the medium. For exoelectrogenic bacteria, a depletion in the carbon source (electron donors) or the electron acceptors is a critical growth-limiting factor (inhibition of the electron mobility through the electron transfer chain). (iv) The death-phase (or decline phase) is characterized by a dramatic decrease of the concentration of alive bacteria. This decline occurs when the growth-limiting factor becomes predominant and problematic for bacteria viability. For example, a lack of nutrient may lead to bacteria death.

2.3.3. Bacteria counting and OD_{600}/cfu correlation.

The correlation between the measured optical density and the colony-forming unit per milliliter is evaluated by counting on LB-agar plate. This technique only counts the cultivable bacteria. Bacteria cultured as described in part. 2.3.2 and sampled at an optical density of 0.8, transferred in an MR1 medium without lactate and fumarate and finally diluted at 10^{-5}, 10^{-6} and 10^{-7}. 50 µL of each dilution is spread out on LB-Agar plates (triplicate), incubated at 37°C for 24h and then counted **(Figure 2.22)**.

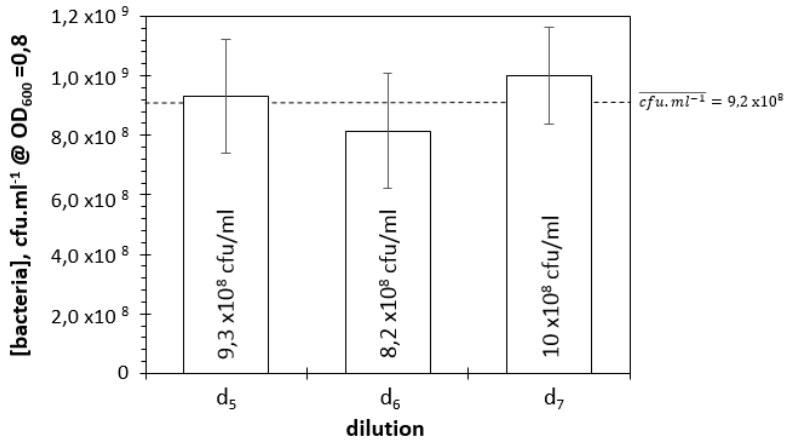

Figure 2.22 – Number of colony-forming unit (cultivable bacteria) per milliliter of culture at an optical density of 0.8. cfu.ml^{-1} (condition SOg_4) are determined by counting the number of bacteria which form a colony after 24h at 37°C for 50 µL of culture at a dilution d_x: $cfu.ml^{-1} = 20 * Nb(counted\ bacteria) * 10^x$ where x is the factor of dilution. Caption: d_x mean diluted 10^{-x}.

At an optical density of 0.8, the average number of colony-forming unit per milliliter is determined at 9.2 x10^8 cfu.ml^{-1}. Based on this proportional law the growth curve for the condition SOg_4 (see part. 2.3.4) may be plotted as function of the bacteria concentration **(Figure 2.23)**.

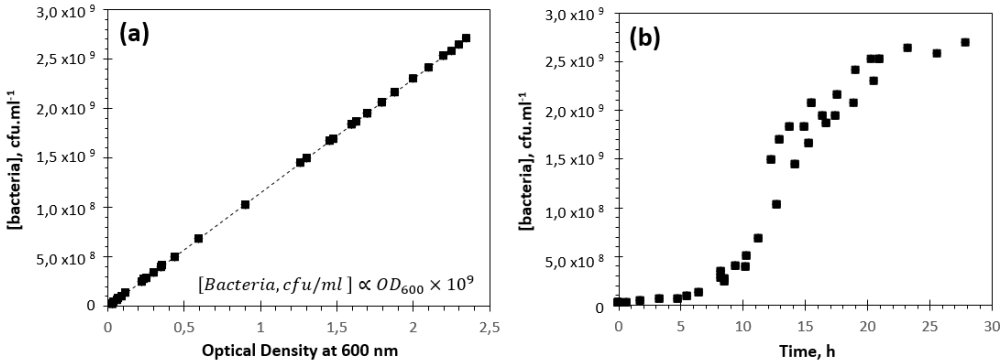

Figure 2.23 – Correlation between the optical density at 600 nm and the concentration of bacteria. **(a)** Linear correlation between the concentration of bacteria and the OD at 600 nm, [bacteria, cfu.ml^{-1}] = f(OD_{600}). **(b)** Growth curves of the condition SOg_4 expressed in concentration of bacteria, [bacteria, cfu.ml^{-1}] = f(time, h).

2.3.4. Growth conditions effect on *S. oneidensis* multiplication.

In this section, the effect of the nature and the concentration of both electron donor and acceptor on bacteria growth is studied. Also, the effect aerobic or anaerobic growth conditions is evaluated.

First of all, pre-cultivated *S. oneidensis* cells growing in an MR1 medium without addition of lactate as sole carbon source, in aerobic or anaerobic condition, leads to a stable OD_{600} value, equivalent to the initial optical density (ca. 0.03) during 20h of measurement. This indicates that there is no unintended carbon source in the medium composition and that such a carbon source is necessary to achieve *S. oneidensis* growth in MR1 medium. Based on this result, four growth conditions (cf. **Table 2.2**) are assessed to optimize bacteria density at the stationary phase. For aerobic condition, the medium is aerated before inoculation and the cultivation is carried in a flask with a vent cap which allows gas exchange in sterile conditions. On the contrary, for anaerobic condition, the medium is flushed with nitrogen for 30 min and sealed in a flask before inoculation to prevent the presence of oxygen. The results interpreted below are reported on the **Figure 2.24**.

Condition	[Lactate], mM	[Fumarate], mM	Pre-cultivated bacteria inoculation	Aerobic growth	Anaerobic growth
SOg_1	30	0	2% *	X	
SOg_2	30	30	1% $^{\Upsilon}$		**X**
SOg_3	15	15	1% $^{\Upsilon}$	X	
SOg_4	30	30	2% *	X	

Table 2.2 – Growth conditions to evaluate the effect of electron donor (carbon source) and acceptor concentration, anaerobic and anaerobic condition: without artificially add electron donor (SOg_1), with high concentration of electron donor (lactate) and acceptor (fumarate) in absence of competitive oxygen as acceptor (SOg_2) or in presence of oxygen (SOg_4), with low concentration of electron donor and acceptor in presence of oxygen (SOg_3). Caption: * 2 mL of inoculum in 50 mL of buffer, $^{\Upsilon}$ 1 mL of inoculum in 50 mL of buffer.

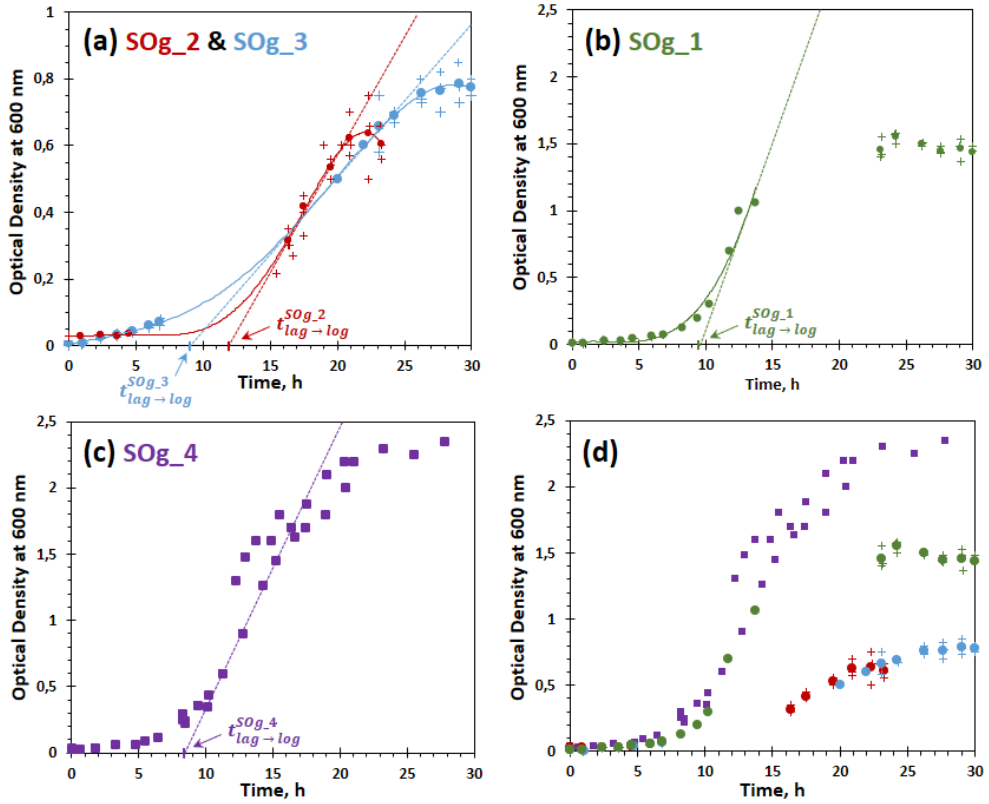

Figure 2.24 – Resulting growth curves in various conditions. **(a)** **SOg_2**, MR1-L/F medium concentrated at 30 mM, inoculated with 1% (0.5 mL in 50 mL) of pre-cultivated *S. oneidensisis* in anaerobic condition and **SOg_3** in aerobic condition with only 15 mM lactate and fumarate. **(b)** **SOg_3**, MR1-L medium (30 mM) inoculated at 2% (1 mL in 50 mL) of pre-cultivated *S. oneidensis* in aerobic condition. **(c)** **SOg_4**, MR1-L/F (30 mM) inoculated at 2% in aerobic condition. **(d)** Superposition of growth curves.
Caption: **+** triplicate curves, **•** average curves, **■** aggregated data for the same **SOg_4** condition.

Condition	Lag-phase duration, ca. h	Growth-rate in log-phase, OD_{600} unit.h^{-1}	Max OD_{600} in stationary-phase
SOg_1	9.5	0.28	1.4 to 1.6
SOg_2	12	0.07	0.6 to 0.7
SOg_3	9	0.04	0.7 to 0.8
SOg_4	8.5	0.22	2.2 to 2.4

Table 2.3 – Growth curves characteristic parameters for previously defined conditions of growth. The lag-phase, the log-phase and the stationary phase are respectively defined by the lag-phase duration, the maximum growth-rate in log-phase ($\Delta OD_{600}/\Delta t$, ca. OD_{600} unit.h^{-1}) and the maximum optical density measured during the stationary phase.

2.3.4.1. Lag-phase.

The duration of the lag-phase is similar for the three aerobic conditions (15 mM and 30 mM of lactate and/or fumarate) and varies between 8h and 9h (SOg_1/3/4). In anaerobic condition, this duration increase to 12h (SOg_2). The lag-phase is characteristic of a reactivation and adaptation of the bacteria to the medium, that depends on the pre-culture conditions. Here the pre-culture step is carried out in an oxic LB broth medium. In the case of an anaerobic growth the inoculum is transferred into an anoxic medium requiring a transition phase of adaptation of the bacteria for a growth condition where oxygen is removed and replaced by another electron acceptor, the fumarate. In contrast, for the aerobic growth, the pre-culture and culture conditions are closer. As a matter of fact, the μ_{lag} growth-rate during the lag-phase is not zero

and a slow increase of the optical density is observed. The transitional phase of growth acceleration between lag- and log-phase also occurs earlier ($t < t_{lag-\log}$).

2.3.4.2. Log-phase.

For the conditions SOg_2 and SOg_3, in anaerobic or aerobic conditions but under-concentrated in *lactate and fumarate (15 mM)*, growth-rates in log-phase are low in comparison with the calculated growth-rates in conditions SOg_1 and SOg_2 (aerobic condition, *30 mM lactate and/or fumarate*). In log-phase, the growth-rate is maximized and most of the cells are viable and cultivable. Even at low lactate concentration, the growth-rate in condition SOg_3 is similar to the growth-rate observable in condition SOg_2. This low growth-rate can be explained by strict growth conditions (low concentration of donor and acceptor of electrons or absence of oxygen) which lead to smaller population of cultivable bacteria at the beginning of the exponential cell division. On the contrary, for most favorable aerobic conditions as SOg_1 (30 mM of lactate) and SOg_4 (30 mM of lactate and fumarate), high growth rates are measured, between 0.2 and 0.3 h^{-1}. These conditions lead to an intense cell division. The slightly smaller growth-rate for the aerobic condition SOg_3 emphasizes the effect of the low availability of critical nutrients (15 mM of lactate and fumarate).

These results suggest that the presence of a sole electron donor (lactate) at 15 mM is sufficient for the growth of *S. oneidensis*. On the contrary, they point out that bacterial growth is favored when both oxygen and fumarate are present as co-acceptors, in a concentration-dependent manner.

2.3.4.3. Stationary-phase.

At the stationary-phase, the bacteria concentration is maximized and cell division only maintains the ratio of alive and dead cells. For the less favorable conditions SOg_2 (anaerobic) and SOg_3 (aerobic), the bacteria density reach an OD_{600} values of 0.65 and 0.75, respectively. Despite a concentration of lactate and fumarate two time less for the aerobic condition (15 mM vs. 30 mM), the highest bacteria density at the stationary-phase confirms the low influence of the decrease in the carbon source concentration. The main difference between these two conditions is the presence or the absence of oxygen as electron acceptor.

Supposing that, during log-phase, the increase of bacteria density is linearly related to the decrease of critical nutrient concentration for growth, the effect of oxygen as co-electron acceptor can be confirmed. Between condition SOg_2 (anaerobic) and SOg_3 (aerobic), the presence of oxygen is accompanied with an increase of maximal OD_{600} in stationary-phase, even if the medium is less concentrated in lactate. It confirms our previous conclusion that oxygen significantly contributes to the growth of the aero-anaerobic optional *S. oneidensis* strain.

2.3.4.4. Effect of the initial inoculum amount.

For the aerobic conditions SOg_1 and SOg_4 the amount of inoculum (prepared from the second pre-culture) is doubled from 1 mL to 2 mL for 50 mL of MR1-L and MR1-L/F buffer.

For the first condition (SOg_1), even if the oxygen is the sole electron acceptor, the optical density reach 1.4 which is ca. 2 times higher than the strictest conditions SOg_2 and SOg_3. Moreover, the lag-time ($t_{lag-log}$) and the growth-rate (μ_{log}) defined by the slope in log-phase are similar to the results obtained for the most favorable condition SOg_4. For the fourth condition (SOg_4) in presence of oxygen with fumarate as co-acceptor of electrons concentrated at 30 mM, the highest optical density is 2.3 indicating the valuable effect of the addition of a soluble molecular electron acceptor.

Based on the previous hypothesis, the cooperative effect of oxygen and fumarate is confirmed by the increase of the maximal bacteria density in stationary-phase from 1.5 in to 2.3 in OD_{600} by adding a fumarate electron acceptor in supplement to oxygen dissolved in solution. In fact, redox couple implying the reduction of oxygen into water has a higher standard potential than succinate/fumarate redox couple. A reactional cooperation can be hypothesized, first the dissolved oxygen in solution is consumed until oxygen concentration becomes too low. During the recovery of the oxygen by natural dissolution of atmospheric oxygen in the medium, fumarate is used as reducer for cathodic reaction. A reactional equilibrium between both oxygen and fumarate occurs.

2.3.5. Conclusion.

As part of the tested conditions, lactate is necessary for cell division but low concentrations are sufficient for the growth and the establishment of the maximum bacteria density at the stationary-phase. On the contrary, the depletion in electron acceptors seems to be a critical limiting factor. Oxygen availability as co-electron acceptor as well as a molecular electron acceptor in solution such as fumarate allow reaching higher bacteria density than in anaerobic condition. Moreover, the presence of oxygen during both the pre-culture and culture steps limits the lag-time before acceleration and maximization of the growth-rate in log-phase. Based on these results, the condition SOg_4 has been chosen to culture *Shewanella oneidensis*. For the rest of the study, *S. oneidensis* is cultured in an aerated MR1 basal medium (2% of pre-cultured inoculum) supplemented with 30 mM of lactate as sole electron donor, fumarate and oxygen as cooperative electron acceptors.

Moreover, a correlation between OD_{600} values and concentration of bacteria has been carried out and led to the conclusion that an OD_{600} of 0.8 correspond to 9.2 $x10^8$ $cfu.ml^{-1}$.

2.4. CARBON-*SHEWANELLA ONEIDENSIS* BIOELECTRODE

In a MFC, the anodic platinum catalyst is replaced by an electroactive bacterium. This micro-organism is responsible for the degradation of a fuel (small organic molecule such as lactate or glucose) by metabolic oxidation resulting in the production of a bio-energy converted into electrons. By EET, electrons are transfer to an external acceptor of electrons which can be molecular (fumarate, oxygen, …) or a solid anode. After a preliminary study on *Escherichia coli*, a more efficient electroactive strain has been chosen. *S. oneidensis* was selected for its ability to

transfer electrons by direct and indirect pathways, in comparison with *G. sulffureducens* only able to perform DET.

In this part we have evaluated the impact of external parameters on the bacteria adhesion, multiplication and viability at a carbon felt surface by electrochemical monitoring in various conditions. The effect of the state of growth (lag-, log-phase and stationary phase) of the inoculum was determined as well as the effect of the presence of oxygen. Moreover, the complexity and suitability of the MFC electrolyte was assessed. By this way, the adaptability of the bacterium strain for simplest to highly complex and more adapted medium was also assessed. Finally, the effect of the symmetrical application of carefully selected electrodes potentials, applied to the working (bio-anode) and the counter electrodes (cathode), was investigated in a single-compartment and a dual-compartments configuration.

Most of the experiments were carried out in single-compartment reactors with a three-electrodes configuration. The working and the counter electrodes consist in a 1 cm^3 and a 2 cm^3 carbon felt electrodes, respectively, and an Ag/AgCl/KCl (sat.) electrode is used as reference. To polarize the system, a potential is applied to the working electrode via a third annex electrode (Ag/AgCl/KCl reference) and the opposite potential is applied to the counter electrode by the same methodology. For example, for a working electrode poised at +0.3 V:

$$E_{we \to ref} = +0.3\ V, E_{ce \to ref} = -0.3\ V \text{ and } \Delta E_{apply} = |E_{ce \to ref} - E_{we \to ref}| = 0.6\ V.$$

The choice of the applied potential to the working electrode will be explained in part 2.4.4.

For aerobic condition, a glass reactor with vent-cap (0.2 µm) allows atmospheric exchange and natural oxygen renewal in sterile conditions. For anaerobic condition (see part. 2.4.1), sealed reactors with deaerated (argon bubbling) electrolytes and inoculums are employed. The batch reactor is periodically fed with a 30 mM equivalent amount of sodium lactate solution. The fumarate is removed from the inoculum by centrifugation and medium replacement (MR1-LF by MR1-L). In case of electrode polarization, the system is left at the OCV until stabilization for 1 hour.

2.4.1. Effect of the oxygen

Numerous electroactive bacteria such as *G. sulffureducens* are strict anaerobic and must be cultured in deaerated medium. In opposite, *S. oneidensis* is a pseudo anaerobic or aero-anaerobic optional bacteria. In this part, the influence of the presence or absence of oxygen is evaluated. Bacteria are cultivated as previously described in aerobic condition with lactate and fumarate as electron donor and acceptor (condition SOg_4). Then an inoculum is prepared by transferring the bacteria sampled at OD_{600} = 2.2 in MR1 medium supplemented with sodium lactate. The inoculum is diluted at an optical density of 0.7 and the working electrode is symmetrically polarized at +0.3 V. All the working electrodes present similar weight, volume and surface (1 cm^3 for the working electrode and 2 cm^3 for the counter electrode). Both anodic current and open circuit potential (OCP) are measured in time, periodic cyclic voltammogram are performed to evaluate the transfer mechanism patterns.

As shown on **Figure 2.25.a**, the polarization duration is divided in two regions, from the beginning of the polarization to day 7 and from day 7 to day 11. In the first period, both aerobic (in blue) and anaerobic (in green) conditions lead to similar results. Except at day 1, the anodic current increases quite linearly without significant difference between the two cases. At day 1, the current measured in anaerobic condition is slightly higher (10 times) than in aerobic condition. Meanwhile, at day 1 the OCP in aerobic condition (-0.025 V vs. Ag/AgCl/KCl) is closed to the standard carbon felt OCP while in anaerobic condition the working electrode OCP is more negative (-0.4 V vs. Ag/AgCl/KCl). The OCP can be related to the rate of electrode colonization [210]. The bacteria cultured until stationary phase are conditioned to respire (oxidize) lactate and to reduce molecular electron acceptors (fumarate or oxygen). As a consequence, at the beginning of the polarization, the oxygen is a competitor in solution which easily accepts electrons compared to the electrode. A delay of acclimation is necessary to facilitate electron transfer to the electrode and to make it more favorable. Once this delay is passed, the OCP values in aerobic and anaerobic conditions converge with time until being quite equivalent **(Figure 2.25.b)**. However, after day 7, the two systems show a different behavior. In presence of oxygen, the anodic current continues to increase whereas in absence of oxygen the current is stabilized or slightly decreased. Altogether, these data indicate that the presence of oxygen does not significantly impact the anodic current generated by *S. oneidensis* in the carbon felt under a positive polarization. However, oxygen seems to enhance produced anodic current.

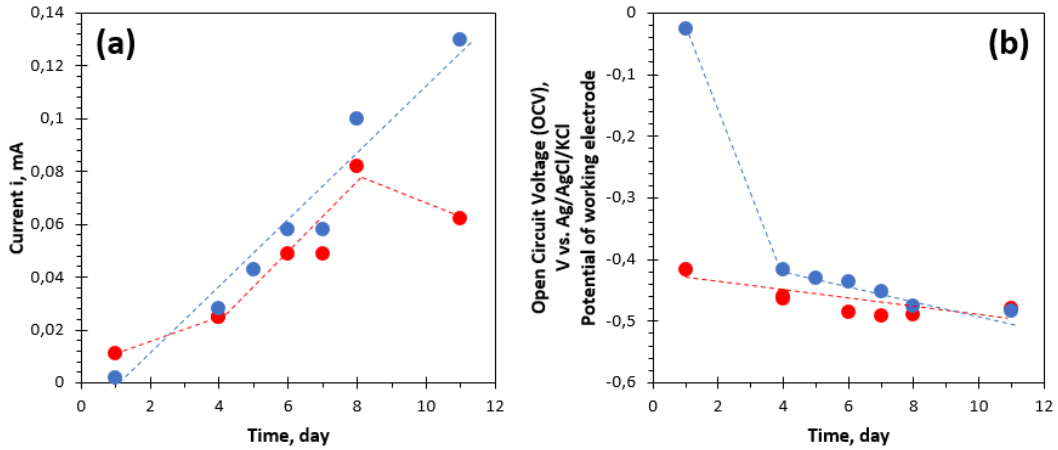

Figure 2.25 – Effect of the presence or absence of oxygen in solution during the incubation of a 1 cm³ carbon felt under polarization ($E_{working} = +0.3\ V$) in a sealed or open to air single-compartment. Bacteria are sample at an OD_{600} = 2.1, transferred in MR1 medium supplemented with lactate at 30 mM and diluted or concentered to an OD_{600} = 0.6-0.7. **(a)** Current monitoring by chronoamperometric methods at $E_{working} = +0.3\ V$ and **(b)** OCP monitoring (potential of the working electrode in open circuit): • **Aerobic condition** in blue, • **Anaerobic condition** in red (sealed reactor, N_2 bubbling).
Both current and OCP measurement were repeated several times and confirms the observed trends.

Cyclic voltammetry curves exhibit different behaviors **(Figure 2.26)** according to the electron transfer at the interface between *S. oneidensis* and the carbon fibers surface. Two domains are distinguished: (i) the mediated electron transfer reaction with a range of potential from -0.45 to 0 V vs. Ag/AgCl/KCl with a reversible redox system around -0.4 V vs. Ag/AgCl/KCl and (ii) the direct electron transfer region of potential from 0 to 0.8 V vs. Ag/AgCl/KCl. Both

electrochemical signatures are referred to sigmoidal waves characteristic to the establishment of bacteria layers. In both aerobic and anaerobic conditions mediate and direct electron transfer waves are not separated and the redox reversible mediator couple (riboflavin) is not visible. In aerobic condition, the wave intensity increases with time while it decreases between day 8 and day 11 for the anaerobic condition. The loss in wave intensity confirms the conclusions based on the anodic current measured by chronoamperometry. In both cases at day 5, the riboflavin redox system is visible around -0.4 V vs. Ag/AgCl/KCl and then the signal of the riboflavin is superposed to the oxidative wave. At day 11, another redox system is observable around -0.6 V vs. Ag/AgCl/KCl. From now, the nature of this redox couple is uncertain but probably secreted by the bacteria, in these experimental environment.

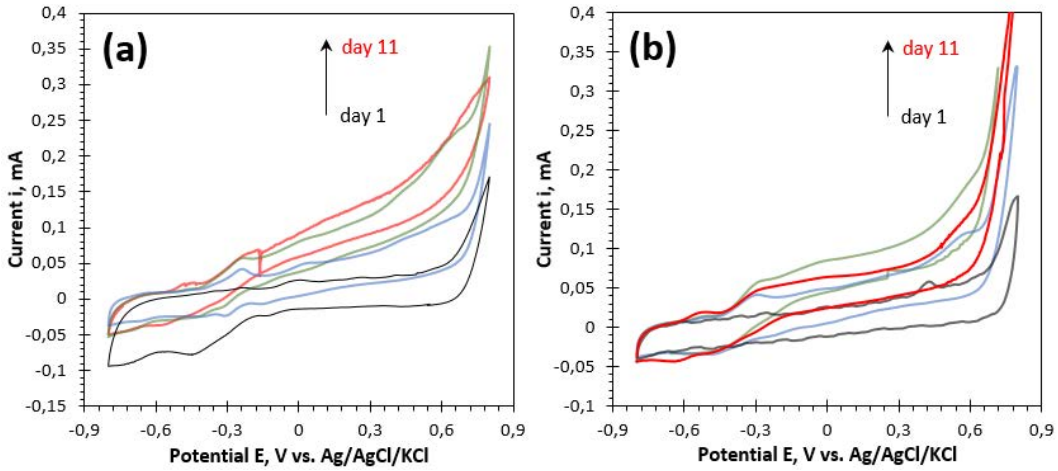

Figure 2.26 – Effect of the presence or absence of oxygen in solution during the incubation of a 1 cm^3 carbon felt under polarization ($E_{working} = +0.3\ V$) in a sealed or open to air single-compartment. Bacteria are sample at an OD_{600} = 2.1, transferred in MR1 medium supplemented with lactate at 30 mM and diluted or concentered to an OD_{600} = 0.6-0.7. The Mediated Electron Transfer occurs between -0.4 and 0 V vs. Ag/AgCl/KCl and the Direct Electron Transfer occurs between 0 and 0.8 V vs. Ag/AgCl/KCl.
Cyclic voltammograms **(a)** in aerobic condition **(b)** in anaerobic condition.
Caption: **— day 1** in black, **— day 5** in blue, **— day 8** in green and **— day 11** in red.

Scanning electron microscopies on **Figure 2.27** shows the extent of colonization of the carbon felt incubated in an aerated or deaerated medium at the peripheral surface and inside the felt at around 300 µm in depth. In both aerobic and anaerobic conditions, the carbon fibers at the surface of the felt are highly colonized. These images suggest that a homogeneous layer of bacteria is first established and then bacteria are deposited or divide on the upper surface of this layer. After sufficient time under polarization, the adhering bacteria are embedded in a biofilm **(Figure 2.27.a, Figure 2.27.d)**. In certain cases, a large number of bacteria is visible on specific locations **(Figure 2.27.b)**. The most relevant hypothesis to explain this organization is the adhesion of a few bacteria due to the polarization and then an intense division from the deposited bacteria. The reason of the colonization of these specific regions is uncertain but potentially related to a heterogeneous surface repartition of the current density at the electrode surface. Density of current, and therefore bacteria, are preferentially localized on the most electrically conductive regions.

Observation of the inner volume of the felt reveals a less extensive colonization. In aerobic condition, a layer of biofilm and exopolysaccharides (EPS) is observable on the inner fibers but no bacteria are visible **(Figure 2.27.c)**. For deaerated medium condition, the inner fibers are colonized by a few bacteria only **(Figure 2.27.e)**. When the surface and the core of the felts are compared, the observed lower colonization of the latter could be expected as it requires diffusion of the bacteria through the tortuosity of the carbon porous network, that can be made more difficult by the high density of cells grown on the surface **and carbon hydrophobicity**.

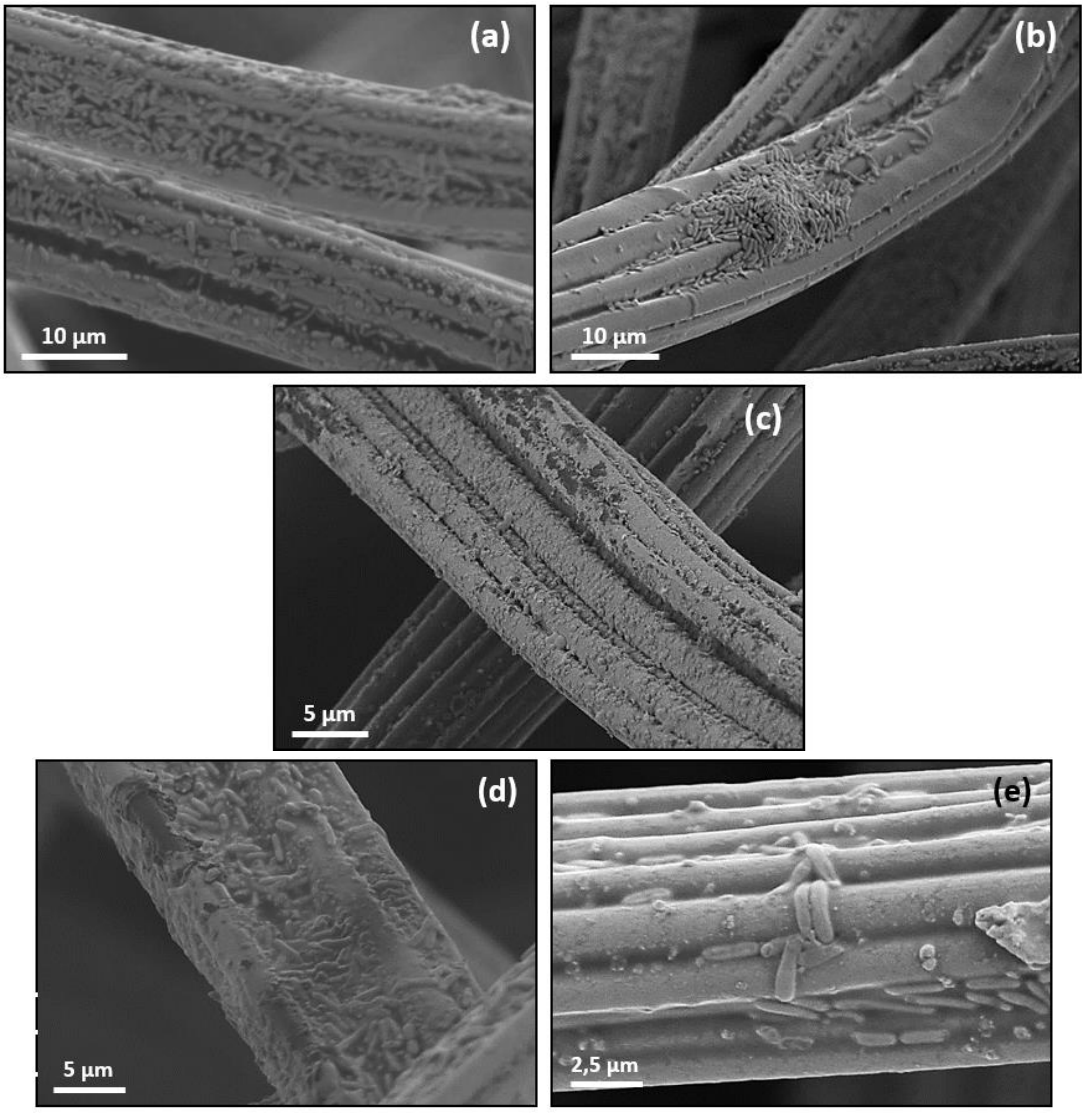

Figure 2.27 – SEM observation of 1 cm^3 carbon felt incubated under polarization ($E_{working} = +0.3\ V$) in a sealed or open to air single-compartment. Bacteria are sample at an OD_{600} = 2.1, transferred in MR1 medium supplemented with lactate at 30 mM and diluted or concentered to an OD_{600} = 0.6-0.7.
(a-c) SEM observations of carbon felt fibers in aerobic condition, at the peripheral surface (a, b) and inside the felt (c). **(d, e)** SEM observation in anaerobic condition, at the peripheral surface (d) and inside the felt (e).

Difference of colonization between the surface and the core of the felt must be explained by the triple-phase boundary hypothesis (bacteria, electron donor and acceptor, oxygen availability). In aerobic condition, at the surface of the felt: (i) A sufficient number of bacteria is directly available in the electrolyte to deposit on the fibers, to replace existent inactive bacteria and/or participate to EET (direct or indirect via riboflavin mediator). (ii) A solid

and highly conductive electron acceptor (working electrode) as well as mediators in solution (riboflavin). Moreover, nutrients (electrode donor) are directly available in sufficient concentration. (iii) Oxygen is also directly available. As a consequence, the felt surface presents all the conditions necessary for a preferential adhesion of the bacteria and EET. On the contrary, in anaerobic condition: bacteria, solid electrode, mediators and nutrients are available, but oxygen is absent. In this condition, the electrode is the sole electron acceptor. Overcoming diffusive limitation becomes more than optional to access a wider surface of solid fibers to perform DET.

In other words, difference between aerated and deaerated conditions should find its origin in the competition between the fibers surface and oxygen as electron acceptors in the aerobic condition, whereas the electrode is the sole electron acceptor in anaerobic conditions.

2.4.2. Effect of the bacterial state of growth

As pointed out earlier (cf. part 2.3.2), the growth of a bacterium is divided in three parts: (i) the lag-phase, (ii) the log-phase or exponential phase and (iii) the stationary-phase. These three phases exhibit different dynamics of growth and the state of growth of the bacteria influences their biological activity and should, in particular, modify their electroactivity. To evaluate this influence, *S. oneidensis* was grown in condition SOg_4 (cf. part 2.3.4) and bacteria were sampled **(Figure 2.28.b)**: (i) at the beginning of the log-phase just after the step of growth-rate acceleration until the community reaches a maximum growth-rate ($OD_{600} = 0.5, [S.oneidnesis] = 5.8\ 10^8\ cfu.ml^{-1}, \mu = \mu_{lag} \rightarrow \mu_{log}$). (ii) At the middle of the log-phase ($OD_{600} = 1, [S.oneidensis] = 1.2\ 10^9\ cfu.ml^{-1}, \mu = \mu_{log}$). (iii) At the end of the log-phase just before the step of deceleration until the stationary phase ($OD_{600} = 1.7, [S.oneidensis] = 2\ 10^9\ cfu.ml^{-1}$, $\mu = \mu_{log} \rightarrow \mu_{stat}$) . (iv) At the stationary phase ($OD_{600} = 2.2, [S.oneidensis] = 2.5\ 10^9\ cfu.ml^{-1}, \mu = \mu_{stat}$).

Then, the sampled bacteria culture is prepared as an inoculum. The resultant electron acceptors (sodium fumarate) are removed from the solution by centrifugation and the bacteria pellet is transferred in a MR1-L medium (MR1 medium without sodium fumarate and supplemented in sodium lactate at 30 mM). To free the system from current intensity variation due to the bacteria density ($i \propto n_{bac} * i_{bac}$), all the prepared bacteria inoculum are diluted or concentrated in MR1-L medium at an OD_{600} of 0.7 corresponding to 8 10^8 cfu.ml^{-1}. The experience is carried out in a three-electrodes single-compartment reactor without any oxygen restriction (in aerobic condition). Anodic current is measured by chronoamperometric methods at +0.3 V vs Ag/AgCl/KCl and the working electrode potential is monitored at the OCV in time **(Figure 2.28, Figure 2.29)**. Working and counter electrode are symmetrically polarized at $E_{we} = +0.3\ V\ (vs. E_{ce} = -0.3\ V\ and\ \Delta E_{apply} = 0.6\ V)$, the working *and* the counter electrode potential are fixed and not allowed to change during the polarization duration.

Corresponding current and OCP measurements are available on **Figure 2.28.a** and **Figure 2.29** with the various states of growth presented on **Figure 2.28.b**.

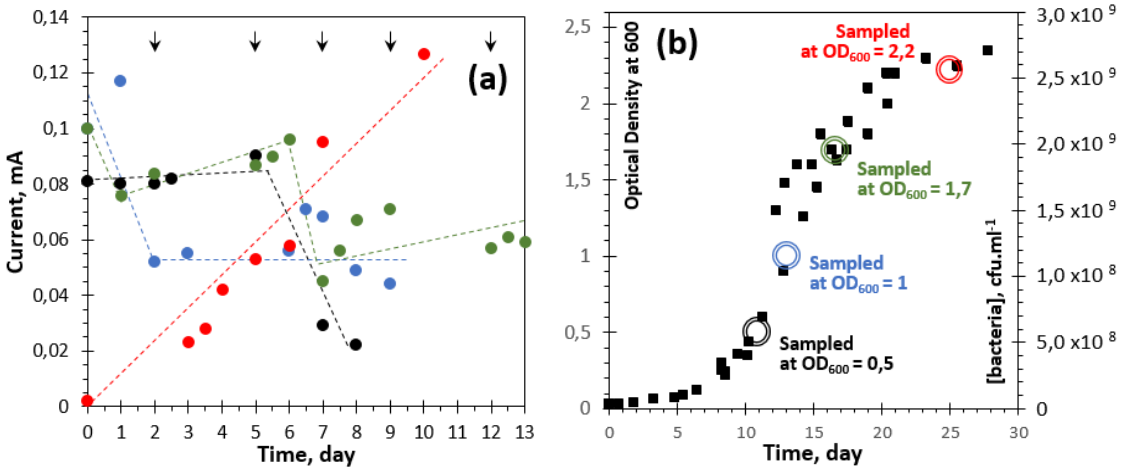

Figure 2.28 – Electrochemical characterization of the bacteria metabolism for various Optical Density (bacteria state of growth). Bacteria are sample after specific growth time, transferred in MR1 medium supplemented with lactate at 30 mM and diluted or concentered to an OD_{600} = 0.7. The reactors consist in a single-compartment. Carbon felt 1 cm^3 and 2 cm^3 electrode as WE and CE are symmetrically polarized $E_{working} = +0.3\ V$.

All the reactors are leaved for 1 hour at the OCV for stabilization before any measurements. Black arrows represent the addition of lactate at an equivalent of 30 mM.

(a) Current monitoring for Optical Density of the sampled bacteria solution: • **OD_{600} = 0.5** in black (1/4 of the log-phase), • **OD_{600} = 1** in blue (1/2 of the log-phase), • **OD_{600} = 1.7** in green (3/4 of the log-phase), • **OD_{600} = 2.2** in red (stationary-phase). **(b)** Growth curve for *S. oneidensis* (growth condition SOg_4) with spot at the time and the state of growth at the sampling.

Dashed lines only exhibit trends.

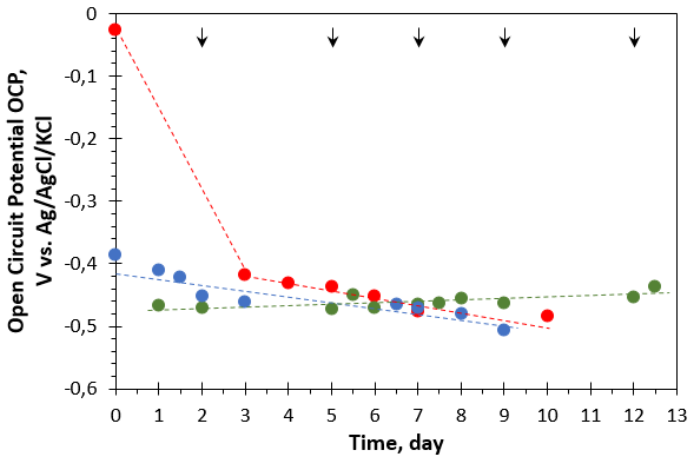

Figure 2.29 – Electrochemical characterization of the bacteria metabolism for various Optical Density (bacteria state of growth). Same experiment than presented on figure 2.28.a. The working electrode Open Circuit Potential (OCP) is measured before chronoamperometric measurent (cf. fig. 2.28.a). Day 0 represents the first current/OCP measurement, 12 hours after the beginning of the polarization.

Caption: • **OD_{600} = 0.5** in black (1/4 of the log-phase), • **OD_{600} = 1** in blue (1/2 of the log-phase), • **OD_{600} = 1.7** in green (3/4 of the log-phase), • **OD_{600} = 2.2** in red (stationary-phase).

Dashed lines only exhibit trends.

For inoculums prepared from bacteria sampled at **the beginning (OD_{600} = 0.5, black dots) or end (OD_{600} = 1.7, green dots) of the logarithmic phase**, the monitored current is already at its stable value (80 µA) after the 12 first hours of polarization. For ***low OD_{600} (0.5) cultures***, a dramatic current loss is observed after 5 days of polarization, from 90 µA to 20 µA in only 3 days, despite a regular feeding of the bacteria. It indicates that the current loss is not related to a depletion of nutrient leading to a starving phase but to a permanent deactivation or bacteria

death. For bacteria sampled at ***the end of the log-phase (1.7)*** the current abruptly decreases from ca. 90 µA to 45 µA at day 6. However, it then increases slowly, up to ca. 60 µA, and remains quite stable for the last 5 days of experiment. This would suggest that more mature bacteria are less sensitive to a transitory lack of nutrients. In parallel, the monitored open circuit potential of the working electrode colonized by both bacterial suspensions is stable on time at ca. -0.45 V vs. Ag/AgCl/KCl. It has been already demonstrated that the biofilm formed slightly modifies the OCP value [210]. Thus it can be suggested that, in these conditions, the key steps of colonization occur within the first 5 days of contact between the felt and the bacteria, while the longer term fate of the cells has a lower impact on the OCP.

For bacteria sampled in the ***middle of the log-phase (OD_{600} = 1)***, an overshoot of current is noticed the first day with a maximum current intensity at 120 µA. This is probably related to a fast contact between bacteria and electrode, favoring EET. This effect is observed here, and not for bacteria sampled at the beginning of the log phase (or at least at a lowest scale), because the middle log phase corresponds to the maximal growth rate. This initial sharp increase of the anodic current is followed by a dramatic drop, down to 52 µA, the following day. After bacterial feeding at day 3, the current remains stable which may indicate that the population of viable and *active* bacteria remain stable or that a limitation exists in the interactions between the bacteria and the electrode. The first hypothesis would in fact correspond to the fact that the bacteria have entered the stationary state. In favor of this hypothesis, we observed a peak in current at day 6 after addition of 30 mM to the batch, allowing to temporary increase the ratio of dividing vs dying cells thanks to the supply of additional nutrients. In term of working electrode potential, the OCP decreases from -0.385 V vs. ref to -0.452 V vs. ref for the first 2 days and remains stable until day 6, when it slightly decreases. Interestingly, these variations closely parallel the evolution of the anodic current, showing a stronger correlation between colonization and electron transfer.

To summarize, whereas distinct and complex behaviors were observed in the first days of colonization, all bacterial populations harvested in the log phase provide similar anodic currents between 60 µA to 80 µA and OCP (-0.45/0.5 V vs. Ag/AgCl/KCl) after 1 week under a +0.3 V polarization. Among these, the most stable system on the long term seems to be obtained with bacteria sampled at an OD fixed at 1.7 **(Figure 2.28.a** green**)**.

The anodic current behavior for bacteria harvested in ***stationary phase at optical density of 2.2*** is very different. The current increases quasi linearly with polarization time, from 2 µA to 130 µA (and probably continues to increase after day 10). In comparison, with bacteria sampled during the log-phase (OD_{600} = 1 and 1.7), here the OCP of the working electrode evolved from less negative initial potential (-0.026 V vs. Ag/AgCl/KCl) to more conventional bio-anode potential (-0.430 V at day 4 and -0.476 V vs. Ag/AgCl/KCl at day 7). Hypothesis to explain the evolution of the current and the initial OCP can be find in the external parameters such as the state of growth of the bacteria, their adhesion at the carbon fiber surface and the EET pathways.

(i) **Growth rate hypothesis:** As previously defined, the growth rate μ varies with the state of growth. In opposition with bacteria sampled in log-phase, the rate of growth of bacteria harvested in stationary phase converge to zero. The dynamic of bacteria division only occurs to keep the population of living bacteria constant. Therefore, the low current and high OCP at day 0 may be explained by low reactivity of the bacterial population, that may include a lower sensitivity to the effect of polarization. After a phase of adaptation and acclimation (analog to the lag-phase), the ability of the bacteria to divide actively is restored and the carbon fibers are more intensely colonized, as indicated by the OCP decrease and fast current increase. However, after day 3, the decrease of the OCP is very slow and not sufficient to explain the linear increase of the current.

(ii) **Electronic transfer hypothesis:** *S. oneidensis* is able to transfer electrons by both direct and mediated transfers. Flavin redox shuttles are involved in the mediated electron transfers while the cytochromes are involved in the direct transfer, via a chain of iron redox systems, named heme. In log-phase, the color of the bacteria pellet is red related to the iron content of the cytochroms. On the contrary, in the stationary phase, the pellet is quite white. It means a variation in cytochrome concentration or structure which can lead to a lack in electron transfer by this pathway. On the cyclic voltamogram **(Figure 2.30)**, at the beginning of the polarization time the influence of the direct electron transfer wave (from ca. 0 to 0.8 V vs Ag/AgCl/KCl) is low and increase with time. The same phenomenon is observable for the mediated transfer wave (from ca. -0.4 to 0 V vs Ag/AgCl/KCl) and the redox system corresponding to the flavin is less- or non-observable. The progressive rises of both transfer pathways may explain the increase of the current even if the OCP is stabilized (cytochromes reactivation and/or division of bacteria with more active cytochromes).

(iii) **Oxygen hypothesis:** The oxygen in solution is a competitor to the electron transfer to the electrode. Moreover, these bacteria harvested in stationary phase only grow and established their maximal density in the presence of a molecular acceptor of electron (sodium fumarate and oxygen as co-acceptor). The inoculum is initially more adapted to a molecular electron acceptor and is more likely to first react with it. Noticeably, the initial OCP is close to that obtain in part 2.4.2 for aerobic conditions (-0.026 V vs Ag/AgCl/KCl), where the oxygen vs. electrode competition is in favor of the former, whereas it becomes close to that of anaerobic conditions (ca. -0.450 V vs. Ag/AgCl/KCl) as the electrode is the sole electron acceptor.

Scanning electron microscopy observations confirm that the density of bacteria at the surface of fibers increases with the state of growth of harvested bacteria. For the situation while bacteria are sampled at 0.5 or 1.7 in optical density, the repartition of bacteria is quite similar **(Figure 2.31.a to Figure 2.31.d)**. The density at 1.7 in OD_{600} is more important due to the higher viability of the bacteria. For bacteria sampled at an optical density of 2.2 in stationary phase, the carbon fibers at the peripheral surface of the felt are entirely and homogeneously recovered

with bacteria. In a few spots, most of the time at the intersection of fibers, the density of EPS (exopolysacharrides) and bacteria is higher **(Figure 2.31.e, Figure 2.31.f)**. However, at 1.7 in optical density, the bacteria can colonize the fibers by dividing on each other on specific spots. In other words, the most likely explanation is to consider the adhesion of few bacteria on the fibers and then the multiplication of these bacteria at the surface of the felt by taking advantage to their « log-phase » behavior.

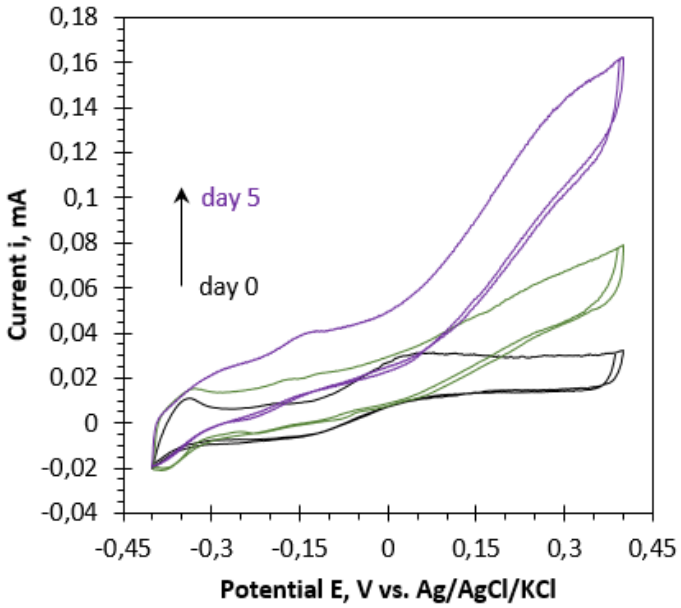

Figure 2.30 – Cyclic voltammetric characterization of a single-compartment MFC (without membrane) for a symmetric polarization of the 1 cm³ carbon felt working and counter electrodes: $\Delta E = 0.6\ V$ and $E_{working} = -E_{counter} = +0.3\ V$. Bacteria are sampled at a maximal Optical Density (in stationary phase, OD_{600} = 2.2) and transferred in MR1 medium supplemented with 30 mM Lactate.
Caption: **— day 0** in black, **— day2** in green, **— day 5** in purple.

To summarize, bacteria have been harvested at four states of growth (beginning, middle, end of the log-phase and at the stationary phase). Bacteria sampled during the log-phase overall present the same behavior. After 12h of polarization at +0.3 V, the anodic current is equal to ca. 80 µA. The stability of the current then varies with time as a function of the chosen state of growth. The bacteria sampled at an optical density of 1.7 are less sensitive to the variation of experimental conditions such as the variation of bacteria density, oxygen content and more particularly, of electron donor (lactate, carbon source) concentrations. Bacteria sampled in stationary phase present a different behavior. The monitored current increases linearly during the polarization but the initial OCP of the working electrode is 20 time higher than the OCP with other selected states of growth. In conclusion, in order to obtain a stable anodic current in a minimal duration, bacteria in log-phase are preferable while bacteria in stationary phase exhibit a long-term current increase with a high bacteria covering of the carbon fibers.

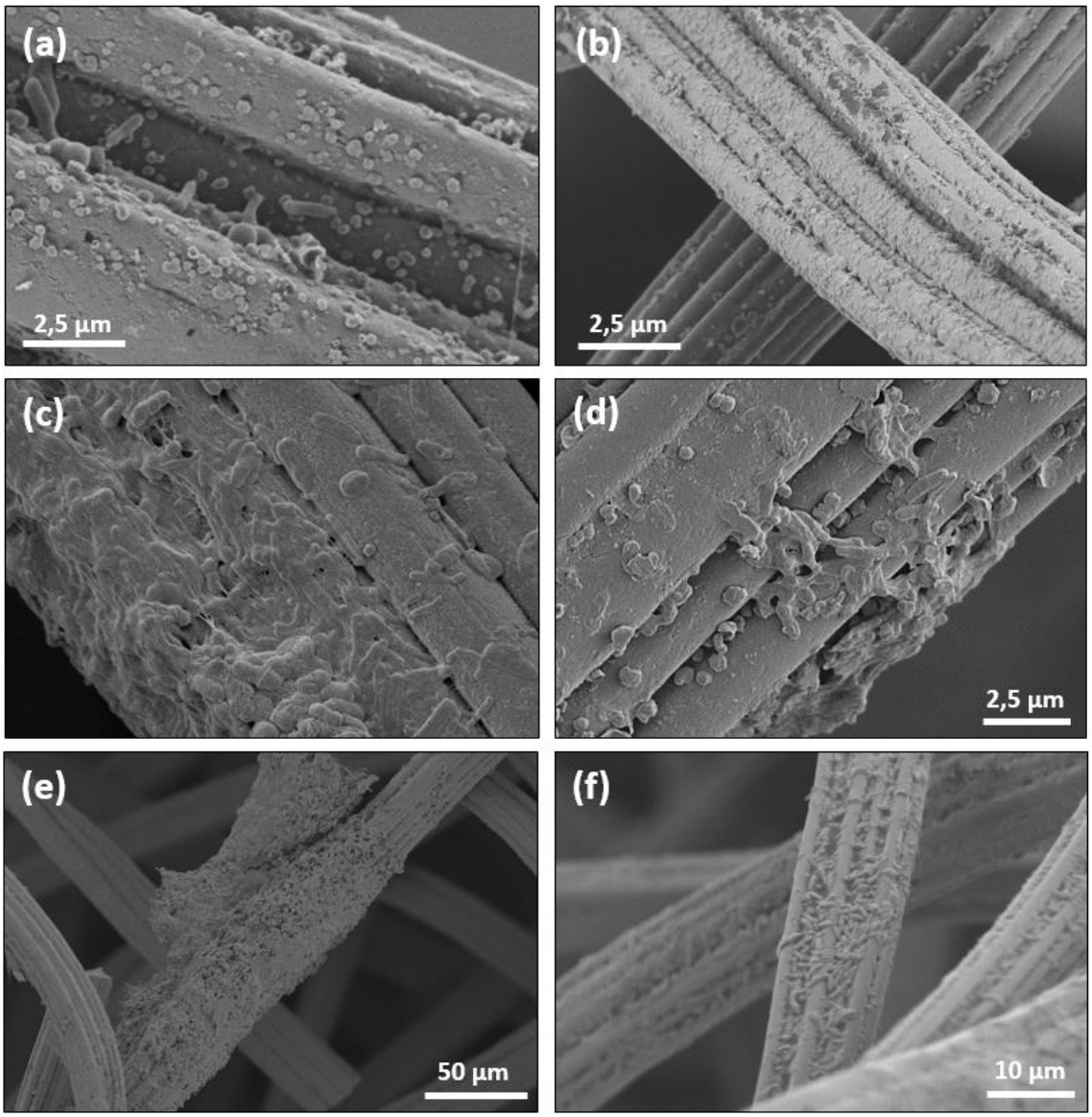

Figure 2.31 – SEM characterization of the bacteria metabolism for various Optical Density (bacteria state of growth). Bacteria are sample after specific growth time, transferred in MR1 medium supplemented with lactate at 30 mM and diluted or concentered to an OD_{600} = 0.7. The reactors consist in a single-compartment. Carbon felt 1 cm^3 and 2 cm^3 electrode as WE and CE are symmetrically polarized $E_{working} = +0.3\ V$**.**
For bacteria sampled at an OD_{600} of: **(a, b)** 0.5 at day 8, **(c, d)** 1.7 at day 13, **(e, f)** 2.2 at day 10.

2.4.3. Effect of the electrolyte nature

MR1 medium is a complex basal medium especially developed for the culture of *S. oneidensis* and similar bacterium strains. This medium is composed of a phosphate-based buffer associated to solutions of minerals, vitamins and amino acids (cf. 2.3.1). The medium is also supplemented with an electron donor (sodium lactate, MR1-L) and electron acceptors (oxygen and/or sodium fumarate, MR1-L/F). The aim of this section is to compare the effect on the bacteria behavior at the electrode surface between a basic PBS-L buffer (Phosphate Buffered Saline, PBS supplemented with 30 mM of sodium lactate) as an electrolyte and a complete MR1-L medium.

Figure 2.32.a and Figure 2.32.b indicate the evolution of the anodic current (at 0.3 V vs. Ag/AgCl/KCl) and OCP of a polarized working electrode (at +0.3 V) in a MR1-L and in a PBS-L electrolyte. The inoculum is prepared with bacteria sampled at the end of the log-phase at 1.7 in optical density and transfer in the appropriate medium (MR1-L or PBS-L). The innoculum is diluted in the corresponding electrolyte until an OD_{600} of 0.7. Two geometries (1 cm^3 cubic or cylindrical carbon felt) were tested. As previously demonstrated, in MR1-L medium (green and blue plots) the current varies between 80 µA and 100 µA. The current of the cylindrical (disk-shape) electrode is slightly higher than the current monitored for the cubic electrode, but this difference is not significant. In both cases, a short overshoot of current is measured after the 12 first hours of polarisation (ca. 120 µA to ca. 80 µA at day 2). In comparison, for the cyclindrical carbon felt immersed in a PBS-L bacteria solution, a high current is measured from day 1 to day 2 (360 µA). The anodic current then decreases to a more conventional value from day 2 to day 5 (70 µA) and varies between 70 µA and 110 µA. In term of working electrode OCP, the potential evolves around -0.45 ± 0.03 V vs. Ag/AgCl/KCl but no significant differences are observable between the three experimental conditions. Since the OCP variation which refers to the electrode colonization is equivalent for MR1 or PBS electrolyte, bacteria adhesion cannot explain the initial overshoot of current. However, in the PBS electrolyte, there is no electron shuttle (riboflavin) in solution while the riboflavin is present in the MR1 medium formulation (at 1.33 10^{-9} mM). This is clearly visible on the cyclic voltammogram performed at day 1 **(Figure 2.32.c)**: a reversible couple of peaks is present for MR1-L around -0.4 V vs. Ag/AgCl/KCl while it is absent in PBS-L electrolyte. In addition to the absence of riboflavin as initial redox shuttle in solution to promote MET, the current intensity of the DET wave of oxidation is 2.5 time higher than the oxidative wave in MR1-L electrolyte. Based on the observation of (i) an anodic current overshoot at day 2 and 3 in relation with a stable OCP at low value, (ii) a high DET oxidation wave and (iii) the absence of the riboflavin redox signal around -0.4 V vs. Ag/AgCl/KCl, the hypothesis of an high and fast electron transfer at the surface of the felt can be done. Moreover, in MR1-L electrolyte, electron shuttles represent an external reserve of electron (redox mediator in reduced state) dispersed in solution. In absence of shuttles, electrons produced by the oxidation of lactate, in absence of an electron acceptor (during innoculum and reactor preparation, from 10 to 24h), are accumulated in the redox transfer chain of the bacteria and fastly delivered in presence of an electron acceptor (electrode). At day 13, apart from the difference in oxidative wave intensity, the electrochemical behaviors are equivalent. A reversible couple of faradaic peaks is observed at ca. -0.5 V vs. Ag/AgCl/KCl. The nature of this couple is uncertain but probably related to a bacteria metabolite acting as a mediator in solution.

As a conclusion, in long-term polarization experiments, the substitution of the MR1 medium electrolyte by a simpler PBS electrolyte (higher salt concentration, absence of vitamins and minerals) is not detrimental to the anodic current production. Yet, an overshoot of current is observed at the inoculation time that will need further efforts to be clearly explained.

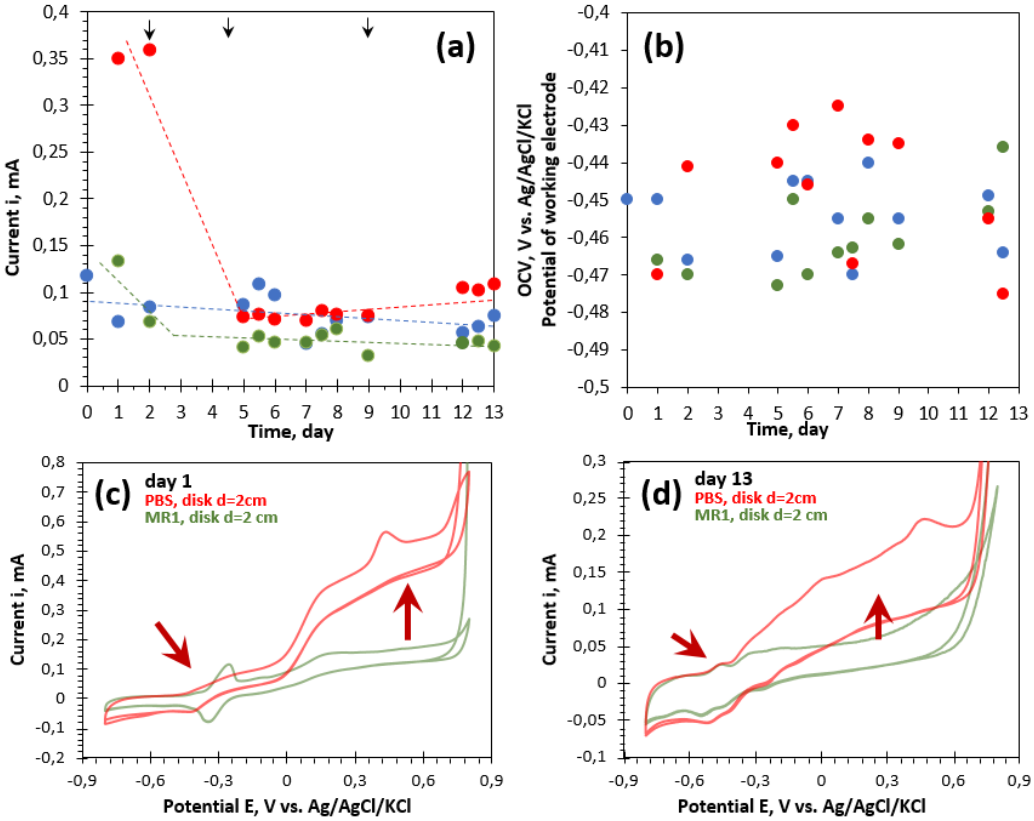

Figure 2.32 – Effect of the electrolyte nature (MR1 medium supplemented with 30 mM of lactate) and the electrode geometry (1 cm³), during the incubation of a 1 cm³ carbon felt under polarization ($E_{working} = +0.3\ V, \Delta E = 0.6\ V$). Bacteria are sample at an OD_{600} = 1.5-1.6, transferred in MR1 medium supplemented with lactate at 30 mM and diluted to an OD_{600} = 0.6-0.7.

(a) Current monitoring by chronoamperometric method at $E_{working} = +0.3$ V and **(b)** OCP monitoring (potential of the working electrode in open circuit): • **Disk working electrode in MR1-L with bacteria** in green, • **Disk working electrode in PBS-L with bacteria** in red (radius $r \sim 1\ cm$, thickness $e \sim 0.3\ cm$, Volume $V \sim 1\ cm^3$), • **Cubic working electrode in MR1-L with bacteria** in blue (1 *cm* square in shape).

Black arrows represent the addition of lactate at an equivalent of 30 mM (0.6 mL of a lactate solution at 1 M). The reactors are polarized for 12h before the first measurement at day 0. All the reactors are leaved for 1 hour at the OCV for stabilization before any measurements.

(c-d) Cyclic voltammogram for the disk electrodes in — **PBS-L** (in red) and —**MR1-L** (in green) electrolytes at day 1 (c) and day 13 (d).

2.4.4. Effect of the Polarization Potential.

To perform a microbial fuel cell, it is common to apply a potential of polarization in order to support the bio-anode colonization and to increase the performance of the MFC. However, the applied potential appears highly dependent on the micro-organism which can be a bacterium, a consortium of bacteria or inoculums sampled from real environment, such as domestic or industrial wastewaters [180], garden composts [211] or marine soils [139]. Most of the time, the potential is empirically determined by the experiment and there is no general law to predict the ideal potential of polarization with efficiency and accuracy. The positive effect of a polarization phase for bacteria adhesion, biofilm formation and current establishment is an emerging consensus but the sign and the intensity of the applied potential is a matter of discussion [201]. As an example, for pure *D. desulfuricans*, it has been demonstrated that currents are only measured at -0.16 V vs. SCE [212] while *G. sulfurreducens* benefits from more positive applied potential (ca. 0.26 V vs. SCE, between 0 to 0.4 V vs. Ag/AgCl [213] or 0.51 V vs Ag/AgCl [154]

depending on the quoted study). For mixed cultures and real inoculum, the situation is more complex, due to the multiplicity of bacterium strains, the synergic behavior of these strains and/or the domination of a specific strain. Moreover, the origin of inoculum influences its composition [214]. However, it is admitted that the use of a potential higher than the standard potential of the electron donor (lactate) to be degraded is preferable [210]. Note that potential higher than the equilibrium potential favors electron deficiency at electrode surface, then encouraging oxidation reaction by bacteria. In most cases, the polarization as well as the measurement are carried out in strict anaerobic condition in order to limit the competition with oxygen reaction for electron collection and to ensure the bacteria viability of strict anaerobic strains such as *G. sulfurreducens*.

Reactor set-up and experimental conditions.

In this section, the effect of the polarization is first evaluated **for potentials from -0.3 V to +0.5 V (2.4.4.1)**. This evaluation is carried out with a single-compartment reactor in a three-electrodes configuration. *S. oneidensis* is cultured according to the aerobic protocol SOg_4 (cf. part 2.3.3). Then the inoculum is prepared from bacteria sampled at an optical density of 1.5-1.6 (log-phase) or 2.2 (stationary phase) and transferred in MR1-L medium (without sodium fumarate as electron acceptor). Finally, the inoculum is diluted to 0.7 unit of optical density corresponding to ca. 8 10^8 cfu.ml^{-1}. The bacteria/MR1-L electrolytes are not deaereted and the reactors are equipped with vent-caps (0.2 µm) to allow atmospheric exchange. The batch reactors are assembled and operated in sterile conditions. The working and counter electrodes are respectively a 1 cm^3 (1 cm in length) and a 2 cm^3 (2 cm in length) carbon felt. The potential is symmetrically applied to the working and the counter electrodes, with the support of a fourth annex Ag/AgCl/KCl electrode to apply a well-defined potential to both working and counter electrode in a specific difference of potential, for example:

$$E_{we}^{vs\ ref} = +0.3\ V\ \left(\Delta E_{we \to ref} = +0.3\ V\right), E_{ce}^{vs\ ref} = -0.3\ V\ \left(\Delta E_{ce \to ref} = -0.3\ V\right)$$
$$\text{and, as a consequence, } \Delta E_{apply} = \Delta E_{we \to ce} = 0.6\ V.$$

In a second step (2.4.4.2), by conserving the same conditions of experiment as previously described, the influence of polarization time and potential is evaluated in a complete microbial fuel cell. The bio-anode is mounted in a dual-compartments reactor. A bacteria/MR1-L electrolyte is used as anolyte while $K_3Fe(CN)_6$ is used as catholyte, to perform ferricyanide reduction into ferrocyanide ($Fe(CN)_6^{3-} + e^- = Fe(CN)_6^{4-} at\ E^0 = 350\ mV$) [2]. The working and counter electrode are respectively a 1 cm^3 (1 cm in length) and a 2 cm^3 (2 cm in length) carbon felt and both compartment are separated by an ultrafiltration or a Nafion® membrane (50.8 µm thick 212 NRE, Sigma-Aldrich). Polarization curves, power curves and electrodes potential are monitored as function of time.

[2] Ferricyanide electrolyte is used at the lab-scale due to its high stability in optimized situation. This cathodic system can be easily replaced by an air cathode or an open-to-air cathode for up-scaled MFC.

2.4.4.1. Single-compartment reactor: How the potential of polarization affects the bio-anodic current?

As previously stated, various external parameters affect bacteria adhesion and biofilm formation at the surface of the electrode. The polarization of the anode in a defined field of potential represents another mean to form an efficient bio-anode.

Effect of the electrode polarization for bacteria harvested at the stationary phase (OD_{600} = 2.2)

Reactors prepared from ***S. oneidensis bacteria sampled at the stationary state of growth*** were subjected to three conditions of polarization E_{we} = -0.3 V, E_{we} = +0.3 V or non-polarized condition. Before measurement the working and the counter electrodes are allowed to stabilize at the OCV to limit the bias induced by the polarization. The current is monitored by chroamperometry at 0.3 V vs. Ag/AgCl/KCl and electron transfers patterns and mechanisms are characterized by cyclo voltammetry **(Figure 2.33)**.

At -0.3 V, the monitored current is equivalent to zero for the first days and increases slowly until ca. 10 µA at day 6. However, the measured current is positive. This applied potential is close to the standard potential of redox system pyruvate/lactate ($E^0 = -0.39\,V\ vs.\ Ag/AgCl/KCl\ sat.$) but remains higher. As referred previously (cf. 2.2.1), in this condition, the electrode presents a lack in electrons and the reaction direction corresponding to the electron transfer to the electrode (oxidation) is promoted. The cyclic voltammogram shows a sigmoidal wave of oxidation characteristic of the formation of a biofilm from around -0.1 V vs. Ag/AgCl/KCl at day 0 and day 1 **(Figure 2.33.b)**. Thereafter, a degradation of the signal is observed. At day 2, the sigmoidal wave is characteristic of planktonic cells in solution without permanent contact with the electrode leading to a non-turnover system. However, the measured current is not zero which probably indicates a favorable transfer by MET.

The anodic current observed **in absence of polarization** (self-determination of the electrode potentials) is higher with MR1-L medium than PBS-L electrolyte (37 µA vs 28 µA at day 5). Moreover, for both conditions, the measured current is clearly lower than for **working electrode polarized at +0.3 V** (121 µA at day 7). More specifically, **at +0.3 V** the current increases significantly (from 25 µA at day 0 to 121 µA at day 7). For a non-polarized electrode or an electrode poised at a positive potential, the patterns measured by cyclic voltammetry are similar and shown two successive waves of oxidation at -0.4 V vs. Ag/AgCl/KCl and 0 V vs. Ag/AgCl/KCl, respectively. In all cases, the reversible peaks of the riboflavin are not observed.

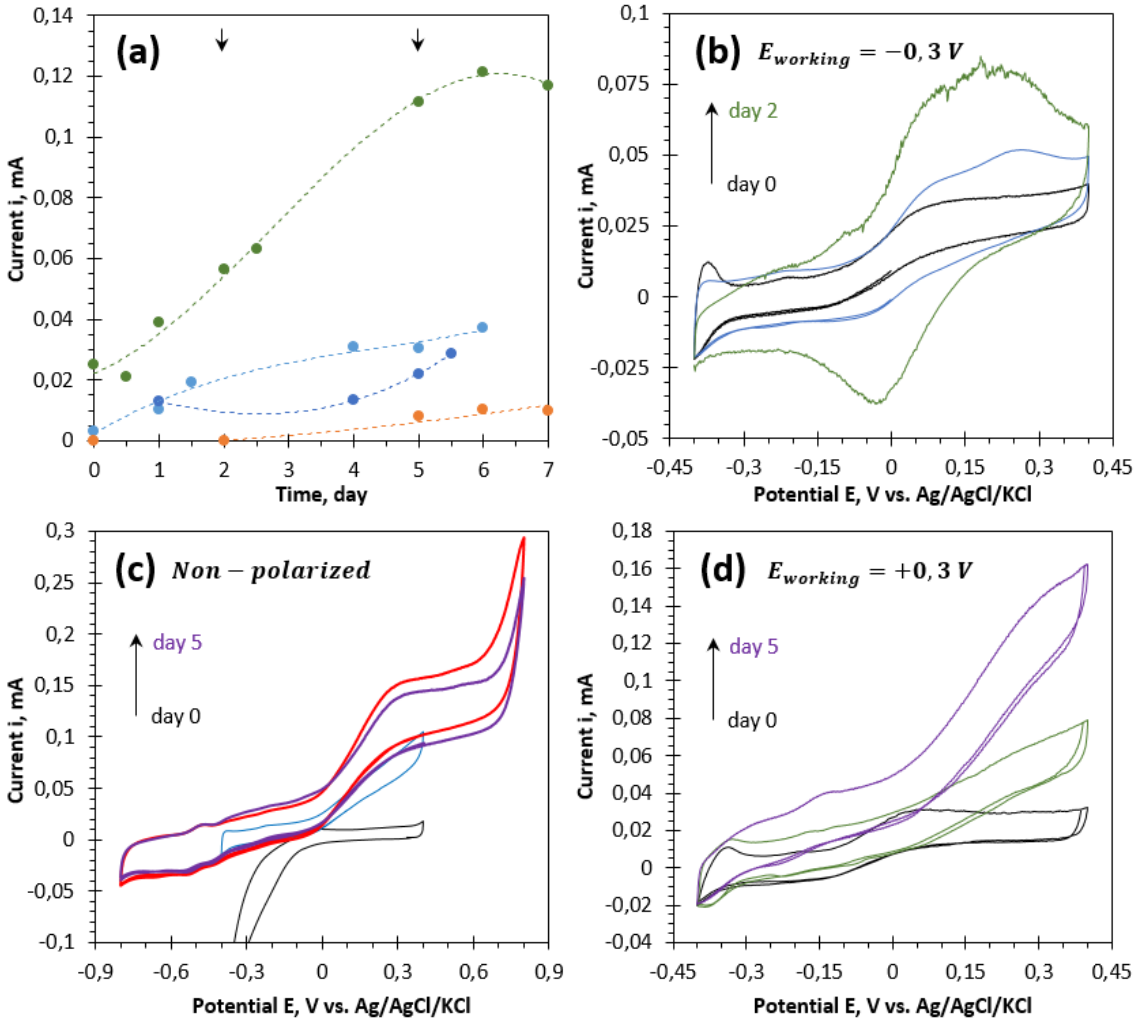

Figure 2.33 – Electrochemical characterization of a single-compartmented MFC (without membrane) for a symmetric polarization of the 1 cm³ carbon felt working and counter electrodes: $\Delta E = E_{counter}^{apply} - E_{working}^{apply} = x$ and $E_{counter} = E_{working} = x/2$. Bacteria are sampled at a maximal Optical Density (in stationary phase, OD_{600} = 2.2) and transferred in MR1 medium supplemented with 30 mM Lactate.
(a) Working electrode current monitoring as function of time (1h of acclimation before measure) by chronoamperometric technic: — MR1-L medium, $E_{working} = -0.3\ V$ in orange, — **MR1-L** medium, no potential applied, **unpolarized** in light blue. — **PBS-L** medium, no potential applied, **unpolarized** in dark blue. — MR1-L medium, $E_{working} = +0.3\ V$ in green. *Black arrows represent the addition of lactate at an equivalent of 30 mM (0.6 mL of a lactate solution at 1 M). Before measurement, reactors are allowed to stabilized at OCV for 1h.*
(b-d) Cyclic voltammogram for each polarization at specific day-time: (b) $E_{working} = -0.3\ V$. (c) MR1-L medium, non-polarized. (d) $E_{working} = +0.3\ V$.
Caption: — **day 0** in black, — **day 1** in blue, — **day2** in green, — **day 4** in red, — **day 5** in purple.

Effect of the electrode polarization for bacteria harvested in log-phase at OD_{600} = 1.6

In the case of ***bacteria harvested in the last quarter of the log-phase at around 1.6 in OD_{600}*** **(Figure 2.34)** in a working electrode polarized at **E_{we} = -0.3 V**, the current remains stable at a low value quasi-equivalent to zero (3 µA at day 15). As for bacteria harvested at the stationary phase, the current measured for a **non-polarized working electrode** is superior and slowly increase until 20 µA at day 15. For **positive potential (E_{we} = +0.3 and +0.5 V)**, the working electrode shows a high initial current (60 µA at a polarization of +0.5 V and 70 µA at an electrode poised at +0.3

V). For a polarization at +0.3 V, the current stabilizes around 65 to 70 µA while the monitored current continues to increase at a poised potential of +0.5 V (120 µA at day 14 and 90 µA at day 15) but the signal shows high instability. It can be suggested that, for the higher polarization (E_{we} = +0.5 V), more bacteria are engaged in a EET at the surface of the fibers so that the system is more sensitive to lactate depletion at the vicinity of the fibers. Compared to bacteria harvested in stationary phase at the same time of measurement, for non-polarized or positively-polarized working electrode the current is lower for an equivalent working electrode potential, as shown on **Table 2.4** at day 7. For a non-polarized working electrode, the measured current evolves from 8 µA for bacteria sampled at OD_{600} = 1.6 to 37 µA for bacteria sampled at the stationary phase. The current increases by 4.5 times. At E_{we} = +0.3 V, the current tripled from 42 µA (OD_{600} = 1.6) to 121 µA in stationary phase. However, this difference is less significant for a negative polarization at E_{we} = -0.3 V while the effect increases with the potential of polarization. This result may be related to the higher extent of carbon fibers colonization previously observed for felt incubated with bacteria from the stationary phase **(Figure 2.33)**.

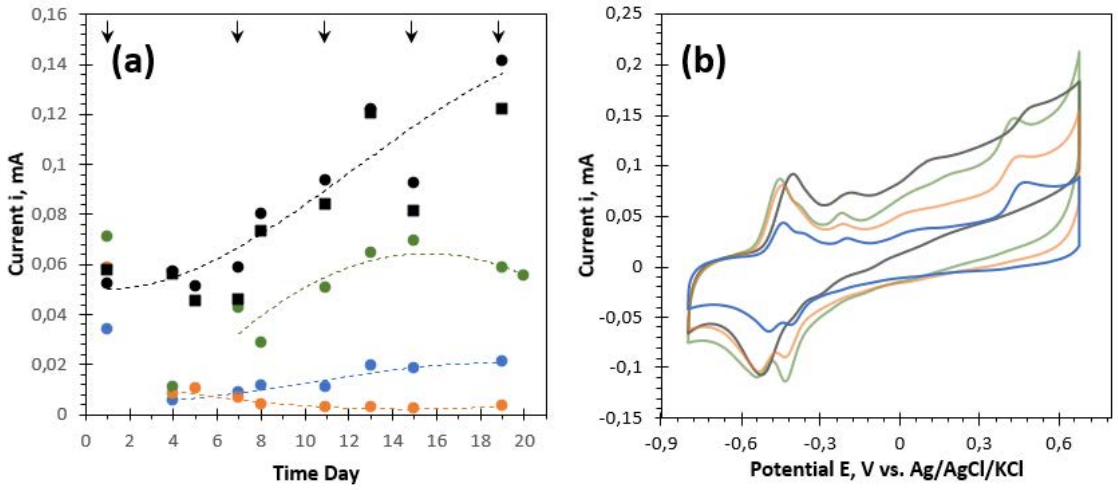

Figure 2.34 – Electrochemical characterization of a single-compartmented MFC (without membrane) for a symmetric polarization of the 1 cm^3 carbon felt working and counter electrodes: $\Delta E = E_{counter} - E_{working} = x$ and $E_{counter} = E_{working} = x/2$. Bacteria are sampled at OD_{600} = 1.4-1.6 (3/4 of the log-phase) and transferred in MR1 medium supplemented with 30 mM Lactate.

(a) Working electrode current monitoring in time (1h of acclimation before measure) by chronoamperometric technic: — MR1-L medium, $E_{working} = -0.3\ V$ in orange, — **MR1-L** medium, no potential applied, **unpolarized** in light blue. — **PBS-L** medium, no potential applied, **unpolarized** in dark blue. — MR1-L medium, $E_{working} = +0.3\ V$ in green. — MR1-L medium, $E_{working} = +0.5\ V$ in black.

Black arrows represent the addition of lactate at an equivalent of 30 mM (0.6 mL of a lactate solution at 1 M). Before measurement, reactor is allowed to stabilized at OCV for 1h.

(b) Cyclic voltammogram at day 8 for each polarization. Caption: — $E_{working} = -0.3\ V$ in orange, — **Unpolarized** in blue, — $E_{working} = +0.3\ V$ in green, — $E_{working} = +0.5\ V$ in black.

OD_{600} of sampling	Non-polarized WE	E_{we} = -0.3 V	E_{we} = +0.3 V	E_{we} = +0.5 V
1.7	8 µA	6.2 µA	42 µA	--
2.2	37 µA	10 µA	121 µA	70 µA

Table 2.4 – Recapitulative table of the current measured at day 7 for bacteria sampled at the end of the log-phase (OD_{600} = 1.7) and in stationary phase (OD_{600} = 2.2)

Insights in the corresponding electron transfer mechanisms can be obtained from the cyclic voltammograms acquired at day 8 **(Figure 2.34.b)**. The faradaic peaks for bacteria sampled at stationary phase at a polarization of -0.3 V is not visible and replace by a classic sigmoidal wave of oxidation. It means that bacteria from log-phase are able to aggregate, to form a biofilm and perform both DET and MET even if the electrode is polarized at a negative potential closes to the standard potential of the pyruvate/lactate redox couple. The intensity of the wave of oxidation increases with the potential of polarization. Moreover, for the non-polarized electrode and the electrodes polarized at -0.3 V and +0.3 V, the redox signal of the riboflavin is splitted in two reversible peaks characteristic of two redox couple. The first couple is centered at ca. -0.4 V vs Ag/AgCl/KCl and the second one at -0.5 V vs. Ag/AgCl/KCl. In comparison with the absence of polarization, at -0.3 V and +0.3 V, these peaks are not symmetric. The reason of this splitting is difficult to explain at this time but may reflect the presence of riboflavin both in solution and adsorbed at the surface of the fibers.

SEM images displayed on **Figure 2.35** support the effect of the four conditions of polarization tested on carbon felts incubated in bacteria/MR1-L electrolytes. The lowest density of bacteria is observed at a negative polarization (E_{we} = -0.3 V). These bacteria are embedded in a dense biofilm **(Figure 2.35.g, Figure 2.35.h)**. Under non-polarized condition, an accumulation of bacteria is distinguished with a thin layer of polymeric substances **(Figure 2.35.e, Figure 2.35.f)**. At positive working electrode polarization, the density of bacteria increases with the intensity of the applied potential **(Figure 2.35.a to Figure 2.35.d)**. In comparison with a negative potential, the biofilm is thinner and less dense.

To summarize, for bacteria sampled in both log- or stationary phase and electrodes polarized in a single-compartment reactor, both the sign and value of the potential influence the biofilm. A positive potential higher than the standard potential of reaction of the pyruvate/lactate redox couple is preferable to improve the anodic current [215], the accumulation of bacteria at the fiber surfaces and the formation of a biofilm. Most of the time, controversy remains in the choice of the applied potential in anaerobic condition [215,216]. In the literature, it appears that both negative [214,217,218] and positive [217,219] potential of polarization can promote the adhesion of *S. oneidensis* and to a lesser extent promote the electron transfer by both MET and DET in specific range of potential [201]. In any case, our observations lead to the conclusion that in a single-compartment reactor the application of a positive potential of polarization is favorable to prepare and acclimate the bio-anode in order to improve its electrochemical performances.

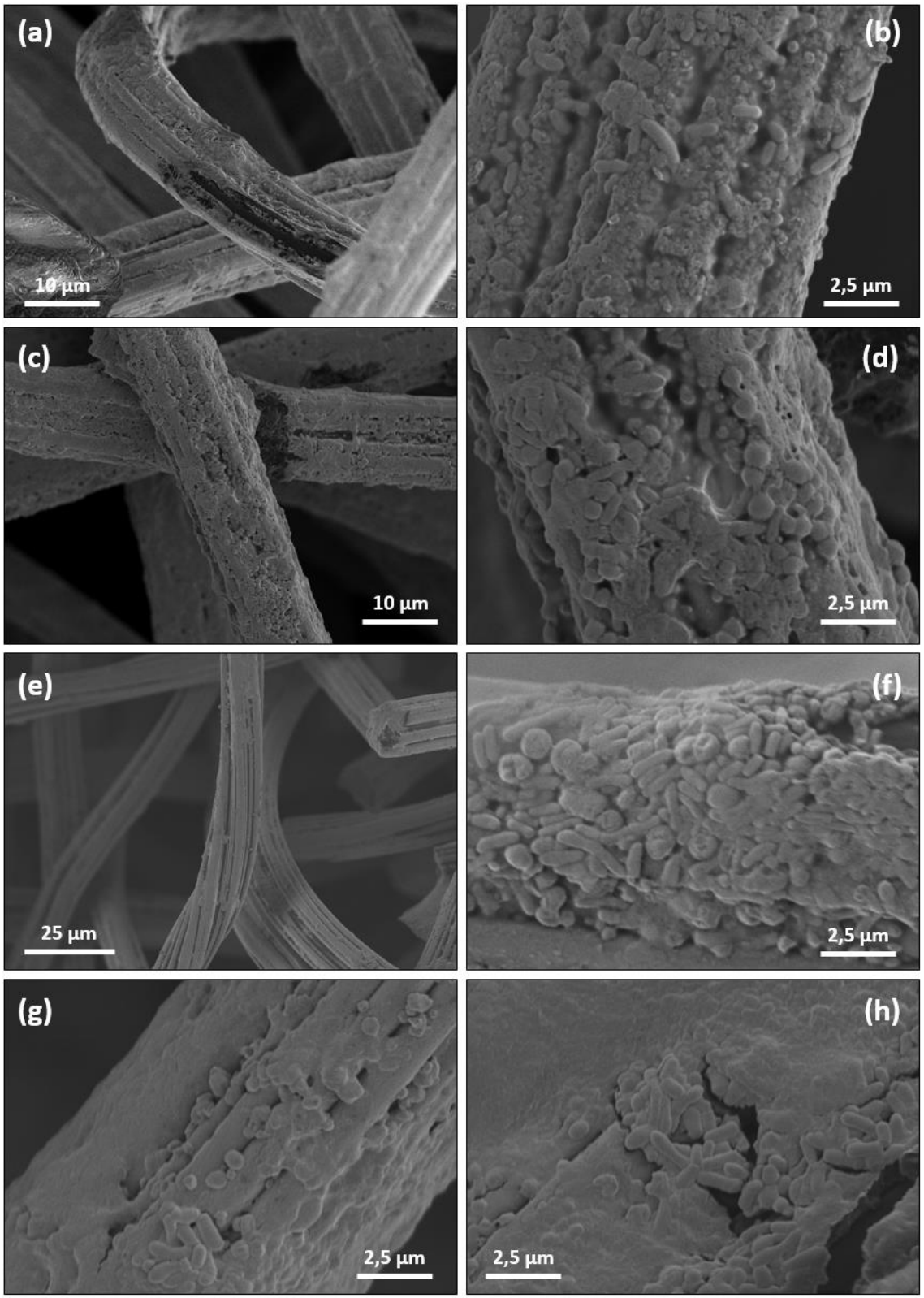

Figure 2.35 – SEM observations of symmetrically polarized carbon felt electrodes in bacteria/MR1-L electrolyte based on inoculum prepared with bacteria sampled in log-phase (OD_{600} = 1.6) and diluted at an OD_{600} of 0.7. **(a, b)** $E_{we} = +0.3\ V\ (E_{ce} = -0.3\ V, \Delta E_{apply} = 0.6\ V)$, **(c, d)** $E_{we} = +0.5\ V\ (E_{ce} = -0.5\ V, \Delta E_{apply} = 1\ V)$, **(e, f)** Non-polarized and **(g, h)** $E_{we} = -0.3\ V\ (E_{ce} = +0.3\ V, \Delta E_{apply} = 0.6\ V)$,

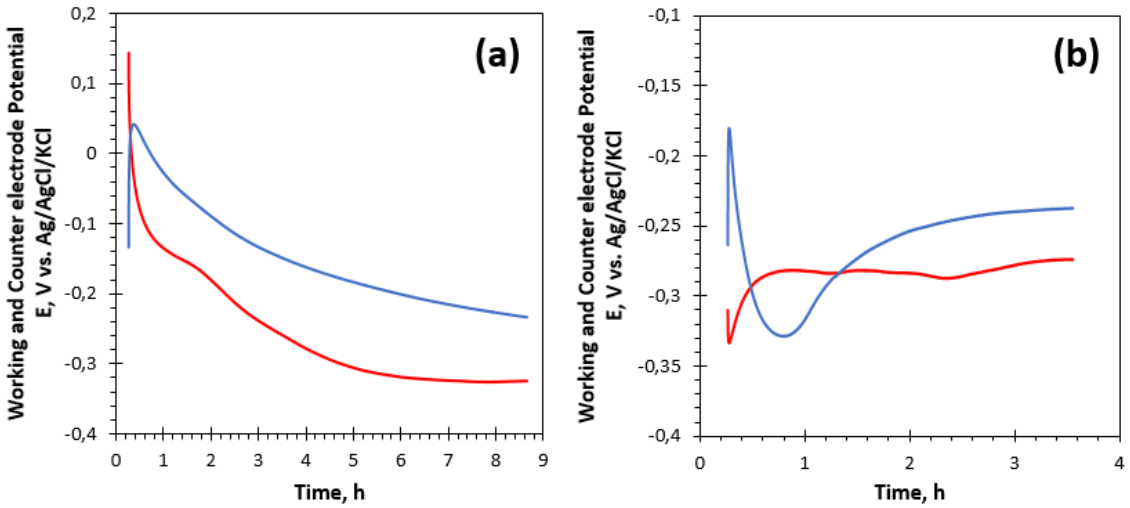

Figure 2.36 – Monitoring of the working electrode potential (E_{we}) and of the counter electrode potential (E_{ce}) of a reactor with non-polarized electrode at **(a)** day 1 and **(b)** day 3.
Caption: **— Working electrode OCP** in red, **— Counter electrode OCP** in blue.

However due to the absence of a separator between the bio-anode and the cathode, the counter electrode is exposed to the bacteria and may be poisoned by the bacteria. In absence of polarization, the resulting variation on the difference of potential may lead to the inversion of the electrode roles (working electrode OCP begins to be less negative than the counter electrode). As shown on **Figure 2.36**, this phenomenon is intensified without an applied potential at one or both electrodes and occurs without predictable behavior. Moreover, the **Figure 2.37** indicates a high colonization of the working electrode but also a contamination of the counter electrode due to the periodic inversion of potential reported on **Figure 2.36**. To avoid this issue, dual-compartments reactors appear well-adapted. Note that this phenomenon is also observed in polarized configuration at a lesser proportion leading to better performances.

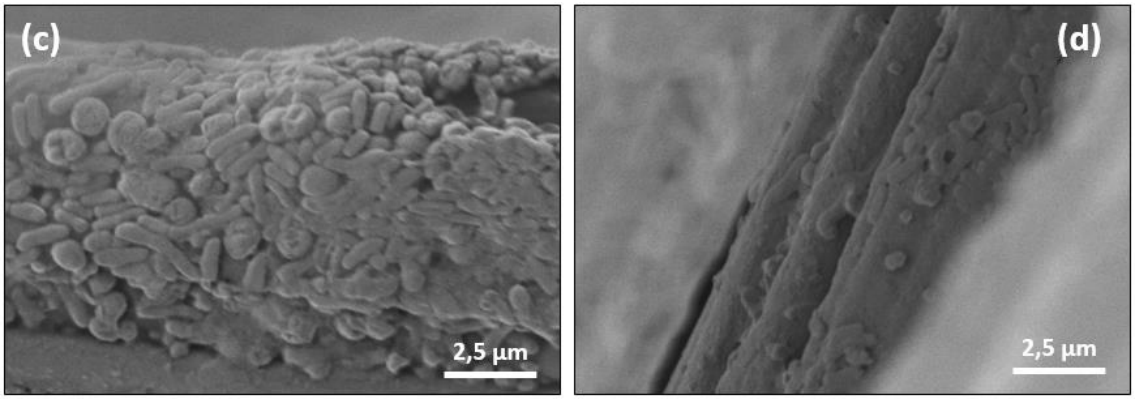

Figure 2.37 – Scanning electronic microscopy of a defined **(a)** working electrode and a defined **(b)** counter electrode non-polarized observed after 19 days of incubation in a bacteria MR1-L electrolyte based on inoculum prepared with bacteria sampled in log-phase (OD_{600} = 1.6) and diluted at an OD_{600} of 0.7. The picture indicates a high colonization of the working electrode but also a contamination of the counter electrode due to the periodic inversion of potential reported on **Figure 2.36.b**.

2.4.4.2. Dual-compartments reactor: implications and performance as function of the potential of polarization.

In a dual-compartments configuration, the reactor is divided in two parts by a separator, also named membrane. The aim of the membrane is to avoid the bacterium diffusion from the anodic side to the cathodic side and prevents the cathode (counter electrode) colonization or poisoning by anodic cells. The membrane can also be used to limit the diffusion of oxygen from the cathodic side (reduction of the oxygen in water, $E^0 = 1.23\,V\ vs.\ NHE$) which may deactivate or lead to the death of anaerobic strict bacteria. Various membrane can be used to separate the compartments (cf. 1.5.3). The most used membranes allow specifically the migration of charged species (cations CEM, anions AEM or protons PEM exchange membranes). But, other less specific membranes, such as ultrafiltration membranes (pore size from 0.2 µm to 0.45 µm), can be used to simply avoid catholyte contamination by the bacteria.

Reactor set-up and experimental conditions.

In this part, the polarization step is characterized (as in part 2.4.4.1) in a dual-compartments configuration. The anodic and cathodic sides are first separated by an ultrafiltration membrane with pore sized fixed at 0.2 µm **(Figure 2.39, Figure 2.40)**. In a second time the ultrafiltration membrane is replaced by a Nafion® membrane (NRE-212, ca. 50.8 µm in thickness, Sigma-Aldrich) as a proton exchange membrane **(Figure 2.43)**. To check the permeability of the membrane to *S. onedensis*, one side was filled with 20 mL of bacteria solution and the other side was filled with MR1-L/F medium and left at least 5 days. No contamination of the side initially free of bacteria was observed (by optical density measurement and counting on plate, **Figure 2.38**).

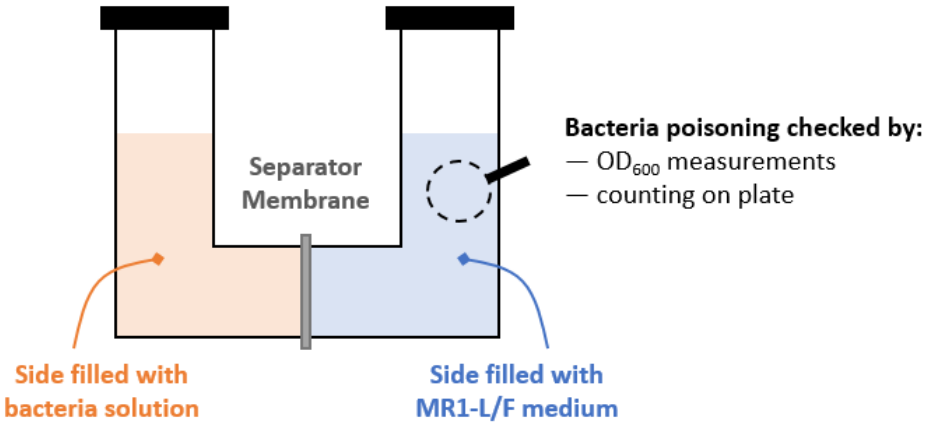

Figure 2.38 – Schematic representation of the configuration and the test use to check the non-permeability of the ultrafiltration membrane separator and of the Nafion® membrane to the bacteria

For MFC preparation, the anolyte is composed by a prepared inoculum with bacteria sampled at 1.6 in optical density, transferred and diluted at OD_{600} = 0.7 in MR1-L medium. The catholyte consists in a 10 mM $K_3Fe(CN)_6$ supplemented with 150 mM NaCl (support electrolyte). The working electrode also defined as the bio-anode is a 1 cm^3 untreated carbon felt (geometric surface A_{geo} = 6 cm^2) and the cathode a 2 cm^3 carbon felt. The cathode volume and surface is

conventionally doubled to ensure the non-limitation of the measured performance due to the cathodic reduction. The anodic and cathodic carbon felts are sterilized and respectively immersed in sterilized MR1 medium and catholyte. Both anodic and cathodic sides are equipped with vent-caps to ensure atmospheric exchanges in sterile condition and with a micro-Ag/AgCl/KCl (sat.) reference. The bio-anode and cathode electrodes poised potentials are applied against the references. For example, for a positive polarization at +0.3 V:

$$E_{bio-anode \rightarrow ref_{catholyte}} = +0.3\ V,\ E_{cathode \rightarrow ref_{catholyte}} = -0.3\ V, \text{ and } \Delta E_{apply} = \Delta E_{bio-anode \rightarrow cathode} = 0.6\ V.$$

As in the case of a single-compartment, the reactors are allowed to stabilized at the OCV for 1h before measurements. Polarization and power curves are determined with a Biologic VSP potentiostat in fuel cell configuration. In this configuration, the cathode is considered as the working electrode, the anode as the counter electrode and the cathodic Ag/AgCl/KCl electrode is used as reference electrode. An incremental series of current i (corresponding to an equivalent density of current $j\ (mA.cm^{-2}) = i/A_{geo}$) is applied to the working electrode and the potential of the anode and the cathode are measured against the reference. The MFC difference of potential (e.m.f.) is calculated as $\Delta E = E_{cathode} - E_{anode} = f(j)$ (polarization curve) and the power as $P(mW.cm^{-2}) = \Delta E * j = j^2 * R = f(j)$ (with R, the equivalent applied resistance).

Results for non-optimized reactors with ultrafiltration membranes.

(Figure 2.39 and Figure 2.40, main results are summarized in Table 2.5 and Table 2.6)

Figure 2.39 displays the evolution of the polarization curves and the power curves during 19 days of symmetrical polarization with an anode polarized at $\boldsymbol{E_{anode}^{apply} = +0.3\ V}$ $(vs.\ E_{cathode}^{apply} = -0.3\ V\ and\ \Delta E_{apply} = 0.6\ V)$. The anodic and the cathodic compartments are separated by an ultrafiltration membrane with a pore size of 0.2 µm. In this condition, the bio-anode potential is equal to -0.4 V vs. Ag/AgCl/KCl at day 2. Then, the anode OCP varies around -0.45 V vs. Ag/AgCl/KCl between -0.39 V and -0.48 V vs. Ag/AgCl/KCl. This anodic potential is close to the redox potential of the flavin shuttle. The current density at E_{anode} = 0 V vs. Ag/AgCl/KCl evolves from 10 mA/m² at day 2 to 30 mA.m^{-2} at day 19. The current profile $\left(i = f(E_{cathode})\right)$ of the cathode is unstable in time. In optimized condition (regular renewal of the catholyte), this profile should remain stable in time **(Figure 2.39.a)**. The evolution of the MFC polarization curves **(Figure 2.39.c)** is a result of the anodic and cathodic current profile. The OCV of the MFC is stable around 0.65 V and the maximum current density decrease from ca. 95 mA.m^{-2} to 50 mA.m^{-2}. The slope of the polarization curves is related to the internal resistance of the MFC $(R_{INT} = \Delta E/j)$. In the present case, the internal resistance R_{INT} increases with time. In parallel, the power curves indicate a loss in power from ca. 20 mW.m^{-2} (day 2) to ca. 7 mW.m^{-2} (day 19).

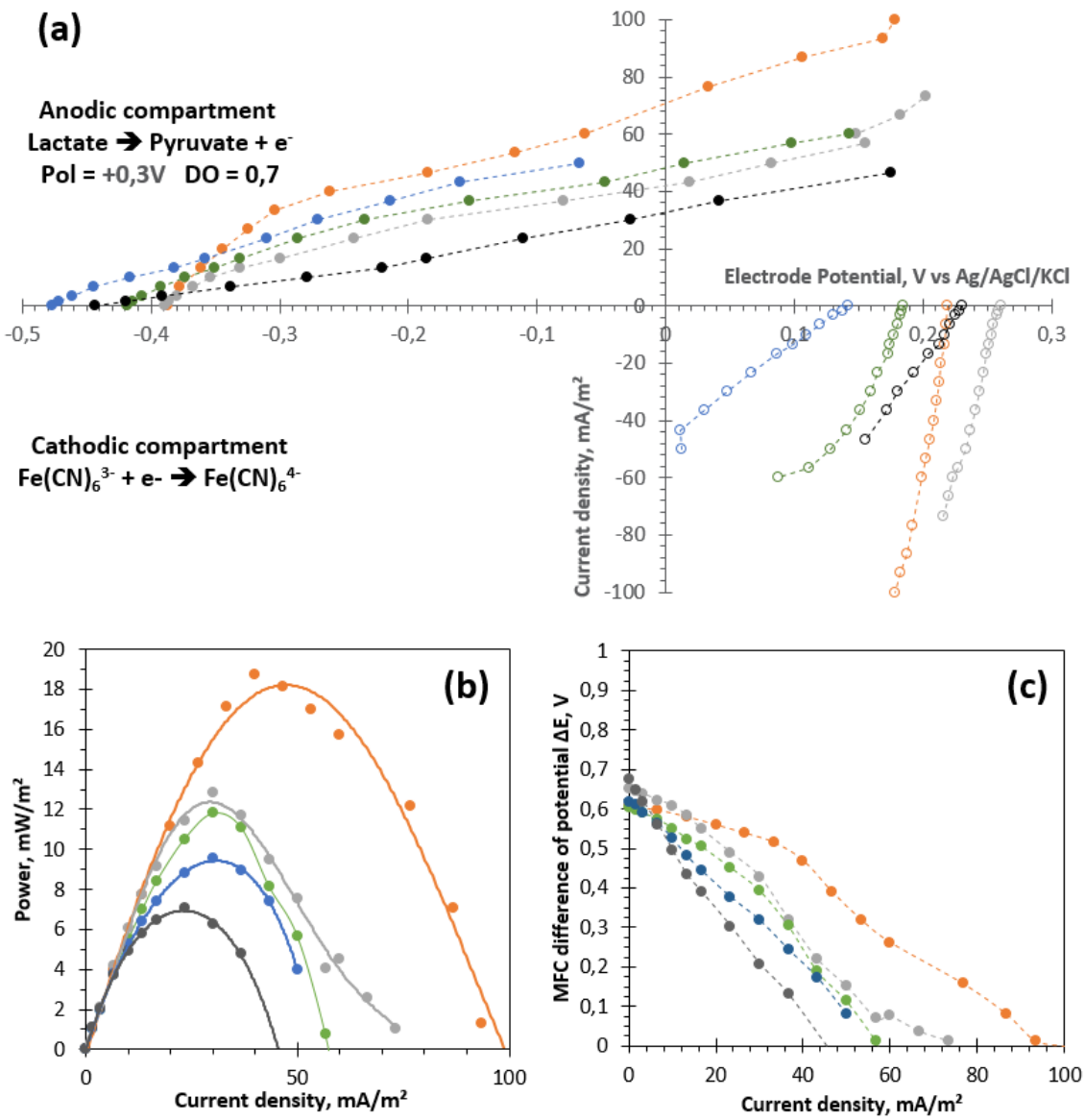

Figure 2.39 – Electrochemical characterization of a dual-compartment MFC (with a Nafion® NRE-212, 50 µm thick, Sigma-Aldrich) composed of 2 compartment separated by a Nafion® membrane. Both anode (working electrode) and cathode (counter electrode) are a 1 cm^3 carbon felt (1 cm square in shape). The anode is incubated with *S. oneidensis* sampled at OD_{600} = 1.4 transferred in a MR1-L medium and diluted at a OD_{600} = 0.7 and polarized (vs. counter electrode) at $\boldsymbol{E_{working} = E_{anode} = +0.3\ V}$. The cathode is immersed in a 10 mM $K_4Fe(CN)_6$ and 150 mM KCl. *Before measurement, reactor is allowed to stabilized at OCV for 1h.*

(a) Anodic (•) and cathodic (○) current in function of the electrode potential in time. **(b)** Power curves in time. **(c)** Polarization curves in time.

Caption: •, ○, — **day 2** in orange. •, ○, — **day 5** in gray. •, ○, — **day 6** in green. •, ○, — **day 15** in blue. •, ○, — **day 19** in dark.

Day	2	5	6	15	19
OCP, E_{anode}(j=0), V	-0.39	-0.39	-0.42	-0.48	-0.45
j(E=0), mA.m^{-2}	70	40	50	55	35
MFC OCV, ΔE(i=0), V	0.606	0.65	0.605	0.62	0.675
j_{max}, j(ΔE=0), mA.m^{-2}	100	75	55	55	45
P_{max}, mW.m^{-2}	19	13	12	9	7

Table 2.5 – Compiled data from **Figure 2.39**.

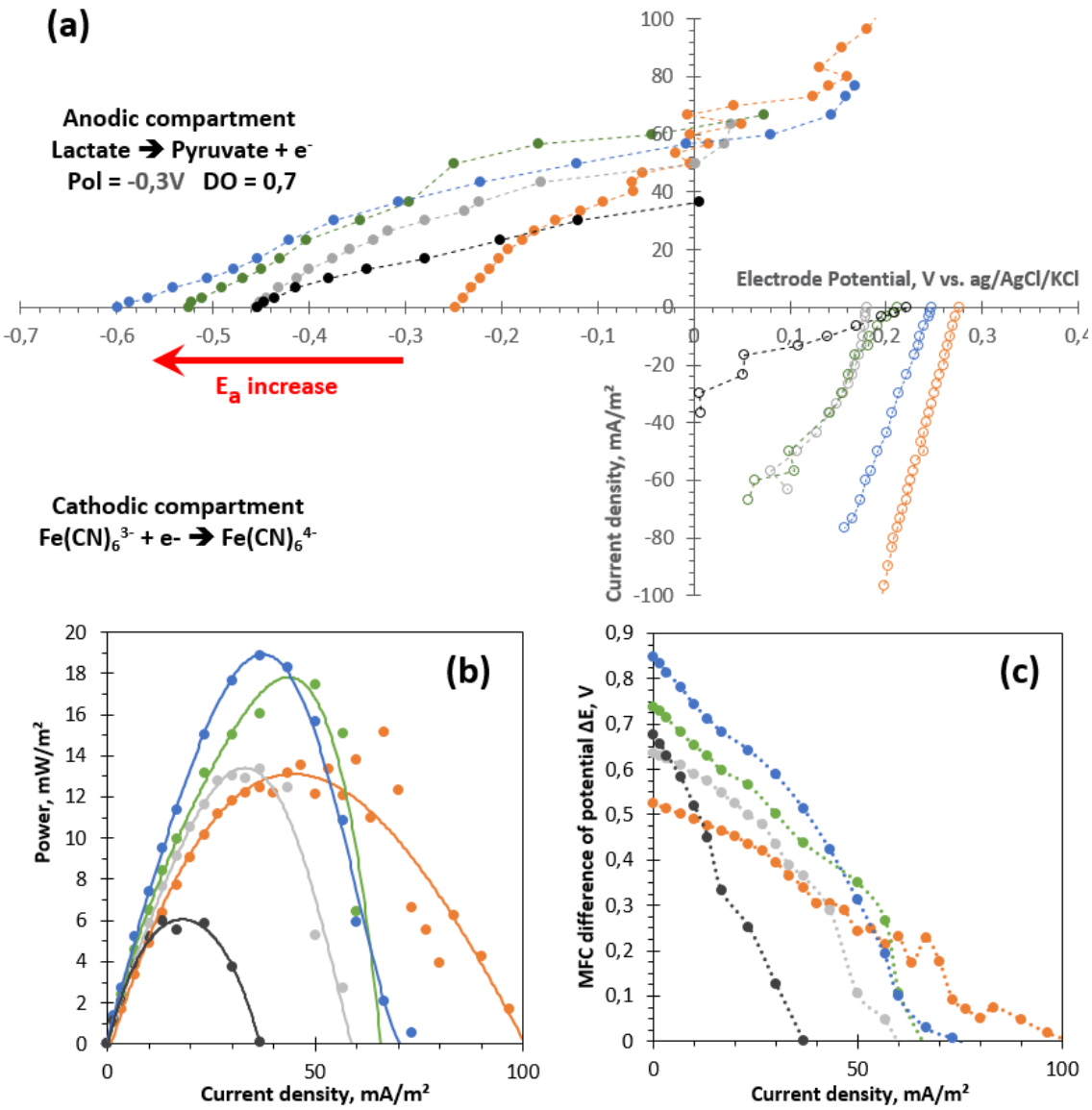

Figure 2.40 – Electrochemical characterization of a dual-compartment MFC (same as figure 2.37). The anode is incubated with *S. oneidensis* sampled at OD_{600} = 1.4 transferred in a MR1-L medium and diluted at a OD_{600} = 0.7 and polarized (vs. counter electrode) at $\boldsymbol{E_{working} = E_{anode} = -0.3\ V}$. The cathode is immersed in a 10 mM $K_4Fe(CN)_6$ and 150 mM KCl. Before measurement, reactor is allowed to stabilized at OCV for 1h.
(a) Anodic (•) and cathodic (○) current in function of the electrode potential in time. **(b)** Power curves in time. **(c)** Polarization curves in time.
Caption: •, ○, — **day 2** in orange. •, ○, — **day 5** in gray. •, ○, — **day 6** in green. •, ○, — **day 15** in blue. •, ○, — **day 19** in dark.

Day	2	5	6	15	19
OCP, E_{anode}(j=0), V	-0.25	-0.45	-0.52	-0.6	-0.45
j(E=0), $mA.m^{-2}$	60	50	57	60	39
MFC OCV, ΔE(i=0), V	0.53	0.65	0.75	0.85	0.7
j_{max}, j(ΔE=0), $mA.m^{-2}$	100	60	70	70	38
P_{max}, $mW.m^{-2}$	13	13	17	19	6

Table 2.6 – Compiled data from **Figure 2.40**

Figure 2.40 describes the evolution of the characteristic curves in similar reactor configuration but for a negative anodic polarization fixed at $\boldsymbol{E_{anode}^{apply}} = \boldsymbol{-0.3\ V}$ $\left(E_{cathode}^{apply} = +0.3\ V\ and\ \Delta E_{apply} = 0.6\ V\right)$. At the open-circuit, the bio-anodic potential (OCP) regularly increases (in absolute value) from -0.25 V (day 2) to -0.6 V vs. Ag/AgCl/KCl (day 15). At the short-circuit potential (ΔE = 0), the measured anodic density of current remains stable at around 60 mA/m². At day 19, the anodic OCP and the short-circuit current have respectively decreased at -0.45 V vs. Ag/AgCl/KCl and 38 mA.m^{-2}. This loss in voltage and current is explained by the depletion in lactate due to the absence of feeding since day 13. As for the previous case (anode poised at +0.3 V), the cathodic current profile is unstable and would require optimization **(Figure 2.40.a)**. But, as the cathodic reaction is based on the couple $Fe(CN)_6^{3-}/Fe(CN)_6^{4-}$ which is not supposed to be used for applied MFC, we did not pay too much attention. The MFC OCV shown on **Figure 2.40.c** increases from 0.5 V (day 2) to 0.85 V (day 15) and the maximal power from 12 mW.m^{-2} to 20 mW.m^{-2}. The initial maximal density of current j_{max} is about 100 mA.m^{-2} and decreases to 60 mA.m^{-2} at day 5. At day 6, the recovered j_{max} is equal to 25% of the loss $(j_{max} = 70\ mA.m^2)$. This loss may be related to a lack of optimization of the feeding time and the increase of the internal resistance (slope of the polarization curves). j_{max} remains stable until day 15 and decrease to 40 mA.m^{-2} at day 19, which again may be due to the absence of feeding.

The structure of the bacteria and of the biofilm observed by SEM **(Figure 2.41)** can be correlated to the evolution of the characteristic parameters of the MFC under polarization (anodic OCP, MFC OCV, MFC Power and the maximal current delivered) shown in **Figure 2.39**, **Table 2.5**, **Figure 2.40** and **Table 2.6**. For a working electrode symmetrically poised $\boldsymbol{E_{anode}^{apply}} = \boldsymbol{+0.3\ V}$ $\left(vs.\ E_{cathode}^{apply} = -0.3\ V\ and\ \Delta E_{apply} = 0.6\ V\right)$ the bacteria are distinctly deposited and form a layer of bacteria on the fiber. This bacterial layer is embedded in a thin and dense biofilm which forms a sheath around the fibers **(Figure 2.41.a to Figure 2.41.d)**. On the contrary, at negative working electrode polarization at $\boldsymbol{E_{anode}^{apply}} = \boldsymbol{-0.3\ V}$ $(vs.\ E_{cathode}^{apply} = +0.3\ V\ and\ \Delta E_{apply} = 0.6\ V)$, a large quantity of biomass (EPS, bacteria, …) is produced and stuck in the porosity of the carbon felt. The fibers are embedded in a thick and porous biofilm structure composed of a high density of bacteria and EPS. Moreover, and unlike at a positive poised potential, at -0.3 V the fibers may be compared to an interconnected network in which bacteria and biofilm are connected to the carbon. Indeed, bacteria are clearly visible (and in contact) in the bridge between the fibers and supported by the EPS polymeric structure **(Figure 2.41.e, Figure 2.41.f, red arrows)**. Due to the tight biofilm sheath around the fibers at positive polarization, the bacteria are less visible than the bacteria embedded in the softer and more porous biofilm structure formed at E_{anode} = -0.3 V. These structure can be correlated to the characteristic parameters expressed above. As previously defined, the bio-anodic OCP is related to a variation of the structure at the surface of the fibers. Here, depending on the potential, the interaction of bacteria with the fiber surface can be transitory, so that bacteria grow between the fibers, or permanent, leading to bacteria growth on the fibers.

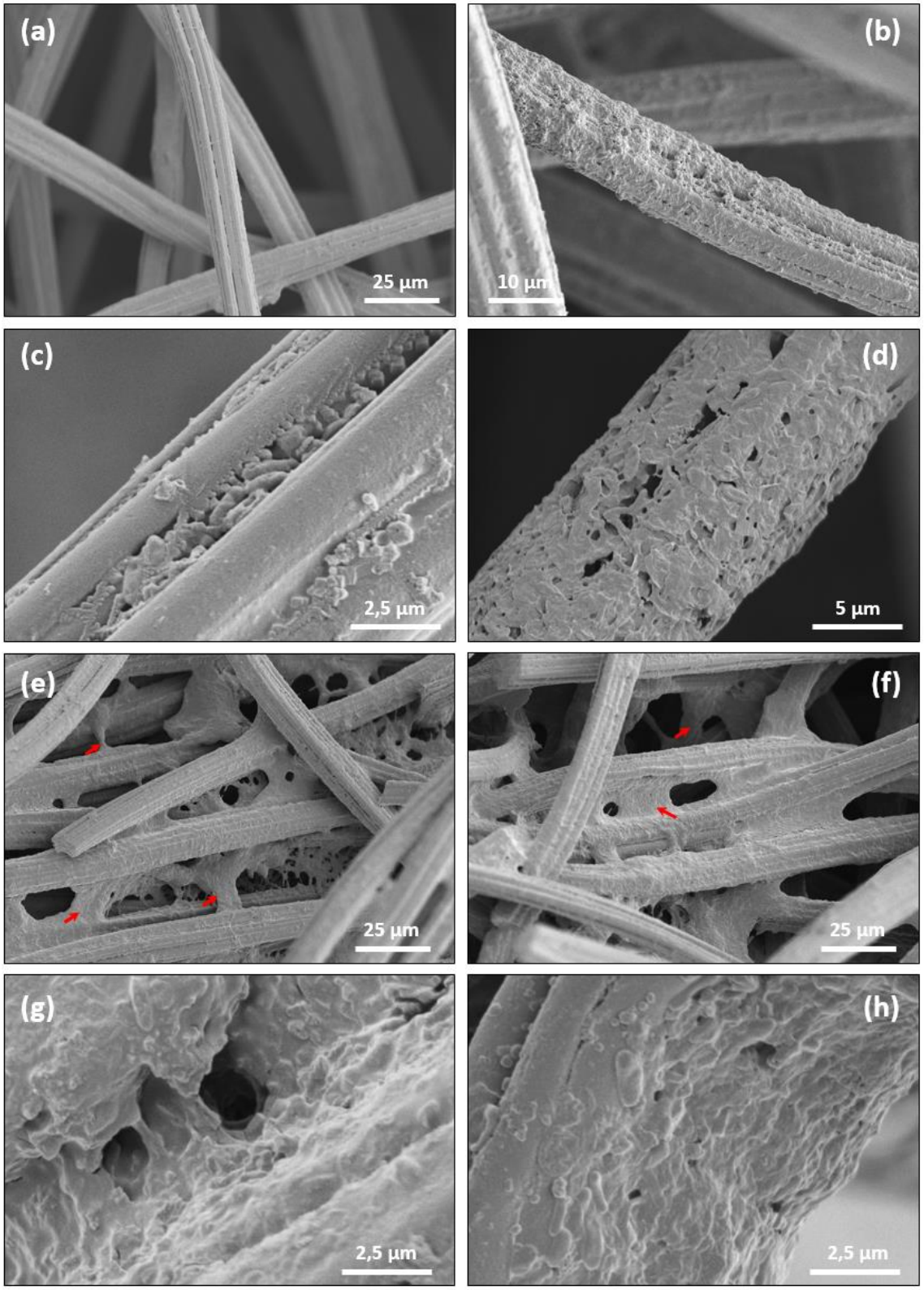

Figure 2.41 – Scanning electronic microscopy of carbon-felt bio-anodes after 19 days in dual-compartments reactors (described above). The bio-anode was incubated for 19 days in a bacteria/MR1-L anolyte prepared with bacteria sampled in log-phase (OD_{600} = 1.6) and diluted at an OD_{600} of 0.7.
Each bio-anode is polarized at a specific potential: **(a-d)** $E_{anode} = +0.3\ V$ $(E_{cathode} = -0.3\ V, \Delta E_{apply} = 0.6\ V)$, electrochemical characterization available on **Figure 2.39** and **(e-h)** $E_{anode} = -0.3\ V$ $(E_{cathode} = +0.3\ V, \Delta E_{apply} = 0.6\ V)$, electrochemical characterization available on **Figure 2.40**.

Thus, in the case of **a positive polarization (E_{anode} = +0.3 V)**, after a short time of polarization, the bio-anodic OCP reaches a stable value between -0.39 V and -0.48 V vs. Ag/AgCl/KCl **(Figure 2.39.a)**, indicating a fast and intense colonization in the first days of polarization, as confirmed by SEM. Then a stable situation remains in term of fibers colonization and the MFC OCV (at j = 0 mA/m²) remains stable around 0.65 V from the day 2 to the last day of measurement (day 19). The decrease in current and power densities is directly correlated to the increase of the internal resistance observed on the polarization curves **(Figure 2.39.b, Figure 2.39.c)**. Both charge and mass transfer can explain the loss in performance for long time polarization: (i) A lack of charge transfer probably due to a deficient biofilm in term of electronic conductivity. (ii) A lack of mass transfer caused by a limitation of the nutrients and electron shuttles diffusion through the dense biofilm. As a consequence, the bacteria accessibility to the carbon source is limited and leads to a depletion in lactate concentration in the biofilm. The lack in electron shuttles diffusion may limit the MET by the bacteria embedded in the biofilm but not directly connected to the conductive fibers or to a structural electron transfer chain (chain of bacterial cytochrome or conductive pili). Moreover, the MET carried out by the bacteria in the electrolyte needs to proceed through the biofilm. If this diffusion is hindered, the external transfers are limited. These hypotheses are in agreement with the sign and value of the poised potential since +0.3 V vs. Ag/AgCl/KCl corresponds to the DET domain and may promote initial fast bacteria adhesion at the surface. Finally, the absence of bio-anodic OCP degradation during the starvation phase (measured at day 19 after 5 days without lactate renewal) indicates a high resistance of the biofilm structure. It means that the biofilm structure and the carbon-bacteria interaction are resilient.

For **a negative polarization at E_{anode} = -0.3 V**, the progressive decreases of the bio-anodic OCP from -0.25 V (day 2) to -0.6 V vs. Ag/AgCl/KCl (day 15) indicates a modification of the bio-anode on the long term with a progressive colonization of the carbon felt for at least the first 15 days of polarization being observed. The MFC OCV and the bio-anodic potential (even if the cathodic current profile is unstable) increase. The current loss between day 2 and day 5 is partially recovered at day 6 and then its value is stable. This loss can be attributed to a transitional phase during which the fibers are partially coated by a layer of bacteria that produce the biofilm. However, the partial recovery of the current density and its stabilization in turn-over condition suggests that the initial loss cannot only be attributed to limited mass transfer but may also results from the surface modification by bacteria adsorption and biofilm formation. Increasing of the power density is in accordance with the increasing of the bacteria density. At day 19, the observed important loss in bio-anodic OCP suggests a higher sensitivity to nutrient availability than bacterial structure formed on a bio-anode poised at +0.3 V. These results are in accordance with the predictable behavior of the bio-anode at -0.3 V vs. Ag/AgCl/KCl where the MET is promoted. As a consequence, the bacterial adhesion required for DET can occur but at a limited rate, leading to a slow increase of the bio-anode OCP and of MFC performance.

To conclude, in this first dual-compartments configuration, both anodic (working) and cathodic (counter) electrodes are separated by a larger distance than in single compartment systems and by a non-ion-conductive separator supposed to increase the internal MFC

resistance. Therefore, the explanation referring to the competition between the oppositely polarized electrodes for the bacteria in a single-compartments is no longer applicable. In dual-compartments, only one electrode polarized at a specifically chosen potential is available. The other potential is applied at the cathodic side and its sphere of influence on the bacteria is limited. In this condition, beyond the sign and the intensity of the applied potential, the polarization appears favorable for anode to be colonized by the bacteria and the electron transfer to occur. Based on these considerations and that the density of power delivers at day 2 by the reactor with a bio-anode polarized at +0.3 V (19 $mW.m^{-2}$) is equivalent to the power delivered by the negatively-polarized reactor at day 15, two bacterial comportments are promoted: (i) For a bio-anode negatively poised at E_{anode} = -0.3 V, MET is promoted and the colonization of the felt by the bacteria occurs slowly due to the EET mechanism via electron shuttles. In this condition a high quantity of biomass bridging the carbon fibers is produced. (ii) For positively poised bio-anode at E_{anode} = +0.3 V, DET is promoted and the colonization occurs in the very first days before stabilization of the bio-anode OCP.

Results for an optimized reactor with a Nafion® membrane.

(Figure 2.42, main results are compiled in Table 2.7)

To optimize the performances in dual-compartments configuration: (i) the ultrafiltration membrane used as separator is replaced by a Nafion® membrane (NRE-212, ca. 50.8 µm in thickness, Sigma-Aldrich). This membrane is less resistive (less damageable for R_{INT}) and dedicated to proton diffusion but subjected to biofouling. (ii) The distance between the electrodes is decreased from 5 to 2 cm. (iii) The 10 mM $K_3Fe(CN)_6$ (150 mM NaCl) catholyte is regularly changed to avoid instability due to the depletion in final cathodic electron acceptors. The negative polarization is chosen based on the previous results.

Figure 2.42 displays the electrochemical behavior of the optimized reactor as described above. The progressive increase of the bio-anodic OCP is verified with a similar potential increase. Until day 7, the maximal current density remains stable at 140 $mA.m^{-2}$ and the slopes of the polarization curves are similar. At day 5, the power density (20 $mW.m^{-2}$) is equivalent to the power density of the non-optimized reactor at day 15, with higher maximal current density (140 $mA.m^{-2}$ vs. 100 $mA.m^{-2}$). The MFC OCV and the bio-anodic OCP increase. Moreover, the catholyte renewal permits to stabilize the current profile of the cathode.

During the time of polarization, the effect of a stress due to a depletion in nutrient (lactate) is evaluated. Between day 5 and day 9, no lactate is provided to the bacteria. The bacteria in colonization and division phases consume the available lactate. At day 9, the performances are degraded due to the lack in lactate in the electrolyte. The power is decreased by a factor 1.6 (from ca. 25 to 15 $mW.m^{-2}$) in 2 days. The ability of the bacteria to reactivate and/or divide and colonize are evaluated by adding an equivalent of 30 mM sodium lactate at day 9. The lactate solution added to the batch is deaerated to avoid performance variation due to a punctual and drastic change of the oxygen concentration. At day 12 after 3 days in turn-over condition, the MFC performance is not only recovered but highly improved: the power density is increased by 160% (65 $mW.m^{-2}$) and the maximal current density by 720%

(330 mA.m^{-2}). Moreover, the performances continue to increase until the end of monitoring. At day 15, the maximal density of power and current are equivalent to 80 mW.m^{-2} and 380 mA.m^{-2}, the MFC OCV reaches 0.9 V.

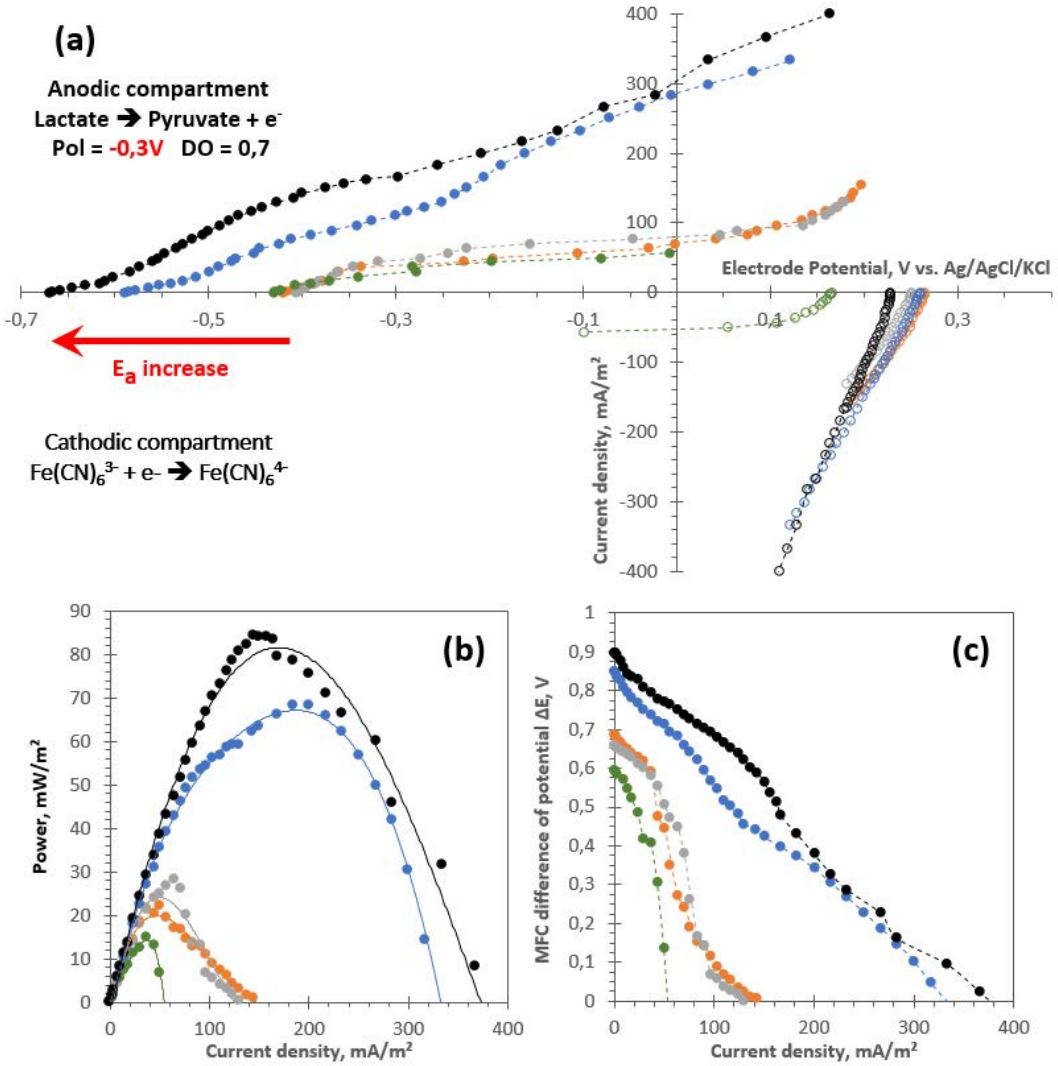

Figure 2.42 – Electrochemical characterization of a dual-compartment MFC (same as **figure 2.20**). The anode is incubated with *S. oneidensis* sampled at OD_{600} = 1.4 transferred in a MR1-L medium and diluted at a OD_{600} = 0.7 and polarized (vs. counter electrode) at $\boldsymbol{E_{working} = E_{anode} = -0.3\ V}$. The cathode is immersed in a 10 mM $K_4Fe(CN)_6$ and 150 mM KCl. **Space between electrodes and catholyte renewal optimization**. Before measurement, reactor is allowed to stabilized at OCV for 1h.

(a) Anodic (•) and cathodic (○) current in function of the electrode potential in time. **(b)** Power curves in time. **(c)** Polarization curves in time.

Caption: •, ○, — **day 5** in orange. •, ○, — **day 7** in gray. •, ○, — **day 9** in green. •, ○, — **day 12** in blue. •, ○, — **day 15** in dark.

Day	5	7	9	12	15
OCP, E_{anode}(j=0), V	-0.42	-0.4	-0.42	-0.6	-0.68
j(E=0), mA.m^{-2}	70	80	70	280	300
MFC OCV, ΔE(i=0), V	0.7	0.65	0.6	0.85	0.9
j_{max}, j(ΔE=0), mA.m^{-2}	140	125	40	330	390
P_{max}, mW.m^{-2}	20	25	15	65	80

Table 2.7 – Compiled data from **Figure 2.42**

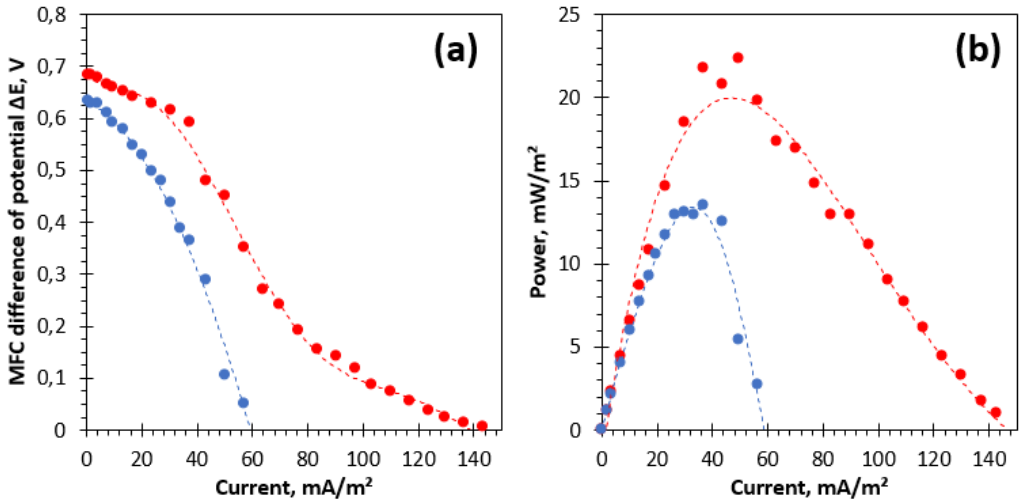

Figure 2.43 – MFC performance comparison between **a non-optimized reactor** with an ultrafiltration membrane in red and **an optimized reactor** in blue, **5 days after the beginning of the polarization at E_{anode} = -0.3 V** ($E_{cathode}$ = +0.3 V and ΔE_{apply} = 0.6 V). **(a)** Polarization curves and **(b)** power curves.

To summarize, thanks to a few modifications in the design of the reactor, the MFC performances are improved **(Figure 2.43, Figure 2.42)**: (i) changing the ultrafiltration membrane for a more selective Nafion® membrane allows to decrease the internal resistance due to the isolative membrane [178]. Moreover, a Nafion® membrane limits mutual poisoning of the anolyte and the catolyte by faradaic species. (ii) by significantly reducing the distance between the electrodes (from 5 to 2 cm), the travel of the protons from the anode to the cathode is also reduced. (iii) by improving the stability of the catholyte composition, oxidized $Fe(CN)_6^{3-}$ species are always available to accommodate electrons arrival from the bio-anode. In addition, it appears that the bacteria and biofilm structuration resulting of a polarization of the anode at -0.3 V better accommodates the variation of nutrient availability.

2.5. How encapsulated Shewanella oneidensis in silica gel depend on the applied potential of polarization?

2.5.1. General assessments on micro-organisms encapsulation.

As previously demonstrated, the formation of an electroactive biofilm at the surface of an electrode depends in many parameters and more particularly on the bacterium or the community of bacteria employed as exoelectrogenic micro-organisms. The global architecture of the biofuel cell, more specifically the bio-electrode nature, geometry and surface chemistry also influences the biofilm formation. The strategy employed to enhance the biofilm formation (natural formation or electrode perturbation) is determinant to build an active and productive bio-anode or bio-cathode. The performance of a bio-electrode is directly related to the bacterium metabolism and on its ability to perform EET. Both parameters are dependent on the mass and the charge transfers, themselves dependent on many parameters such as the thickness, the conductivity, the porosity and the bacterial percolation of the electrode. But it is also strongly impacted by the ability of various substrates (carbon sources), electroactive mediators, products of the respiration and protons to diffuse actively through the biofilm. For example, a limited diffusion of protons (as a product of the electron donor bio-oxidation)

acidifies the biofilm, leading to the degradation of the bacterial community activity or, in worst case, conducting to the death of the bacteria.

Recent studies have described innovative strategies to artificially improve the biofilm electronic transfer, by doping the electrode via direct immobilization of conductive groups and mediators or by coating the surface with specific conductive polymers [136,147], polymers grafted with mediators such as AQDS [73] or conductive carbon dispersed in a polymer matrix [220]. As an example, in 2007, Qiao *et al.* demonstrated the efficiency of a PANI/CNT paste on metallic foams as bio-anodic based material (cf. 1.5.1.2, **Figure 1.18**) [147] and in 2013, Nguyen *et al.* proved the enhancement of their MFC performances by substituting a basic carbon cloth with a SWCNT-coated mesoporous polysulfone matrix electrode [221].

Based on these technological advances, the concept of artificial biofilm was introduced to overcome the constraints and the variability introduced by the bacterium physiology and the formation of an adhesive and conductive biofilm. In an artificial biofilm, planktonic cells (single and distinct bacteria in suspension) are embedded in a chosen matrix that allows EET between these organisms and the electrodes. To serve as an artificial biofilm, the matrix must contain nontoxic materials such as natural polymers, carbon, non-reactive metals or cytocompatible artificial (i.e. synthetic) polymers. The choice of the matrix depends on the ability of the bacterium strain to transfer electrons by both MET and DET pathways or only one of them. As an example, in 2008, Srikanth *et al.* proved the ability of *G. sulfurreducens* to transfer electrons even if suspended in a pectin matrix at the surface of a graphite paper [222]. *G. sulfurreducens* only performs DET, but the structured artificial biofilm demonstrated an electro-activity. Another option was developed by Yu *et al.* in 2011 with *S. oneidensis* as an electro-active model bacterium. The concept consists in the production of a paste by associating *S. oneidensis* with a mixture of a conductive polymer (polypyrrole) and a graphite powder. The paste is applied on a carbon fiber surface which is used as a collector of electrons [223]. They demonstrated acceptable viability of the encapsulated cells and MFC performances were significantly enhanced in comparison with the carbon fibers paper alone.

In controlled conditions, an artificial biofilm based on bio-organic materials can present excellent properties of cytocompatibility, supporting an acceptable viability of the encapsulated micro-organism. However, inorganic matrices such as silica gel represent a valuable alternative to organic biofilms. An inorganic matrix can be mechanically resistant, mesoporous, less sensitive to the degradation in a non-ideal environment (seawater, wastewater, effluent) and presents an enhanced resistance towards biodegradation (bacteria metabolism, enzymatic attack). It can be prepared in cytocompatible conditions. Thanks to these advantages, the silica gel was selected here as an inorganic material for bacteria encapsulation in a carbon felt in order to create a 3D inorganic artificial biofilm in the porosity of a conductive matrix.

2.5.2. How to produce a silica gel for micro-organisms encapsulation?

A silica gel is an inorganic matrix produced with silica precursors via the sol-gel process. The sol-gel process corresponds to the abbreviation « solution-gelation » and corresponds to an

inorganic polymerization of inorganic precursors in *solution*. Through condensation reactions, the size of the polymers increases until they are able to form an interconnected network of silica colloidal species (percolation). The *gelation* occurs and forms a solid monolith entrapping the reaction solvent. Two reactional pathways are available to obtain a silica gel, the alkoxide pathway and the aqueous pathway. Both pathways were clearly described by Brinker and Scherer in 1990 [224] and by Jolivet in 1998 [225].

2.5.2.1. Alkoxide pathway.

The alkoxide pathways consists in the hydrolysis and condensation of silica precursors composed of a single-silicon atom bound to four alkoxy groups (−OR). Tetraethoxysilane (TEOS, $Si(OCH_2CH_3)_4$) is the most commonly used silica precursor. But others precursors are available such as the tetramethoxysilane (TMOS, $Si(OCH_3)_4$) or the Triethoxymethylsilane (MTEOS, $H_3CSi(OCH_3)_3$). The latter belongs to the family of ORMOSILs for *or*ganically *mo*dify *sil*icates that allow to introduce specific function to the silica gel by grafting specific groups directly on the precursor. Due to the $Si-C$ bond stability in the conditions of inorganic polymerization, these functional groups remain in the silica gel.

To polymerize and form a gel, silica precursors must in a first step be made reactive. The hydrolysis of the precursors consists in replacing at least one of the four alkoxy ligands by reactive hydroxyl groups $(-OH)$ via the following reaction. This reaction is generally catalyzed in acidic (H^+) or basic (OH^-) conditions.

$$\underline{\text{Hydrolysis:}}\ (RO)_3 - Si - \boldsymbol{OR} + H_2O \xrightarrow{H^+ \text{ or } HO^-} (RO)_3 - Si - \boldsymbol{OH} + \boldsymbol{ROH}$$

Following hydrolysis, the precursors react with each other and form a polymeric chain by two possible reactions of condensation: (i) an oxolation in which, two unprotected precursors react, form an $Si-O-Si$ link and produce a molecule of water as co-product. (ii) in an alkoxolation, a silanol group reacts with Si-OR group to form a $Si-O-Si$ bond and a molecule of alcohol (ROH). This reaction is generally catalyzed in basic (OH^-) conditions.

$$\underline{\text{Oxolation:}}\ (RO)_3 - Si - \boldsymbol{OH} + \boldsymbol{HO} - Si - (OR)_3 \rightarrow (RO)_3 - \boldsymbol{Si} - \boldsymbol{O} - \boldsymbol{Si} - (OR)_3 + \boldsymbol{H_2O}$$
$$\underline{\text{Alkoxolation:}}\ (RO)_3 - Si - \boldsymbol{OH} + \boldsymbol{RO} - Si - (OR)_3 \rightarrow (RO)_3 - \boldsymbol{Si} - \boldsymbol{O} - \boldsymbol{Si} - (OR)_3 + \boldsymbol{ROH}$$

In most conditions, hydrolysis and condensation occur simultaneously. However, the solution pH regulates the relative kinetics of the two reactions and also impact on the structure of the resulting gels. In acidic conditions, the condensation occurs preferentially at the ends of the growing polymeric chain. This results in an inorganic network formed of long chains, with a porosity in the microporous domain (below 2 nm). Due to this structure, the gel is transparent. In basic catalytic conditions, condensation preferentially occurs on partially substituted silicon atoms, leading to cyclic and then particulate polymers. The resulting silica gel is opaque and presents a higher mesoporosity (2 to 50 nm).

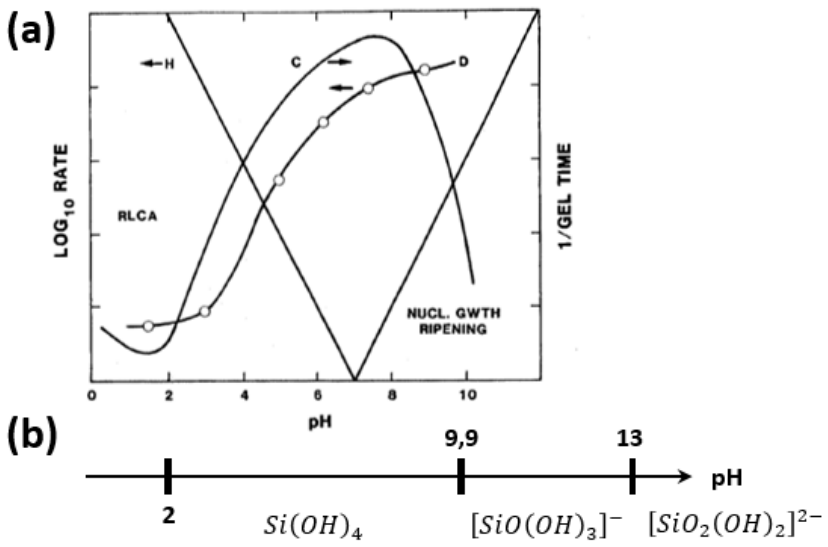

Figure 2.44 – (a) Main parameters of the hydrolysis-condensation reaction leading to the formation of a silica gel (H, Hydrolyze; C, Condensation; D, gel dissolution) and **(b)** pH domains of silicified species predominance. *(partially extract from Brinker and Scherer 1990 and Jolivet 1998* [224,225]*)*

2.5.2.2. Aqueous pathway.

In the aqueous pathway, silica precursors are silicic acids. Their condensation is therefore spontaneous unless the pH values are very low or very high: in these situations, silicic acid bear a charge that makes condensation unfavorable due to repulsive electrostatic interactions **(Figure 2.44.b)**. This is typically the case for the most commonly used precursor of aqueous silica gels, sodium silicates, that contain negatively-charged polysilicic acids and sodium ions at pH > 12. From these solutions, the condensation can be triggered by addition of an acid below pH 9-10, where the neutral $Si(OH)_4$ is prevalent. **(Figure 2.44)**.

2.5.2.3. Alkoxide pathway by gas vapor deposition.

The aqueous pathway has the advantages of using solvent-free and cheap precursors and to be relatively simple (no hydrolysis, gelation induced by a change in pH). However, the alkoxide route is more flexible as the control of hydrolysis/condensation rates, that can be tuned by both the amount of added water and pH conditions, allow to control the gel structure. Another interesting possibility of silicon alkoxides is to process them in the gas phase, allowing the formation of thin coatings. For this, the volatile alkoxide in its liquid state is equilibrated in a closed chamber containing the sample to be coated or its flown over it in its vapor state. Since water is necessary to achieve hydrolysis, the sample can be humid and/or the relative humidity in the chamber can be fixed with a salt solution [226]. The thickness of the deposited dense silica layer usually increases with the process duration.

2.5.2.4. Micro-organisms encapsulation into a silica gel.

In 1989, Carturan *et al.* perform the first encapsulation of a micro-organism into a silica gel by the traditional alkoxide route based on a TEOS silica precursor dissolved in ethanol and addition of acidic water [227]. By encapsulating the yeast *Saccharomyces cerevisae* in a silica gel, Carturan demonstrated the possibility to obtain the survival of a cell during and after the process

of encapsulation. However, *S. cervisae* is commonly used as a laboratory model or as a brewer's or a baker's yeast for the fermentation of alcoholic beverage and therefore resists to high concentration of alcohol and to low pH. As a consequence, this yeast is particularly well-adapted to the encapsulation by the alkoxide route which needs a low pH and produces one to four equivalent of alcohol per reactive molecule of TEOS. More recently, Dickson *et al.* (2009) demonstrated the feasibility of the encapsulation of *Synechocys sp. PCC6803* by the same alkoxide route as Carturan [228]. They have demonstrated the activity of a photo-sensitive micro-organism in the matrix of silica, emphasizing the transparency of the gel obtained with TEOS or TMOS in acidic condition to natural light. Moreover, the encapsulated bacteria were able to produce H_2 after 5 days of entrapment in the silica gel.

Yet, for most bacteria, the alcohol concentration appears as a key parameter to minimize in order to enhance their viability. In 2003, Ferrer *et al.* encapsulated an *E. coli* strain in a silica gel made by the alkoxide route, but the sol precursor solution was pre-hydrolyzed and 96% of the formed alcohol was extracted by evaporation *in vacuo* [229]. An increase in bacteria viability was demonstrated as well as a preservation of the bacteria structural integrity for a long period. However, the corresponding protocol is tedious and requires an acidification of the sol to prevent its fast gelation. In contrast, the aqueous route shows multiple advantages. The silica precursors are already hydrolyzed and stabilized at a basic pH. As a consequence, no alcohol is produced during the inorganic polymerization that takes place by addition of acid until reaching a neutral pH. However, this simplicity is accompanied by a higher salinity of the sol. The precursors are stabilized at basic pH by sodium cations and during the neutralization chloride anions are added and increases the global salinity of the sol. Such a high salinity may induce the death of a wide range of micro-organisms. However, recently the group of Rousseau *et al.* demonstrated that salinity tolerance is a key parameter for biofuel cell performance to increase [230]. Therefore, silica gel made by the aqueous way responds to the future necessity to increase the ionic strength of electrolyte or bacteria « containers ». For sensitive bacteria, it is possible to decrease the salt concentration of sodium silicate solutions by an acidification on an ion-exchange membrane [231].

Another way to decrease the salinity without decreasing the total silica concentration is to replace a part of the silicate by another precursor. The addition of silica nanoparticles *via* Ludox (colloidal suspension of silica nanoparticles) is an option. Due to the surface chemistry of the nanoparticles ($Si - \boldsymbol{OH}$), during the inorganic polymerization, silicates may condense with the hydroxo groups at the surface of the silica nanoparticles and form a cement around them [232,233]. Several studies have already demonstrated that this approach preserve the viability and the metabolic activity of *E. coli* a few days after the encapsulation [233,234]. A viability of around 30% to 50% after 21 days was demonstrated by epifluorescence in layer of silica gel made by the aqueous route [235]. The viability was also proven to be enhanced by the formation of an hybrid inorganic-organic silica-gel [234,236]. This strategy consists in the addition of polymers or adjuvants recognized as protectants for bacteria such as alginate, gelatin, PVA or glycerol. Glycerol appears as the most efficient adjuvant with 60% of the viability remaining at day 15 and 50% at day 30. Finally, a comparison between the alkoxide route and the aqueous route confirms the

damageable effect of the produced methanol on bacteria during the hydrolysis-condensation of TMOS while the aqueous route should not affect bacteria integrity [232].

Despite the advantages of the aqueous route, only a few papers about artificial biofilm made by this pathway are available in the literature [133,237,238] whereas the formation of a layer of silica (by gas vapor deposition of TEOS) at the surface of a biofilm was more extensively studied. In 2010, Luckarift *et al.* deposited a layer of silica by vapor deposition on a biofilm of *S. oneidensis* bacteria and demonstrated an enhancement of the power by ca. 200% from 0.15 to 0.3 µW.cm^{-2} **(Figure 2.45)**. This enhancement was attributed to the stabilization of the biofilm structure, growth, chemistry and viability. In 2013, Sizemore *et al.* streamlined the process of biofilm silicification [239,240]. More recently, Strack *et al.* proceeds following the same protocol and immerged the MFC in seawater, and observing significant performance in an unusual real environment (seawater) [241].

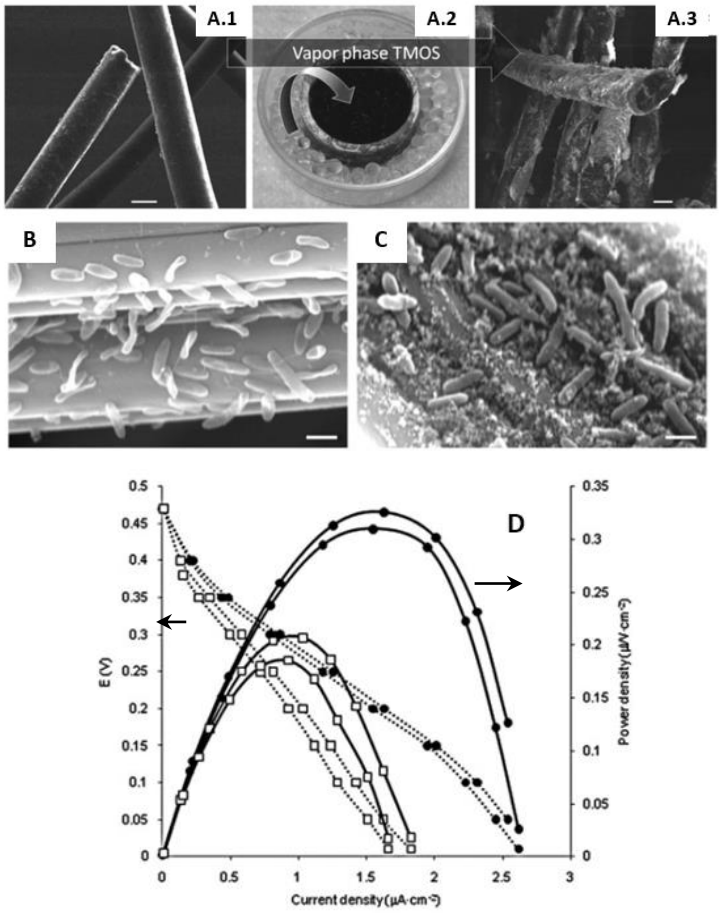

Figure 2.45 – Process of biofilm silicification and resulting MFC performance. **(A.1)** Carbon fiber untreated, **(A.2)** Close chamber dedicated to silica gel formation by gas vapor deposition, **(A.3)** Silicified carbon fibers *(from Sizemore et al.* [240]*)*. **(B)** *S. oneidensis* at the surface of a carbon felt fiber, **(C)** Colonized carbon fibers recover by a layer of silica gel by gas vapor deposition, **(D)** Polarization and Power curves presenting performance enhancement with an artificial biofilm (•) vs untreated colonized fibers (□) (from Luckarift *et al.* [239])

It is important to point out the difference that exists between a silica coating formed *via* the alkoxide vapor deposition and the silica gel obtained by aqueous routes. In the first case, the structure of the layer is dense but the cells are already deposited on a surface so that it cannot

be considered as a 3D encapsulation. In contrast, gels obtained by the aqueous process are more porous, contain more water and fully embed the bacteria. But in all cases, the formation of an artificial biofilm should permit to control the cells division and the therefore the structure of cellular organization. In the following part, the bacteria strains *S. oneidensis* will be encapsulated in an artificial biofilm synthetized by the aqueous route. Before complete gelation, the silica precursor solution will be mixed with the bacteria and impregnated in the carbon felt to ensure the electronic conductivity. Then, the effect of the polarization will be evaluated for the entrapped bacteria into silica gel.

2.5.3. Hybrid Silica gel/Carbon felt as an electrode.

2.5.3.1. Gel formation and structure.

The formulation of a silica gel is based on the mixing of four components: (i) a volume of sodium silicate at a final concentration fixed between 0.1 and 0.5 M, (ii) a volume of Ludox HS-40, (iii) a volume of water or buffer to introduce components to be encapsulated and (iv) a volume of acid concentrated at 3 M.

The standard silica gel composition contains 1 mL of 0.35 M SiNa (sodium silicate, Sigma-Aldrich), 1 mL of commercial Ludox HS-40 (Sigma-Aldrich) and 0.25 mL of milli-Q water (to proceed to an encapsulation). The sol is neutralized with ca. 130 µL of 3M HCl. The quantity of HCl must be re-evaluated at each sodium silicate batch preparation. At this step, the concentration of sodium silicate and Ludox HS-40 are equal to 0.16 M and 3.8 M respectively resulting in a global silica concentration of ca. 4 M. By varying this quantity, the effect of each silica source was evaluated. The increasing of both sodium silicate and Ludox HS-40 increases the global silica loading of the gel making them more resilient with lower SiO_2 loading. In term of gelation time, the influence of the sodium silicate concentration is predominant over the effect of Ludox HS-40 loading increase. However, the gelation time must be fixed by a compromise as same gelation time can be reach with low concentrated sodium silicate and highly concentrated Ludox HS-40 sol and conversely. The mechanical stability of the gel is a key parameter for the formation of an artificial biofilm. In a tight (dense) silica gel, the bacteria are trapped and cannot deform the gel to increase the available space in order to divide. In this case, the bacteria multiplication is limited. For a softer cohesive silica gel, less concentrated in silica, the silica network can be distorted around the encapsulated bacteria which may divide and colonize the available space in the gel.

Figure 2.46 displays scanning electron microscopy of the silica gel composed of 1 mL 0.35 M SiNa, 1 mL Ludox HS-40 and 0.25 mL milli-Q water neutralized with 130 µL of 3M HCl. The sol is impregnated in a carbon felt and then the hybrid SiO_2-carbon felt is left until the gelation point. The hybrid SiO_2-carbon felt is freeze dried to preserve the structure of the gel state as effectively as possible. SEM observation reveals an entire impregnation of the carbon felt by the silica gel. Most of the fibers are entirely or partially recovered by the gel and a significant proportion of the porosity is filled with silica gel (to compare, cf. **Figure 2.6**). The microstructure of the silica gel at the surface of the carbon fibers reveals a multi-scaled hybrid

material: (i) Even if the silica gel fills a part of the porosity, the macro-porosity of the carbon felt remains open **(Figure 2.46.a to Figure 2.46.d)**. (ii) The silica gel presents an inherent roughness and tortuosity at the microscopic scale **(Figure 2.46.f)**. (iii) Finally, the porosity of the silica gel at the nanoscale (2 to 50 nm in function of the gel composition) ensures the diffusion of small molecules through the gel.

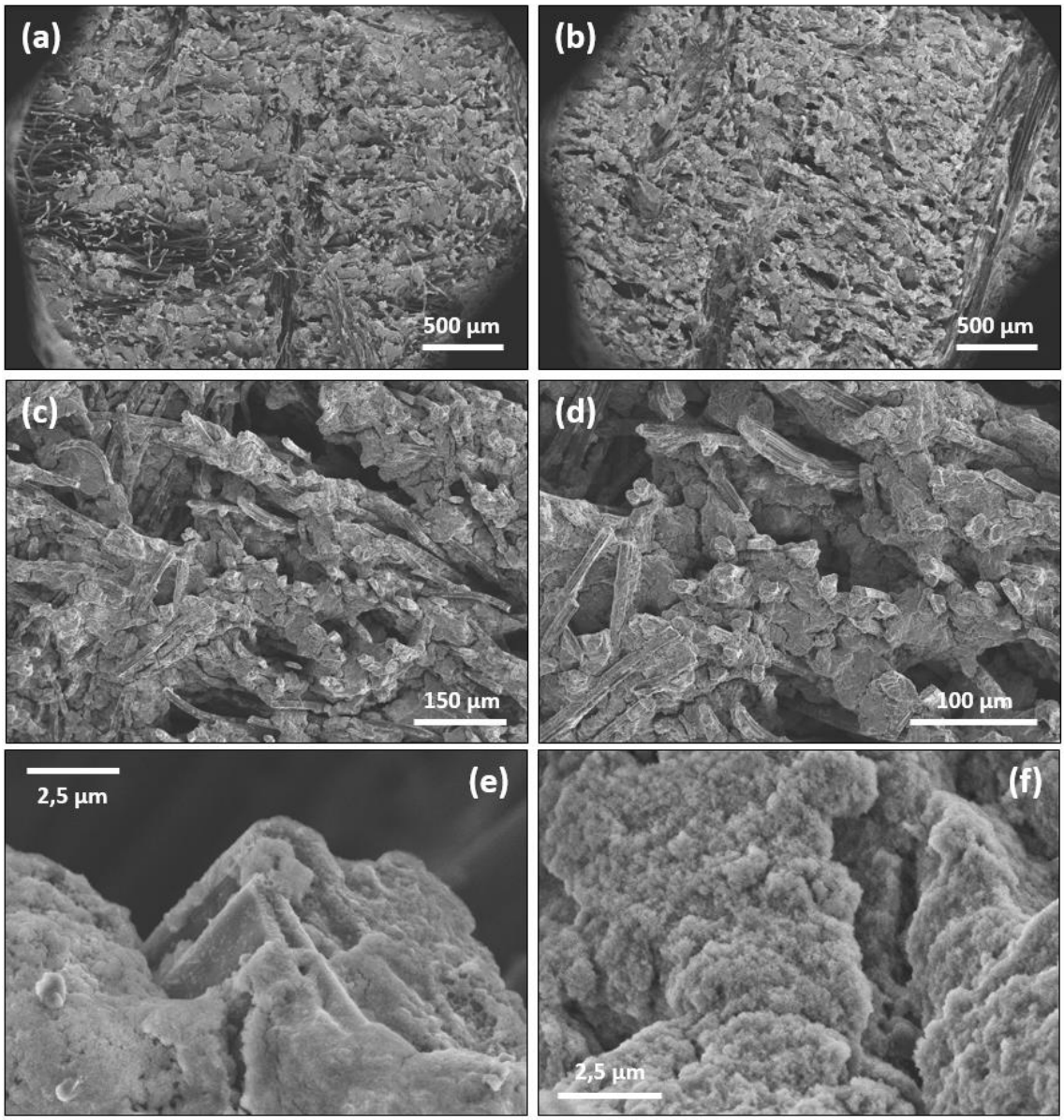

Figure 2.46 – Scanning electron microscopy of a silica gel formed by the aqueous route and impregnated in the carbon felt. Homogeneity and gel structure (x40). **(a, b)** Global picture of the silica gel incorporation between the fibers. **(c, d)** Carbon felt fibers embedded in the silica gel (x300 and x150). **(e)** Closer observation of the silica gel including a carbon fiber (x8 500). **(f)** Multi-scale structure of the silica gel from micro- to nano-scale (x20 000)

To encapsulate a micro-organism, the basic sol must be neutralized before the addition of 2 mL of bacteria suspension (based on the proportion for 2.25 mL of sol). The employed bacteria solution is concentrated at an optical density of 0.7. To palliate the silicate dilution due to the addition the bacteria solution, the initial sodium silicate solution is over-concentrated at 0.66 M. The global sodium silicate concentration of the gel is equal to 0.15 M and the global quantity of bacteria into the gel is equivalent to an OD_{600} = 0.3 equivalent to 3.8 10^8 cfu.mL^{-1}.

Figure 2.47 show that for an inoculum of *S. oneidensis* strain encapsulated into a silica gel, the bacteria are embedded into the gel and sometimes difficult to distinguished. However, their structural integrity appears well-preserved even if trapped in a pure inorganic matrix without protectant such as glycerol or PVA.

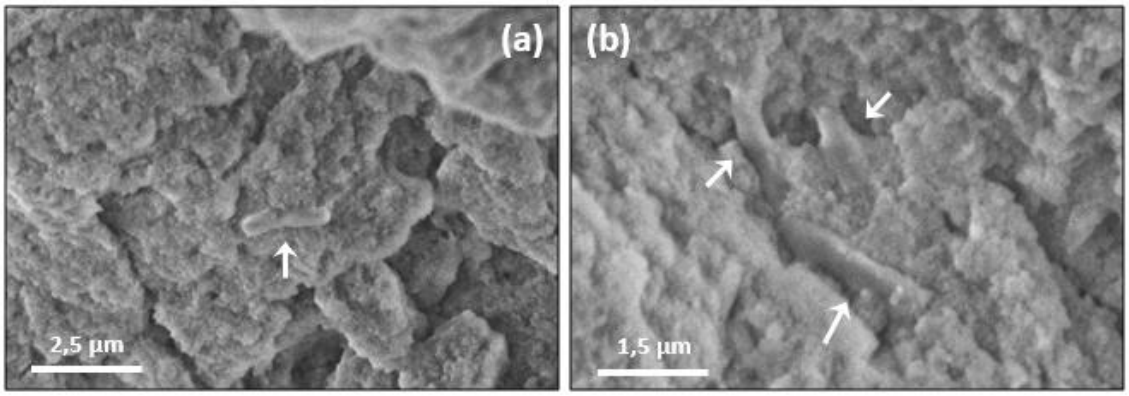

Figure 2.47 – Scanning electron microscopy and bacteria (white arrows) encapsulated into a silica gel formed by the aqueous route with sodium silicate and Ludox HS-40.

2.5.3.2. Electrochemical behavior.

To start with, the electrochemical behavior of an electrode corresponding to a raw carbon felt impregnated by a silica sol (composed as previously, cf 2.5.3.1) was studied by including a solution of redox probes directly in the composition of the sol. The 0.25 mL of water is replaced by 0.25 mL of a 150 mM NaCl and 0.33 mM $K_3Fe(CN)_6$ or $Ru(NH_3)_6Cl_3$ aqueous solution. The final concentration of probes into the gel is ca. 0.037 mM.

The electrochemical measurements are carried out in a three-electrodes configuration in a single-compartment reactor. The cyclic voltammogram **(Figure 2.48)** indicates a reversible redox system centered on the predictable potential of the redox couple. The pattern measured for both probes are similar to those obtained for raw carbon felts. In absence of probes in the electrolyte, the intensity of the peak of reduction and of oxidation are 2 times lower than in presence of probes in the electrolyte (concentrated at 0.33 mM). At high scan rate, an elliptic signal is visible. This phenomenon is also observable for raw carbon felts. Two hypothesis can explain the current increase at E_{pic}: (i) the probes diffuse into the gel to react at the surface of the fibers. This hypothesis means that the silica gel is sufficiently soft and/or porous to allow the diffusion of a probe from the bulk solution without lag-time. In fact, electrochemical measurements performed with a platinum wire embedded into a similar silica gel showed a lower influence of the gel tortuosity and compactness on the electrochemical pattern **(Figure 2.50)**. (ii) Raw fibers without silica gel coating remain available and are a preferential sites of reaction for redox species from the electrolyte. No potential shift or oxidative/reductive peak splitting that would confirm this hypothesis are observed.

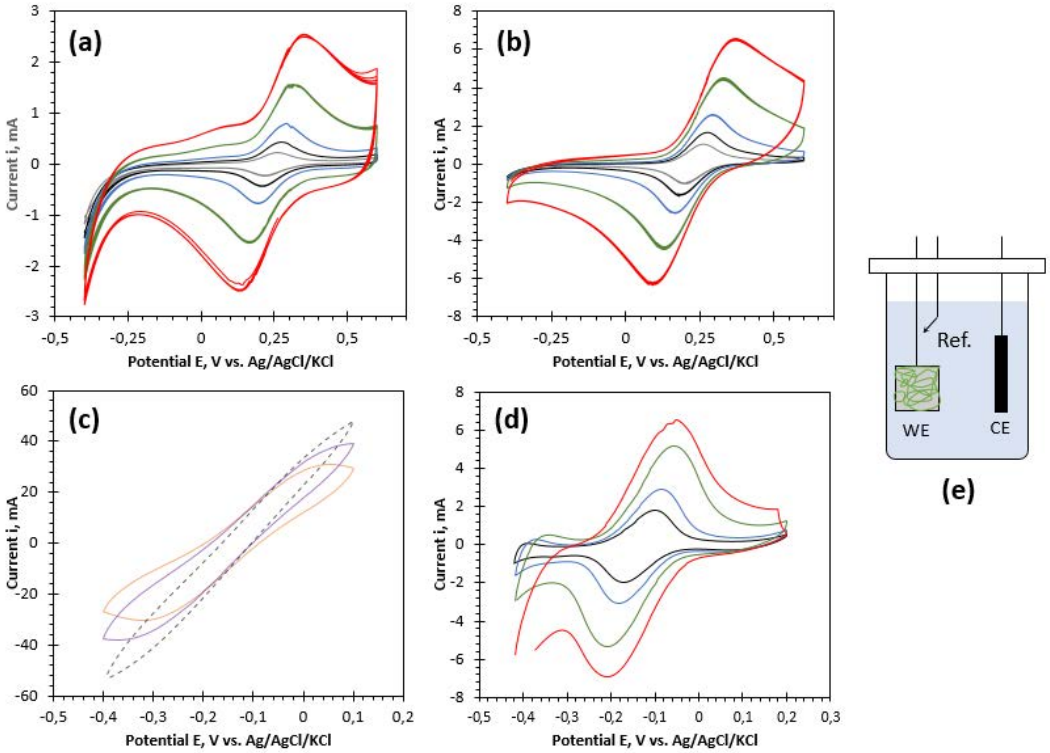

Figure 2.48 – Electrochemical characterization of a 1 cm^3 raw carbon felt impregnated by a silica gel as working electrode (WE). Platinum wire and Ag/AgCl/sat. KCl are respectively used as counter and reference electrodes.
Silica gel formulation: 1 mL 0.35 M SiNa + 1 mL commercial Ludox HS-40 (8.7 M) + 0.25 mL X.
(a) Silica gel concentrated at 0.037 mM (X = 0.33 mM $K_3Fe(CN)_6$ aqueous solution) and 150 mM NaCl electrolyte.
(b) Silica gel prepare as previously (a) and 150 NaCl + 0.33 M $K_3Fe(CN)_6$ aqueous electrolyte.
(c, d) Silica gel concentrated at 0.037 mM $Ru(NH_3)_6Cl_3$ (X = 0.33 M $Ru(NH_3)_6Cl_3$ aqueous solution) and 150 NaCl + 0.33 M $Ru(NH_3)_6Cl_3$ aqueous electrolyte. **(e)** Electrochemical reactor configuration.
Caption: — 5 $mV.s^{-1}$ in gray, **— 10 $mV.s^{-1}$** in black, — 20 $mV.s^{-1}$ in blue, — 50 $mV.s^{-1}$ in green and — 100 $mV.s^{-1}$ in red, — 500 $mV.s^{-1}$ in orange, — 1 $V.s^{-1}$ in purple and **- - - 3 $V.s^{-1}$** in black (dotted line).

Figure 2.49 displays the electrochemical behavior of a SiO_2-carbon felt (silica gel impregnated into a carbon felt with the protocol presented in part 2.5.3.2) embedded in 3 cm of silica gel loaded with a solution of probes concentrated at 0.33 mM (final Fe-probe concentration = 0.037 mM). In this condition, the difference of peak potential (DPP) is dramatically increased resulting in an important loss in reversibility (ΔE_p increased by 3.3 times or 230%). Moreover, the faradaic peaks are not Gaussian and, for scan rates higher than 20 $mV.s^{-1}$, the reversible oxidative peak is no more observable in the chosen electrochemical range. The redox probes used for the characterization of the SiO_2-carbon felt electrode are reversible. The cyclic voltammogram presented on the **Figure 2.50** in similar condition with a platinum wire (embedded in a silica gel) proves its reversibility (ΔE_p independent on the scan rate). As a consequence, the loss in reversibility must be attributed to a lack in mass transport. It is related to the problem of diffusion of probe because the pores of silica gel are less adapted. Silica gel matrix is negatively-charged and probably slows down the diffusion through the hybrid SiO_2-Carbon felt and eventually traps the probes. The distance of diffusion increases with the addition of silica gel. Moreover, the reductants produce from the reduction of the oxidants ($K_3Fe(CN)_6$) into the gel can be kept into the gel.

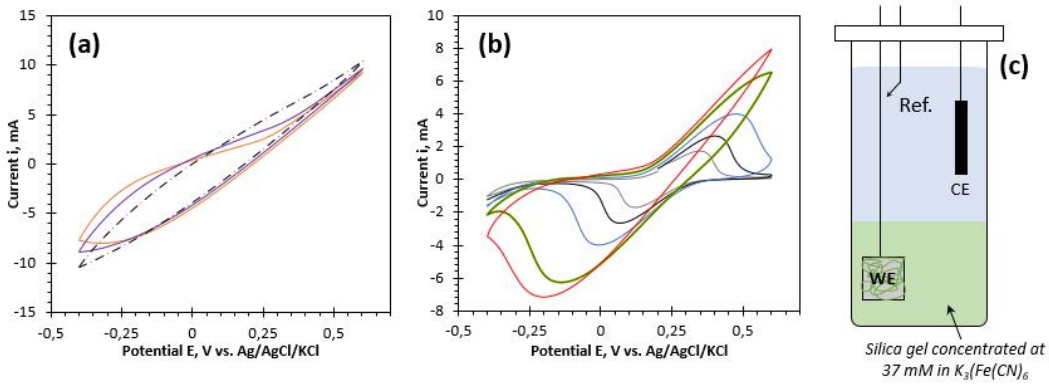

Figure 2.49 – Electrochemical characterization of *a 1 cm³ raw carbon felt impregnated by a silica gel* as working electrode (WE). The WE is then *fully encapsulated in a silica gel concentrated in $K_3Fe(CN)_6$ at 37 mM* (green on **Figure 2.49.e**). Platinum wire and Ag/AgCl/sat. KCl are respectively used as counter and reference electrodes. Silica gel formulation: 1 mL 0.35 M SiNa + 1 mL commercial Ludox HS-40 (8.7 M) + 0.25 mL H_2O.
(a, b) Electrochemical responses of the working electrode fully encapsulated in a silica gel concentrated in probes.
(c) Electrochemical reactor configuration.
Caption: — 5 mV.s^{-1} in gray, **— 10 mV.s^{-1}** in black, — 20 mV.s^{-1} in blue, — 50 mV.s^{-1} in green and — 100 mV.s^{-1} in red, — 500 mV.s^{-1} in orange, — 1 V.s^{-1} in purple and **- - - 3 V.s^{-1}** in black (dotted line).

Finally, the coefficient of diffusion has been calculated into a gel composed of 1 mL of 0.35 M sodium silicate solution, 1 mL of Ludox HS-40 and 0.25 mL of a 150 mM NaCl + 0.33 mM $K_3Fe(CN)_6$ aqueous solution. Then, the sol is neutralized with 3 M HCl aqueous solution and cast around 2.5 cm of a platinum wire. A twisted platinum wire is used as counter electrode and the cyclic voltammetry is carried out in a three-electrode configuration in a single-compartment reactor filled with a 150 mM NaCl electrolyte **(Figure 2.50)**. The Randles-Sevick model (cf. 2.2.3.2) is applied based on the following parameters: A_c = 0.39 cm² and $[K_3Fe(CN)_6]$ = 3.7 10^{-5} mol.cm^{-3}. The resulting coefficient of diffusion is equal to 0.33 10^{-7} cm².s^{-1} thus dramatically lower than the tabulated value (0.77 10^{-5} cm².s^{-1}). This result confirms the previous observation: in comparison with a raw electrode in a bulk solution of probes, the encapsulated probes present a slower diffusion.

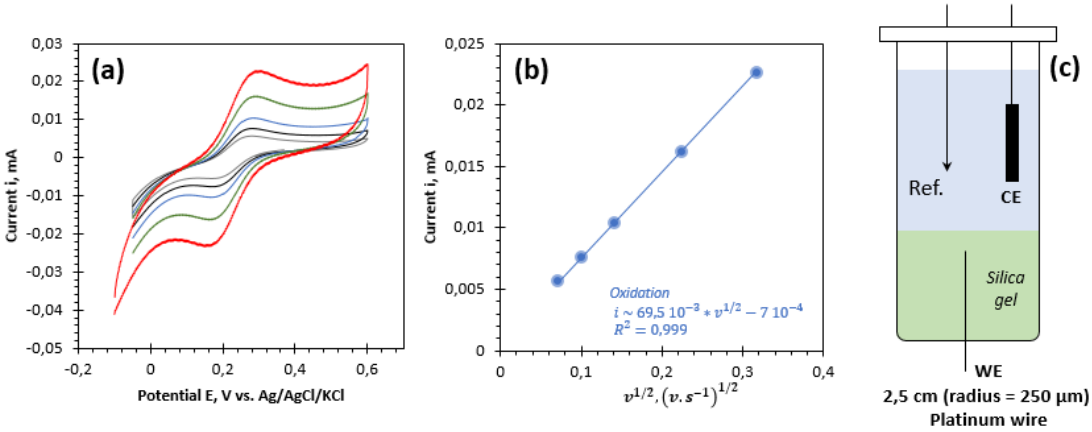

Figure 2.50 – Electrochemical characterization (diffusion coefficient determination) of *a 2.5 cm (radius = 250 µm) platinum* (WE). The WE is then *fully encapsulated in a silica gel concentrated in $K_3Fe(CN)_6$ at 37 mM* (green on **Figure 2.50.e**). Platinum wire and Ag/AgCl/sat. KCl are respectively used as counter and ref. electrodes.
Silica gel formulation: 1 mL 0.35 M SiNa + 1 mL commercial Ludox HS-40 (8.7 M) + 0.25 mL mQ H_2O.
(a, b) Electrochemical responses of the working electrode fully encapsulated in a silica gel concentrated in probes.
(c) Electrochemical reactor configuration. **(e)** Electrochemical reactor configuration.
Caption: — 5 mV.s^{-1} in gray, **— 10 mV.s^{-1}** in black, — 20 mV.s^{-1} in blue, — 50 mV.s^{-1} in green and — 100 mV.s^{-1} in red.

2.5.4. Bacteria viability in a silica gel.

S. oneidensis viability into a formulated silica gel is evaluated by epifluorescence and plate counting. For epifluorescence, the silica gel is synthetized in sterile conditions and an inoculum of *S. oneidensis* is added to the composition (based on the formulation 3 on **Table 2.8**). Then the silica gel is immersed in a MR1-L medium and conserved at room temperature (18°C) in sterile conditions. At day 2 and day 10, a part of the gel is incubated in a solution of fluorescent dyes ([syto9] = 5 µM and [Propidium Iodide] = 27 µM in milli Q sterile water) and mounted between slide and slip for observation in epifluorescence microscopy. On **Figure 2.51**, the green signal indicates the living bacteria and the red color indicates potentially dead bacteria. It appears that most of the bacteria are alive after 2 and 10 days of encapsulation. The signal of the dead bacteria is insignificant in comparison with the fluorescence of the living ones. The concentration of living bacteria is also determined by the plate counting methodology. Four silica gels with 19% of Ludox HS-40 loading and a sodium silicate concentration fixed at 0.1, 0.2, 0.26 and 0.3 M are prepared as described on **Table 2.9**. For all the formulation the global volume of silica gel is equal to 2.6 mL and 4 10^8 cfu.mL^{-1} (bacteria.mL^{-1}) are encapsulated based on an inoculum sampled at OD_{600} = 1.7. The silica gels are conserved in a MR1-L medium under sterile conditions at 18°C. After 4 days, the bacteria are extracted from the gel: the silica gel is broken with a sterile spatula, then the silica gel is diluted in 5 mL of MR1 medium and the cells are extracted by stirring with glass beads.

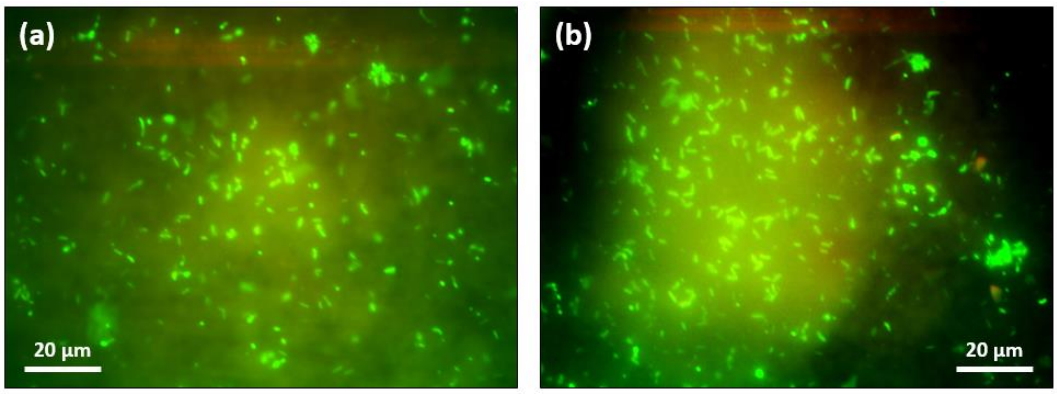

Figure 2.51 – Characterization of the bacteria viability by epifluorescence (Syto9/Propidium Iodide) at **(a)** 2 days and **(b)** 10 days after the encapsulation

Figure 2.52 indicates the viability of the encapsulated cells of the four different silica gels **(Table 2.8)**. Based on previous experiments, for a sodium silicate superior to 0.2 M, the bacteria are trapped and not allowed to divide due to the tightness of the inorganic network. For the **formulation 1 (0.1 M SiNa)** the rate of living bacteria is about 119%. Even if the inorganic network is stronger for the **formulation 3 (0.26 M SiNa)**, the same percentage of viable and cultivable bacteria after 4 days of encapsulation is observed. The monitored alive/dead *S. oneidensis* bacteria by epifluorescence presented similar results **(Figure 2.51)**. On the contrary, for an intermediate situation **(formulation 2, 0.2 M SiNa)** a loss of viable bacteria of ca. 17% appears. Moreover, for the highest concentration of sodium silicate **(formulation 4, 0.3 M SiNa)** only 50% of the encapsulated *S. oneidensis* are viable after 4 days of encapsulation. Analyses of these results are complex since a high number of living cells can mean that cell division has

occurred or that bacteria have well - sustained the encapsulation. It would be tempting to relate the first effect to formulation 1 (at low silicate concentration) and the second one to formula 3 (high silicate concentration). A better understanding of this would require a more systematic study as a function of time.

To survey the external electron transfer of the bacterium in a soft inorganic network which increases the space around the bacteria and potentially allows the cells division, the formulation 1 (0.1 M SiNa) must be chosen. On the contrary, to maximize the viability of bacteria in a tight silica gel, the optimal condition is the third one (formulation 3, 0.25 M SiNa).

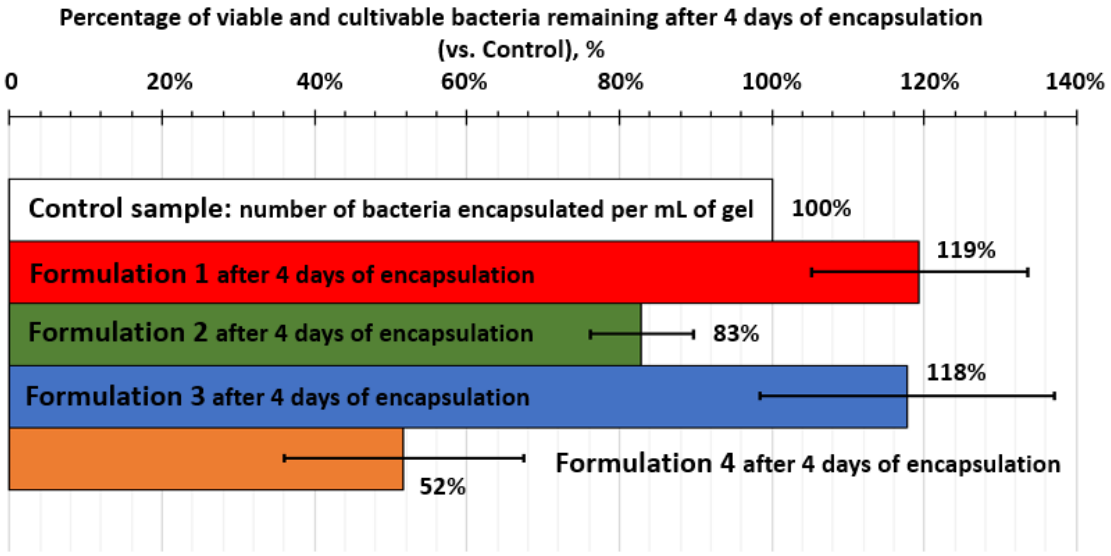

Figure 2.52 – Evaluation of the number of bacteria viable and cultivable into various formulation of silica gel by counting on LB-Agar plate. Percentage of viable and cultivable bacteria after 4 days of encapsulation (vs. Control: number of bacteria encapsulated at t=0)
Caption: □ Control: number of bacteria included into the silica gel at t = 0,
■ **Formulation 1:** 0.1 M SiNa/19% Ludox HS-40, ■ **Formulation 2:** 0.2 M SiNa/19% Ludox HS-40,
■ **Formulation 3:** 0.25 M SiNa/19% Ludox HS-40, ■ **Formulation 4:** 0.3 M SiNa/19% Ludox HS-40.

Formulation:	**1**	**2**	**3**	**4**
V(SiNa, 0,66 M)	0,38 mL	0,76 mL	1 mL	1,14 mL
[SiNa]final	**0,1 M**	**0,2 M**	**0,25 M**	**0,3 M**
V(Ludox HS-40)	0,5 mL	0,5 mL	0,5 mL	0,5 mL
[Ludox HS-40]final	**19 %**	**19 %**	**19 %**	**19 %**
V(S. Oneidensis, DO(init) = 1,7	0,5 mL	0,5 mL	0,5 mL	0,5 mL
DO(S. Oneidensis)final	**0,33**	**0,33**	**0,32**	**0,33**
[S. Oneidensis]final	**4 10^8 cfu/mL**	**4 10^8 cfu/mL**	**4 10^8 cfu/mL**	**4 10^8 cfu/mL**
V(MR1-L)	1,12 mL	0,74 mL	0,5 mL	0,36 mL
V(HCl, 3 M)	0,081 mL	0,095 mL	0,12 mL	0,186 mL
Global volume of Silica Gel	2,6 mL	2,6 mL	2,6 mL	2,6 mL

Table 2.8 – Composition of the four formulation of silica gel (with 2.5 mL) with 4 10^8 bacteria encapsulated per milliliter. These compositions refer to the results of viability test presented on **Figure 2.52**.

2.5.5. *S. oneidensis* immobilized hybrid Silica Gel/Carbon felt as a bio-anode for Microbial Fuel Cell: Effect of the polarization.

In the field of microbial fuel cell and more generally in the field of microbial electrochemical systems (cf. part 1.2.3), the encapsulation of bacteria within an artificial biofilm demonstrated an increase of the performance in comparison with bacteria immobilized on a conductive surface. If encapsulated, the bacteria are trapped close to the electrode and are not allowed to multiply. Other basic advantages must be taken into account: (i) the process of encapsulation limit the production of a natural biofilm and a potential clog of the carbon felt and the separator. (ii) Specific function can be artificially added to the composition of the artificial biofilm. As an example, specific groups responsible for the proton diffusion can be added to the inorganic structure in order to promote their migration through the biofilm and limit local acidification. By adding a conductive phase (CNT, carbon black, …) or redox functional groups, it is also possible to enhance the electronic transfer and replace the intrinsic bacterial pathways of transfer through the biofilm (bacteria aggregation, c-cytochromes and conductive pili). (iii) By the encapsulation process, the bacteria are trapped into the gel. As a direct consequence, these electrodes can be used as a bio-anode or a bio-captor without contaminating the medium with bacteria. The synthetized bio-anode is therefore ready-to-use. Moreover, the electrolyte is not contaminated by bacteria during the experiment.

The encapsulation of *S. oneidensis* into a silica gel is carried out by the aqueous route. Bacteria are cultivated according to the aerobic protocol SOg_4 (described in part 2.3) until 1.7 in optical density. Then, the inoculum is diluted at an optical density of 1 (corresponding to 1.2 10^9 cfu.ml^{-1}) and transferred in the appropriate medium (MR1-L or PBS-L). The silica sol is formulated by mixing a volume of Ludox HS-40 to a volume of sodium silicate ([SiNa] = 3.5 M). The volume of sol is balanced to 2 mL with a MR1-L or a PBS-L medium. After neutralization with a 3 M HCl solution, 1.5 mL of bacteria solution is added to the sol and stirred. Before complete gelation, the sol is incorporated into a 1 cm^3 carbon felt (formulation on **Table 2.9**). The hybrid *S. oneidensis* encapsulated SiO_2-carbon felt electrode is left until complete gelation. Finally, the electrode is mounted as a bio-anode in a three-electrode configuration single-compartment reactor and submitted to chronoamperometric measurements at 0.3 V vs. Ag/AgCl/KCl each day during 9 days. Two compositions of silica gel are evaluated and the only parameters which changes is the final loading in Ludox HS-40: 11% for the « Low-ludox concentrated Silica Gel » and 28% for the « High-ludox concentrated Silica Gel ».

Figure 2.53 displays the current evolution for these two systems, in a PBS-L or MR1-L electrolytes. For experiments involving **MR1-L based silica gel in a MR1-L electrolyte**, the currents are the highest and include between 40 to 80 µA in the first 5 days of measurement. The anodic current delivered by an electrode with high loading of Ludox HS-40 (28%, in red) is quite stable in time with a slightly decrease of the current between day 2 and 5. On the contrary, for silica gel with a lower loading of Ludox HS-40 (11%, in blue), the current is more variable and increases from 50 to 110 µA between day 5 and day 9. The observed variability of the anodic current is related to the electron transfer mechanism **(Figure 2.53.a** and **Figure 2.53.b)**. For a low-Ludox silica gel, the inorganic network is soft and malleable. In this condition, the bacteria

can divide and develop a biofilm into the structure of the inorganic network. The cyclic voltammetry reveals a classic sigmoidal wave of oxidation from -0.45 V vs. Ag/AgCl/KCl and the intensity of the oxidative wave increase with time (from 50 µA at day 1 to 150 µA at day 9 at 0.3 V vs. Ag/AgCl/KCl, cf. **Figure 2.54.a**). This behavior is characteristic to the development of a biofilm, including the division of the bacteria. On the contrary, for silica gel loaded with a higher quantity of Ludox HS-40, the network is tighter and rigid. In this case, the bacteria are trapped in the inorganic network in a limited volume. The cyclic voltammetry corresponding to this silica gel composition indicates a stable wave of oxidation at day 1, 3 and 9 with a slightly loss at day 9. This behavior confirmed the limited ability of the bacteria to divide in this condition **(Figure 2.54.b)**.

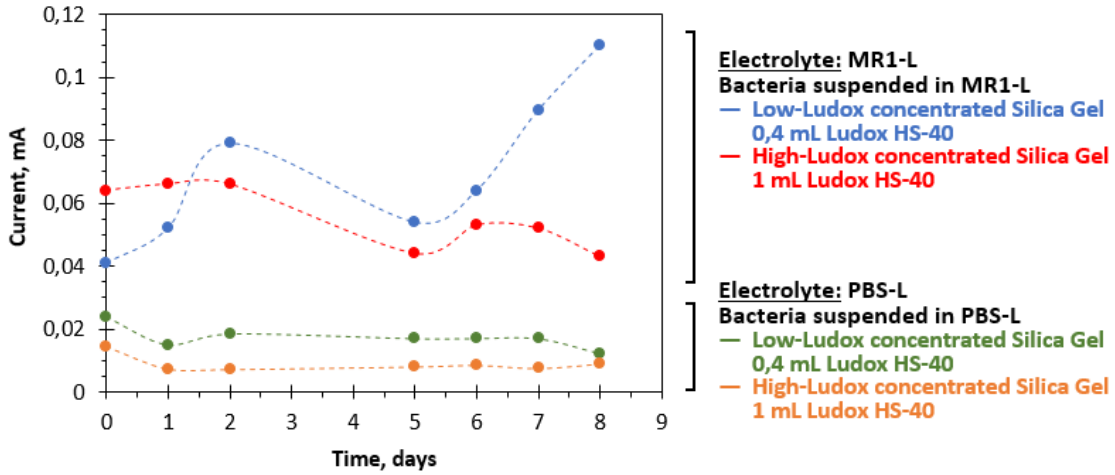

Figure 2.53 – Current monitoring of *S. oneidensis* encapsulated in an artificial biofilm made of silica gel impregnated in a raw carbon felt. Ludox, sodium silicate and global silica concentrations effects are evaluated as well as the effect of the electrolyte nature (MR1-L or PBS-L). Silica gel formulation are tabulated in **Table 2.9**.
Caption: — $[Ludox\text{-}HS\text{-}40]_{final}$ = 11%, MR1-L, $[SiNa]_{final}$ = 0.1 M, DO_{final} = 0.4 in blue. — $[Ludox\text{-}HS\text{-}40]_{final}$ = 28%, MR1-L, $[SiNa]_{final}$ = 0.1 M, DO_{final} = 0.4 in red. — $[Ludox\text{-}HS\text{-}40]_{final}$ = 11%, PBS-L, $[SiNa]_{final}$ = 0.1 M, DO_{final} = 0.4 in green. — $[Ludox\text{-}HS\text{-}40]_{final}$ = 28%, PBS-L, $[SiNa]_{final}$ = 0.1 M, DO_{final} = 0.4 in orange.

	Low-Ludox concentrated Silica Gel — MR1-L — PBS-L			High-Ludox concentrated Silica Gel — MR1-L — PBS-L		
Sol Components			**final concentrations**			**final concentrations**
V(Ludox HS-40)	0,4 mL	=>	11% of Ludox HS-40	1 mL	=>	28% of Ludox HS-40
V(SiNa, 3.5 M)	0,1 mL	=>	0,1 M	0,1 mL	=>	0,1 M
V(MR1-L) or V(PBS-L)	1,5 mL			0,9 mL		
V(HCl, 3 M)	0,105 mL	=>	pH = 6,5-7,5	0,130 mL	=>	pH = 6,5-7,5
V(Bacteria susp. OD=1)	1,5 mL	=>	OD(final) = 0,4	1,5 mL	=>	OD(final) = 0,4

Table 2.9 – Formulation of the silica gel subjected to chronoamperometric measurements presented on **Figure 2.53**. All the final concentrations are similar in low- or high-Ludox concentration with MR1-L or PBS-L medium/electrolyte. The only parameter which variates is the Ludox HS-40 from low- (11%) to high- (28%) concentration.

In **PBS-L electrolyte with PBS-L based silica gel**, the anodic currents are dramatically lower (at 0.3 V vs. Ag/AgCl/KCl) in both low or high condition of Ludox HS-40 loading **(Figure 2.53)**. This behavior can be explained by CV curves. Initially, a wave of oxidation is observable but, rapidly, the wave is transformed in a non-symmetrical system of faradaic peaks **(Figure 2.54.c, Figure 2.54.d)**: (i) an intense peak of oxidation centered at 0 V vs. Ag/AgCl/KCl and (ii) a non-symmetrical and probably independent peak of reduction centered at -0.3 V vs. Ag/AgCl/KCl in the case of a tighten inorganic network **(Figure 2.54.d)**. In the case of a soft inorganic network, the faradaic peak of reduction shifts from -0.3 to 0 V vs. Ag/AgCl/KCl and is less intense than in high loading of Ludox HS-40 **(Figure 2.54.c)**. The observed pattern is comparable to the electrochemical pattern observed for planktonic *Geobacter* cells deposited on a conductive support [56]. Moreover, the PBS-L electrolyte/medium is less favorable to the bacteria division, due to low concentration in nutrients and high salinity.

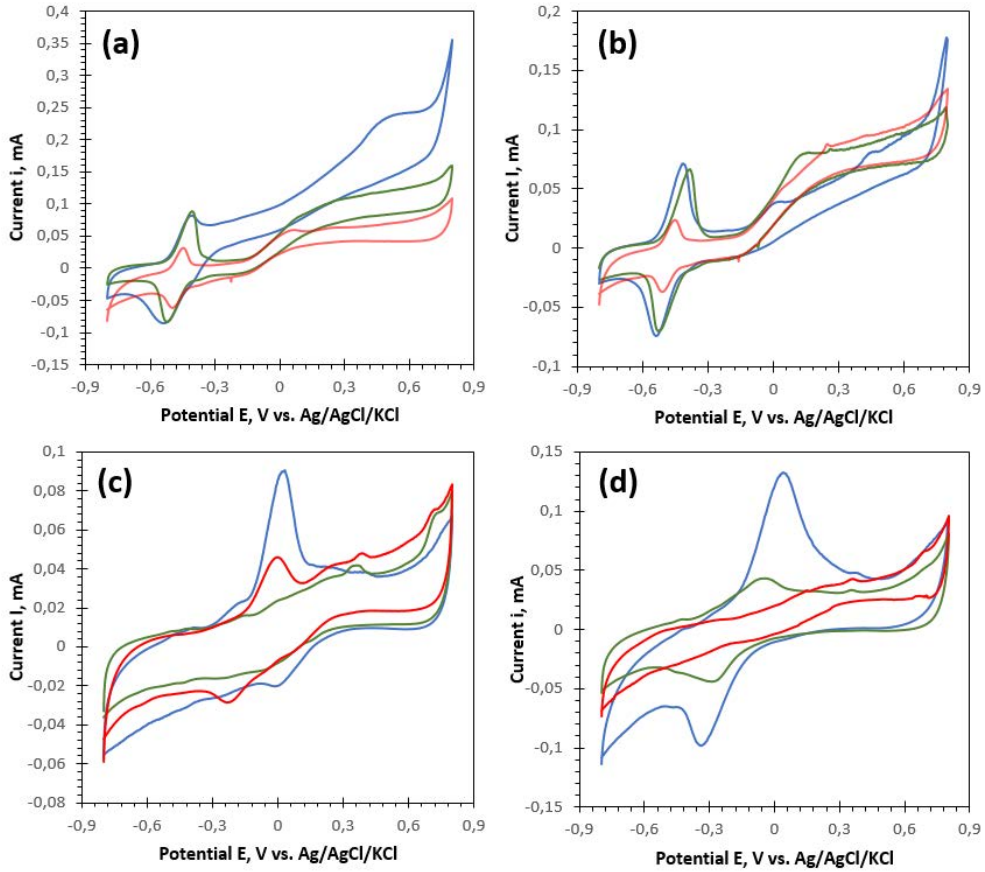

Figure 2.54 – Cyclic voltammetry of *S. oneidensis* encapsulated in an artificial biofilm made of silica gel impregnated in a raw carbon felt. Final OD_{600} of the bacteria in the silica gel is 0.4 equivalent to 4.6 10^8 cfu/ml.
Caption: — **day 1** in red, — **day 3** in green, — **day 9** in blue.
(a) [Ludox-HS-40]$_{final}$ = 11%, MR1-L, $[SiNa]_{final}$ = 0.1 M, DO_{final} = 0.4. **(b) [Ludox-HS-40]$_{final}$ = 28%, MR1-L,** $[SiNa]_{final}$ = 0.1 M, DO_{final} = 0.4. **(c) [Ludox-HS-40]$_{final}$ = 11%, PBS-L,** $[SiNa]_{final}$ = 0.1 M, DO_{final} = 0.4. **(d) [Ludox-HS-40]$_{final}$ = 28%, PBS-L,** $[SiNa]_{final}$ = 0.1 M, DO_{final} = 0.4.

The same behavior is observable by varying the sodium silicate concentration **(Figure 2.54)** with a low Ludox HS-40 loading fixed at ca. 10%. At a final concentration of sodium silicate fixed at 0.1 M, a variation is observable in the intensity of the wave of oxidation between day 2 and day 11 with a slight decrease at day 7 **(Figure 2.55.a)**. A single redox couple of faradaic peaks

is also noticeable at ca. -0.45 V vs. Ag/AgCl/KCl corresponding to the flavin presents in the composition of the electrolyte (MR1-L). For a higher final concentration of sodium silicate (0.25 M), the wave of oxidation is less significant but an irreversible faradaic peak of oxidation centered at 0.1 V vs. Ag/AgCl/KCl is visible **(Figure 2.55.b)**. In opposition to the previous observation, with tight silica gel (increasing of the Ludox HS-40 loading), the peak intensity is stable. Also, the redox couple of faradaic peak at -0.45 V vs. Ag/AgCl/KCl is duplicated in two systems (as previously observed, cf. 2.4.4.1). Moreover, the intensity of the first couple at -0.48 V vs. Ag/AgCl/KCl decreases by a factor 3 between day 2 and day 11 while the peak intensities of the second system remains stable (-0.45 V vs. Ag/AgCl/KCl). The hypothesis of a flavin immobilized at the surface of the carbon felt and a flavin free to diffuse into the gel potentially explain the splitting of the flavin electrochemical signature.

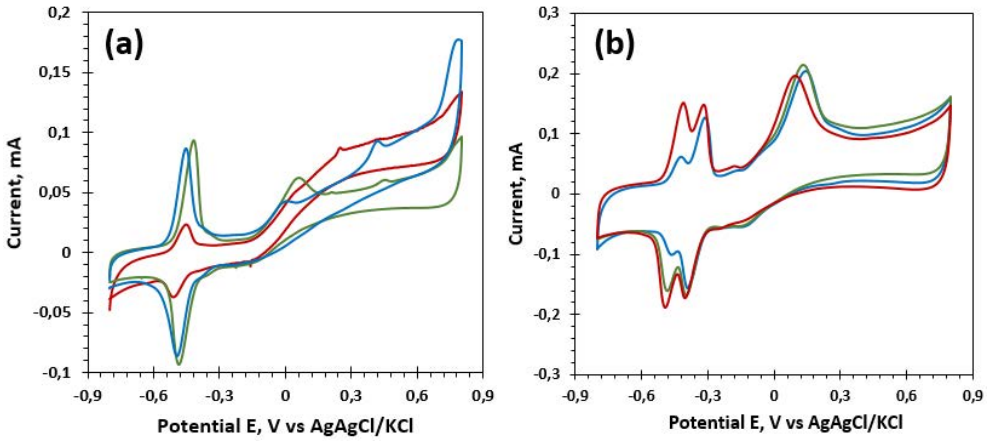

Figure 2.55 – Cyclic voltammetry of bio-anodes: Encapsulation of *S. oneidensis* a silica gel with different composition. The silica gel is incorporated into the carbon felt. The sodium silicate concentration is set-up at: **(a)** $[SiNa]_{final}$ = 0.1 M, and **(b)** $[SiNa]_{final}$ = 0.25 M.
Caption: — **day 2** in red, — **day 7** in green, — **day 11** in blue.

To summarize, the electrochemical behavior of the bacteria changes as function of its ability to divide in a more or less tight inorganic network. Moreover, the limited mobility of the bacteria into the silica gel probably participate in the biofilm-led or planktonic-led bacterial behavior.

Until now, the SiO_2/bacteria-carbon felt electrodes were not polarized at a specific potential. The MFC were simply linked to a 100 Ω-resistance to ensure the electrons circulation in the external circuit from the bio-anode to the cathode. The effect of the electrode polarization was then evaluated for the following silica gel formulation incorporated in 1 cm^3 carbon felt. The gel is concentrated at 0.2 M in sodium silicate and loaded with 10% of Ludox HS-40. Four similar SiO_2/bacteria bio-anodes are mounted in a three-electrodes configuration with a carbon felt as counter electrode and an Ag/AgCl/KCl reference. Two of the synthetized bio-anodes are polarized at $E_{we} = +0.3\ V$ ($E_{ce} = -0.3\ V\ and\ \Delta E_{apply} = 0.6\ V$) and the two other bio-anodes are non-polarized and linked to the counter electrode with a 100 Ω-resistance.

Figure 2.56 indicates the monitored current in cyclic voltammetry between -0.8 and 0.8 V vs. Ag/AgCl/KCl for a bio-electrode with a silica gel remaining intact during the entire

experiment duration **(Figure 2.56.a)** and a bio-electrode with a broken silica gel **(Figure 2.56.b)**. To rationalize the experiment, the silica gel is artificially broken with a spatula, but the phenomenon was naturally observed in PBS-L electrolyte. Silica gels made by the aqueous route are sensitive to high phosphate concentration which leads to a lack in integrity of the network. In this last case, the MR1-L electrolyte progressively becomes turbid and the measured optical density at 600 nm increases. Moreover, when the electrolyte is sampled (in sterile condition) and spread out on a reach LB-Agar plate incubated at 30°C, a dense bacterial mat (form and color characteristic to *S. oneidensis* is observed after 24h of incubation. For **an intact silica gel (Figure 2.56.a)**, no effect of the polarization is observed, both polarized and non-polarized cyclic voltammograms are equivalent. On the contrary, for **broken silica gel (Figure 2.56.b)**, the significant oxidative wave of oxidation is observable under polarization but not for non-polarized SiO_2/bacteria-electrode. As previously demonstrated, this increase of the wave of oxidation in parallel with the bacterial seeding of the electrolyte can be related to a conventional electrode colonization under polarization as described in part 2.4.4 **(Figure 2.56.b)**.

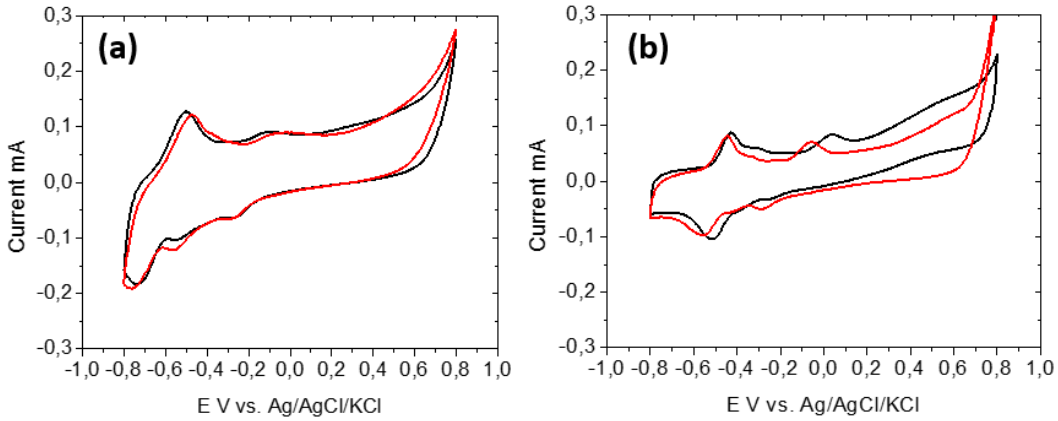

Figure 2.56 – Effect of the polarization on encapsulated bacteria into a silica gel incorporated into a carbon felt. **(a)** for an intact silica gel and **(b)** for a broken silica gel with bacteria releasing into the solution. The electrolyte corresponds to an MR1-L medium.
Caption: Bio-anode **— non-polarized** in red and **— polarized at +0.3 V** in black.

To summarize, when the silica gel remains intact, no effect of the potential of polarization is observed. However, when the silica gel breaks, we observed the spontaneous formation of a biofilm at the surface of carbon fibers free of silica gel. This formation is monitored *via* the presence of an oxidative wave in cyclic voltammetry. This conclusion confirms the effect of the electrode polarization when the bacteria are not immobilized on the electrode or into an artificial biofilm. For trapped bacteria, a polarization of the electrode is inefficient. The bacteria are not able to migrate due to their encapsulation in a tight silica gel. As a consequence, even if the bacteria are sensitive to the applied potential, no effect are observable by electrochemical techniques.

2.6. CONCLUSION

In this chapter, simple single- and dual-compartments microbial fuel cells were mounted with carbon felts as working electrode and counter electrode. The bio-anode was formed by the colonization of the working electrode in a bacteria solution under various experimental

conditions. Experimental parameters such as the presence or the absence of oxygen, the state of growth of the bacterium at the sampling for MFC inoculation, the complexity of the inoculated electrolyte and the potential of electrode polarization were studied:

(i) It was demonstrated that the oxygen is less or not damageable for *S. oneidensis* than for other electroactive bacteria such as *G. sulfurreducens*. After a period of positive polarization at the working electrode (7 days), the current continues to increase in presence of oxygen while the current stabilizes (or slightly decreases) in anaerobic condition. This behavior is due to the aero-anaerobic optional specificity of *Shewanella* strains, specific growth and working condition in MFC

(ii) The anodic current variations clearly changed as a function of the state of growth of *S. oneidensis*. For bacteria sampled in log-phase and polarized at a positive potential, the anodic current measured at only 12h of the polarization is already high and stable. It appears that bacteria sampled at the end of the log-phase are more stable in time and more resistant to the stress associated with the variation of lactate concentration. Bacteria harvested in stationary presents a lower current at the inoculation time, and a linear increase with time.

(iii) Concerning the complexity of the electrolyte, no difference was observed between a classic MR1-L medium and a PBS-L medium on the long term. However, at the inoculation time and for 2 days after, the current in PBS-L electrolyte is 4 to 5 times higher than in MR1-L electrolyte. This behavior was attributed to the absence of mediator in the PBS-L solution, leading to the cellular accumulation of electrons that are released at the beginning of the MFC function. But the results are not sufficient to clearly conclude and need further experiment since the high initial current may be also attributed to the bacterial stress due to the increasing of the salinity in PBS-L electrolyte (vs. the MR1-L medium of growth).

(iv) In term of electrode polarization, both positive (+0.3 V, +0.5 V) and negative (-0.3 V) potentials were applied to the working electrode. An absence of polarization (working and counter electrodes connected to a resistance) was also evaluated as a control sample. The potentials were strictly and symmetrically applied to both working and counter electrode before surveys (each day). The MFC were left at the OCV to reach a stable state without any more influence of the polarization. All the experiments of polarization were carried out under aerobic condition in order to demonstrate the ability of *S. oneidensis* to acclimate the oxygen without dramatic loss in performance. A positive current was measured, even in aerobic conditions. In single-compartment configuration, the anodic current increases significantly with the polarization at two selected state of growth (3/4 of the log-phase or in stationary phase). The anodic current measured for bacteria harvested in log-phase was already at the stable value after only 12h while the bacteria from the stationary phase reach a higher anodic current from a quasi-inexistent current (from 2 µA to 120 µA in 7 days vs. 60 µA). In

addition, at the same state of the polarization (more than 4 days) at a positive polarization (E_{we} = +0.3 V), the anodic current of the bacteria from the stationary phase is clearly higher than for bacteria sampled in log phase (same volume, weight, surface of working electrode). This phenomenon was explained as a consequence of the initial behavior of the bacteria. In stationary-phase, the bacteria are in a dynamic of division. As a consequence, the bacteria colonize the electrode without fast multiplication. Moreover, these bacteria are more adapted to molecular acceptor of electrons in solution than a solid acceptor of electrons (electrode). After a time of acclimation, bacteria in stationary phase are able to actively divide (fast increasing of the electrolyte measured OD_{600}) and transfer electron. This change of behavior leads to a linear increase of the current. These results point out that it is important to take into account the strong interplay between the bacterial metabolism and the electrochemical conditions.

(v) The dual-compartments configuration appears necessary due to the unintended low (for E_{we} = +0.3 V and -0.3 V) or significant (for non-polarized systems) colonization of the counter electrode in single-compartment. Complete evaluation of the dual-compartment MFC performance lead to the conclusion that more than the sign of the applied potential, the process to polarize the electrode affects the biofilm formation and the resulting MFC performance. For positive polarization, the biofilm is rapidly established and an extended polarization seems damageable for the performance. The resulting biofilm is thin and dense. On the contrary, at negative poised potential, the performance of the MFC slowly increases and the established biofilm filled a significant part of the carbon felt porosity. These biofilms and the performance evolution seem in accordance with the type of EET promoted at the applied potential: DET at +0.3 V (transfer by direct contact, fast establishment of the biofilm) or MET at -0.3 V (transfer *via* electron shuttles)

Finally, *S. oneidensis* was encapsulated in an inorganic network by including cultured bacteria in a silica gel prepared by the aqueous route. An impressive viability of the bacteria was noticed and the electrochemical behavior of the bacteria seems related to the silica gel composition and more particularly to the tightness of the silica network. The higher the silica loading the more the network is tight. As a consequence, the electrochemical response must be related to individual bacteria blocked in their ability to divide but still able to perform EET (single non-reversible peak of oxidation at 0-0.1 V vs. Ag/AgCl/KCl).

To conclude, the entire characterization of the carbon felt (part 2.2) as well as the pathways to increase the colonization of the bio-anode by the bacterium *S. oneidensis* allows a better understanding of the bacteria/electrode interaction and an evaluating of their individual effect. Three groups parameters were evaluated to act on the electrode colonization: (i) the cultivation of *S. oneidensis* in optimized batch condition (part. 2.3), (ii) the electrode perturbation *via* external parameters such as the oxygen availability, the state of growth, the electrolyte nature, the electrode polarization and the reactor geometry (part 2.4), (iii) the

encapsulation of the bacteria in an artificial biofilm composed of carbon felt and silica gel (part 2.5). Further efforts will be necessary to improve our understanding of the biofilm formation under polarization. For instance, FIB SEM exploration of the biofilm structure, mass spectrometry analysis of the biofilm composition and well as SECM (scanning electrochemical microscopy) study to map the surface of the fibers during the establishment of the biofilm would constitute valuable and innovative approaches.

In parallel, the optimization of the conductive support is an important option to consider. In particular, an observation of the colonized carbon felts at the surface and inside of the felt has shown a large variation of colonization extent as a function of the depth. This low colonization of the inner volume of the felt may be attributed to the hydrophobicity of the felt limiting the diffusion of the bacterial electrolyte into the carbon felt. To improve the colonization efficiency, we have synthesized carbon-based nano-fibers with specific electrode geometry, carbon fibers size, density and porosity, as presented in the following chapter 3.

CHAPTER 3

ELECTROSPUN CARBON PAPER AS A BIO-ANODE FOR MICROBIAL FUEL CELL

FROM MACRO TO MICRO-SCALE

Table of Contents – Chapter 3

3.1. INTRODUCTION AND OBJECTIVES

In the previous chapter, a commercial carbon felt composed of micrometric fibers was used as an anode to colonize by *S. oneidensis* bacteria in order to perform a bio-anode for MFC. Various experimental parameters, such as the oxygen availability, the electrolyte nature and the polarization, were evaluated as enhancer of the colonization in specific conditions. In this chapter, structural parameters will be demonstrated as another parameter to influence and improve MFC performances.

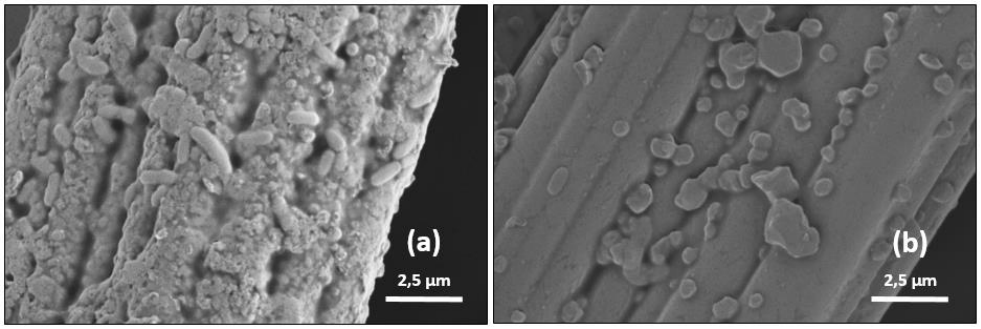

Figure 3.1 – Scanning electronic microscopy of a carbon felt fibers at **(a)** the peripheral surface of the felt or **(b)** 300-400 µm deep in the felt, after 20 days of incubation in a single-compartment reactor polarized at +0.3 V (cf. part. 2.4.4.1)

However, an observation of the fibers at the peripheral surface and of the inner fibers (at 300 µm in depth) of the carbon felt has demonstrated an absence of colonization of the inner volume of the felt even if polarized in the most favorable conditions. SEM observation shows, that raw fibers were at the best covered with a heterogeneous thin and non-colonized layer of EPS (exopolysaccharides) and often unmodified **(Figure 3.1)**. This phenomenon was attributed to diffusive limitation of the bacterial electrolyte into the hydrophobic structure of the carbon felt together with the immediate availability of required conditions for bacteria viability and working condition at the liquid/solid interface (cf. part. 2.4.1). Recently (may 2016), similar observations were reported by Blanchet *et al.* with natural community of bacteria from wastewater **(Figure 3.2)**. They found out that the global volume of carbon felt colonized ranged between 8 and 32% of the whole carbon felt volume which corresponds to the colonization of 300 µm in depth of the felt. This result is in agreement with a simple calculation based on our own SEM images (20 to 30%).

Three options can be developed to increase of the relative percentage of electrode colonized by *S. oneidensis*. (i) A modification of the carbon felt surface should allow **enhancing the hydrophilicity of the carbon felt** (cf. part. 2.2.3.3) but, as already mentioned, the process leads to a degradation of the electrochemical surface activity and requires careful washing in the case of an acid treatment (to remove residual acid that can be toxic for the bacteria). In the case of a hydrophilic treatment by alginate deposition, it is necessary to store the resulting electrode in a strictly sterile environment to prevent the contamination and the proliferation of bacteria. (ii) Raw carbon felt can be specifically **dimensioned to satisfy the diffusive limitation**. But, the carbon felt structure corresponds to wide carbon fibers randomly looped without chemical bonds between them to maintain the structure. As a consequence, dimensioning the

felt to a lower thickness induces a lack of handling capacity and the breakdown of the carbon felt structure. (iii) The last considered option is to **synthetize a new material** exhibiting key structural requirements to improve its performance as a bio-electrode.

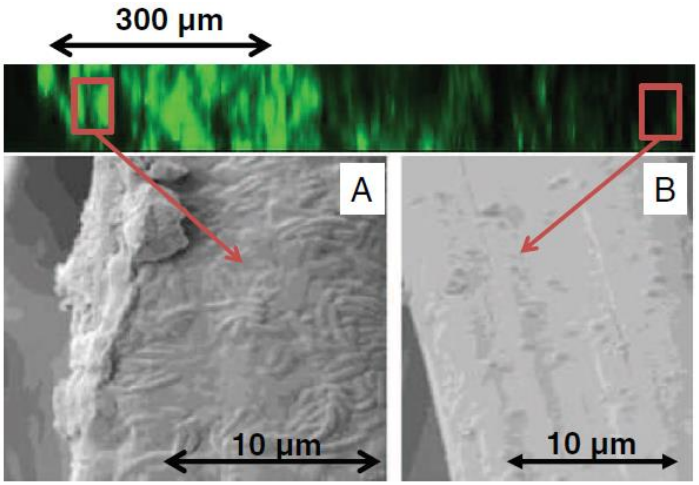

Figure 3.2 – Sectional views of a carbon felt bio-anode (37 day of incubation) observed by epifluorescent microscopy (on top) and SEM of two different fibers **(A)** on the surface of the carbon felt and **(B)** 1 mm deep in the carbon felt (*from Blanchet et al., 2016* [242])

In this chapter, a new and innovative electrode material for microbial fuel cell technology will be synthetized based on the use of poly(acrylonitrile) and the electrospinning process. This two-dimensional electrode, named **electrospun carbon paper (abbreviate ES-carbon paper) will meet important requirements: (i)** the thickness of the fibers mat is fixed in between 100 and 300 µm. **(ii)** The porosity (distance between two fibers) must be in agreement with the dimension of a bacteria, i.e. fixed between 1 and 5 µm. **(iii)** For the mat to accommodate deformation keeping mechanical strength, expected carbon fibers diameter is 200 nm with an accepted distribution between 100 and 400 µm.

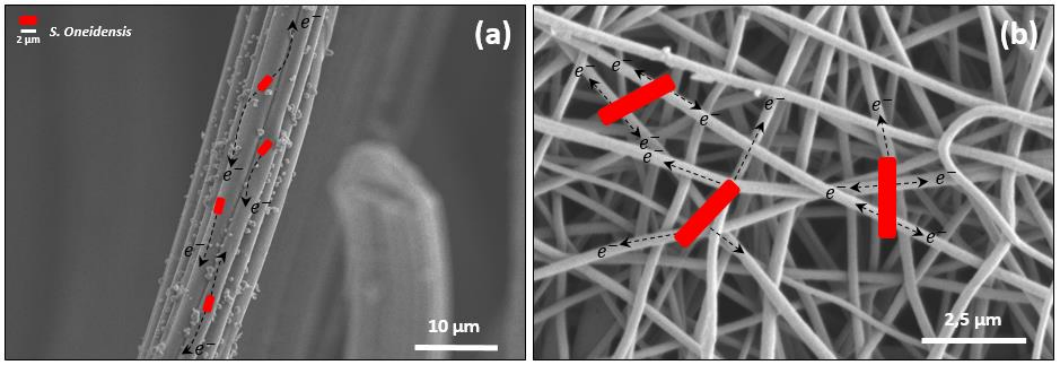

Figure 3.3 – Schematic representation of *S. oneidensis* on a **(a)** carbon felt fibers and **(b)** a mat of conductive fibers synthetized by electrospinning. The bacterium (at the proper scale) is in red and the electron pathways are represented with dashed arrows.

This structure makes it very different to the carbon felt in terms of interactions with the bacteria. In a carbon felt, the fibers diameter (12 µm) is ca. 6 times higher than typical dimension of *S. oneidensis* (ca. 1.5 to 2 µm) and the pores are much wider (50-100 µm). On the contrary, the fibers diameter of a home-made electrospun carbon paper is expected at 200 nm, which is

10 times less than the length of *S. oneidensis.* As a consequence, in a carbon felt the bacterium is supported by 1 fiber which only offer 1 pathway to transfer electron. In our ES-carbon paper electrode, it can be expected that the bacterium will be supported by at least 2 or 3 individual fibers offering 4 to 6 potential pathways to transfer electrons **(Figure 3.3)**. If one of the fibers in contact with the cells is inactive (isolated by EPS, broken, non-correctly connected to the conductive structure), another one may be used as electron acceptor for DET. Once these fiber mats have been prepared and characterized, their impact on, *S. oneidensis* viability will be evaluated. Finally, the material will be characterized as an electrode for electrochemistry and mounted in a dual-compartments MFC. To conclude the MFC performance will be compared to equivalent experiment implying conventional carbon felt. At the end of the chapter, a side project consisting in the direct encapsulation of *S. oneidensis* within an electrospun fiber will be mentioned.

3.2. HOME-MADE SYNTHETIZED ELECTROSPUN CARBON PAPER BY ELECTROSPINNING PROCESS

3.2.1. General assessments about electrospinning process

The electrospinning process, patented by J.F. Cooley and W.J. Morton in 1900 and 1902 [243,244], allows to form mats of fibers with various thickness (nano- to micro-fibers) and architecture (randomly looped or aligned fibers, bulk or core-shell structures) [245–248]. By applying a high voltage (from 1 to more than 30 kV) to a needle supplied with a solution, a high field of potential is formed between the needle and a grounded substrate. It results in a perturbation of the solution droplet at the tip of the needle, the formation of a so-called Taylor cone. A liquid jet which forms a fiber between the needle and the collector is then observed. During its flying time, elongation and thinning of the fibers occur due to electrostatic repulsion and ambient parameters such as the temperature and the air relative humidity. Finally, the fiber is deposited on a collector.

Otherwise, a competitive phenomenon to electrospinning, named electrospray, can occur during the applying of the voltage, resulting in the fast deposition of small droplets at the grounded substrate surface [249–251]. Electrospray can be avoided by carefully choosing electrospinning experimental parameters.

A compromise has to find between viscoelastic behavior, surface tension and fluidity to make the solution of precursor electrospinnable. In fact, a sufficient fluidity of the solution is necessary to make it injected without solidification. But, the solution also need to be sufficiently viscous to form a fiber (and to avoid electrospray). Moreover, even a sufficient viscosity is necessary, a compromise is required for the surface tension of the solution droplet to be overcame by the applied high voltage. Suitable electrospinning parameters (described below) must be identify and tune to perform electrospinning process and to form various fibers geometry, architecture and structuration:

(i) Solution properties. To perform the electrospinning of a solution, its inherent properties need to be set-up. The viscosity is one of the most important parameters that needs to be empirically evaluated. Most of the time, polymers are used as base

for the preparation of the precursor solution. To adjust the viscosity of the electrospun solution, concentration and molecular weight of the polymer are the two main parameters to play with. In the case of sol-gel chemistry, the maturation time of the solution is studied to find the optimum state of maturation for electrospinning. The conductivity of the solution is another parameter to determine. Moreover, to form a fiber, electrospinning forces (field of potential) need to overcome the surface tension of the solution to form a Taylor cone. This surface tension can be adapted by adjusting the chemical structure of the polymer or by adding surfactants to the solution.

(ii) **Electric field and injection speed** must be adjusted to achieve electrospinning process. Generally, by increasing the applied potential, fibers diameter decreases whereas an increase of the injection speed increases fibers diameter as well as the quantity of electrospun matter.

(iii) **The distance between the needle and the substrate** has a direct impact on the flying time of the fibers (for a fixed applied potential). The longer this distance, the longer the flying time and therefore the duration of contact of the fiber with the atmosphere. Higher distance may help to dry the fibers before deposition on the substrate.

(iv) **Ambient parameters.** The temperature of the atmosphere directly in contact with the fiber during flying time helps to dry the fibers or to maintain the polymer in the liquid state before electrospinning (for example, agarose solution must be kept above 40°C to avoid instant gelation). The air velocity can also aid to dry the fibers but, more importantly, allows the renewal of the atmosphere and the elimination of the evaporating solvent. Finally, air relative humidity is an important parameter. Most of the time, by increasing the %RH the fibers diameter increases. Moreover, for certain polymers, a low or high relative humidity are necessary.

(v) **The collector** must be electrically conductive and grounded or fixed at a potential of opposite sign. Planar substrate or roller are used to collect the fibers. The rotation of the roller adds a second spinning force and aids to form fibers. For specifically formulated precursor solutions, the rotation of a roller collector leads to the alignment of the fibers [252].

(vi) Finally, **the needle gauge** influences the fibers sizes. By using atypical needles conformation, it is possible to perform coaxial electrospinning leading to the formation of a core-shell fiber.

By adjusting all these parameters, a large diversity of mats can be synthetized and can be used in many fields of research: batteries, fuel cell, medicine (scaffold, …), filtration membrane, material for isolation, textile, …

3.2.2. Electrospinning of Poly(acrylonitrile) solution

In this chapter, the anodic material obtained by the electrospinning process is named « electrospun carbon paper » and abbreviated as « ES-carbon paper ». To elaborate this electrospun carbon paper, poly(acrylonitrile) (PAN) is used as base polymer of the formulation. PAN has been widely studied in bulk material as well as in fibrous materials for various applications. In the electrospinning process, polymeric solutions composed of PAN from 100 000 to 200 000 in molar weight dissolved in dimethylformamide solvent at 7 to 20 w.% are intensively used due to their ideal behavior and simplicity to electrospun. Indeed, highly stable electrospinning behavior is achieved for PAN solution concentration fixed between 7 and 20 w.%. Other electrospinning parameters were determined empirically and considered as efficient if a stable Taylor cone was obtained at the needle. After SEM characterization, the parameters can be adjusted as function of observed instabilities.

(i) Injection speed: $10\ \mu L.min^{-1} < v_{inj} < 40\ \mu L.min^{-1}$
(ii) Applied tension between needle and substrate: $E > 10\ kV$
(iii) Distance between needle and substrate: $8\ cm < d < 20\ cm$
(iv) Relative humidity: $\%RH < 70\ \%$. Due to the insolubility of PAN in water, for relative humidity superior to 70 %RH, the gelation of the polymeric solution is observed at the needle tip limiting the electrospinning process. For relative humidity lower than 35 %RH, highly stable fibers mats were obtained while for highest relative humidities, nodules are observed and the fibers randomly merged to form fibrils.
(v) Substrate: PAN solution can be electrospun on aluminum or baking paper on planar or rotating roller supports. The best fibers homogeneity is obtained with roller support due to the addition of the rotating spinning force to the applied field of potential.

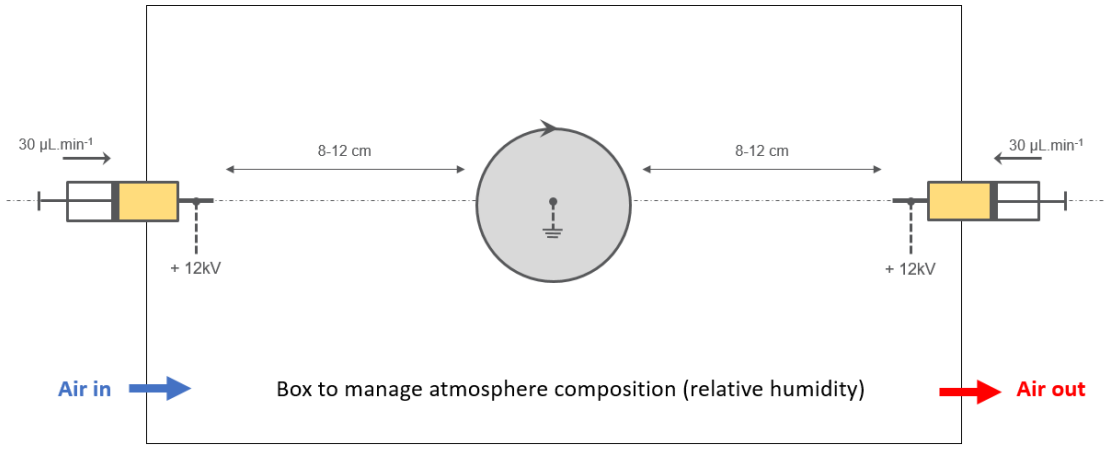

Figure 3.4 – Schematic representation of the electrospinning set-up to perform dual-electrospinning process and to produce PAN-fibers mats

In this work, poly(acrylonitrile) (PAN, 130 000 in molecular weight, Sigma-Aldrich US) solution concentrated at 10 and 15 w.% are electrospun with or without addition of adjuvants such as poly(ethylene glycol) (PEG, 10 000 in molecular weight, Sigma-aldrich) or iron chloride ($FeCl_3$, Sigma-Aldrich). Poly(ethylene glycol) acts as a surfactant and is supposed to allow the formation of more homogeneous mats in term of thickness. Iron chloride is known for its

catalytic effect during the stabilization and the carbonization/graphitization process. All the mats are electrospun with a dual-electrospinning system equipped with a conductive and grounded rotating roller centered between two needles **(Figure 3.4)**. Humidity is monitored and regulated by sparging water vapor or dry air in a closed environment. The tension is applied with a high voltage generator provided by Electrospinz company (E < 35 kV, New Zealand).

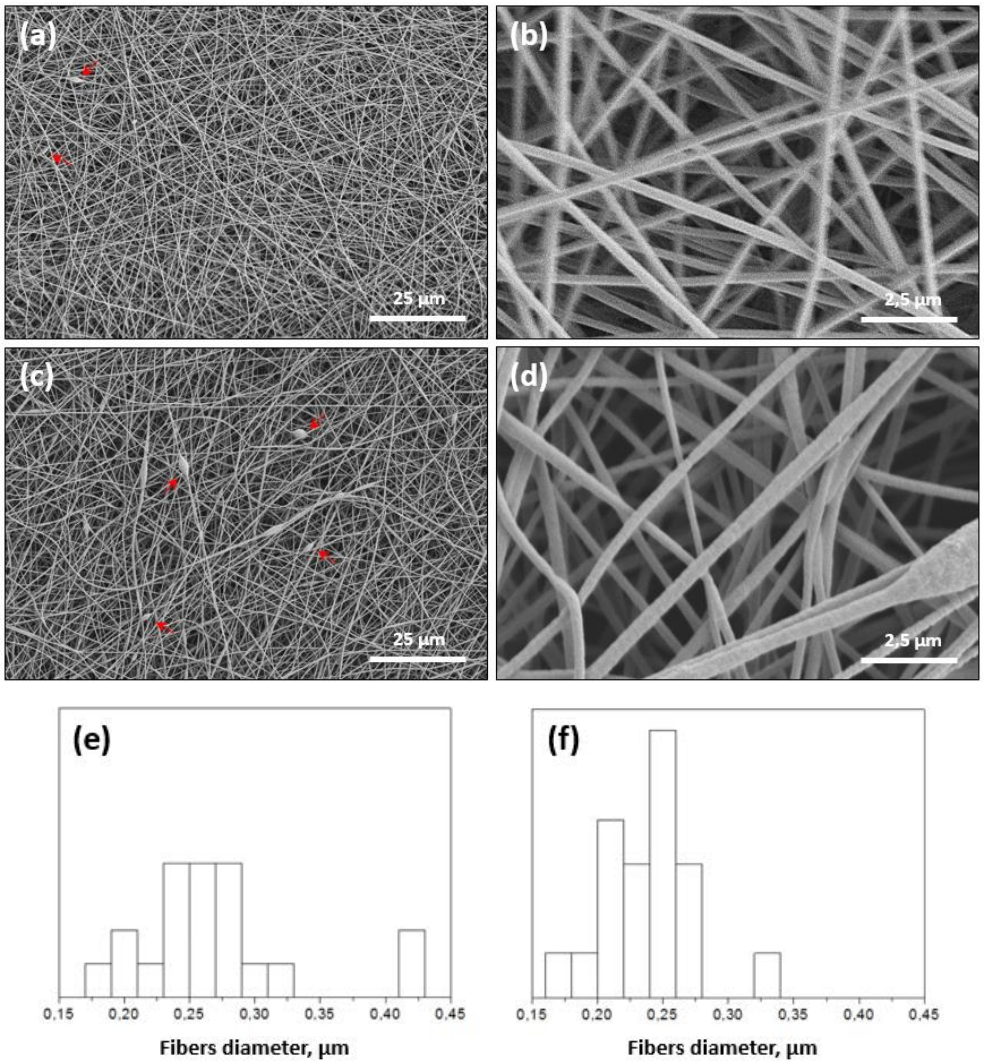

Figure 3.5 – Electrospun fibers for a polymer solution concentrated at **(a, b, e)** 10 w.% in PAN and at **(c, d, f)** 10 w.% PAN + 2 w.% PEG at 30 %RH of humidity. Scanning electron microscopy (a-d) and distribution of fibers diameters (e, f)

Figure 3.5 displays scanning electron microscopy of the fibers mats obtained for PAN solutions concentrated at 10 w.% with or without addition of 2 w.% of PEG, at a relative humidity between 30 and 35 %RH. For the pure PAN solution, the injection speed, and the tension are fixed at 34 µL.min^{-1} and 14 kV. The addition of 2% PEG slightly changes the chosen parameters: v_{inj}= 28 µL.min^{-1} and E = 15 kV. In both cases, the mat is electrospun on a grounded rotating roller (ca. 440 rpm) equipped with an aluminum foil. The set-up is as previously described on **Figure 3.4** with a distance of ca. 10 cm between the needle and the substrate.

For polymer solution without PEG, the resulting mat thicknesses are between 100 and 150 µm with an inhomogeneity in the thickness of ca. 50 µm between the center of the mat and

their extremities. With the addition of 2% PEG, this homogeneity is solved and mat thickness is more homogeneous over the 20 cm of its full length. A few nodules and instabilities are observed in both cases (2 to 5 in a SEM field of 420 x 300 µm, at a x 8 000 magnification) but remain in a limited amount. The fibers diameter is centered at 0.240 ± 0.034 µm for the 10 w.% PAN solution and 0.270 ± 0.063 µm (12.5 % of diameter increase) in the presence of PEG. Even the dispersion in fibers diameters is narrow, both of the diameters with or without PEG can be considered as equivalent.

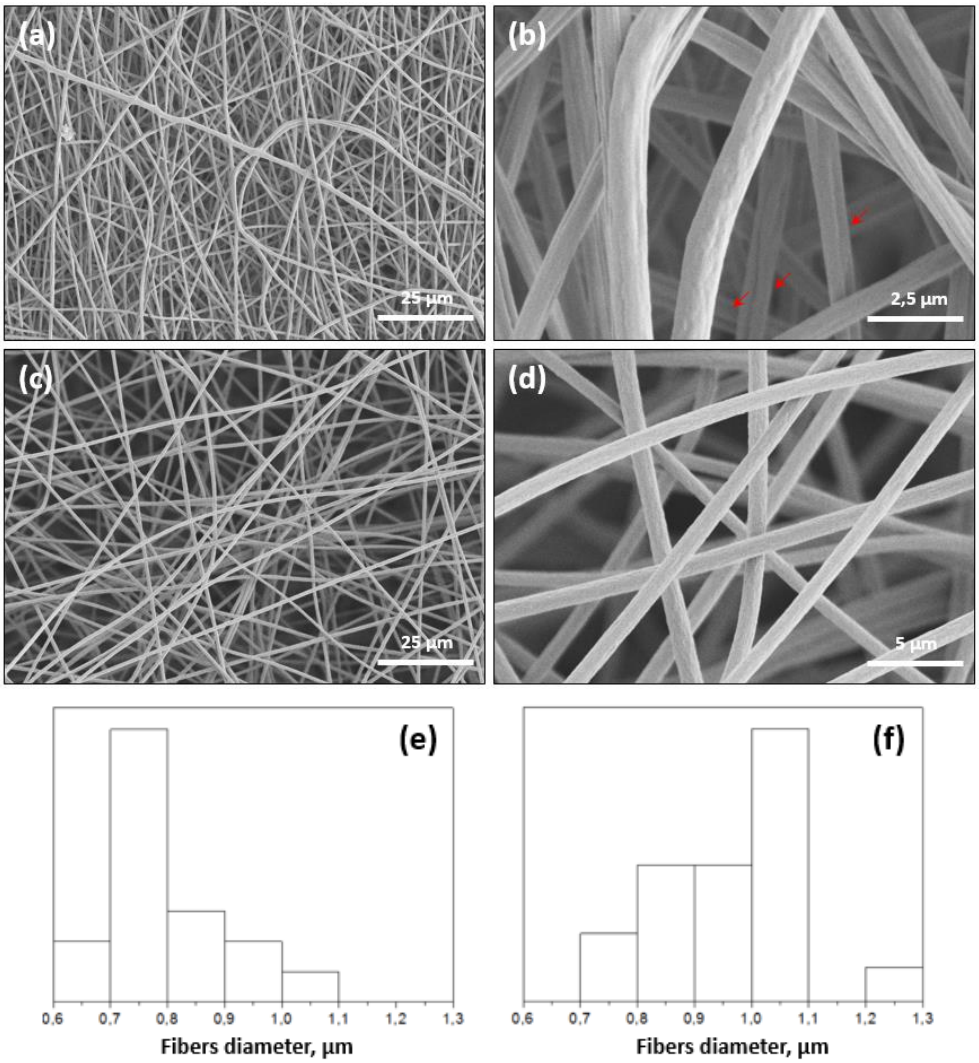

Figure 3.6 – Electrospun fibers for a polymer solution concentrated at **(a, b, e)** 15 w.% in PAN and at **(c, d, f)** 15 w.% PAN + 2 w.% PEG at 30 %RH of relative humidity. Scanning electron microscopy (a-d) and distribution of fibers diameters (e, f)

In comparison, **Figure 3.6** presents the characterization by SEM of a electrospun PAN solution concentrated at 15 w.% with or without 2 w.% of PEG. For the solution without PEG, injection speed is fixed at 26 µL.min^{-1} and the tension at 15 kV. With PEG, the conditions are very similar: v_{inj}= 28 µL.min^{-1} and E = 17 kV. Other experimental conditions and electrospinning set-up are equivalent to those previously described. The measured mat thickness is ca. 120 µm for the same amount of solution electrospun (ca. 1.5 mL) as for 10 w.% solutions. An equivalent density of fibers is observed but with no apparent nodules or instabilities. At high magnification,

the fibers surfaces appear rougher than for the 10 w.% solution of PAN. Specific fibers organization (red arrows) emphasizes a hypothetical welding of fibers during the electrospinning process. Without PEG addition, the measured fibers diameter is 0.800 ± 0.150 µm. With 2 w.% of PEG this diameter increases to 0.966 ± 0.114 µm (21 % of diameter increase).

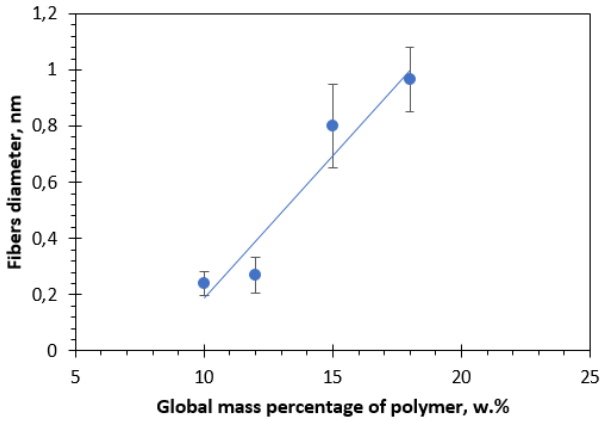

Figure 3.7 – Correlation between the measured fibers diameter and the global percentage of polymers (PAN + PEG) to perform electrospinning (results from **Figure 3.5** and **Figure 3.6**)

The effect of the addition of PEG on the fibers diameter is therefore more significant for the highest PAN concentration. This can be related to the variation in the solution viscosity probably resulting from highest chain-chain interaction between PAN nitrile- and PEG hydroxo-groups for highest PAN concentration. This effect was observed not only during the preparation of the mixture but the solution was also found instable upon ageing, leading to the formation of a gel after 5 to 6 hours. Such an increase in viscosity therefore explain the increase in fibers diameter (see part. 3.2.1). In addition, the dispersion in fibers diameters is more important at 15 w.% of PAN than at 10 w.% revealing a significant polydispersity probably related to the observed random fusion between fibers. The fibers diameter seems to evolve quite linearly with the total amount of polymer involved in the electrospinning process (PAN + PEG dissolved in dimethylformamide solvent) **(Figure 3.7)**.

Finally, the effect of the relative air humidity is explored by electrospinning of a 10 w.% PAN solution at 30 %RH and 60 %RH. An increase of the relative humidity lead observed to the gelation of the fiber during the flying time (since PAN is hydrophobic). Therefore, an increase of the fibers diameter should be observed, due to a lower influence of the applied potential on the fiber stretching in a field of high potential. As expected, by doubling the relative humidity, the fibers diameter has almost doubled from 0.24 ± 0.034 µm (30 %RH) to 0.45 ± 0.055 µm (60 %RH) **(Figure 3.8)**. Contrary to the mechanical increasing related to the viscosity of the polymer solution, the increase is here due to the gelation of the fibers during the flying time. In consequence, the fusion of fibers observed at 15 w.% of PAN is not relevant to explain the increasing in diameter at higher relative air humidity. These fibers [3] are therefore 27 to 50 times thinner than in carbon felts, as function of relative air humidity, respectively. However, as such,

[3] Electrospinning condition: 10 w.% PAN, 34 µL.min^{-1}, 14 kV, ca. 8-10 cm between needle and substrate, 30% RH or 60 %RH.

they form an isolating matrix and must therefore be converted into a conductive network before being used as an electrode.

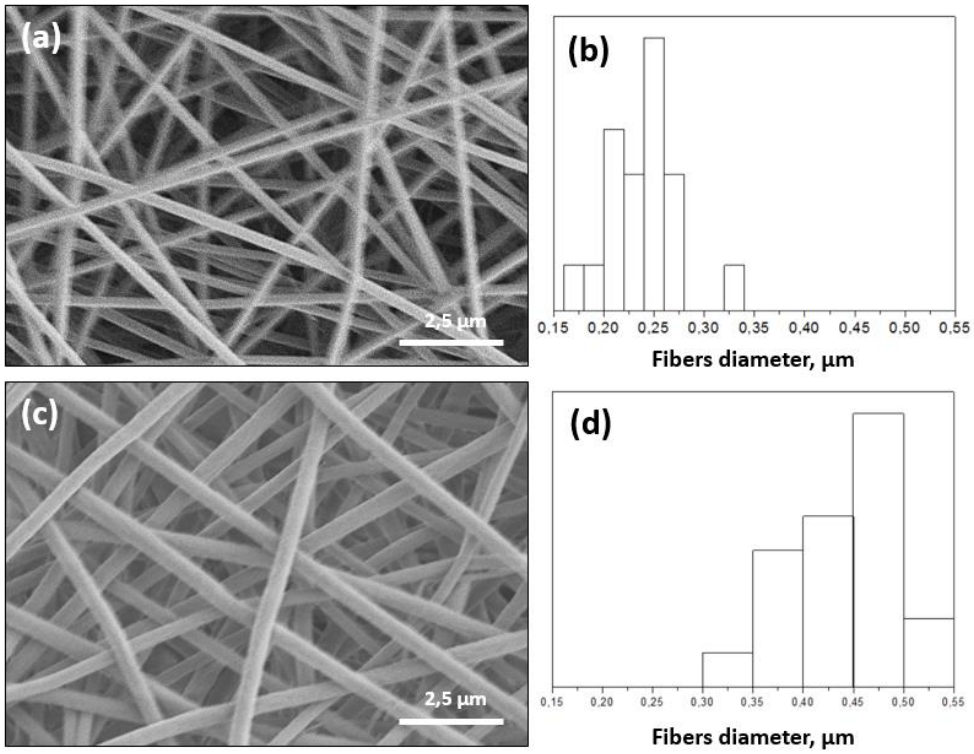

Figure 3.8 – Effect of doubling the relative humidity of the atmosphere during electrospinning process of a polymer solution concentrated at 10 w.% PAN. **(a, b)** 30 %RH and **(c, d)** 60 %RH of relative humidity.

3.2.3. Stabilization, carbonization and graphitization of electrospun fibers mats: from non-conductive to conductive fibers

To improve the electronic conductivity in order to form a ES-carbon paper electrode composed of randomly looped electrically conductive fibers, a process of carbon conversion is required. The carbon conversion is generally composed of two main steps: (i) stabilization under air and (ii) carbonization under inert atmosphere [253].

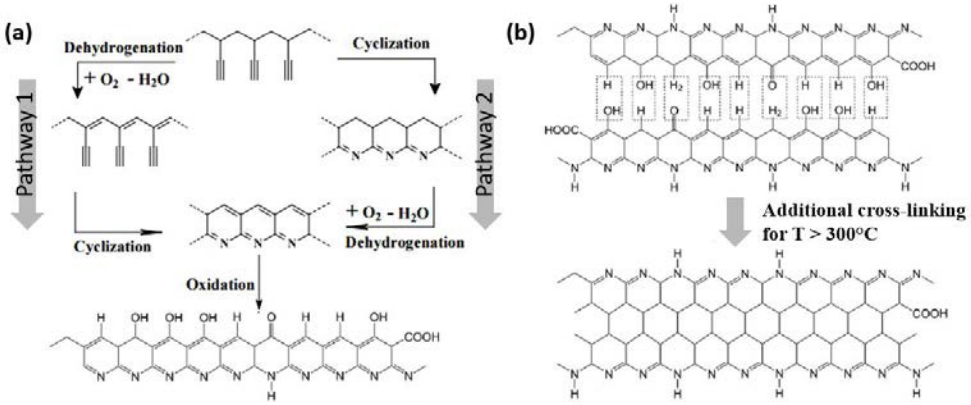

Figure 3.9 – Pathways of PAN stabilization in temperature under air: **(a)** typical sequence under 300°C and **(b)** additional cross-linking for temperature higher than 300°C [254,255]

(i) **The stabilization process** is crucial as part of the heat treatment leading to the carbon conversion. This initial step is necessary for converting electrospun fibers into conductive carbon fibers [256–262]. If the stabilization is not carefully controlled, the deterioration resulting in important weight loss occurs by degradation (burning) and chain scission [262]. However, the absence of stabilization, or too short or too long stabilization step also lead to the deterioration of the material accompanied with a low electronic conductivity. Therefore an optimum has to be find in order to ensure a sufficient conductivity [263].

Poly(acrylonitrile) stabilization process has already been studied with the help of various characterization technics: scanning electron microscopy, X-ray diffraction [258,260,261], Fourier transform infrared spectroscopy (FTIR) [258,260] and differential scanning calorimetry (DSC and/or ATG) [258]. Complex steps occur and contribute to the stabilization process. Three pathways of stabilization are reported and potentially occur simultaneously as a function of heat treatment temperature: nitrile reaction, C=C conjugation and oxidation. These sub-processes of the stabilization involve cyclisation by analog-polymerization of the nitrile groups, and dehydrogenation [264,265]. Three reaction pathways are available to perform the first step of the carbon conversion leading to a « ladder configuration » [264,266] **(Figure 3.9.a)**. In case of oxidation, at temperatures above 300°C, an additional cross-linking reaction occurs **(Figure 3.9.b)** [264]. In term of energy of activation, the cross-linking step exhibits the highest energy of activation followed by the cyclization and nitrile-analog polymerization process [267]. The stabilization is performed under air; oxygen initiate the formation of activated centers in order to promote cyclisation.

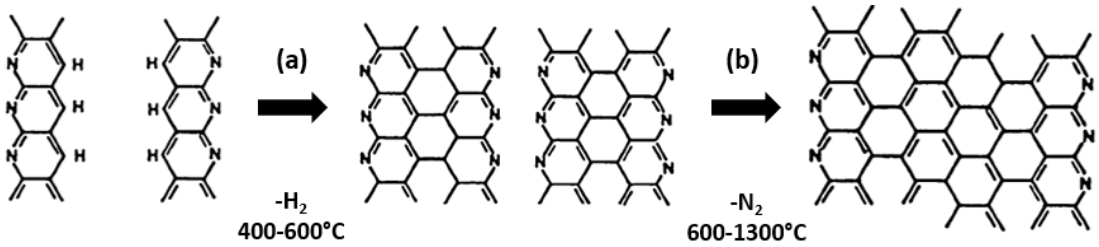

Figure 3.10 – Carbonization pathway at higher temperature than during stabilization process (600 to 1300°C). **(a)** Dehydrogenation and **(b)** denitrogenation [254].

(ii) **The carbonization process** occurs at higher temperatures under non-reactive atmosphere such as nitrogen. The carbonization is an aromatic growth which occurs by analog-polimerization. During this step, volatile non-carbon atoms i.e. oxygen, hydrogen and nitrogen are removed by dehydrogenation, deoxygenation and denitrogenation leading to water and nitrogen formation [254,264]. The carbonization leads to the formation of highly-conjugated and conductive layers of carbon also named graphite ribbons, with a small concentration of nitrogen **(Figure 3.10)**.

3.2.3.1. Experimental procedure

To produce conductive electrospun carbon paper, a solution of precursor (10 w.% PAN in DMF solvent) is electrospun on a grounded rotating roller (440 rpm) in a dual-electrospinning set-up. The process is conducted for 1h leading to an average electrospun volume of 2 times 1.5 mL to achieve a mat thickness of ca. 300 µm. The electrospinning process is carried out under 60 %RH of relative humidity.

Then, a heat treatment is applied to the PAN-fibers mat in order to proceed to the carbon conversion and to transform the isolative mat into a conductive mat made of 100-300 nm sized fibers **(Figure 3.11)**. In a first step, the polymeric chains of PAN which composes the fibers are stabilized under air at 220°C (at 5 °C.min^{-1}) for 3h. In a second step, the stabilized mat is taken off its aluminum foil and carbonized at a temperature between 750 and 950°C (at 5 °C.min^{-1}) for 1h30 under nitrogen atmosphere (with less than 2 ppm of O_2). Finally, to achieve a more extended carbonization/graphitization, an optional heat treatment at 1500°C (at 5 °C.min^{-1}) for 1h30 under pure argon atmosphere is performed to improve electric conductivity.

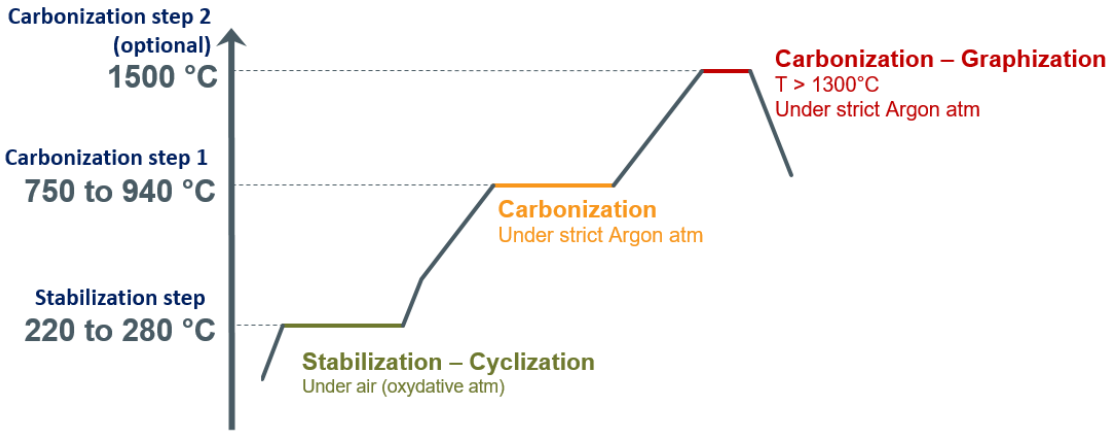

Figure 3.11 – Schematic representation of the heat treatment cycle applied to mats to transform them into conductive carbon paper made of conductive 100-300 nm-fibers.

The resulting electrospun carbon papers are characterized by scanning electron microscopy, Fourier transform infrared spectroscopy, impedance spectroscopy, electrochemistry and Raman spectroscopy. Moreover, the effect of iron chloride ($FeCl_3$) added at 0.5 w.% to the initial polymer solution has been evaluated, since iron chloride is supposed to act as a catalyst for both stabilization and carbonization processes.

3.2.3.2. Scanning Electronic Microscopy characterization

From a macroscopic point of view, raw mats are white while stabilized mats are brown after 3h at 220°C under air and dark brown after 3h at 280°C under air. For the mat electrospun with a PAN solution including 0.5 w.% of iron chloride catalyst, the mats are dark brown or dark at 220°C and 280°C. The color of the fiber mat is indicative to the rate of cyclization/dehydrogenation and oxidation. The darker the mat, the more the mat is stabilized.

Figure 3.12 displays scanning electron microscopy observations at different states of the carbon conversion. First, the randomly looped organization of the fibers and their integrity are preserved all along the conversion. However, the fibers seem to crack probably under the stress caused by intensive fibers shrinking under high temperature (1500 °C, 1h30, Ar, **Figure 3.12.d**). An evaluation of the fibers diameter after each step of the whole heat treatment **(Figure 3.13)** indicates a low effect of the stabilization at 220°C. The fibers diameter decreases from 0.489 ± 0.063 µm (raw mat) to 0.446 ± 0.055 µm (stabilized at 220°C) resulting in 9% of loss in fibers diameter [4]. After a treatment of carbonization at 850°C (1h30, nitrogen atm.) the fibers diameter, fell down to 0.283 ± 0.038 µm corresponding to 42% of diameter loss in comparison with the raw fibers. For a treatment at 950°C (1h30, nitrogen atm.) and an optional treatment at 1500°C (1h30, argon atm.), the results are similar with diameters losses equivalent to 44% and 43%, respectively. This measurement clearly indicates that the fibers are not degraded during the stabilization process under air, i.e. the temperature of degradation of the material is not reached. In contrast, fibers shrinking mainly occurs during the carbonization step, where ca. 50% of the fibers diameter is lost after 1h30 at 850°C or 950°C. An additional treatment at higher temperature (1500°C) for more 1h30 does not lead to a higher fibers diameter loss but the stress induces fibers to break down. However, the macroscopic structure of the electrospun carbon paper remain smooth and mechanically resistant to electrode processing.

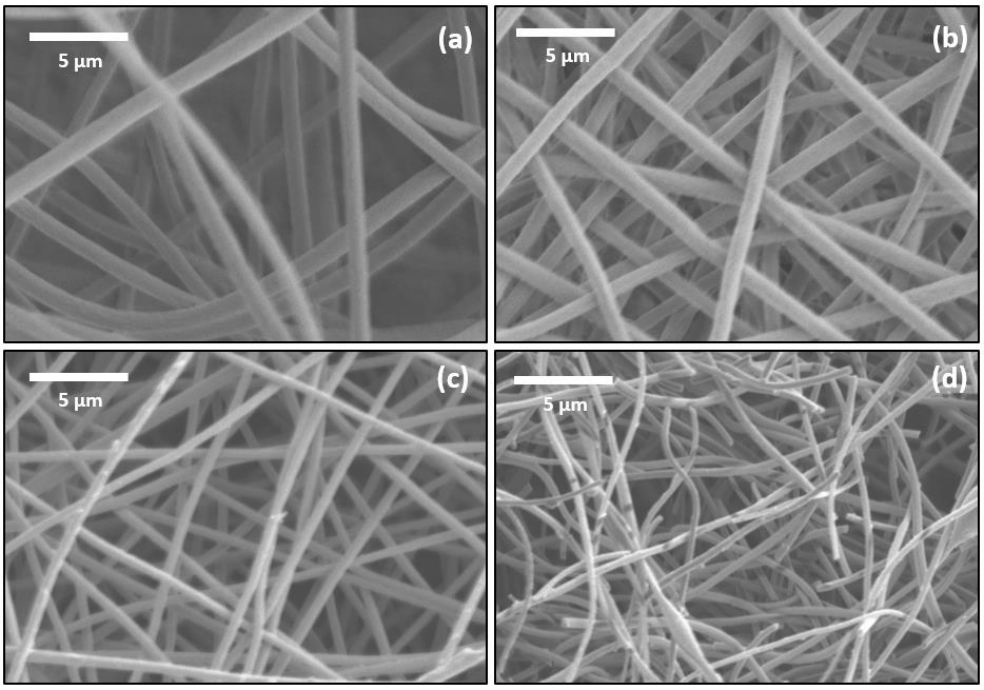

Figure 3.12 – Scanning electron microscopy of a raw fibers mat under carbon conversion by successive heat treatments: **(a)** Control, raw mat, **(b)** after stabilization at 220°C during 3h under Air, **(c)** after carbonization at 850°C during 1h30 under nitrogen atmosphere and **(d)** after an optional carbonization at 1500°C during 1h30 under argon atmosphere (O_2 < 2 ppm)

[4] Loss in fibers diameter means the reduction induced by heat treatment, in comparison with the diameter of non-treatment electrospun fibers **(Figure 3.12.a)**: $\% \, \emptyset \, loss = \frac{\emptyset \, cosidered \, fiber}{\emptyset \, control \, fiber}$

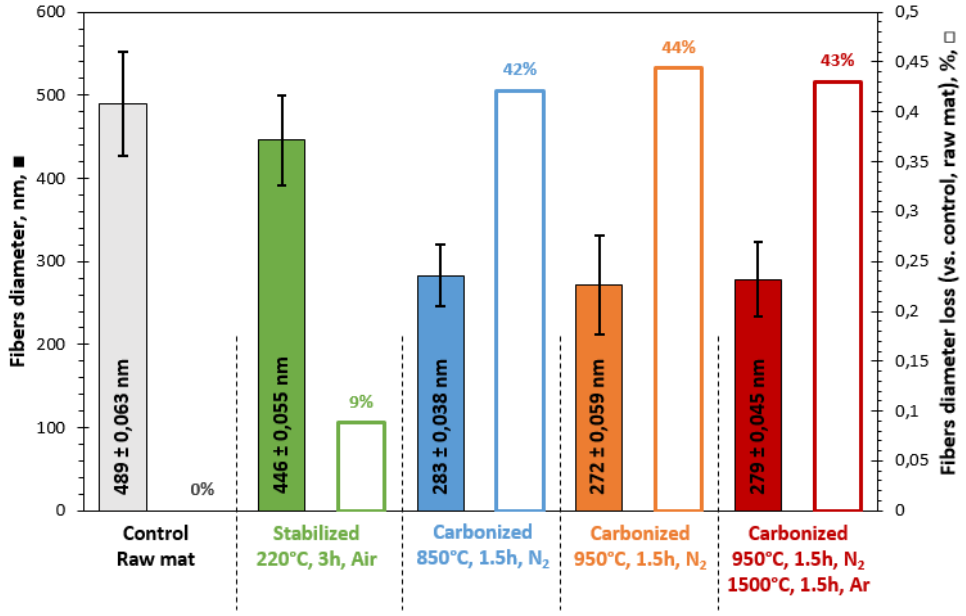

Figure 3.13 – Carbon fibers diameter at different states of the carbon conversion process. For each successive treatment, the average fibers diameter (on the left) and the percentage of diameter loss vs. the raw carbon fibers diameter (on the right) are displayed. ■ Fibers diameter, □ Fiber diameters loss vs. raw mat fibers diameter. Caption: ■ □ **Control raw mat**, ■ □ **stabilized at 220°C**, ■ □ **Carbonized at 850°C**, ■ □ **Carbonized at 950°C**, ■ □ **Carbonized at 1500°C**.

3.2.3.3. Fourier transform infrared spectroscopy characterization

Carbon conversion of electrospun mats, based on the 10 w.% PAN solution with or without 0.5 w.% $FeCl_3$ as a catalyst, is monitored by FTIR at various state of the heat treatment from the raw mat to the carbonization step under argon atm. at 1500°C **(Figure 3.14)**. A group of bands characteristic the PAN are observable on the FTIR spectrum: 2939 cm^{-1}, 1456 cm^{-1} refer to CH_2 stretching and bending; 2240 cm^{-1} refer to C≡N stretching; bands in between 1070 and 1400 cm^{-1} are related to C-O bond and the band at 1070 cm^{-1} more particularly refers to C-O-C. The intensity of these bands progressively decreases with increasing of the temperature during the carbon conversion process. This is a consequence of cyclization, dehydrogenation and oxidation step, occurring during the stabilization and carbonization process. At the stabilization step, the spectrum is becoming less precise and the bands are less thin and separate. The bands characteristic of unsaturated bonds between 1070 and 1400 cm^{-1} are more intense. This result was predictable due to the progressive transformation of the PAN structure into « ladder structure » **(Figure 3.14.b** blue spectrum**, Figure 3.9)** Ultimately, The FTIR spectrum is simplified into a characteristic FTIR signal of carbon by increasing the temperature of treatment from 750°C (green) to 1500°C (dark red).

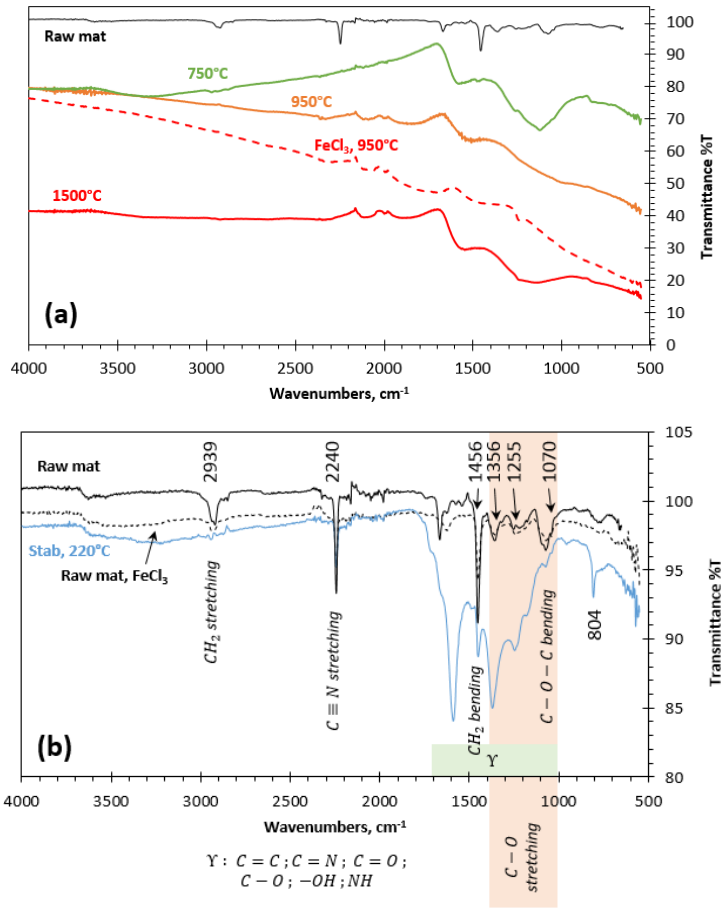

Figure 3.14 – FTIR characterization at various state of the carbon conversion process from the raw ES-mat to the conductive ES-carbon paper. **(a)** Superposition of all the spectra and **(b)** raw and stabilized mat spectra. For electrospun 10 w.% PAN solution: **— raw mat**, **— after stabilization at 220°C** (3h, Air), **— after carbonization at 750°C** (1h30, N_2 atm.), **— after carbonization at 950°C** (1h30, N_2 atm.), **— after carbonization at 1500°C** (1h30, Ar atm.) For electrospun 10 w.% PAN + 0.5 w.% $FeCl_3$ solution: **- - - raw mat**, **- - - after carbonization at 950°C** (1h30, N_2 atm.)

3.1.1.1. Raman spectroscopy characterization

In the present case, ES-carbon papers with or without addition of iron (II or III) are characterized by Raman spectroscopy and spectra are reported on **Figure 3.15**. This study has been done in collaboration with Ivan Lucas (LISE, UPMC, Paris). Two main bands are observable at 1350 cm^{-1} (D-band) and 1600 cm^{-1} (G-band). As shown on **Table 3.1**, wavenumbers of both D- and G-bands are in agreement with tabulated values [268]. D-band refers to the disorder in the carbon structure and the G-band refers to the graphitic structure. The R-value is defined as the ratio of the D- and G-bands intensities. This ratio evolves with the degree of graphitization and more precisely to the degree of graphitic plan alignment. Moreover, R-value is sensitive to the concentration of graphitic plan and to the graphitic plan assemble. The decrease of the R-value is characteristic of an increase of the sp^2 (graphitic) nature of the carbon structure and as a consequence indicates an increase of the its electronic conductivity. Moreover, the separation between D- and G-band as well as the width of the bands (FWHM, full width at half-maximum) are characteristic of the PAN transformation from a disordered state to a more graphitic state. The same observations may be applied to the second harmonic bands between 2000 and 3500 cm^{-1} [268].

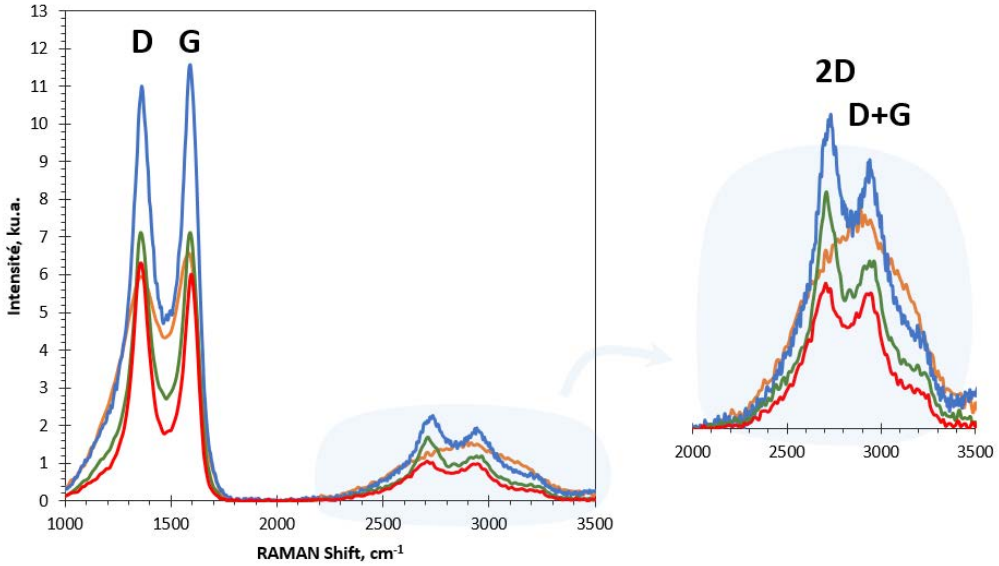

Figure 3.15 – Raman spectroscopy analysis of electrospun carbon paper based on the electrospinning of 10 w.% PAN with or without iron (II or III) chloride catalyzer. All the mats are stabilized at 280°C under air for 3h and then carbonized for 1h30 at: — 940°C (N_2), — 1500°C (N_2), — 940°C (Ar, with $FeCl_2$), — 940°C (Ar, with $FeCl_3$).

As shown on Figure 3.15 and reported on **Table 3.1**, for **electrospun carbon paper based on a 10 w.% PAN solution**, the R-values are equivalent for a sample carbonized at 940°C (1h30, N_2) and at 1500°C (1h30, Ar). The R-values are low compared to those tabulated ones observed for equivalent or lower temperature (1.95 reported at 900°C compared to 0.95 at 940°C here) [268]. In parallel the FWHM values for D- and G-bands are larger for ES-carbon paper carbonized at 940°C (non-measurable, **Figure 3.15** orange) than for 1500°C-carbonization. Moreover, the second harmonic are clearly non-separated. These results confirm an increase of the graphitic nature of the converted fibers with an increase of the carbonization temperature. **By addition of 0.5 w.% of $FeCl_3$** as a catalyst, equivalent R-value and FWHM-values are measured for a 940°C-carbonization, in comparison to a 1500°C-carbonization without catalyst. This result confirms the benefit of the addition of $FeCl_3$ to limit the temperature of carbonization (and stabilization). Finally, by replacing $FeCl_3$ by $FeCl_2$, an equivalent R-value is observed (0.95) but the bands exhibit a wider FWHM.

ES solution	Heat treatment 1/ Stabilization at 280°C (Air, 3h)	D-band cm-1	G-band cm-1	R-value ID/IG	FWHM cm-1
PAN 10 w.% (DMF)	2/ Carbonized at 940°C (N2, 1h30)	1360	1590	0,95	--
	2/ Carbonized at 1500°C (Ar, 1h30)	1360	1590	1,00	D-band: 92 G-band: 70
PAN 10 w.% + FeCl3 0,5 w.% (DMF)	2/ Carbonized at 940°C (N2, 1h30)	1355	1595	1,05	D-band: 92 G-band: 70
PAN 10 w.% + FeCl2 0,5 w.% (DMF)	2/ Carbonized at 940°C (N2, 1h30)	1345	1575	0,93	D-band: 123 G-band: 106

Table 3.1 – Characteristic parameters in Raman spectroscopy for the conditions tested on **Figure 3.15**. D-band and G-band correspond to the bands characteristic to Disordered structures and Graphitized structures, respectively. R-Value correspond to the ratio of the D-band intensity (ID) and the G-band (IG). FWHM signifies full width at half-maximum and cannot be determined for the last condition due to the lack in D-band and G-band separation.

3.1.1.2. Electrical and electrochemical characterization

To characterize the electronic conductivity of electrospun carbon paper, impedance spectroscopy measurements are performed. Surface, $\sigma(S)$, (2 points on the electrode surface separated by 1 cm) and transversal, $\sigma(T)$, (2 points on top and down surfaces of the electrode) conductivities have been evaluated for different treatment of the 10 w.% PAN i.e. after (i) the 3h of stabilization at 220°C (Air) and after 1h30 of carbonization at (ii) 750°C, (ii) 850°C, (iii) 950°C (N_2) or 1500°C (Ar). **Figure 3.16** displays the variation of the conductivity as function of the heat treatment.

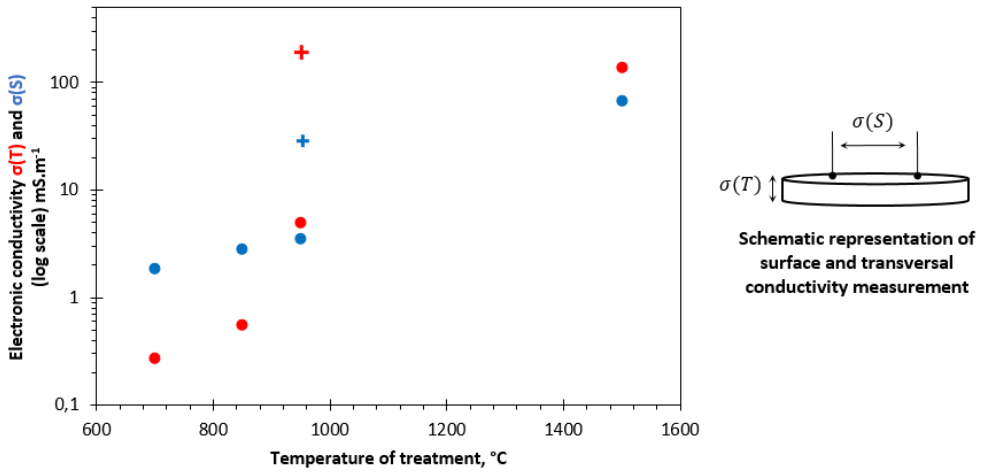

Electrospun solution:	10% PAN (DMF)					+0,5 w.% $FeCl_3$
Temperature (1h30)	220°C (Air)	700°C (N2)	850°C (N2)	950°C (N2)	1500°C (Ar)	950°C (N2)
Transversal conductivity σ(T)	ca. 0	0,3 mS/m	0,6 mS/m	5 mS/m	140 mS/m	190 mS/m
Surface conductivity σ(S)	ca. 0	2 mS/m	3 mS/m	4 mS/m	70 mS/m	70 mS/m

Figure 3.16 – Evaluation of the transversal **σ(T) and planar σ(S)** electronic conductivity as function of the applied heat treatment.
Caption: **For 10 w.% PAN solution, • σ(T)** and **• σ(S). For 10 w.% PAN + 0.5 w.% $FeCl_3$, + σ(T)** and **+ σ(S).**

First, the conductivities increase with the temperature from a non-electrically conductive electrospun mat of fibers to a highly conductive carbon paper (0 to 136 $mS.m^{-1}$ from the stabilized mat to the carbon paper carbonized at 1500°C). As predictable, the carbonization is responsible for the electrical conductivity enhancement. **Second,** at low temperature of carbonization (< 900°C), conductivities measured in the plane, $\sigma(S)$, are higher than in the bulk, $\sigma(T)$, by a factor of 5 to 7. This behavior must be explained by the continuity of the conductive fiber network in the plane. In the bulk (perpendicularly to the plane), carbon papers are organized in layers of randomly looped fibers, resulting in a more complex electron transfer. For highest temperatures, this trend is reversed (i.e. $\sigma(T) > \sigma(S)$). Two phenomena may occur to explain this change: (i) cyclization, dehydrogenation and denitrogenation are completed and lead to a rearrangement at the fibers junctions which facilitate electron transfers from a layer of fibers to another. (ii) As observed on SEM pictures at high temperature (> 900°C), the fibers break and the continuity of the planar network is no more ensured **(Figure 3.12)**. **Third,** by adding 0.5 w.% of $FeCl_3$ to the initial electrospun solution, planar and transversal electronic

conductivities at only 950°C are equivalent to the ones measured after a carbonization at 1500°C. These results confirm the catalytic effect of iron chloride for carbonization process.

As supplementary information, **Figure 3.17** displays the Nyquist plots determined by impedance spectroscopy. For carbonization temperature superior to 800 °C (green, blue and black series of dots) pure resistance are obtained while a more complex situation is observed at 750°C. At this temperature, the carbonization appears incomplete and a second contribution represented by non-perfect half-circle is observed between 1500 and 2600 Ω. By varying AC voltage, it is possible to determine if this contribution is due to the material or to the interface. At various voltage (from 20 to 100 mV) the measured Nyquist plot and impedance are equivalent leading to the conclusion that this contribution indicates the conductivity of the material. The non-pure resistance can be explained by a partial carbonization.

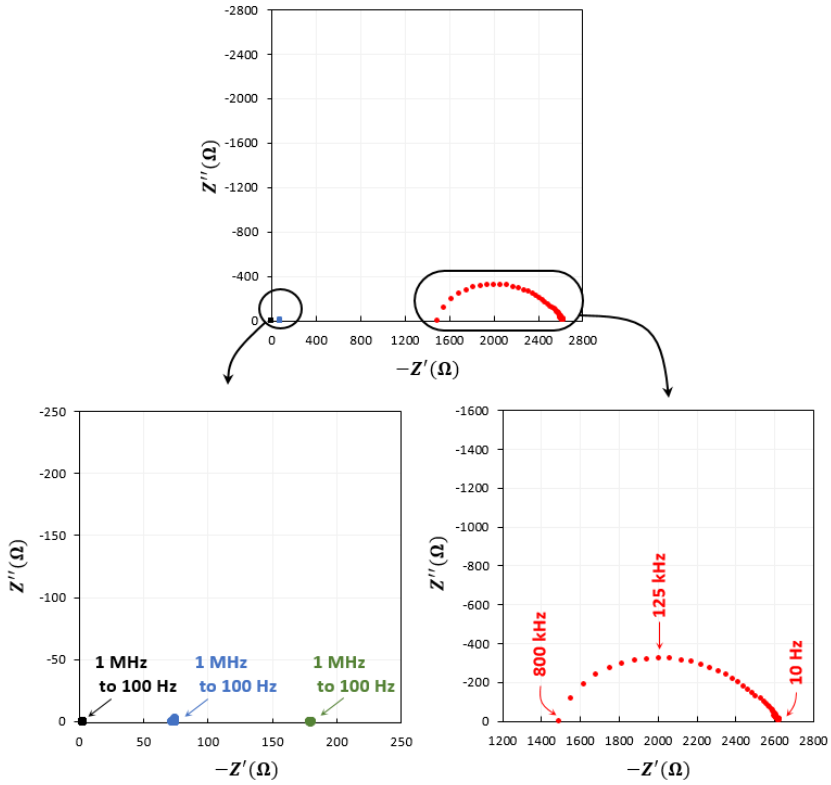

Figure 3.17 – Determination of the transversal electronic conductivity by impedance spectroscopy for four systems: ES-carbon papers • **stabilized at 220°C (air, 3h)** and **carbonized during 1h30 at** • **750°C (N_2)** or • **850°C (N_2)** or • **1500°C (Ar)**. Conductivity is determined by the formula $\sigma(T) = A/(R * l)$ with A the surface area, l the thickness and R the material participation to the resistance determined at 100 Hz for the carbonized samples or at 800 Hz for the sample only stabilized at 220°C.

Electrochemical characterization by cyclic voltammetry

Finally, the electrospun carbon paper [5] (disk of 1.5 cm in diameter) is characterized by cyclic voltammetry in an aqueous solution of NaCl (150 mM) supplemented or not with ferricyanide probes ($K_3Fe(CN)_6$) concentrated at 0.3 mM **(Figure 3.18)**. In a saline solution, a

[5] Mats are based on the electrospinning of a solution of 10% PAN without addition of catalyst. Then, mats are stabilized at 220°C under air atm. for 3h and carbonized at 940°C for under nitrogen atm. for 1h30.

square capacitive signal is achieved and measured capacitive currents lead to a calculated capacitive surface area of $A_c = 1.5\ m^2$ for ca. 7 cm² of geometric surface and a volume of electrode equal to 70 cm³. When the same experiment carried out in presence of 0.3 mM of ferricyanide probe, the monitored faradaic signal indicates both peaks of reduction and oxidation for speed rate between 1 and 50 mV.s^{-1}. The investigated range of potential (-0.8, 0.8 V vs. Ag/AgCl/KCl) is not sufficient to observe the oxidation of $Fe(CN)_6^{4-}$. Based on the measured currents, the faradic surface is evaluated at only 650 cm² (5% of the global capacitive surface). However, this surface remains 4.6 times higher than the faradaic surface of the carbon felt. By considering a quasi-irreversible reaction and an exchange coefficient of 0.23 [269], the percentage of active surface area increases by a factor of 8% of the global capacitive surface **(Figure 3.18.c)**. For high speed rate, the electrochemical behavior of ES-carbon papers is similar to the carbon felt in equivalent conditions. An elliptic signal is observed. The difference of peaks potentials increases from 160 to 600 mV (> 59 mV which is the limit for a perfectly reversible mono-electronic reaction) between 1 and 50 mV.s^{-1} **(Figure 3.18.d)**. This result indicates the quasi-reversibility of the system. Practical option to improve the faradaic surface and reversibility will be presented in conclusion. But, this result also indicates that the faradaic surface is enough to use this ES-carbon paper as electrode.

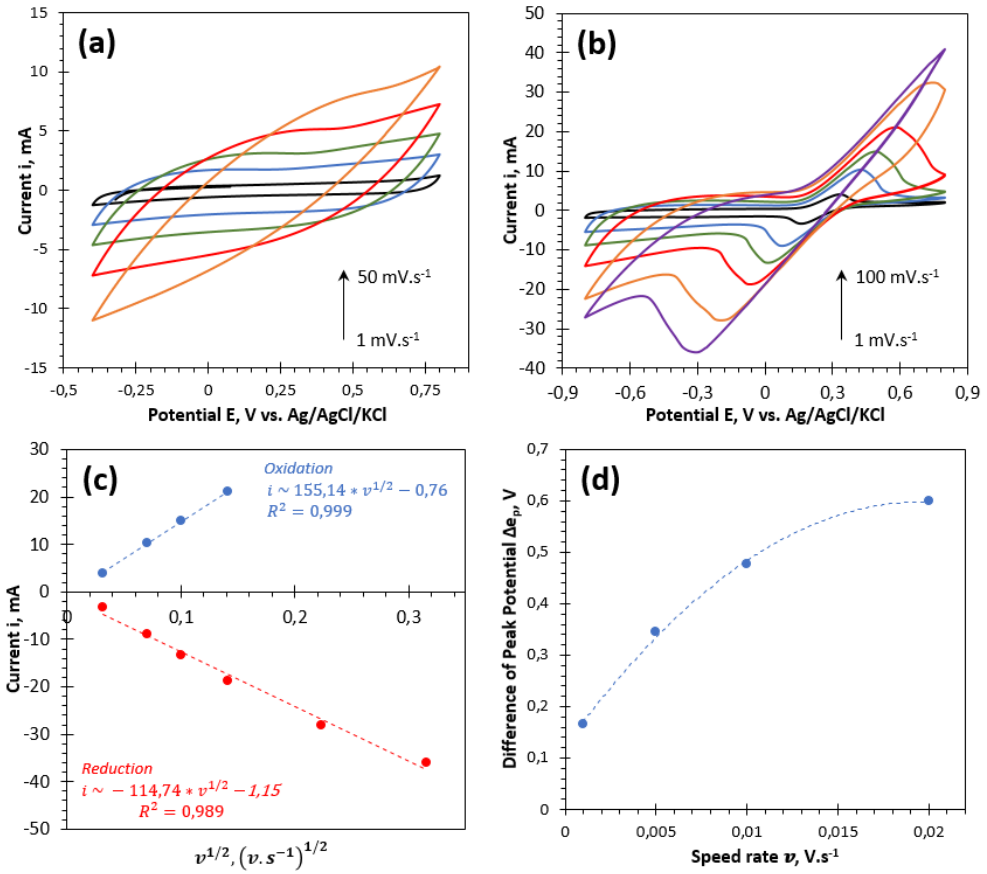

Figure 3.18 – Electrochemical characterization of an electrospun carbon paper based on the stabilization (220°C, Air, 3h) and carbonization (940°C, N_2, 1h30) of a mat based on the electrospinning of a 10 w.% PAN solution. **(a)** Capacitive participation measured by cyclic voltammetry (speed rate from 1 to 50 mV.s^{-1}) in a saline electrolyte (NaCl, 150 mM). **(b)** Faradaic participation measured by cyclic voltammetry (see above) in a saline solution supplemented with 0.3 mM of $K_3Fe(CN)_6$. **(c)** Randles-Sevcik plot based on the results of **Figure 3.18.b**. **(d)** Evolution of the difference of peaks potential for each speed rate.
Caption (a, b): **— 1 mV.s^{-1}**, **— 5 mV.s^{-1}**, **— 10 mV.s^{-1}**, **— 20 mV.s^{-1}**, **— 50 mV.s^{-1}**, **— 100 mV.s^{-1}**.

3.2. BACTERIA VIABILITY ON ELECTROSPUN CARBON PAPER

S. oneidensis viability on ES-carbon paper is evaluated for various structural and incubation conditions by epifluorescence and inhibition test on LB-Agar plate. The objective is to determine the potential bacteria adhesion and multiplication at the ES-carbon paper surface as function of the precursor solution composition and the heat treatment applied to the fibers mat. Moreover, inhibition test allows to qualitatively determine if the electrode is toxic for the bacteria. Before both tests, ES-carbon papers are autoclaved for 1h and illuminated with UV germicidal irradiation in a sterile environment for 12h in order to ensure the material sterility before testing.

(i) **Inhibition tests** are divided in two parts. In a first part, a bacteria solution of *S. oneidensis* [6] is spread out on an LB-Agar plate (analog to agars for counting on plate, cf. part. 2.3) in order to obtain a dense bacterial film after 24h of incubation at 37°C. Disks of ES-carbon paper at various states of carbon conversion are disposed on LB-Agar and then incubated at 37°C. If the material is toxic for bacteria, no bacteria should be seen under the disk. Four compositions and states of conversion are evaluated: PAN fibers mats with or without iron (III) chloride catalyst, both being stabilized for 3h under air at 220°C and two PAN fibers mats stabilized at 220°C and then carbonized at 700°C for the first and at 950°C for the second.

After incubation, forming colonies are observed under and around the three disks that were carbonized and/or stabilized without incorporation of iron catalyst (see schematic representation on **Figure 3.19**). To confirm these results, the four disks were taken off the agar plate and rinsed with sterile PBS to preserve only the bacterial colonies formed on the paper, and then transferred on a new LB-Agar (without bacteria spread out). After 24h of incubation at 37°C a dense circle of bacterial colonies is observed around the three papers without iron catalyst. On the contrary, no bacteria growth is observed around the fibers mat including $FeCl_3$ and stabilized at 220°C **(Figure 3.19)**.

As a conclusion of the inhibition test, the PAN fibers mats are not toxic at the stabilization and the carbonization states, except when iron was present in the initial formulation. This needs further explanations: *S. oneidensis* is a DMRB (dissimilatory metal-reducing bacteria) implying its ability for iron respiration. As a consequence, the observed apparent toxicity of the iron (II) chloride into the precursors solution is difficult to explain. It will be necessary to evaluate the potential toxicity of the material after carbonization and to evaluate the nature of iron in the carbon structure of the fibers to better understand this effect.

[6] Bacterial growth since the protocol SOg_4 (see part. 2.3) stopped at OD_{600} = 1.7 and then transferred in an MR1-L medium without fumarate but concentrated at 30 mM in lactate and diluted at an OD_{600} = 0.7.

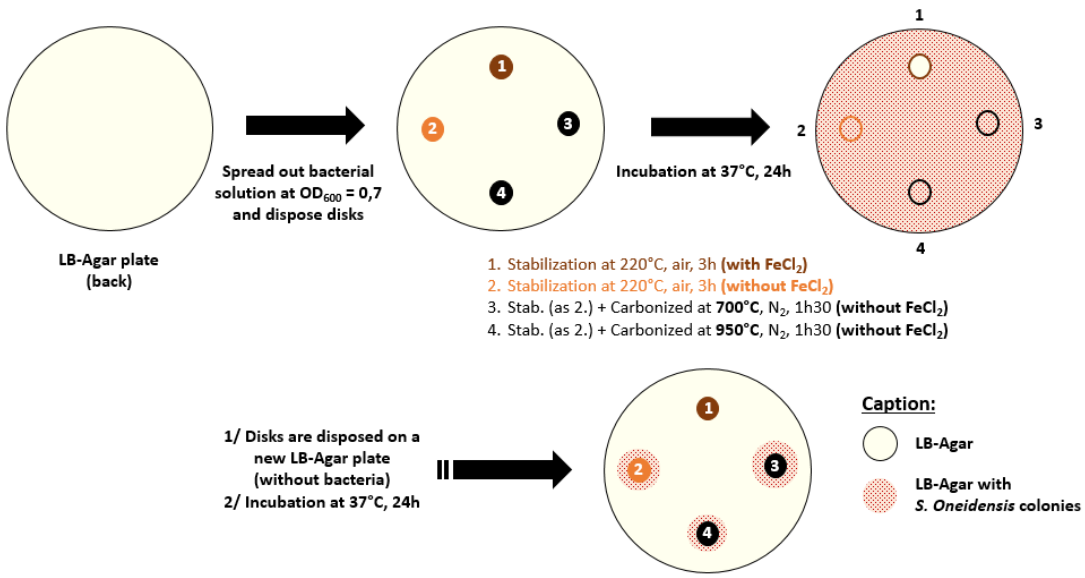

Figure 3.19 – Schematic representation of inhibition test on LB-Agar plate. Evaluation of the material toxicity for bacterial growth.

(ii) Epifluorescent microscopy viability tests are performed for an ES-carbon paper stabilized at 220°C for 3h under air and carbonized at 950°C for 1h30 under N_2. The aim is to evaluate how ES-carbon papers are colonized after five days in four different conditions of incubation:

1. ES-carbon paper **incubated in bacterial culture** (OD_{600} = 0.7, MR1-L medium) for 10 min and then transferred in **pure MR1-L medium** (30 mM Lactate) for 5 days.
2. ES-carbon paper **immersed in a fumarate solution** (1 M) for 10 min (adsorption of fumarate) and then transferred in **a bacterial culture (OD_{600} = 0.7, MR1-L medium)**.
3. ES-carbon paper **immersed in a solution of fumarate and lactate** (1 M) for 10 min (adsorption of fumarate) and then transferred **in a bacterial culture (OD_{600} = 0.7, MR1-L 30 mM Lactate)**.
4. ES-carbon paper **directly incubated in the bacterial culture** (OD_{600} = 0.7, MR1-L 30 mM Lactate).

After 5 days of incubation at 30°C and 150 rpm, electrodes are observed by epifluorescence after being incubated in a solution of fluorescent dyes ([syto9] = 5 µM and [Propidium Iodide] = 27 µM in milli Q sterile water) and mounting between slide and slip for observation **(Figure 3.20)**.

The first condition consists in incubating a ES-carbon paper in MR1-L medium (30 mM Lactate and 0 mM Fumarate) after impregnation of the electrode with a bacteria culture. And inversely, both 2 and 3 conditions consist in the impregnation of the electrode with a solution of fumarate (cond. 2) or with a solution of fumarate and lactate (cond. 3) and then, their incubation in the bacteria culture. For these three conditions, most of the bacteria are dispersed

on the entire electrode and seem mainly alive (green on epifluorescence pictures). Moreover, a part of the adhesive bacteria is organized in clusters within which a part of the bacteria is dead (red). The existence of these clusters indicates favorable localization for bacteria to adhere and multiply. For the condition 1, after a short time of exposition to the bacteria, the clusters existence can be explained by a non-homogenous repartition of the bacteria during the exposition and then high multiplication rate from adhesive bacteria. For both conditions 2 and 3, lots of bacteria are available during the incubation in the bacterial solution for 24h. Situations are equivalent in term of living/dead bacteria ratio, indicating the predominant effect of the fumarate deposited at the surface of the electrode. The clusters are probably due to a heterogeneous repartition of the fumarate which increases the electron acceptor behavior of the domains covered with fumarate. Finally, condition 4 seems to confirm previous conclusions. In absence of impregnation of lactate and fumarate at the fibers surface, the covering of the electrode by bacteria is homogeneous and most of the bacteria seem alive.

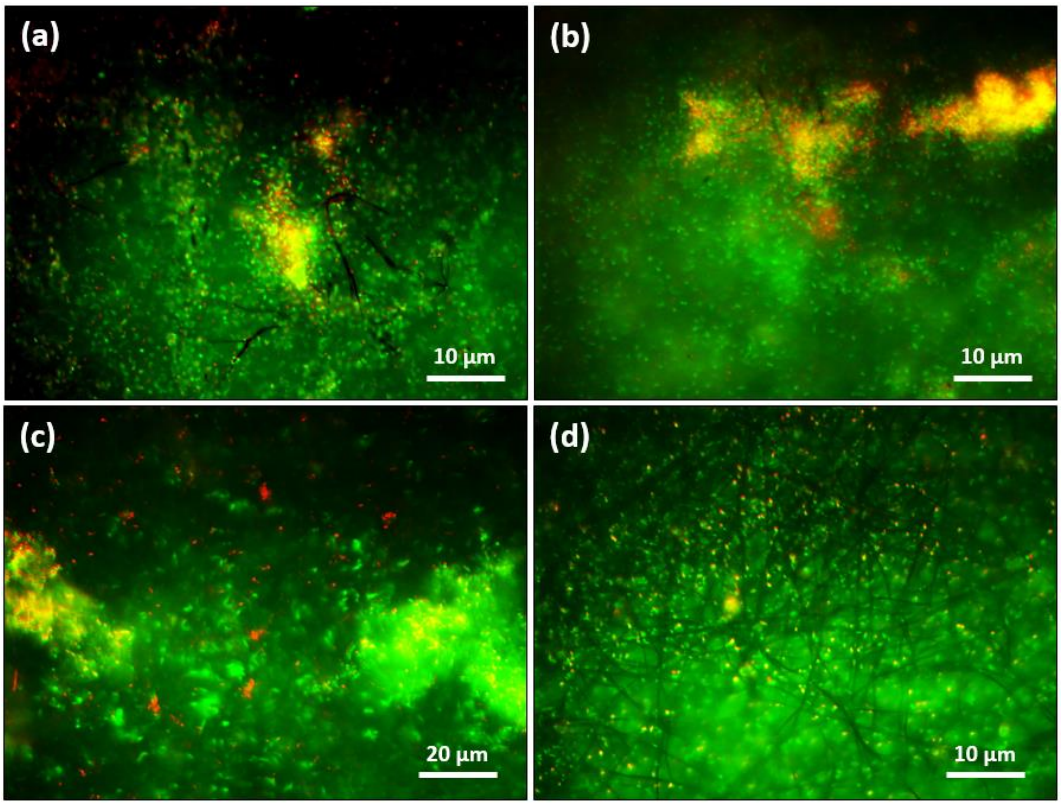

Figure 3.20 – Characterization of the bacteria viability by epifluorescence (Syto9/Propidium Iodide). Electrospun carbon papers are incubated in various condition for 5 days. **(a)** ES-carbon paper incubated in bacterial culture (OD_{600} = 0.7, MR1-L medium) for 10 min and then transferred in pure MR1-L medium (30 mM Lactate). **(b)** ES-carbon paper immersed in a fumarate solution (1 M) for 10 min (adsorption of fumarate) and then transferred in a culture (OD_{600} = 0.7, MR1-L 30 mM Lactate). **(c)** ES-carbon paper immersed in a solution of fumarate and lactate (1 M) for 10 min (adsorption of fumarate) and then transferred in a culture (OD_{600} = 0.7, MR1-L 30 mM Lactate). **(d)** ES-carbon paper directly incubated in the bacterial culture (OD_{600} = 0.7, MR1-L 30 mM Lactate).

To conclude, the ES-carbon paper synthesized by stabilization of an iron-free PAN fibers mat at 280°C and then carbonization at 950°C (N_2) appears non-toxic and adapted to *S. oneidensis* colonization to form a bio-anode for MFC.

3.3. ES-CARBON PAPER AS A BIO-ANODE

The ES-carbon paper chosen for MFC investigation corresponds to the fibers mat electrospun based on a 10 w.% PAN (in DMF) solution, then stabilized at 220°C for 3h under air and carbonized for 1h30 at 950°C under nitrogen atmosphere. Before being mounted as an anode in a dual-compartments MFC, the ES-carbon paper is sterilized. All the parts of the reactor are subjected to the same sterilization (Nafion® is only sterilized with UV light).

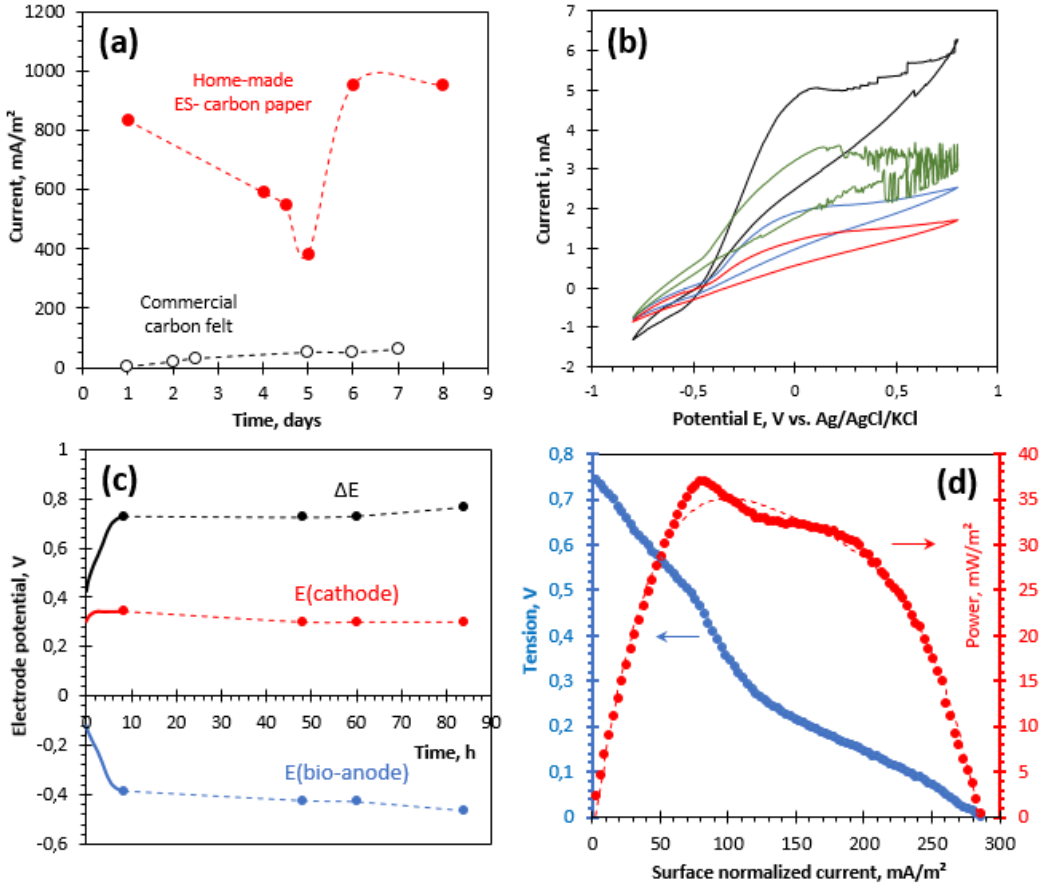

Figure 3.21 – Electrochemical characterization of a dual-compartments reactor based on the use of: a ES-carbonpaper (electrospinning of a 10 w.% PAN solution stabilized at 220°C and carbonized at 940°C, $\sigma_T = 5\ mS.m^{-1}\ and\ \sigma_P = 3.4\ mS.m^{-1}$) as anode and a 2 cm³ carbon felt as cathode. The anolyte consists in a solution of *S. oneidensis* sampled in log-phase (OD_{600} = 1.7) diluted in an MR1-L medium at OD_{600} = 0.7. The catholyte is a 150 mM NaCl supplemented in 10 mM $K_3Fe(CN)_6$. A Nafion® membrane is used as a separator. Both anodic and cathodic sides are aerated with vent-cap. The system is not polarized. **(a)** Comparison between the anodic current provided by an ES-carbon paper at 0.3 V vs. Ag/AgCl/KCl in comparison with a standard 1 cm³ carbon felt in the same condition of measurement and incubation (Current normalized by the geometric surface area). **(b)** Cyclic voltammetry monitoring of the system at: **— day 1,** — day 4, — day 5, — day 7. **(c)** OCP monitoring of: • **the anode**, • **the cathode** and • **the MFC OCV** as function of the time (continuous line = continuous measurement). **(d)** Characterization of the whole MFC at day 3: • **Polarization curve**, • **Power curve** (current and power normalized by the geometric surface area).

Figure 3.21 displays the entire electrochemical characterization of the MFC based on the use of a ES-carbon paper for 9 days of monitoring. The monitoring of electrodes OCP indicates an impressive stability of the cathodic reduction. The optimization proposed in chapter 2 (see part. 2.4.4) are applied here. The anode OCP fastly decreases from -0.1 to -0.385 V vs. Ag/AgCl/KCl in less than 10h and then slightly decreases to -0.465 V vs. Ag/AgCl/KCl after 3.5

days. The global MFC OCV reaches 0.73 V vs. Ag/AgCl/KCl after 10h and then slowly increases while the anode OCP decreases **(Figure 3.21.c)**. This OCP behavior is analog to the carbon felt OCP under positive polarization in dual-compartments (see 2.4.4, **Figure 2.39**) and indicates a fast colonization at the beginning of MFC working condition. Cyclic voltammetry indicates an intense wave of oxidation at -0.5 V vs. Ag/AgCl/KCl which decreases until day 5 together with the current measured by chronoamperometry at 0.3 V vs. Ag/AgCl/KCl (from 0.84 to 0.38 $A.m^{-2}$ between day 1 and day 5). After feeding the reactor with an equivalent 30 mM volume of lactate at day 5, the current reaches a more stable value of ca. 1 $A.m^{-2}$ at day 6. The cyclic voltammetry at day 7 is in accordance with chronoamperometric measurements **(Figure 3.21.a and Figure 3.21.b)**. By comparing the anodic current normalized by the geometric surface area of anode with the ES-carbon paper and with the conventional carbon felt, an increase by a factor 10 (100 $mA.m^{-2}$ for the carbon felt vs. 1 $A.m^{-2}$ for the ES-carbon paper) is obtained. The same order of increase is observed by volume normalization. Normalizing the current measured by the capacitive surface area is not relevant due to the uncertain rate of colonized fibers. Moreover, the ratio between the bacteria and the fiber dimension leads to a lack of surface occupation.

Finally, both polarization and power curves indicate reasonable performances after only 2 days of anode colonization in MFC working condition. The maximum power and current are 35 $mW.m^{-2}$ and 280 $mA.m^{-2}$, respectively. The MFC OCV is equal to 0.75 V. These performances are higher to those obtained for an optimized dual-compartments MFC with a carbon felt bio-anode polarized at -0.3 V.

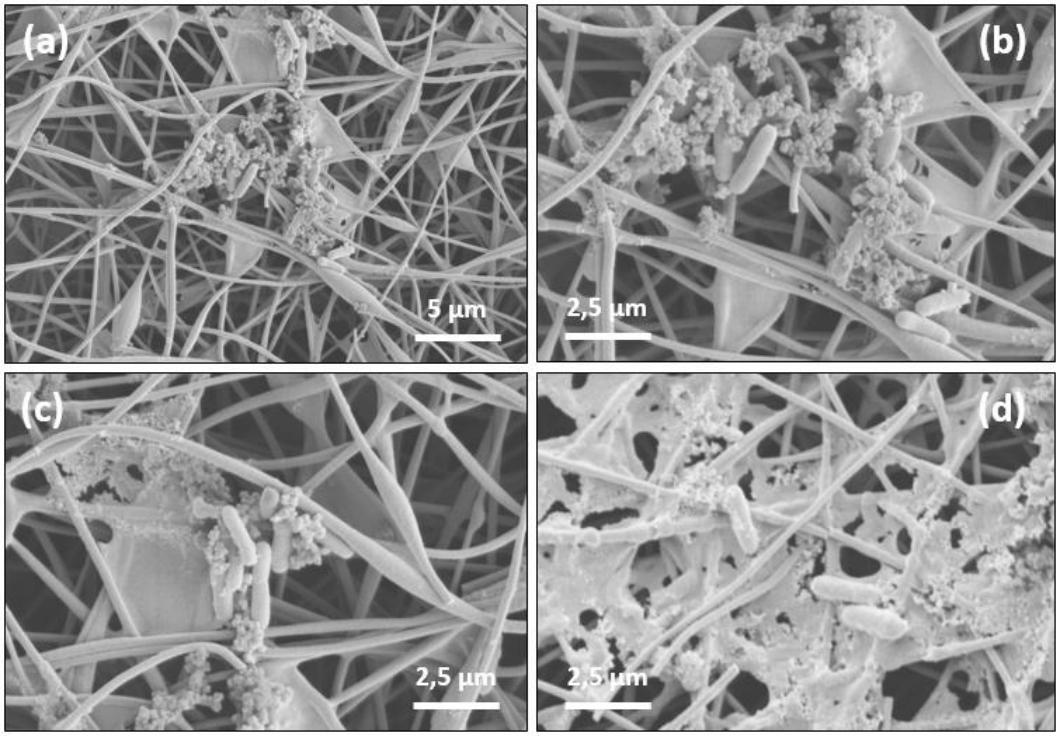

Figure 3.22 – Scanning electron microscopy of a ES-carbon paper after **2 days** of colonization as a bio-anode in a dual-compartments MFC. *S. oneidensis* colonizing the **(a-c)** side facing the bacterial solution and **(d)** the side facing the Nafion® membrane.

Figure 3.22 displays SEM observation of a ES-carbon paper bio-anode after only 2 days. A few colonies are observed on both top (facing bacteria electrolyte) and down (facing Nafion®) faces of the ES-carbon paper. Ribbons and particles of EPS are also observable near to the bacteria colonies. At day 10, most of the top surface of the bio-anode is colonized by a thin layer of individual bacteria **(Figure 3.23.e and Figure 3.23.f)**. On the top of the bacteria layer, a thick (> 10 µm) and porous biofilm composed of bacteria and EPS (exopolysaccharides) is formed **(Figure 3.23.b to Figure 3.23.d)**. Finally, a wide SEM field of observation indicates a large covering of the bio-anode after only 10 days **(Figure 3.23.a)**. The biofilm cracks are probably due to the non-regulated (air) drying of the structure.

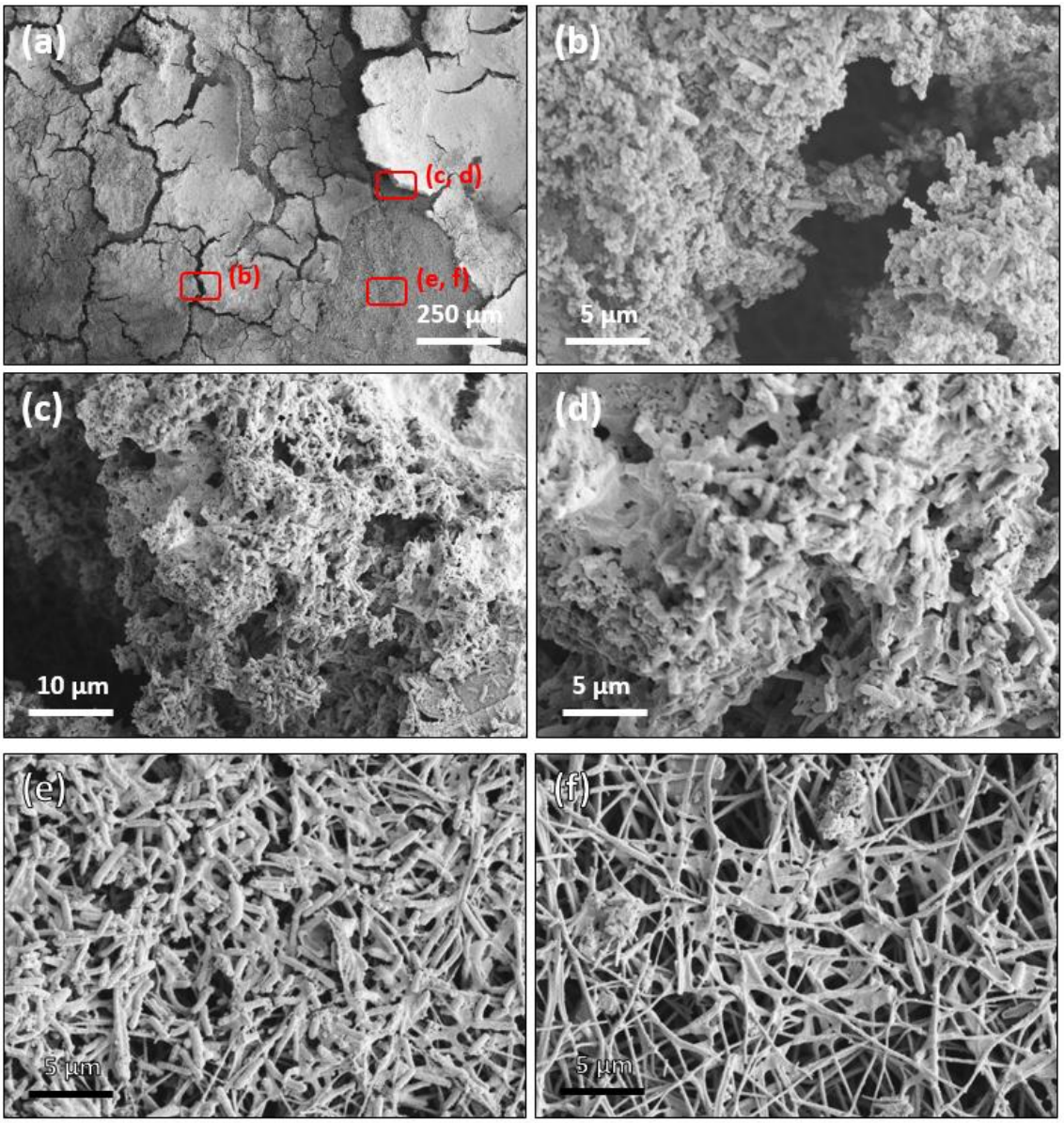

Figure 3.23 – Scanning electron microscopy of a ES-carbon paper after **10 days** of colonization as a bio-anode in a dual-compartments MFC. *S. oneidensis* colonizing the side facing the bacterial solution. Pictures **(b-f)** are taken in specific regions indicated in red on picture **(a)**.

3.4. CONCLUSION

In this chapter, an electrode (ES-carbon paper) was synthetized by the electrospinning of a 10 w.% PAN solution. The fibers mat was stabilized at 220°C for 3h under air atmosphere and then carbonized at 950°C under nitrogen atmosphere for 1h30. Various carbon conversion conditions have been tested and this condition was selected as a compromise between electronic conductivity enhancement, electrochemical behavior, surface chemistry and bacteria viability at the surface of the fibers. A significant improvement of the MFC performance is demonstrated by moving from a 3D carbon felt to a 2D ES-carbon paper. An enhancement by a factor 10 of the anodic current at +0.3 V vs. Ag/AgCl/KCl was observed in comparison with a carbon felt incubated in a dual-compartments MFC reactor, in the same conditions. The maximum anodic current density measured at +0.3 V vs. Ag/AgCl/KCl for ES-carbon paper is about 1 $A.m^{-2}$, while only 160 $mA.m^{-2}$ is measured for a 1 cm^3 carbon felt bio-anode.

Even if non-polarized and in aerobic conditions, a bio-anode based on the colonization of a ES-carbon paper in MFC presents highest oxidative wave from -0.5 V to 0.8 V vs. Ag/AgCl/KCl. Performances higher than those obtained for a carbon felt anode polarized at -0.3 V vs. Ag/AgCl/KCl in optimized reactor at day 5, are reached in only 2 days. Moreover, the rate of electrode covering is clearly higher than for a carbon felt polarized at -0.3 V vs. Ag/AgCl/KCl. A thick and porous biofilm was obtained after 10 days in a MFC. To enhance the MFC performances, the rate of bacteria loading into the ES-carbon paper may be improved by hydrophilic surface treatment or by bacteria solution filtration on the ES-carbon paper.

3.5. SIDE PROJECTS: *S. ONEIDENSIS* ENCAPSULATION IN AN ELECTROSPUN FIBER

Complementary to the production of an efficient ES-carbon paper for bacteria colonization in a MFC, another option was evaluated. Similarly to the use of silica gel as an artificial biofilm included into a carbon felt matrix, here the objective is to encapsulate *S. oneidensis* bacteria directly into a fiber synthetized by the electrospinning of a polymer solution composed of 7 w.% PVA, and concentrated in bacteria at an OD_{600} = 1.5-1.7. PVA is a cytocompatible and non-toxic polymer.

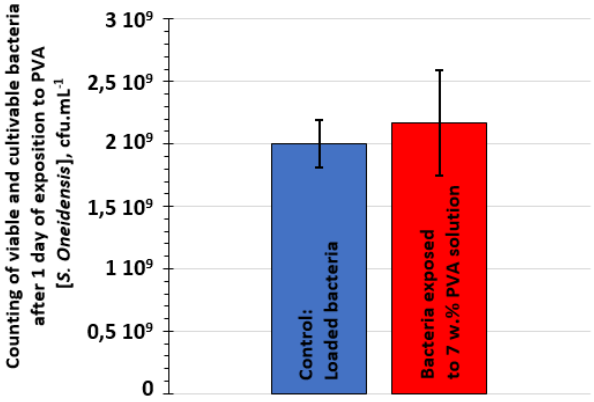

Figure 3.24 – *S. oneidensis* viability into a 7 w.% PVA solution after an exposition of 2-3h evaluated by counting on LB-Agar Plate.

First, the viability of *S. oneidensis* in a liquid solution of PVA is evaluated by counting on LB-Agar plate. The polymer solution is composed of 1 mL of 10 w.% PVA (Mowiol H88, 150 000 in molar weigh) and 0.5 mL of bacteria at OD_{600} = 5. The final concentration of PVA is ca. 7 w.% and the final optical density of the polymer is equivalent to OD_{600} = 1.7. As shown on **Figure 3.24**, after 2 to 3h of exposition to PVA aqueous solution, ca. 100% of the bacteria remained alive.

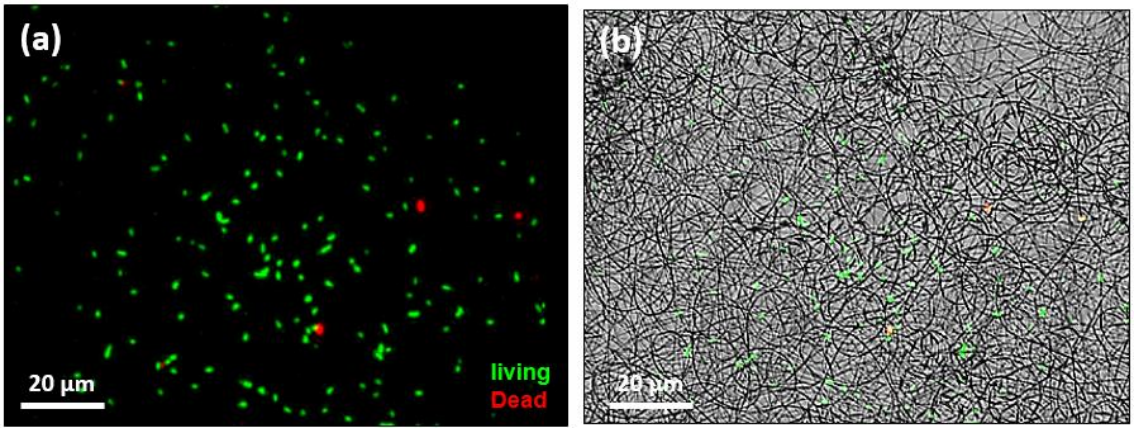

Figure 3.25 – Evaluation of living/dead bacteria ratio after electrospinning of a 7 w.% PVA containing an 2 10^9 cfu (bacteria)/mL by epifluorescence. Living bacteria are represented in green and dead bacteria in red. **(a)** Superposed signal of living and dead bacteria. **(b)** Superposition of pictures (a) on an optical image of electrospun fibers on ITO. The living and dead bacteria signals are clearly visible on polymer nodules.

Second, to evaluate the survival of the bacteria to the electrospinning process, 10 v.% of Syto9/Propidium Iodide fluorescent dyes solution is added to the polymer/bacteria solution. After 5 minutes of stirring, the solution is electrospun on an ITO slide for 30 minutes at 15 kV with a 30 µL.min^{-1} solution injection speed. The substrate is separated from the needle by 10 cm and the relative humidity is set at 60 %RH. Based on the hypothesis that the fiber remains liquid during the electrospinning process (slow water evaporation) and thanks to the high air relative humidity, the fluorescent dyes should be able to diffuse to the cells, allowing to stain living and dead bacteria. Then, the fibers are analyzed by epifluorescence **(Figure 3.25)**. Most of the bacteria seems to remain viable after the electrospinning process, 3 dead bacteria are visible for more than 50 living bacteria. Moreover, the superposition of both living and dead bacteria signals to an optical image of the fibers suggests the localization of the bacteria into the fibers. More precisely, it appears that the bacteria are localized into nodules **(Figure 3.25.b)**. This result is confirmed by SEM observation on **Figure 3.26**. The PVA fibers electrospun measures 0.320 ± 0.080 µm in diameter and are randomly looped. Lots of nodules are also visible and patchy dispersed in the fibers mat. These nodules measure 0.920 ± 0.355 µm in diameter for an average length of 2.14 ± 0.36 µm. By considering the thickness of the polymeric walls, these dimensions are more or less similar to the dimensions of a bacillus *S. oneidensis* (1.5-2 µm x 0.5 µm). Moreover, in the rest of the mat, the fibers are regular and do not present equivalent nodules. Based on epifluorescence and SEM results it is possible to conclude that the encapsulation of *S. oneidensis* bacteria into PVA fibers was achieved.

However, for this option to be viable, it will be necessary to crosslink the water-soluble PVA fibers without hindering the diffusion of ions or molecules from or into these fibers. Obtaining PVA hydrogel seems the better option and can be performed by a crosslinking of PVA with STMP (trisodium trimetaphosphate) [270] or glyoxal [271]. Moreover, the fibers need to be electronically conductive in order to ensure electronic transfer to the electron collector. Since carbonization is not possible because of the presence of the cells, addition of carbon suspensions is relevant. In particular including carbon black or CNT [272–274] at the percolation rate (that can be very low for a fiber), electronic conductivity may be obtained.

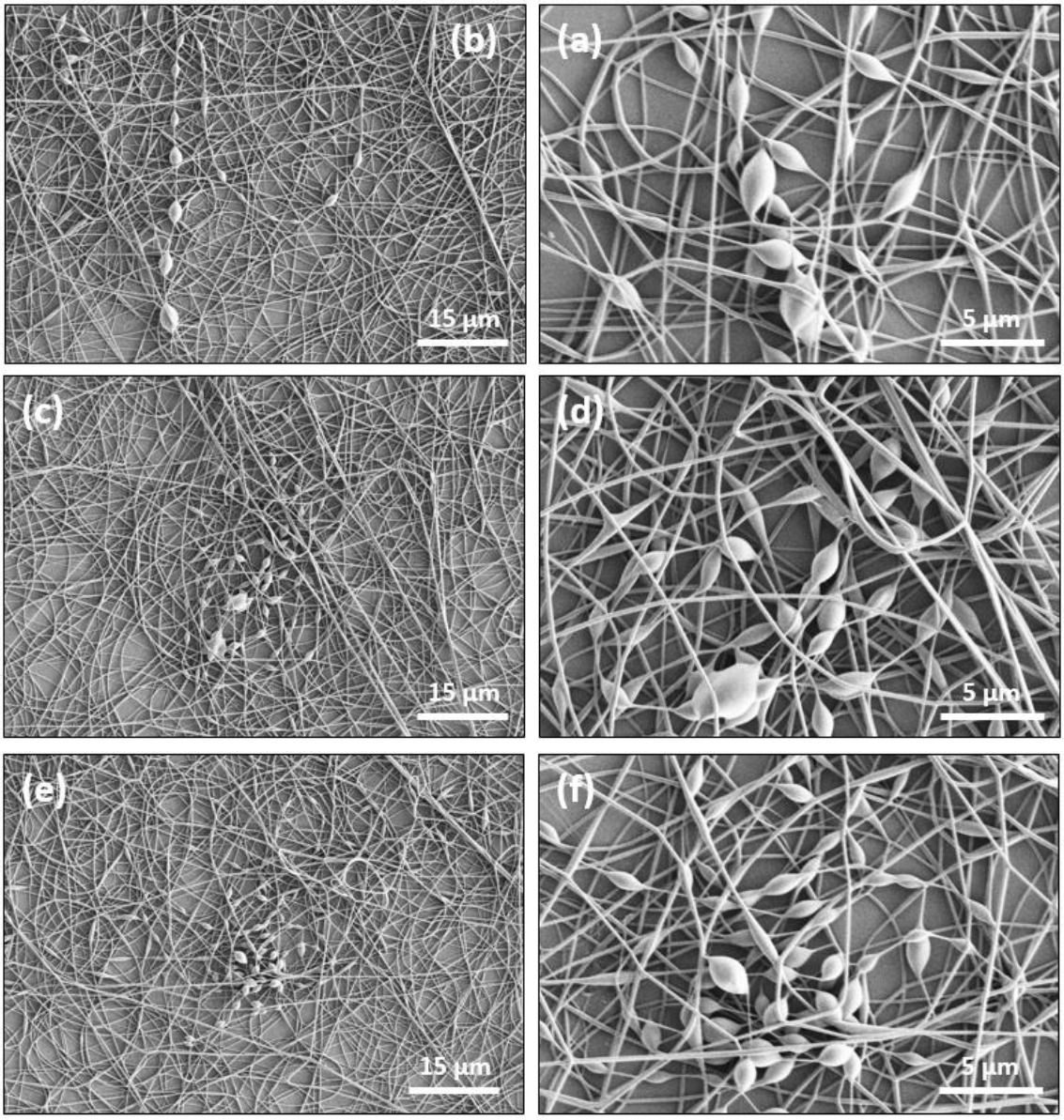

Figure 3.26 – Scanning electron microscopy characterization of PVA fibers including 2 10^9 cfu (bacteria)/mL of polymer solution.

In conclusion, electrospinning of bacteria into a compatible polymer-based fiber is an innovating process to produce an artificial biofilm but needs further work to be viable. In our opinion, a few points must be studied in the next years: (i) a solution must be found to enhance the dispersion of the bacteria in the fibers. The observed heterogeneity may be related to instability caused by bacteria which can be compared to micro-particles. (ii) The polymer must be crosslinked or electrospun into a coaxial system (encapsulation of PVA/bacteria fibers into a sheath made of an insoluble polymer in water. (iii) A cytocompatible pathway must be found to improve electronic conductivities of the polymeric fibers.

GENERAL CONCLUSION AND PERSPECTIVES

GENERAL CONCLUSION & PERSPECTIVES

Microbial Fuel Cell and more generally Microbial Electrochemical Systems are known for several decades. Even if the ability of certain bacterium strains to transfer electron produced by their metabolism of short organic sources to electrodes is quite well-known, better understanding of the complex relation existing between bacteria and electrically-conductive material remains crucial to increase MFC performances and to develop innovative systems. Indeed, in an MFC the external transfer of electrons by a bacterium to a conductive collector appears at the anode and can occur by two main routes: (i) the MET pathways take the benefit of electrochemical mediators to indirectly transfer electron from the bacterium to the anode surface, and ii) the direct pathways take the advantage of membrane-bounded cytochromes or conductive pili that are developed extracellularly to establish connections with other bacteria or with a conductive matrix. Whatever the considered mechanism, the anode colonization has to be encouraged and facilitated the anode colonization in MFC.

Based on this general need of understanding, a global Microbial Fuel Cell device was studied here by focusing on the interactions existing between a specific electro-active bacterium strain and a carbon-based material acting as an anode in order to better understand complex bacterium/anode relation and propose simple and efficient pathways to improve anode colonization and formation of electrically-conductive biofilms. *Shewanella oneidensis* was selected as a bacterium of choice due to its ability to grow and multiply in both aerobic and anaerobic conditions and to transfer electrons by both MET and DET.

This thesis work is based on the hypothesis that bacterial colonization (i.e. adhesion, multiplication and/or biofilm formation) is a key factor in MFC performance, that can be stimulated by different experimental and structural parameters, summarized on the following figure. After developing a protocol of growth for *S. oneidensis* in aerobic conditions, a carbon felt was used as a bio-anode supporting material (chapter 2). Then, bio-anodes were subjected to variations of several experimental parameters: (i) oxygen availability, (ii) bacterial state of growth and (iii) the nature of the electrolyte. Based on previous conclusions, the effect of symmetric polarization of both anode and cathode was evaluated in a range of potential from -0.3 V and +0.5 V vs. Ag/AgCl/KCl. The polarization process was carried out in single- and dual-compartments MFC in unusual aerobic conditions, that are unusual compared to general MFC working conditions. In a second time, the replacement of the biofilm formation under polarization condition was evaluated by the encapsulation of *S. oneidensis* into an artificial biofilm. This biofilm is composed of an inorganic matrix and carbon felt. Finally, structural parameters were demonstrated as particularly efficient to improve both bacterial colonization and MFC performances (part. 2.5.5 & chapter 3).

Experimental MFC working condition, under positive polarisation

Several experiments in single-compartment MFC allow to conclude that ***S. oneidensis* is able to adapt its behavior in order to perform EET under aerobic condition**. This particular

behavior compared to others electroactive bacterium, such as the anaerobic strict *G. sulfurreducens*, is explained by the aero- anaerobic optional growth condition of *S. oneidensis*. Moreover, we demonstrated the beneficial effect of bacterial growth in a medium with at least two acceptors of electrons (oxygen and fumarate). These acceptors allow an acclimation of bacteria to transfer electrons by various reactional pathways. **Two electrochemical behaviors of *S. oneidensis* were demonstrated as function of the bacterial state of growth**. It appears that bacteria harvested in log-phase, and more particularly at the early-end of the log-phase, are able to transfer a high and stable anodic current at the inoculation (around 260 $mA.m^{-2}$ for aerobic condition at OD_{600} = 0.7, E_{we} = +0.3 V). At the opposite, bacteria harvested in stationary phase achieved a slow increase of current from quite 0 to more than 320 $mA.m^{-2}$ (in the same conditions). This difference in explained by the initial metabolism of harvested bacteria. In the stationary phase, bacteria only divide to maintain the number of living bacteria and are more adapted to transfer electron to molecular acceptors. As a consequence, the colonization only occurs by adhesion and oxygen present in solution is preferred to transfer electron. After a time of acclimation (lag-phase), bacteria recover their ability to divide intensively and colonize the surface more actively, by multiplication, in order to perform EET. At the opposite, bacteria in log-phase are already able to colonize the felt fibers by both adhesion and multiplication, resulting in a fast increase of the monitored current. Finally, on longer term MFC working condition, **the change of electrolyte from a specific medium (MR1) to a simple phosphate salt buffer (PBS, pH 7) demonstrated no damageable effect** on the measured current. Moreover, with a bacteria inoculated PBS electrolyte, an overshoot of potential is observed at the inoculation time. This phenomenon was supposed to be related to the absence of riboflavin and to the stress engendered by the increase of salinity.

The polarization appears as the main parameter to influence the colonization of the carbon felt and to increase MFC performances. In single-compartment MFC configuration, both anodic current and electrode colonization are directly correlated to positive polarization (+0.3 and +0.5 V). Under non-polarized condition, a lower and less reproducible current is measured but it remains higher than the current measured under negative polarization at a potential close to the standard potential of lactate oxidation into pyruvate. Based on these results, we demonstrated that the colonization is favored after a short time under positive polarization. However, we also observed an unintended colonization of the counter electrode not only under positive polarization but, more remarkably, under non-polarized condition. This result suggests a synergetic effect of both fixed anode and cathode potentials. To elucidate this phenomenon and prevent the cathode colonization by bacteria, dual-compartments MFC experiments were carried out in the same polarization condition. When only one electrode defined as the anode is polarized at a specific potential (-0.3 V or +0.3 V), the polarization appears more important than the sign of the applied potential. Two behaviors are observed: (i) under positive polarization, MFC performance (polarization and power curves), anodic OCP and MFC OCV are already at their maximal value after a short time of polarization; however, an extended polarization period seems detrimental to MFC performances. The observed biofilm appears thin and dense around the fibers but is not observed in the porosity of the felt. (ii) Under negative polarization, the previous parameters progressively increase to reach their maximal values after more than 20

days. In this condition, the biofilm is thick, porous and progressively fills the porosity of the felt until reaching a stable situation. These two behaviors seem in agreement with the DET/MET hypothesis. At +0.3 V, the electrode colonization is controlled by DET. A dense colonization of the fibers is needed to perform EET at the surface of the fibers. On the contrary, at -0.3 V, the colonization is driven by MET, the whole porosity of the felt can be used to transfer electrons via mediators. DET can also occur but at a lower rate. Both conditions may lead to the formation of a biofilm with an important kinetic time in the whole porosity of the felt. Hypothetically, bacteria into the porosity progressively migrate, or connect to the conductive network and perform MET at the same time. This process is therefore longer than the one observed for "DET driven colonization".

Structural parameters were evaluated by two different pathways.

First, **bacteria were encapsulated in an artificial biofilm composed of a silica gel incorporated in a carbon felt**. Impressive viability of the bacteria was observed. The electrochemical behavior of these matrices revealed to significantly depend on both the composition of silica network and its mechanical strength. In soft silica gels, bacteria viability is over 100% and the intensity of the DET oxidative wave, characteristic to the establishment of a biofilm, increases with time indicating the development of a microbial structure inside the silica gel. No bacteria growth is observed in the MR1-L electrolyte, indicating that integrity of the silica gel is preserved. For an intermediate concentration of silica, the wave of oxidation remains stable and less than 20% loss of viable bacteria is observed. For highest silica concentration, the oxidative wave is hardly observable and an irreversible peak of oxidation is appearing at 0.1 V vs. Ag/AgCl/KCl, indicating the presence of an addition electroactive system. In PBS-L electrolyte, irreversible peaks of oxidation are also visible that are probably related to an increase of the bacterial stress due to the highest medium salinity. Finally, if the gel preserves its integrity, trapped bacteria are non-sensitive to the polarization. However, when the gel breaks (or is intentionally broken), a wave of oxidation is visible that increases with time. This observation confirms the influence and possible benefit of the polarization on the colonization of a conductive matrix by bacteria in solution.

In a second step, **a home-made electrospun carbon paper was synthetized by stabilization and carbonization of mat composed of PAN fibers** with diameters ranging between 100 and 400 µm. This electrode was synthetized to answer the low extent of colonization of the carbon felt (not more than 300 µm in depth). Synthetized fibers are 27 to 50 times thinner than carbon felt fibers and the mat thickness is fixed at 300 µm. As a direct consequence, a bacterium can be supported by at least 3 fibers leading to at least 6 pathways to transfer electrons. The electrode was fully characterized and then used as bio-anode into a MFC. Impressive performances were observed. After only 10 days under working MFC conditions without polarization, the measured current increases by a factor of 10. After only 3 days, MFC performances have reached highest values than a dual-compartments MFC based on carbon felt anode polarized at -0.3 V. At the end of experiment, a large part of the carbon paper surface was colonized by a layer of bacteria and a thick and porous biofilm has grown on the top. Bacteria were observed in both faces of the electrode (in direct contact with the bacterial

electrolyte or with the Nafion® membrane). Based on these first results, the use of electrospun carbon paper seems to be very promising to increase MFC performances, to create innovative architectures and explore alternative processes of colonization.

Perspectives

For general comprehension of the complex interaction existing between the bacterium and electrode, further studies are necessary to confirm some of our hypotheses and to improve our general understanding on how EET is occurring and, especially, how the composition and the structure of the electrode influences bacteria adhesion, multiplication and EET.

(i) **Concerning the oxygen effect** on *S. oneidensis* colonization and EET, it should be interesting to growth bacteria anaerobically and then inject oxygen, and reversely, to check the ability of bacteria to change its behavior as function of rapid environmental modification of oxygenation. Accordingly, it is necessary to perform longer measurements under both anaerobic and aerobic conditions with a better and quantitative control of oxygen to evaluate the critical concentration before which the performances are deteriorated.

(ii) **Concerning the polarization experiment**, we have so far only evaluated conditions where both working and control electrode potentials were fixed at symmetrically opposite potentials (i.e. if the working electrode is set-up at +0.3 V, the counter electrode is fixed at -0.3 V). It would be interesting to apply non-symmetrical differences of potential to evaluate if it is possible to limit the counter electrode colonization by applying a physiologically non-compatible potential. Finally, to evaluate the stability of the bio-anode formed under polarization, it is important to monitor its performance if the polarization is stopped after a defined polarization time.

(iii) **In a general manner**, to gain a better understanding of these systems at the scale of the bacterium (microns to tens of microns) it is necessary to combine various advanced characterizations. SECM (scanning electrochemical microscopy) will be interesting to map the electrical conductivity and electrochemical reactivity of the surface under colonization. One step further, the combination of confocal optical microscopy with electrochemistry and/or SECM measurement would allow to correlate the observation of the biofilm formation and the resulting effects on electrochemical behavior in real time. However, it will be necessary to genetically modify the bacterial strain to obtain a fluorescent strain without altering its EET ability.

Considering the carbon host, our preliminary results open large perspective for the use of electrospinning to design electrodes. In particular, the possibility to encapsulate cells within the fibers and keep them alive constitutes a promising field of research.

Finally, artificial biofilms produced by the aqueous sol-gel route represents a promising system and should allow producing energy and/or depolluting water while avoiding dissemination or contamination by a supplementary bacterium strain. Into an inorganic matrix, the bacteria are supposed to be protected from rough environmental condition. In a first time,

it is important to evaluate the performance and electrochemical behavior of a SiO_2-carbon felt bio-anode in different medium by increasing acidity, basicity or salinity, that are closer to real environmental situations. Then it would be interesting to study whether the capacity of *S. oneidensis* in solution to reduce heavy metals is preserved into the inorganic network. By this way water will be depolluted and reduced metals trapped into the gel for collection and recycling.

Figure Conclusion – Schematic representation of experimental and structural parameters employed to increase MFC performances and to perform a better understanding of bacteria/electrode interaction

References

[1] Srinivansan, *Fuel cells: from Fundamentals to Applications*, **2006**.

[2] T.R. Ralph, *Principles of Fuel Cells*, Platin. Met. Rev. 50 (**2006**) 200–201.

[3] S. Park, Y. Shao, J. Liu, Y. Wang, *Oxygen electrocatalysts for water electrolyzers and reversible fuel cells: status and perspective*, Energy Environ. Sci. 5 (**2012**) 9331–9341.

[4] A. Bocarsly, *Fuel Cells and Hydrogen Storage*, **2011**.

[5] F. Barbir, CHAPTER 4 – Main Cell Components, Materials Properties and Processes, in: PEM Fuel Cells, **2005**: pp. 73–113.

[6] M.C. Potter, *Electrical Effects accompanying the Decomposition of Organic Compounds.*, Proc. Roy. Soc. London Ser. B. 84 (**1911**) 260–275.

[7] R.A. Bullen, T.C. Arnot, J.B. Lakeman, F.C. Walsh, *Biofuel cells and their development*, Biosens. Bioelectron. 21 (**2006**) 2015–2045.

[8] H. Wang, Z.J. Ren, *A comprehensive review of microbial electrochemical systems as a platform technology*, Biotechnol. Adv. 31 (**2013**) 1796–1807.

[9] B.E.. Logan, K. Rabaey, *Conversion of wastes into bioelectricity and chemicals by using microbial electrochemical technologies.*, Science. 337 (**2012**) 686−690.

[10] B.E. Logan, *Exoelectrogenic bacteria that power microbial fuel cells.*, Nat. Rev. Microbiol. 7 (**2009**) 375–81.

[11] J.K. Fredrickson, J.M. Zachara, *Electron transfer at the microbe-mineral interface: a grand challenge in biogeochemistry.*, Geobiology. 6 (**2008**) 245–53.

[12] J. Larminie, A. Dicks, *Fuel Cell Systems Explained Second Edition*, **2003**.

[13] J.O. Besenhard, *Materials, Handbook of battery*, **2008**.

[14] D. Linden, *Handbook of batteries and fuel cells*, **1984**.

[15] M.L. Perry, T.F. Fuller, *A Historical Perspective of Fuel Cell Technology in the 20th Century*, J. Electrochem. Soc. 149 (**2002**) 59–67.

[16] A.J. Appleby, *From Sir William Grove to today: fuel cells and the future*, J. Power Sources. 29 (**1990**) 3–11.

[17] F.T. Bacon, *Fuel cells, past, present and future*, Electrochim. Acta. 14 (**1969**) 569–585.

[18] E. Ivers-Tiffée, A. Weber, D. Herbstritt, *Materials and technologies for SOFC-components*, J. Eur. Ceram. Soc. 21 (**2001**) 1805–1811.

[19] S. Park, Y. Shao, J. Liu, Y. Wang, *Oxygen electrocatalysts for water electrolyzers and reversible fuel cells: status and perspective*, Energy Environ. Sci. 5 (**2012**) 9331–9341.

[20] L.B. Wingard, C.H. Shaw, J.F. Castner, *Bioelectrochemical fuel cells*, (**1982**).

[21] A.K. Shukla, P. Suresh, S. Berchmans, A. Rajendran, *Biological fuel cells and their applications*, Curr. Sci. 87 (**2004**) 455–468.

[22] C.F. Blanford, R.S. Heath, F. a Armstrong, *A stable electrode for high-potential, electrocatalytic O(2) reduction based on rational attachment of a blue copper oxidase to a graphite surface.*, Chem. Commun. (**2007**) 1710–1712.

[23] M.A. Alonso-Lomillo, O. Rüdiger, A. Maroto-Valiente, M. Velez, I. Rodr'iguez-Ramos, F.J. Muñoz, V.M. Fernández, A.L. De Lacey, *Hydrogenase-Coated Carbon Nanotubes for*

Efficient {H}_2 Oxidation, Nano Lett. 7 (**2007**) 1603–1608.

[24] Y. Degani, a Heller, *Direct Electrical Communication between Chemically Modified Enzymes and Metal Electrodes*, J. Phys. Chem. 91 (**1987**) 1287–9.

[25] S. Cosnier, *Biomolecule immobilization on electrode surfaces by entrapment or attachment to electrochemically polymerized films. A review*, Biosens. Bioelectron. 14 (**1999**) 443–456.

[26] L. Murphy, *Biosensors and bioelectrochemistry*, Curr. Opin. Chem. Biol. 10 (**2006**) 177–184.

[27] D. Grieshaber, R. MacKenzie, J. Vörös, E. Reimhult, *Electrochemical Biosensors - Sensor Principles and Architectures*, Sensors. 8 (**2008**) 1400–1458.

[28] A. Heller, *Miniature biofuel cells*, Phys. C Hem. Chem. Phys. 6 (**2004**) 209–216.

[29] E. Katz, I. Willner, A.B. Kotlyar, *A non-compartmentalized glucose O2 biofuel cell by bioengineered electrode surfaces*, J. Electroanal. Chem. 479 (**1999**) 64–68.

[30] N. Mano, F. Mao, A. Heller, *A miniature biofuel cell operating in a physiological buffer*, J. Am. Chem. Soc. 124 (**2002**) 12962–12963.

[31] N. Mano, F. Mao, A. Heller, *Characteristics of a Miniature Compartment-less Glucose-O2 Biofuel Cell and Its Operation in a Living Plant*, J. Am. Chem. Soc. J. Phys. Chem. B. 124 (**2002**) 6480–8842.

[32] I. Ivanov, T. Vidakovic-Koch, K. Sundmacher, *Recent advances in enzymatic fuel cells: Experiments and modeling*, Energies. 3 (**2010**) 803–846.

[33] D. Leech, P. Kavanagh, W. Schuhmann, *Enzymatic fuel cells: Recent progress*, Electrochim. Acta. 84 (**2012**) 223–234.

[34] Y. Kamitaka, S. Tsujimura, N. Setoyama, T. Kajinob, K. Kano, *Fructose/dioxygen biofuel cell based on direct electron transfer-type bioelectrocatalysis*, Phys. Chem. Chem. Phys. 9 (**2007**) 1793–1801.

[35] W. Gellett, M. Kesmez, J. Schumacher, N. Akers, S.D. Minteer, *Biofuel Cells for Portable Power*, Electroanalysis. 22 (**2010**) 727–731.

[36] P. Cinquin, C. Gondran, F. Giroud, S. Mazabrard, A. Pellissier, F. Boucher, J.-P. Alcaraz, K. Gorgy, F. Lenouvel, S. Phane Mathé, P. Porcu, S. Cosnier, R. Haverkamp, *A Glucose BioFuel Cell Implanted in Rats*, Glucose BioFuel Cell Implant. Rats. PLoS ONE. 5 (**2010**) 1–7.

[37] S. Cosnier, A. Le Goff, M. Holzinger, *Towards glucose biofuel cells implanted in human body for powering artificial organs: Review*, Electrochem. Commun. 38 (**2014**) 19–23.

[38] A. Heller, *Potentially implantable miniature batteries*, Anal. Bioanal. Chem. 385 (**2006**) 469–473.

[39] S.R. Higgins, C. Lau, P. Atanassov, S.D. Minteer, M.J. Cooney, *Hybrid Biofuel Cell : Microbial Fuel Cell with an Enzymatic*, ACS Catal. 1 (**2011**) 994–997.

[40] K. Lewis, *Symposium on Bioelectrochemistry of Microorganisms, IV. Biochemical Fuel Cells*, Bacteriol. Rev. 30 (**1966**) 101–113.

[41] H.J.K. Byung Hong Kim, Doo Hyun Park, Pyung Kyun Shin, In Seop Chang, Mediator-less biofuel cell, US 5976719 A, **1997**.

[42] B.H. Kim, H.S. Park, H.J. Kim, G.T. Kim, I.S. Chang, J. Lee, N.T. Phung, *Enrichment of microbial community generating electricity using a fuel-cell-type electrochemical cell*, Appl Microbiol Biotechnol. 63 (**2004**) 672–681.

[43] H.J. Kim, H.S. Park, M.S. Hyun, I.S. Chang, M. Kim, B.H. Kim, *A mediator-less microbial fuel*

cell using a metal reducing bacterium, Shewanella putrefaciens, Enzyme Microb. Technol. 30 (**2002**) 145–152.

[44] K. Rabaey, N. Boon, M. Höfte, W. Verstraete, *Microbial Phenazine Production Enhances Electron Transfer in Biofuel Cells*, Environ. Sci. Technol. 39 (**2005**) 3401–3408.

[45] K. Rabaey, N. Boon, S.D. Siciliano, M. Verhaege, W. Verstraete, *Biofuel Cells Select for Microbial Consortia That Self-Mediate Electron Transfer*, Appl. Environ. Microbiol. 70 (**2004**) 5373–5382.

[46] I. Shizas, D.M. Bagley, *Experimental Determination of Energy Content of Unknown Organics in Municipal Wastewater Streams*, J. Energy Eng. 130 (**2004**) 45–53.

[47] Y. Ahn, B.E. Logan, *Altering Anode Thickness To Improve Power Production in Microbial Fuel Cells with Different Electrode Distances*, Energy Fuels. 27 (**2012**) 271–276.

[48] R.A. Rozendal, H.V.M. Hamelers, K. Rabaey, J. Keller, C.J.N. Buisman, *Towards practical implementation of bioelectrochemical wastewater treatment*, Trends Biotechnol. 26 (**2008**) 450–459.

[49] L. Huang, S. Cheng, G. Chen, *Bioelectrochemical systems for efficient recalcitrant wastes treatment*, J. Chem. Technol. Biotechnol. 86 (**2011**) 481–491.

[50] H. Liu, R. Ramnarayanan, B.E. Logan, *Production of Electricity during Wastewater Treatment Using a Single Chamber Microbial Fuel Cell*, Environ. Sci. Technol. 38 (**2004**) 2281–2285.

[51] Z. He, F. Zhang, Z. Ge, *Using Microbial Fuel Cells to Treat Raw Sludge and Primary Effluent for Bioelectricity Generation : Final Report*, **2013**.

[52] I.A. Ieropoulos, P. Ledezma, A. Stinchcombe, G. Papaharalabos, C. Melhuish, J. Greenman, *Waste to real energy: the first MFC powered mobile phone*, Phys. Chem. Chem. Phys. 15 (**2013**) 15312–15316.

[53] I. Ieropoulos, C. Melhuish, J. Greenman, I. Horsfield, *EcoBot-II: An artificial agent with a natural metabolism*, J. Adv. Rob. Sys. 2 (**2005**) 295–300.

[54] I. Ieropoulos, J. Greenman, C. Melhuish, I. Horsfield, EcoBot-III: a robot with guts, in: Proc. Alife XII, **2010**: pp. 733–740.

[55] J.M. Tront, A.J.D. Fortner, A.M. Plötze, A.J.B. Hughes, A.A.M. Puzrin, *Microbial fuel cell technology for measurement of microbial respiration of lactate as an example of bioremediation amendment*, Biotechnol. Lett. 30 (**2008**) 1385–1390.

[56] M. Estevez-Canales, A. Berná, Z. Borjas, A. Esteve-Núñez, *Screen-printed electrodes: New tools for developing microbial electrochemistry at microscale level*, Energies. 8 (**2015**) 13211–13221.

[57] J.M. Morris, S. Jin, B. Crimi, A. Pruden, *Microbial fuel cell in enhancing anaerobic biodegradation of diesel*, Chem. Eng. J. 146 (**2009**) 161–167.

[58] J.M. Morris, S. Jin, *Feasibility of using microbial fuel cell technology for bioremediation of hydrocarbons in groundwater.*, J. Environ. Sci. Health. A. Tox. Hazard. Subst. Environ. Eng. 43 (**2008**) 18–23.

[59] H. Guha, K. Jayachandran, F. Maurrasse, *Kinetics of chromium (VI) reduction by a type strain Shewanella alga under different growth conditions*, Environ. Pollut. 115 (**2001**) 209–218.

[60] K.S. Jacobson, D.M. Drew, Z. He, *Use of a Liter-Scale Microbial Desalination Cell As a Platform to Study Bioelectrochemical Desalination with Salt Solution or Artificial Seawater*, Environ. Sci. Technol. 45 (**2011**) 4652–4657.

[61] H. Luo, P.E. Jenkins, Z. Ren, *Concurrent Desalination and Hydrogen Generation Using Microbial Electrolysis and Desalination Cells*, Environ. Sci. Technol. 45 (**2011**) 340–344.

[62] K.S. Jacobson, D.M. Drew, Z. He, *Efficient salt removal in a continuously operated upflow microbial desalination cell with an air cathode*, Bioresour. Technol. 102 (**2011**) 376–380.

[63] K.P. Nevin, T.L. Woodard, A.E. Franks, Z.M. Summers, D.R. Lovley, *Microbial electrosynthesis: feeding microbes electricity to convert carbon dioxide and water to multicarbon extracellular organic compounds.*, MBio. 1 (**2010**) 1–4.

[64] K.B. Gregory, D.R. Bond, D.R. Lovley, *Graphite electrodes as electron donors for anaerobic respiration*, Environ. Microbiol. 6 (**2004**) 596–604.

[65] X. Cao, X. Huang, P. Liang, N. Boon, M. Fan, L. Zhang, X. Zhang, *A completely anoxic microbial fuel cell using a photo-biocathode for cathodic carbon dioxide reduction*, Energy Environ. Sci. 2 (**2009**) 498–501.

[66] B.E. Logan, *Microbial fuel cells*, Wiley-Interscience, **2008**.

[67] K. Rabaey, W. Verstraete, *Microbial fuel cells: novel biotechnology for energy generation*, Trends Biotechnol. 23 (**2005**) 291–298.

[68] B.E. Logan, B. Hamelers, R. Rozendal, U. Schröder, J. Keller, S. Freguia, P. Aelterman, W. Verstraete, K. Rabaey, *Microbial Fuel Cells: Methodology and Technology*, Environ. Sci. Technol. 40 (**2006**) 5181–5192.

[69] D.R. Bond, D.R. Lovley, *Electricity Production by Geobacter sulfurreducens Attached to Electrodes*, Appl. Environ. Microbiol. 69 (**2003**) 1548–1555.

[70] D.H. Park, M. Laivenieks, M. V Guettler, M.K. Jain, J.G. Zeikus, *Microbial utilization of electrically reduced neutral red as the sole electron donor for growth and metabolite production.*, Appl. Environ. Microbiol. 65 (**1999**) 2912–7.

[71] J.B. McKinlay, J.G. Zeikus, *Extracellular Iron Reduction Is Mediated in Part by Neutral Red and Hydrogenase in Escherichia coli*, Appl. Environ. Microbiol. 70 (**2004**) 3467–3474.

[72] U. Schröder, *Anodic electron transfer mechanisms in microbial fuel cells and their energy efficiency*, Phys. Chem. Chem. Phys. 9 (**2007**) 2619–2629.

[73] M. Adachi, T. Shimomura, M. Komatsu, H. Yakuwa, A. Miya, *A novel mediator–polymer-modified anode for microbial fuel cells*, Chem. Commun. (**2008**) 2055.

[74] J.C. Thrash, J.D. Coates, *Review: Direct and Indirect Electrical Stimulation of Microbial Metabolism*, Environ. Sci. Technol. 42 (**2008**) 3921–3931.

[75] K. Rabaey, J. Rodríguez, L.L. Blackall, J. Keller, P. Gross, D. Batstone, W. Verstraete, K.H. Nealson, *Microbial ecology meets electrochemistry: electricity-driven and driving communities.*, ISME J. 1 (**2007**) 9–18.

[76] K. Rabaey, G. Lissens, S.D. Siciliano, W. Verstraete, *A microbial fuel cell capable of converting glucose to electricity at high rate and efficiency*, Biotechnol. Lett. 25 (**2003**) 1531–1535.

[77] E. Marsili, D.B. Baron, I.D. Shikhare, D. Coursolle, J. Gralnick, D.R. Bond, *Shewanella secretes flavins that mediate extracellular electron transfer.*, Proc. Natl. Acad. Sci. U. S. A. 105 (**2008**) 3968–73.

[78] H. von Canstein, J. Ogawa, S. Shimizu, J.R. Lloyd, *Secretion of flavins by Shewanella species and their role in extracellular electron transfer.*, Appl. Environ. Microbiol. 74 (**2008**) 615–23.

[79] V.B. Wang, N.D. Kirchhofer, X. Chen, M.Y.L. Tan, K. Sivakumar, B. Cao, Q. Zhang, S. Kjelleberg, G.C. Bazan, S.C.J. Loo, E. Marsili, *Comparison of flavins and a conjugated*

oligoelectrolyte in stimulating extracellular electron transport from Shewanella oneidensis MR-1, Electrochem. Commun. 41 (**2014**) 55–58.

[80] L. Shi, T.C. Squier, J.M. Zachara, J.K. Fredrickson, *Respiration of metal (hydr)oxides by Shewanella and Geobacter: a key role for multihaem c-type cytochromes*, Mol. Microbiol. 65 (**2007**) 12–20.

[81] J.M. Myers, C.R. Myers, *Role of the tetraheme cytochrome CymA in anaerobic electron transport in cells of Shewanella putrefaciens MR-1 with normal levels of menaquinone*, J. Bacteriol. 182 (**2000**) 67–75.

[82] J.M. Myers, C.R. Myers, *Role for Outer Membrane Cytochromes OmcA and OmcB of Shewanella putrefaciens MR-1 in Reduction of Manganese Dioxide*, Appl. Environ. Microbiol. 67 (**2001**) 260–269.

[83] Y.A. Gorby, S. Yanina, J.S. McLean, K.M. Rosso, D. Moyles, A. Dohnalkova, T.J. Beveridge, I. Seop Chang, B. Hong Kim, K. Shik Kim, D.E. Culley, S.B. Reed, M.F. Romine, D.A. Saffarini ţ, E.A. Hill, L. Shi, D.A. Elias, D.W. Kennedy, G. Pinchuk, K. Watanabe, I. Ishii, B. Logan, K.H. Nealson, J.K. Fredrickson, *Electrically conductive bacterial nanowires produced by Shewanella oneidensis strain MR-1 and other microorganisms*, PNAS. 103 (**2006**) 11358–11363.

[84] M.Y. El-Naggar, G. Wanger, K.M. Leung, T.D. Yuzvinsky, G. Southam, J. Yang, W.M. Lau, K.H. Nealson, Y. a Gorby, *Electrical transport along bacterial nanowires from Shewanella oneidensis MR-1.*, Proc. Natl. Acad. Sci. U.S.A. 107 (**2010**) 18127–18131.

[85] R.M. Snider, S.M. Strycharz-Glaven, S.D. Tsoi, J.S. Erickson, L.M. Tender, *Long-range electron transport in Geobacter sulfurreducens biofilms is redox gradient-driven*, PNAS. 109 (**2012**) 15467–15472.

[86] N. Malvankar, Madelinevargas, K. Nevin, A. Franks, B.-C. Kengoinoue, S. Tündemester, J. Covalla, V. Johnson, M. Rotello, Tuominen, Lovley, *Tunablemetallic-likeconductivityinmicrobial nanowirenetworks*, Nat. Nanotechnol. 6 (**2011**) 573–579.

[87] N.S. Malvankar, M. Vargas, K. Nevin, P. Tremblay, K. Evans-lutterodt, D. Nykypanchuk, *Structural Basis for Metallic-Like Conductivity in Microbial Nanowires*, 6 (**2015**) 1–10.

[88] P.S. Bonanni, D. Massazza, J.P. Busalmen, *Stepping stones in the electron transport from cells to electrodes in Geobacter sulfurreducens biofilms.*, Phys. Chem. Chem. Phys. 15 (**2013**) 10300–10306.

[89] N.S. Malvankar, D.R. Lovley, *Microbial Nanowires: A New Paradigm for Biological Electron Transfer and Bioelectronics*, ChemSusChem. 5 (**2012**) 1039–1046.

[90] B.E. Logan, J.M. Regan, *Electricity-producing bacterial communities in microbial fuel cells.*, Trends Microbiol. 14 (**2006**) 512–520.

[91] O. Monzon, Y. Yang, Q. Li, P.J.J. Alvarez, *Quorum sensing autoinducers enhance biofilm formation and power production in a hypersaline microbial fuel cell*, Biochem. Eng. J. 109 (**2016**) 222–227.

[92] O. Bretschger, a. Obraztsova, C. a. Sturm, I.S. Chang, Y. a. Gorby, S.B. Reed, D.E. Culley, C.L. Reardon, S. Barua, M.F. Romine, J. Zhou, a. S. Beliaev, R. Bouhenni, D. Saffarini, F. Mansfeld, B.-H. Kim, J.K. Fredrickson, K.H. Nealson, *Current Production and Metal Oxide Reduction by Shewanella oneidensis MR-1 Wild Type and Mutants*, Appl. Environ. Microbiol. 74 (**2008**) 553–553.

[93] S. Ishii, K. Watanabe, S. Yabuki, B.E. Logan, Y. Sekiguchi, *Comparison of Electrode Reduction Activities of Geobacter sulfurreducens and an Enriched Consortium in an Air-Cathode Microbial Fuel Cell*, Appl. Environ. Microbiol. 74 (**2008**) 7348–7355.

[94] K.P. Nevin, H. Richter, S.F. Covalla, J.P. Johnson, T.L. Woodard, A.L. Orloff, H. Jia, M. Zhang, D.R. Lovley, *Power output and columbic efficiencies from biofilms of Geobacter sulfurreducens comparable to mixed community microbial fuel cells*, Environ. Microbiol. 10 (**2008**) 2505–2514.

[95] P. Parameswaran, C.I. Torres, H.-S. Lee, R. Krajmalnik-Brown, B.E. Rittmann, *Syntrophic interactions among anode respiring bacteria (ARB) and Non-ARB in a biofilm anode: electron balances*, Biotechnol. Bioeng. 103 (**2009**) 513–523.

[96] R.M. Donlan, *Biofilms: Microbial Life on Surfaces*, Emerg. Infect. Dis. 8 (**2002**) 881–890.

[97] M. Allesen-Holm, K.B. Barken, L. Yang, M. Klausen, J.S. Webb, S. Kjelleberg, S. Molin, M. Givskov, T. Tolker-Nielsen, *A characterization of DNA release in Pseudomonas aeruginosa cultures and biofilms*, Mol. Microbiol. 59 (**2006**) 1114–1128.

[98] Y. Jiao, G.D. Cody, A.K. Harding, P. Wilmes, M. Schrenk, K.E. Wheeler, J.F. Banfield, M.P. Thelen, *Characterization of extracellular polymeric substances from acidophilic microbial biofilms.*, Appl. Environ. Microbiol. 76 (**2010**) 2916–2938.

[99] B. Cao, L. Shi, R.N. Brown, Y. Xiong, J.K. Fredrickson, M.F. Romine, M.J. Marshall, M.S. Lipton, H. Beyenal, *Extracellular polymeric substances from Shewanella sp. HRCR-1 biofilms: characterization by infrared spectroscopy and proteomics.*, Environ. Microbiol. 13 (**2011**) 1018–1049.

[100] A.P. Borole, G. Reguera, B. Ringeisen, Z.-W. Wang, Y. Feng, B. Hong, K. De, *Electroactive biofilms: Current status and future research needs*, Energy Environ. Sci. 4 (**2011**) 4813–4834.

[101] C. Matz, Competition, Communication, Cooperation: Molecular Crosstalk in Multi-species Biofilms, in: Springer Berlin Heidelberg, **2011**: pp. 29–40.

[102] J.C. Biffinger, J. Pietron, R. Ray, B. Little, B.R. Ringeisen, N. -Lincoln Biffinger, *A biofilm enhanced miniature microbial fuel cell using Shewanella oneidensis DSP10 and oxygen reduction cathodes*, Biosens. Bioelectron. 22 (**2007**) 1672–1679.

[103] G. Reguera, K.P. Nevin, J.S. Nicoll, S.F. Covalla, T.L. Woodard, D.R. Lovley, *Biofilm and nanowire production leads to increased current in Geobacter sulfurreducens fuel cells.*, Appl. Environ. Microbiol. 72 (**2006**) 7345–7353.

[104] D.R. Bond, S.M. Strycharz-Glaven, L.M. Tender, C.I. Torres, *On Electron Transport through Geobacter Biofilms*, ChemSusChem. 5 (**2012**) 1099–1105.

[105] C.I. Torres, A. Kato Marcus, B.E. Rittmann, *Proton transport inside the biofilm limits electrical current generation by anode-respiring bacteria*, Biotechnol. Bioeng. 100 (**2008**) 872–881.

[106] K.R. Suzanne T Read, Paritam Dutta, Phillip L Bond, Jürg Keller, *Initial development and structure of biofilms on microbial fuel cell anodes*, BMC Microbiol. 10 (**2010**) 98 (1–10).

[107] F. Zhao, R.C.T. Slade, J.R. Varcoe, *Techniques for the study and development of microbial fuel cells: an electrochemical perspective.*, Chem. Soc. Rev. 38 (**2009**) 1926–1939.

[108] J.H. Hirschenhofer, D.B. Stauffer, R.R. Engleman, M.G. Klett, *Fuel Cell Handbook Fuel Cell Handbook*, **1998**.

[109] M. Aghababaie, M. Farhadian, A. Jeihanipour, D. Biria, *Effective factors on the performance of microbial fuel cells in wastewater treatment – a review*, Environ. Technol. Rev. 2515 (**2015**) 1–19.

[110] K. Brenner, L. You, F.H. Arnold, *Engineering microbial consortia: a new frontier in synthetic biology*, Trend. 26 (**2008**) 483–489.

[111] *Production of Electricity from Acetate or Butyrate Using a Single-Chamber Microbial Fuel Cell*, Environ. Sci. Technol. 39 (**2005**) 658–662.

[112] H.-S. Lee, P. Parameswaran, A. Kato-Marcus, C.I. Torres, B.E. Rittmann, *Evaluation of energy-conversion efficiencies in microbial fuel cells (MFCs) utilizing fermentable and non-fermentable substrates*, Water Reasearch. 42 (**2008**) 1501–1510.

[113] A.M. Speers, G. Reguera, *Electron Donors Supporting Growth and Electroactivity of Geobacter sulfurreducens Anode Biofilms*, App. 78 (**2012**) 437–444.

[114] D. Jiang, B. Li, *Granular activated carbon single - chamber microbial fuel cells (GAC - SCMFCs): A design suitable for large - scale wastewater treatment processes*, Biochem. Eng. J. 47 (**2009**) 31–37.

[115] Y. Zuo, S. Cheng, D. Call, B.E. Logan, *Tubular membrane cathodes for scalable power generation in microbial fuel cells*, Environ. Sci. Technol. 41 (**2007**) 3347–3353.

[116] H. Wang, Z. Wu, A. Plaseied, P. Jenkins, L. Simpson, C. Engtrakul, Z. Ren, *Carbon nanotube modified air-cathodes for electricity production in microbial fuel cells*, J. Power Sources. 196 (**2011**) 7465–7469.

[117] C.E. Reimers, P. Girguis, H.A. Stecher, L.M. Tender, N. Ryckelynck, P. Whaling, *Microbial fuel cell energy from an ocan cold seep*, Geobiology. 4 (**2006**) 123–136.

[118] S.K. Chaudhuri, D.R. Lovley, *Electricity generation by direct oxidation of glucose in mediatorless microbial fuel cells*, Nat. Biotechnol. 21 (**2003**) 1229–1232.

[119] A. ter Heijne, H.V.M. Hamelers, M. Saakes, C.J.N. Buisman, *Performance of non-porous graphite and titanium-based anodes in microbial fuel cells*, Electrochim. Acta. 53 (**2008**) 5697–5703.

[120] L.M. Tender, C.E. Reimers, H.A. Stecher Iii, D.E. Holmes, D.R. Bond, D.A. Lowy, K. Pilobello, S.J. Fertig, D.R. Lovley, *Harnessing microbially generated power on the seafloor*, Nat. Biotechnol. 20 (**2002**) 821–826.

[121] J. Wei, P. Liang, X. Huang, *Recent progress in electrodes for microbial fuel cells*, Bioresour. Technol. 102 (**2011**) 9335–9344.

[122] M. Zhou, M. Chi, J. Luo, H. He, T. Jin, *An overview of electrode materials in microbial fuel cells*, J. Power Sources. 196 (**2011**) 4427–4435.

[123] J. Heilmann, B.E. Logan, *Production of electricity from proteins using a microbial fuel cell.*, Water Environ. Res. 78 (**2006**) 531–538.

[124] C. Santoro, M. Guilizzoni, J.P. Correa Baena, U. Pasaogullari, A. Casalegno, B. Li, S. Babanova, K. Artyushkova, P. Atanassov, *The effects of carbon electrode surface properties on bacteria attachment and start up time of microbial fuel cells*, Carbon N. Y. 67 (**2014**) 128–139.

[125] F. Li, Y. Sharma, Y. Lei, B. Li, Q. Zhou, *Microbial fuel cells: The effects of configurations, electrolyte solutions, and electrode materials on power generation*, Appl. Biochem. Biotechnol. 160 (**2010**) 168–181.

[126] I. Ieropoulos, J. Greenman, C. Melhuish, *Improved energy output levels from small-scale Microbial Fuel Cells*, Bioelectrochemistry. 78 (**2010**) 44–50.

[127] P. Aelterman, M. Versichele, M. Marzorati, N. Boon, W. Verstraete, *Loading rate and external resistance control the electricity generation of microbial fuel cells with different three-dimensional anodes*, Bioresour. Technol. 99 (**2008**) 8895–8902.

[128] P. Aelterman, K. Rabaey, P. Clauwaert, W. Verstraete, *Microbial fuel cells for wastewater treatment*, Water Sci. Technol. 54 (**2006**) 1–9.

[129] K. Rabaey, K. Van De Sompel, L. Maignien, N. Boon, P. Aelterman, P. Clauwaert, L. De Schamphelaire, H.T. Pham, J. Vermeulen, M. Verhaege, P. Lens, W. Verstraete, *Microbial fuel cells for sulfide removal*, Environ. Sci. Technol. 40 (**2006**) 5218–5224.

[130] A. Deeke, T.H.J.A. Sleutels, T.F.W. Donkers, H.V.M. Hamelers, C.J.N. Buisman, A. Ter Heijne, *Fluidized capacitive bioanode as a novel reactor concept for the microbial fuel cell*, Environ. Sci. Technol. 49 (**2015**) 1929–1935.

[131] B. Logan, S. Cheng, V. Watson, G. Estadt, *Graphite Fiber Brush Anodes for Increased Power Production in Air-Cathode Microbial Fuel Cells*, Environ. Sci. Technol. 41 (**2007**) 3341–3346.

[132] J.C. Biffinger, R. Ray, B. Little, B.R. Ringeisen, *Diversifying biological fuel cell designs by use of nanoporous filters*, Environ. Sci. Technol. 41 (**2007**) 1444–1449.

[133] B. Le Ouay, T. Coradin, C. Laberty-Robert, *Silica–carbon hydrogels as cytocompatible bioelectrodes*, J. Mater. Chem. B. 1 (**2013**) 606–609.

[134] A. Jain, J. Connolly, *Extracellular electron transfer mechanism in Shewanella loihica PV-4 biofilms formed at indium tin oxide and graphite electrodes*, Int. J. Electrochem. Sci. 8 (**2013**) 1778–1793.

[135] H. Wang, R. Côté, G. Faubert, D. Guay, J.P. Dodelet, *Effect of the Pre-Treatment of Carbon Black Supports on the Activity of Fe-Based Electrocatalysts for the Reduction of Oxygen*, J. Phys. Chem. B. 103 (**1999**) 2042–2049.

[136] Y. Feng, Q. Yang, X. Wang, B.E. Logan, *Treatment of carbon fiber brush anodes for improving power generation in air-cathode microbial fuel cells*, J. Power Sources. 195 (**2010**) 1841–1844.

[137] S. Cheng, B.E. Logan, *Ammonia treatment of carbon cloth anodes to enhance power generation of microbial fuel cells*, Electrochem. Commun. 9 (**2007**) 492–496.

[138] S.B. Velasquez-Orta, T.P. Curtis, B.E. Logan, *Energy from algae using microbial fuel cells*, Biotechnol. Bioeng. 103 (**2009**) 1068–1076.

[139] D.A. Lowy, L.M. Tender, J.G. Zeikus, D.H. Park, D.R. Lovley, *Harvesting energy from the marine sediment-water interface II. Kinetic activity of anode materials*, Biosens. Bioelectron. 21 (**2006**) 2058–2063.

[140] L. Peng, S.-J. You, J.-Y. Wang, *Carbon nanotubes as electrode modifier promoting direct electron transfer from Shewanella oneidensis*, **2010**.

[141] J.J. Sun, H.Z. Zhao, Q.Z. Yang, J. Song, A. Xue, *A novel layer-by-layer self-assembled carbon nanotube-based anode: Preparation, characterization, and application in microbial fuel cell*, Electrochim. Acta. 55 (**2010**) 3041–3047.

[142] Y. Zhang, G. Mo, X. Li, W. Zhang, J. Zhang, J. Ye, X. Huang, C. Yu, *A graphene modified anode to improve the performance of microbial fuel cells*, J. Power Sources. 196 (**2011**) 5402–5407.

[143] U. Schröder, J. Nießen, F. Scholz, *A generation of microbial fuel cells with current outputs boosted by more than one order of magnitude*, Angew. Chemie - Int. Ed. 42 (**2003**) 2880–2883.

[144] K. Scott, G.A. Rimbu, K.P. Katuri, K.K. Prasad, I.M. Head, *Application of Modified Carbon Anodes in Microbial Fuel Cells*, Process Saf. Environ. Prot. 85 (**2007**) 481–488.

[145] J. Niessen, U. Schröder, M. Rosenbaum, F. Scholz, *Fluorinated polyanilines as superior materials for electrocatalytic anodes in bacterial fuel cells*, Electrochem. Commun. 6 (**2004**) 571–575.

[146] L. Huang, X. Li, Y. Ren, X. Wang, *In-situ modified carbon cloth with polyaniline/graphene as anode to enhance performance of microbial fuel cell*, Int. J. Hydrogen Energy. 41 (**2016**) 11369–11379.

[147] Y. Qiao, C.M. Li, S.-J. Bao, Q.-L. Bao, *Carbon nanotube/polyaniline composite as anode material for microbial fuel cells*, J. Power Sources. 170 (**2007**) 79–84.

[148] X. Xie, L. Hu, M. Pasta, G.F. Wells, D. Kong, C.S. Criddle, Y. Cui, *Three-dimensional carbon nanotube-textile anode for high-performance microbial fuel cells*, Nano Lett. 11 (**2011**) 291–296.

[149] X. Xie, G. Yu, N. Liu, Z. Bao, C.S. Criddle, Y. Cui, *Graphene–sponges as high-performance low-cost anodes for microbial fuel cells*, Energy Environ. Sci. 5 (**2012**) 6862–6866.

[150] S. Inoue, E.A. Parra, A. Higa, Y. Jiang, P. Wang, C.R. Buie, J.D. Coates, L. Lin, *Sensors and Actuators A : Physical Structural optimization of contact electrodes in microbial fuel cells for current density enhancements*, Sensors Actuators A. Phys. 177 (**2012**) 30–36.

[151] H. Richter, K. McCarthy, K.P. Nevin, J.P. Johnson, V.M. Rotello, D.R. Lovley, *Electricity generation by Geobacter sulfurreducens attached to gold electrodes*, Langmuir. 24 (**2008**) 4376–4379.

[152] S.R. Crittenden, C.J. Sund, J.J. Sumner, *Letter Mediating Electron Transfer from Bacteria to a Gold Electrode via a Self-Assembled Monolayer Mediating Electron Transfer from Bacteria to a Gold Electrode via a Self-Assembled Monolayer*, Society. 17 (**2006**) 9473–9476.

[153] D. Pocaznoi, A. Calmet, L. Etcheverry, B. Erable, A. Bergel, *Stainless steel is a promising electrode material for anodes of microbial fuel cells*, Energy Environ. Sci. 5 (**2012**) 9645–9653.

[154] C. Dumas, R. Basseguy, A. Bergel, *Electrochemical activity of Geobacter sulfurreducens biofilms on stainless steel anodes*, Electrochim. Acta. 53 (**2008**) 5235–5241.

[155] J. Champavert, S. Ben Rejeb, C. Innocent, M. Pontié, *Microbial fuel cell based on Ni-tetra sulfonated phthalocyanine cathode and graphene modified bioanode*, J. Electroanal. Chem. 757 (**2015**) 270–276.

[156] D. Park, J. Zeikus, *Impact of electrode composition on electricity generation in a single-compartment fuel cell using Shewanella putrefaciens*, Appl. Microbiol. Biotechnol. 59 (**2002**) 58–61.

[157] D.H. Park, J.G. Zeikus, *Electricity Generation in Microbial Fuel Cells Using Neutral Red as an Electronophore Electricity Generation in Microbial Fuel Cells Using Neutral Red as an Electronophore*, 66 (**2000**) 1292–1297.

[158] I. Gajda, J. Greenman, C. Melhuish, I. Ieropoulos, *Photosynthetic cathodes for microbial fuel cells*, Int. J. Hydrogen Energy. 38 (**2013**) 11559–11564.

[159] S. You, Q. Zhao, J. Zhang, J. Jiang, S. Zhao, *A microbial fuel cell using permanganate as the cathodic electron acceptor*, 162 (**2006**) 1409–1415.

[160] T.R. Eliato, G. Pazuki, N. Majidian, *Environmental Effects Potassium permanganate as an electron receiver in a microbial fuel cell*, Energy Sources. 38 (**2016**) 644–651.

[161] S. Cheng, H. Liu, B.E. Logan, *Power densities using different cathode catalysts (Pt and CoTMPP) and polymer binders (Nafion and PTFE) in single chamber microbial fuel cells*, Environ. Sci. Technol. 40 (**2006**) 364–369.

[162] T.H. Pham, J.K. Jang, I.S. Chang, B.H. Kim, *Improvement of cathode reaction of a mediatorless microbial fuel cell*, J. Microbiol. Biotechnol. 14 (**2004**) 324–329.

[163] S. Oh, B. Min, *Cathode Performance as a Factor in Electricity imp Generation in Microbial Fuel Cells - Environmental Science & Technology (ACS Publications)*, 38 (**2004**) 4900–4904.

[164] B.E. Logan, H. Liu, *Electricity Generation Using an Air-Cathode Single Chamber Microbial Fuel Cell in the Presence and Absence of a Proton Exchange Membrane*, Environ. Sci. Technol. 38 (**2004**) 4040–4046.

[165] M. Brodt, T. Han, N. Dale, E. Niangar, R. Wycisk, P. Pintauro, *Fabrication, In-Situ Performance, and Durability of Nanofiber Fuel Cell Electrodes*, J. Electrochem. Soc. 162 (**2015**) 84–91.

[166] P.N. Pintauro, M. Brodt, R. Wycisk, P.N. Pintauro, *Nanofiber Electrodes with Low Platinum Loading for High Power Hydrogen / Air PEM Fuel Cells*, J. Electrochem. Soc. 160 (**2013**) 744–749.

[167] F. Zhao, F. Harnisch, U. Schröder, F. Scholz, P. Bogdanoff, I. Herrmann, *Application of pyrolysed iron(II) phthalocyanine and CoTMPP based oxygen reduction catalysts as cathode materials in microbial fuel cells*, Electrochem. Commun. 7 (**2005**) 1405–1410.

[168] Z. He, L.T. Angenent, *Application of Bacterial Biocathodes in Microbial Fuel Cells*, Electroanalysis. 18 (**2006**) 2009–2015.

[169] A. Bergel, A. Mollica, D. Fe, *Catalysis of oxygen reduction in PEM fuel cell by seawater biofilm*, Trends Biotechnol. 7 (**2005**) 900–904.

[170] A. Aldrovandi, E. Marsili, L. Stante, P. Paganin, S. Tabacchioni, A. Giordano, *Enrico MARSILI*, High. Educ. (**2009**) 1–5.

[171] P. Clauwaert, K. Rabaey, P. Aelterman, L. De Schamphelaire, T.H. Pham, P. Boeckx, N. Boon, W. Verstraete, *Biological denitrification in microbial fuel cells*, Environ. Sci. Technol. 41 (**2007**) 3354–3360.

[172] A. Rhoads, H. Beyenal, Z. Lewandowski, *Microbial fuel cell using anaerobic respiration as an anodic reaction and biomineralized manganese as a cathodic reactant*, Environ. Sci. Technol. 39 (**2005**) 4666–4671.

[173] A. ter Heijne, H.V.M. Hamelers, V. de Wilde, R. a. Rozendal, C.J.N. Buisman, *A Bipolar Membrane Combined with Ferric Iron Reduction as an Efficient Cathode System in Microbial Fuel Cells*, Environ. Sci. Technol. 40 (**2006**) 5200–5205.

[174] Y. Mao, L. Zhang, D. Li, H. Shi, Y. Liu, L. Cai, *Power generation from a biocathode microbial fuel cell biocatalyzed by ferro/manganese-oxidizing bacteria*, Electrochim. Acta. 55 (**2010**) 7804–7808.

[175] G.-C. Gil, I.-S. Chang, B.H. Kim, M. Kim, J.-K. Jang, H.S. Park, H.J. Kim, *Operational parameters affecting the performannce of a mediator-less microbial fuel cell*, Biosens. Bioelectron. 18 (**2003**) 327–334.

[176] R. a. Rozendal, H.V.M. Hamelers, C.J.N. Buisman, *Effects of Membrane Cation Transport on pH and Microbial Fuel*, Environ. Sci. Technol. 40 (**2006**) 5206–5211.

[177] W.-W. Li, G.-P. Sheng, X.-W. Liu, H.-Q. Yu, *Recent advances in the separators for microbial fuel cells*, Spec. Issue Biofuels - II Algal Biofuels Microb. Fuel Cells. 102 (**2011**) 244–252.

[178] J.R. Kim, S. Cheng, S.-E. Oh, B.E. Logan, *Power generation using different cation, anion, and ultrafiltration membranes in microbial fuel cells.*, Environ. Sci. Technol. 41 (**2007**) 1004–9.

[179] F. Harnisch, U. Schr??der, F. Scholz, *The suitability of monopolar and bipolar ion exchange membranes as separators for biological fuel cells*, Environ. Sci. Technol. 42 (**2008**) 1740–1746.

[180] J. Sun, Y. Hu, Z. Bi, Y. Cao, *Improved performance of air-cathode single-chamber microbial fuel cell for wastewater treatment using microfiltration membranes and multiple sludge inoculation*, J. Power Sources. 187 (**2009**) 471–479.

[181] X. Zhang, S. Cheng, X.I.N. Wang, X.I.A. Huang, *Separator Characteristics for Increasing Performance of Microbial Fuel Cells*, 43 (**2009**) 8456–8461.

[182] B.E. Logan, *Scaling up microbial fuel cells and other bioelectrochemical systems*, Applied. 85 (**2010**) 1665–1671.

[183] J.X. Leong, W.R.W. Daud, M. Ghasemi, K. Ben Liew, M. Ismail, *Ion exchange membranes as separators in microbial fuel cells for bioenergy conversion: A comprehensive review*, Renew. Sustain. Energy Rev. 28 (**2013**) 575–587.

[184] B. HP, *Electricity generation by microorganisms.*, Biotechnol. Educ. 1 (**1990**) 163–168.

[185] H. Liu, S. Cheng, B.E. Logan, *Production of electricity from acetate or butyrate using a single-chamber microbial fuel cell*, Environ. Sci. Technol. 39 (**2005**) 658–662.

[186] S. Cheng, H. Liu, B.E. Logan, *Increased Power Generation in a Continuous Flow MFC with Advective Flow through the Porous Anode and Reduced Electrode Spacing*, Environ. Sci. Technol. 40 (**2006**) 2426–2432.

[187] S. Cheng, H. Liu, B.E. Logan, *Increased performance of single-chamber microbial fuel cells using an improved cathode structure*, Electrochem. Commun. 8 (**2006**) 489–494.

[188] G. Gnana kumar, Z. Awan, K. Suk Nahm, J. Stanley Xavier, *Nanotubular MnO2/graphene oxide composites for the application of open air-breathing cathode microbial fuel cells*, Biosens. Bioelectron. 53 (**2014**) 528–534.

[189] J. El-Chakhtoura, M. El-Fadel, H.A. Rao, D. Li, S. Ghanimeh, P.E. Saikaly, *Electricity generation and microbial community structure of air-cathode microbial fuel cells powered with the organic fraction of municipal solid waste and inoculated with different seeds*, Biomass and Bioenergy. 67 (**2014**) 24–31.

[190] Z. Chen, K. Li, P. Zhang, L. Pu, X. Zhang, Z. Fu, *The performance of activated carbon treated with H3PO4 at 80??C in the air-cathode microbial fuel cell*, Chem. Eng. J. 259 (**2015**) 820–826.

[191] C.M. Bruce E. Logan, Keith Scott, Neil D. Gray, Ian M. Head, *Electricity generation from cysteine in a microbial fuel cell*, Water Reasearch. 39 (**2005**) 942–952.

[192] D.R. Lovley, *Bug juice: harvesting electricity with microorganisms.*, Nat. Rev. Microbiol. 4 (**2006**) 497–508.

[193] B. Min, B.E. Logan, *Continuous electricity generation from domestic wastewater and organic substrates in a flat plate microbial fuel cell.*, Environ. Sci. Technol. 38 (**2004**) 5809–5814.

[194] Z. He, S.D. Minteer, L.T. Angenent, *Electricity generation from artificial wastewater using an upflow microbial fuel cell*, Environ. Sci. Technol. 39 (**2005**) 5262–5267.

[195] Z. He, N. Wagner, S.D. Minteer, L.T. Angenent, *An upflow microbial fuel cell with an interior cathode: Assessment of the internal resistance by impedance spectroscopy*, Environ. Sci. Technol. 40 (**2006**) 5212–5217.

[196] B.R. Ringeisen, E. Henderson, P.K. Wu, J. Pietron, R. Ray, B. Little, J.C. Biffinger, J.M. Jones-Meehan, *High power density from a miniature microbial fuel cell using Shewanella oneidensis DSP10*, Environ. Sci. Technol. 40 (**2006**) 2629–2634.

[197] B.E. Logan, K. Rabaey, *Conversion of wastes into bioelectricity and chemicals by using microbial electrochemical technologies.*, Science. 337 (**2012**) 686–90.

[198] G.T.R. Palmore, G.M. Whitesides, *Microbial and Enzymatic Biofuel Cells*, Power. 566 (**1994**) 271–290.

[199] F. Barbir, F. Barbir, CHAPTER 3 – Fuel Cell Electrochemistry, in: PEM Fuel Cells, **2005**. 33–72.

[200] D.P. Lies, M.E. Hernandez, A. Kappler, R.E. Mielke, J.A. Gralnick, D.K. Newman, *Shewanella oneidensis MR-1 Uses Overlapping Pathways for Iron Reduction at a Distance and by Direct Contact under Conditions Relevant for Biofilms*, Appl. Environ. Microbiol. 71 (**2005**) 4414–4426.

[201] J.N. Roy, S. Babanova, K.E. Garcia, J. Cornejo, L.K. Ista, P. Atanassov, *Catalytic biofilm formation by Shewanella oneidensis MR-1 and anode characterization by expanded uncertainty*, Electrochim. Acta. (**2013**).

[202] A.J. Bard, L.R. Faulkner, N. York, C. Bullet, W. Brisbane, S.E. Toronto, *Electrochemical Methods: Fundamentals and Applications*, **1944**.

[203] F. Barbir, F. Barbir, CHAPTER 1 – Introduction, in: PEM Fuel Cells, **2005**: pp. 1–16.

[204] C.G. Zoski, *Handbook of electrochemistry*, Elsevier, **2007**.

[205] M.C. Compagny, *Carbon and Graphite Felt Insulation Thermal Conductivity of Felt*, (**2000**).

[206] E. Frackowiak, F. Béguin, *Carbon materials for the electrochemical storage of energy in capacitors*, Carbon N. Y. 39 (**2001**) 937–950.

[207] B. Trémillon, *Electrochimie analytique et réactions en solution*, **1993**.

[208] J.J. van de G. B. Roffel, *The Diffusion Coefficient of Ferricyanide Ions in Aqueous Potassium Chloride Solutions with and without Polyethylene Oxide Addition Bruin*, J. Chem. Eng. Data. 22 (**1977**) 300–302.

[209] D. Baron, E. LaBelle, D. Coursolle, J. a Gralnick, D.R. Bond, *Electrochemical measurement of electron transfer kinetics by Shewanella oneidensis MR-1.*, J. Biol. Chem. 284 (**2009**) 28865–73.

[210] J. Babauta, R. Renslow, Z. Lewandowski, H. Beyenal, *Electrochemically active biofilms: facts and fiction. A review.*, Biofouling. 28 (**2012**) 789–812.

[211] B. Cercado, N. Byrne, M. Bertrand, D. Pocaznoi, M. Rimboud, W. Achouak, A. Bergel, *Garden compost inoculum leads to microbial bioanodes with potential-independent characteristics.*, Bioresour. Technol. 134 (**2013**) 276–84.

[212] C.M. Cordas, L.T. Guerra, C. Xavier, J.J.G. Moura, *Electroactive biofilms of sulphate reducing bacteria*, Electrochim. Acta. 54 (**2008**) 29–34.

[213] J. Wei, P. Liang, X. Cao, X. Huang, *A new insight into potential regulation on growth and power generation of geobacter sulfurreducens in microbial fuel cells based on energy viewpoint*, Environ. Sci. Technol. 44 (**2010**) 3187–3191.

[214] J.N. Roy, K.E. Garcia, H.R. Luckarift, A. Falase, J. Cornejo, S. Babanova, a. J. Schuler, G.R. Johnson, P.B. Atanassov, *Applied Electrode Potential Leads to Shewanella oneidensis MR-1 Biofilms Engaged in Direct Electron Transfer*, J. Electrochem. Soc. 160 (**2013**) H866–H871.

[215] R.C. Wagner, D.F. Call, B.E. Logan, *Optimal set anode potentials vary in bioelectrochemical systems*, Environ. Sci. Technol. 44 (**2010**) 6036–6041.

[216] A. Kumar, K. Katuri, P. Lens, D. Leech, *Does bioelectrochemical cell configuration and anode potential affect biofilm response?*, Biochem. Soc. Trans. 40 (**2012**) 1308–14.

[217] A. Carmona-Martínez, F. Harnisch, U. Kuhlicke, T.R. Neu, U. Schröder, *Electron transfer and biofilm formation of Shewanella putrefaciens as function of anode potential.*,

Bioelectrochemistry. 93 (**2013**) 23–9.

[218] C. Grobbler, B. Virdis, A. Nouwens, F. Harnisch, K. Rabaey, P.L. Bond, *Use of SWATH mass spectrometry for quantitative proteomic investigation of Shewanella oneidensis MR-1 biofilms grown on graphite cloth electrodes*, **2015**.

[219] L. Peng, S.-J. You, J.-Y. Wang, *Electrode potential regulates cytochrome accumulation on Shewanella oneidensis cell surface and the consequence to bioelectrocatalytic current generation*, **2010**.

[220] P. Liang, H. Wang, X. Xia, X. Huang, Y. Mo, X. Cao, M. Fan, *Carbon nanotube powders as electrode modifier to enhance the activity of anodic biofilm in microbial fuel cells*, Biosens. Bioelectron. 26 (**2011**) 3000–3004.

[221] T.-H. Nguyen, Y.-Y. Yu, X. Wang, J.-Y. Wang, H. Song, *3D Mesoporous Polysulfone-Carbon Nanotube Anode for Enhanced Bioelectricity Output in Microbial Fuel Cells*, Optoelectron. Adv. Mater. Rapid Commun. 4 (**2013**) 1166–1169.

[222] S. Srikanth, E. Marsili, M.C. Flickinger, D.R. Bond, *Electrochemical characterization of Geobacter sulfurreducens cells immobilized on graphite paper electrodes*, Biotechnol. Bioeng. 99 (**2008**) 1065–1073.

[223] Y. Yu, H.-L. Chen, Y.-C. Yong, D. Kim, H. Song, *Conductive artificial biofilm dramatically enhances bioelectricity production in Shewanella-inoculated microbial fuel cells.*, Chem. Commun. 47 (**2011**) 12825–12827.

[224] C. Brinker, G. Scherer, *Sol-Gel Science: The Physics and Chemistry of Sol-Gel Processing*, Academic p, **1990**.

[225] J.-P. Jolivet, *De la solution à l'oxyde : Condensation des cations en solution aqueuse*, Savoirs actuels, **1994**.

[226] J. Young, *Humidity control in the laboratory using salt solutions—a review*, J. Appl. Chem. 17 (**1967**) 241–245.

[227] G. Carturan, R. Campostrini, V. Scardi, E.D.E. Alteriis, *Inorganic Gels for Immobilization of Biocatalysts: Inclusion of Invertase-active Whole Cells of Yeast (Succharomyces cerevisiae) into Thin Layers of SiOz Gel Deposited on Glass Sheets*, J. Mol. Catal. 57 (**1989**) 13–16.

[228] D.J. Dickson, C.J. Page, R.L. Ely, *Photobiological hydrogen production from Synechocystis sp. PCC 6803 encapsulated in silica sol-gel*, Int. J. Hydrogen Energy. 34 (**2009**) 204–215.

[229] M.L. Ferrer, L. Yuste, F. Rojo, F. Del Monte, *Biocompatible sol-gel route for encapsulation of living bacteria in organically modified silica matrixes*, Chem. Mater. 15 (**2003**) 3614–3618.

[230] R. Rousseau, X. Dominguez-Benetton, M.L. Délia, A. Bergel, *Microbial bioanodes with high salinity tolerance for microbial fuel cells and microbial electrolysis cells*, Electrochem. Commun. 33 (**2013**) 1–4.

[231] R.B. Bhatia, C.J. Brinker, *Aqueous Sol - Gel Process for Protein Encapsulation*, Chem. Mater. (**2000**) 2434–2441.

[232] A. Coiffier, T. Coradin, C. Roux, O.M.M. Bouvet, J. Livage, *Sol–gel encapsulation of bacteria: a comparison between alkoxide and aqueous routes*, J. Mater. Chem. 11 (**2001**) 2039–2044.

[233] N. Nassif, O. Bouvet, M. Noelle Rager, C. Roux, T. Coradin, J. Livage, *Living bacteria in silica gels.*, Nat. Mater. 1 (**2002**) 42–4.

[234] N. Nassif, C. Roux, T. Coradin, M.-N. Rager, O.M.M. Bouvet, J. Livage, *A sol–gel matrix to*

preserve the viability of encapsulated bacteria, J. Mater. Chem. 13 (**2003**) 203–208.

[235] C. Depagne, S. Masse, T. Link, T. Coradin, *Bacteria survival and growth in multi-layered silica thin films*, J. Mater. Chem. 22 (**2012**) 12457.

[236] N. Nassif, A. Coiffier, T. Coradin, C. Roux, J. Livage, *Viability of Bacteria in Hybrid Aqueous Silica Gels*, J. Sol-Gel Sci. Technol. 26 (**2003**) 1141–1144.

[237] C.F. Meunier, J.C. Rooke, A. Léonard, H. Xie, B.-L. Su, *Living hybrid materials capable of energy conversion and CO2 assimilation.*, Chem. Commun. (Camb). 46 (**2010**) 3843–3859.

[238] M. Estevez-Canales, D. Pinto, T. Coradin, C. Laberty-Robert, A. Esteve-Núñez, *Silica-immobilization of Geobacter sulfurreducens for constructing ready-to-use artificial bioelectrodes*, Microb. Biotechnol. (**2016**).

[239] H.R. Luckarift, S.R. Sizemore, J. Roy, C. Lau, G. Gupta, P. Atanassov, G.R. Johnson, *Standardized microbial fuel cell anodes of silica-immobilized Shewanella oneidensis*, Chem. Commun. 46 (**2010**) 6048.

[240] S.R. Sizemore, R. Nichols, R. Tatum, P. Atanassov, G.R. Johnson, H.R. Luckarift, Immobilization of Whole Cells by Chemical Vapor Deposition of Silica, in: **2013,** 301–312.

[241] G. Strack, H.R. Luckarift, S.R. Sizemore, R.K. Nichols, K.E. Farrington, P.K. Wu, P. Atanassov, J.C. Biffinger, G.R. Johnson, *Power generation from a hybrid biological fuel cell in seawater.*, Bioresour. Technol. 128 (**2013**) 222–8.

[242] E. Blanchet, B. Erable, M.L. De Solan, A. Bergel, *Two-dimensional carbon cloth and three-dimensional carbon felt perform similarly to form bioanode fed with food waste*, Electrochem. Commun. 66 (**2016**) 38–41.

[243] J. Cooley, Apparatus for electrically dispersing fluids, **1902**.

[244] W. Morton, Method of dispersing fluids, **1902**.

[245] H. Brooks, N. Tucker, *Electrospinning predictions using artificial neural networks*, Polymer (Guildf). 58 (**2015**) 22–29.

[246] W. Teo, R. Inai, S. Ramakrishna, *nanofibers Technological advances in electrospinning of nanofibers*, 6996 (**2016**).

[247] P. Taylor, D. Lukáš, A. Sarkar, L. Martinová, K. Vodsed, D. Lubasová, *Physical principles of electrospinning (Electrospinning as a nano-scale technology of the twenty-first century)*, (**2009**) 37–41.

[248] T.D. Brown, P.D. Dalton, D.W. Hutmacher, *Progress in Polymer Science Melt electrospinning today : An opportune time for an emerging polymer process*, Prog. Polym. Sci. 56 (**2016**) 116–166.

[249] F. Navarro-Pardo, A.L. Martinez-Hernandez, C. Velasco-Santos, *Carbon Nanotube and Graphene Based Polyamide Electrospun Nanocomposites : A Review*, 2016 (**2016**).

[250] P.S. Kumar, S. Jayaraman, G. Singh, *Polymer and nanocomposite nanofiber: Electrospinning parameters and rheology properties.*, (**1920**) 329–354.

[251] S.F. Dehghan, F. Golbabaei, B. Maddah, M. Latifi, H. Pezeshk, M. Hasanzadeh, F. Akbar-, *Optimization of Electrospinning Parameters for PAN-MgO Nanofibers Applied in Air Filtration Somayeh*, 2247 (**2016**).

[252] D.E. Elliott, F.J. Davis, G.R. Mitchell, *Recent progress concerning the production of controlled highly oriented electrospun nanofibrous arrays*, (**2016**).

[253] B.C. Kim, K.S. Yang, M. Kojima, K. Yoshida, Y.J. Kim, Y.A. Kim, *Fabrication of Electrospinning-Derived Carbon Nanofiber Webs for the Anode Material of Lithium-Ion Secondary Batteries*, Adv. Funct. Mater. (**2006**) 2393–2397.

[254] S.K. Nataraj, K.S. Yang, T.M. Aminabhavi, *Polyacrylonitrile-based nanofibers - A state-of-the-art review*, Prog. Polym. Sci. 37 (**2012**) 487–513.

[255] K. Yan, L.-B. Kong, Y.-H. Dai, M. Shi, K.-W. Shen, B. Hu, Y.-C. Luo, Kang, *Design and preparation of highly structure-controllable mesoporous carbons at the molecular level and application as electrode materials for supercapacitors*, J. Mater. Chem. A. (**2015**).

[256] M.L. Minus, S. Kumar, *The Processing, Properties, and Structure of Carbon Fibers*, (**2005**).

[257] N.S. Babu, K.N. Ninan, *Fourier Transform Infrared and Wide-Angle X-Ray Diffraction Studies of the Thermal Cyclization Reactions of High-Molar-Mass Poly (acrylonitrile- co - itaconic acid)*, (**2005**).

[258] M. Jing, C. Wang, Q. Wang, Y. Bai, B. Zhu, *Chemical structure evolution and mechanism during pre-carbonization of PAN-based stabilized fiber in the temperature range of 350 e 600 C*, 92 (**2007**) 1737–1742.

[259] S.A. Podkopayev, G.P. Shveikin, A.G. Fazlitdinova, V.A. Tyumentsev, *Changes of polyacrylonitrile fiber fine structure during thermal stabilization*, J. Mater Sci. (**2010**).

[260] M. Ji, C. Wang, Y. Bai, M. Yu, Y. Wang, *Structural Evolution of Polyacrylonitrile Precursor Fibers during Preoxidation and Carbonization*, 536 (**2007**) 527–536.

[261] M. Yu, C. Wang, Y. Bai, B.O. Zhu, M. Ji, Y. Xu, *Microstructural Evolution in Polyacrylonitrile Fibers During Oxidative Stabilization*, (**2008**) 759–765.

[262] Z. Bashir, *A critical review of the stabilisation of polyacrylonitrile*, Carbon, (**1991**).

[263] Y. Liu, S. Kumar, *Recent Progress in Fabrication, Structure and Properties of Carbon Fibers*, (**2012**) 37–41.

[264] E. Fitzer, D.J. Miller, *the influence of oxygen on the chemical reaction during stabilization of PAN as carbon fiber precursor*, 13 (**1975**) 63–69.

[265] W. Watt, W. Johnson, *Mechanism of oxidation of polyacrylonitrile fibres*, Nature. 257 (**1975**).

[266] M. Mathieu, *Stabilization and carbonization of PAN-based carbon fibers as related to mechanical properties*, 29 (**1991**) 621–628.

[267] Y. Liu, H.G. Chae, S. Kumar, *Gel-spun carbon nanotubes/polyacrylonitrile composite fibers . Part II : Stabilization reaction kinetics and effect of gas environment*, Carbon N. Y. 49 (**2011**) 4477–4486.

[268] C. Kim, S. Park, J. Cho, D. Lee, T. Park, W. Lee, K. Yang, *Raman spectroscopic evaluation of polyacrylonitrile-based carbon nanofibers prepared by electrospinning*, (**2004**) 928–933.

[269] W.J. Blaedel, R.C. Engstrom, *Investigations of the Ferricyanide-Ferrocyanide System by Pulsed Rotation Voltammetry*, Anal. Chem. 50 (**1978**) 476–479.

[270] G. Leone, M. Consumi, M. Aggravi, A. Donati, S. Lamponi, A. Magnani, *PVA / STMP based hydrogels as potential substitutes of human vitreous*, (**2010**) 2491–2500.

[271] Y. Zhang, P.C. Zhu, D. Edgren, *Crosslinking reaction of poly (vinyl alcohol) with glyoxal*, (**2010**) 725–730.

[272] Y. Dror, W. Salalha, R.L. Khalfin, Y. Cohen, *Carbon Nanotubes Embedded in Oriented Polymer Nanofibers by Electrospinning*, (**2003**) 7012–7020.

[273] F. Ko, Y. Gogotsi, a. Ali, N. Naguib, H. Ye, G.L. Yang, C. Li, P. Willis, *Electrospinning of Continuous Carbon Nanotube-Filled Nanofiber Yarns*, Adv. Mater. 15 (**2003**) 1161–1165.

[274] B. Sundaray, V. Subramanian, T.S. Natarajan, K. Krishnamurthy, *Electrical conductivity of*

a single electrospun fiber of poly(methyl methacrylate) and multiwalled carbon nanotube nanocomposite, Appl. Phys. Lett. 88 (**2006**) 143114.

Abbreviations

AEM	Anion Exchange Membrane
BES	Bioelectrochemical System
CEM	Cation Exchange Membrane
CF	Carbon Felt
cfu	colony-forming unit
CNT	Carbon Nanotube
CV	Cyclic Voltammetry
DET	Direct Electron Transfer
DMF	Dimethylformamide
DMRB	Dissimilatory Metal Reducing Bacteria
DPP	Difference in Pic Potential
EET	Extracellular Electron Transfer
EFC	Enzymatic Fuel Cell
ES	Electrospinning
GDL	Gas Diffusion Layer
IET	Indirect Electron Transfer
LB	Luria-Bertani Broth
μ	Growth-rate
MES	Microbial Electrochemical System
MET	Mediated Electron Transfer or Microbial Electrochemical Technology depending on the context
MFC	Microbial Fuel Cell
NHE	Normal Hydrogen Electrode
OCP	Open Circuit Potential
OCV	Open Cicuit Voltage
OD600	Optical Density at λ = 600 nm
PAN	Poly(acrylonitrile)
PBS	Phosphate Buffered Saline
PEG	Poly(ethylene glycol)
PEM	Proton Exchange Membrane
PVA	Poly(vinyl alcohol)
SCE	Saturated Calomel Electrode
SECM	Scanning Electrochemical Microscopy
SEM	Scanning Electronic Microscopy
SHE	Standard Hydrogen Electrode
%RH	Percentage of Relative Humidity